THE UNIVERSITY
of EDINBURGH

THE UNIVERSITY *of* EDINBURGH

IDENTIFICATION OF NOVEL ACCESSORY PROTEINS ENCODED BY INFLUENZA A VIRUS SEGMENT 2 THAT PREVENT INTERFERON INDUCTION

Rute Maria dos Santos Pinto

College of Medicine and Veterinary Medicine

The Royal (Dick) School of Veterinary Studies

The Roslin Institute

Dissertation submitted for the degree of Doctor of Philosophy

The University of Edinburgh

2019

Declaration of authentication

Edinburgh, August 2019

I hereby declare that this thesis entitled "*Identification of novel accessory proteins encoded by influenza A virus segment 2 that prevent interferon induction*" was produced by myself, that the work and illustrations contained herein are my own except where otherwise explicitly acknowledged. This work has not been submitted, either in whole or part, for any other degree or professional qualification of any other institution.

……

Rute Maria dos Santos Pinto

Dedication

I would like to dedicate this dissertation to my grandparents **Victor, Maria Joana, Paulo and Olga**.

Their wealth of knowledge, consistent teaching, patience, encouragement and unconditional love have been absolutely crucial for my personal and professional development and therefore a key for the success of this scientific body of work.

For that I will be eternally thankful.

É com muito gosto que dedico esta dissertação aos meus quatro avós **Victor**, **Maria Joana**, **Paulo e Olga**.

Tê-los presentes na minha vida é uma das minha maiores sortes. Todo a riqueza de conhecimento, o ensino constante, a paciência, a coragem, o carinho e o amor incondicionais por eles cedidos e demonstrados têm sido fundamentais para o meu crescimento pessoal e professional que, entre outros, resultaram no sucesso deste estudo científico.

Por tudo e mais ficarei eternamente grata.

Acknowledgements

Little did I know what an enjoyable and memorable experience this would be. I've got my name attached to the front page of this work, but none if this would have been possible without the help and support of the following people.

Primarily, I would like to thank my supervisor Professor Paul Digard who kindly adopted me into his laboratory and so generously offered me the opportunity to develop a project which I am so passionate about. His broad knowledge and guidance made the success this thesis. I would also like to thank my second supervisor Professor Bernadette Dutia for her patience and encouragement and for kindly providing delicious Victoria sponge cakes which can make any mood as light as the cake itself. Professors Digard and Dutia successfully provided me with the best scientific and academic training a PhD candidate could ever ask for. Our Thursday afternoon meetings were always occasions of intensive and thrilling learning and will truly be missed.

Thank you to previous and current members of the Digard and Dutia laboratories, who have provided essential help and advice. Particularly Dr Helen Wise who so brilliantly initiated this project and Dr Liliane Chung for the training, the friendship and for managing to work beside me without kicking me out the bench. I would like to extend my appreciation to Dr Marlynne Quigg-Nicol (for all the help with the *in vivo* experiments), Dr Lita Murphy (for the support during the writing period), Dr Elly Gaunt (for believing in my crazy ideas), Dr Saira Hussain (for the egg training), Dr Nikki Smith (for keeping us all in order) and Ian Bennet (for advice in molecular biology techniques). Big thanks to Dr Samantha Lycett and Dr Pip Beard for their help with the bioinformatics and histopathology analyses.

It is with delight that I belong to the "Digardians of the Galaxy" and it was a pleasure to work alongside lab friends Dr Seema Jasim, Dr Matty Turntables, Dr Becca Dewar, Dr Mariya Goncheva, Dr Anabel Clements and Dr Carina Conceição. Thanks for the coffee breaks, the lunch breaks, the Friday bars, the karaoke sessions, the Popworld, the FluFighters exhibits, the gossip dinners, the "what bus are you taking?" and honestly… All the fun… Thanks for making that sweet line of people with "I-need-coffee!" faces in the audience of scientific conferences that I was always so proud to belong to. You guys really made it worth it.

Thanks to the newbies Susi Keane, Lizzie Billington and Cal Donnely. Thanks for taking my suggestions (even when they were wrong…). Keep going, guys, I believe in you! If I made it, you'll make it as well. And don't forget… We still have to build a plaque assay throne!

A big thanks to all the members of the virology community at the Roslin Institute. Thanks to Dr Finn Grey and Dr Christine Tait-Burkard for the questions at the internal seminars and to Dr Bob Dalziel for the knowledge sharing and for caringly getting some sense in my head when needed. Thanks to Dr Jack Ferguson and Dr Inga Dry (for the fun times in the lab and for increasing my love for pints), Dr Spring Tan (for the rides in the early mornings) and Elle McLuskey (for being my long hair buddy).

An enormous gratitude to the Microbiology Society for the career development opportunities and the financial support to attend national and international conferences.

A massive appreciation to my MRes supervisors and lab mentors at the MRC-University of Glasgow Centre for Virus Research: Prof Massimo Palmarini, Dr David Bhella, Dr Mariana Varela and Colin Loney, who were vital at the early stages of my virology training, made me believe I could survive this adventure and kept supporting me throughout its entire duration.

Thanks to my first ever Glasgow friends Helena and Mario (now respectful Doctors) for the encouragement and the enjoyable meals with loads of politically incorrect jokes.

Huge thanks to my flatmates, Rui and Joy, for telling me off when I left the kitchen a mess and for making me tidy my room when it desperately needed an intervention. I don't think I could have shared a home with better people. You were the reason why I didn't work on (all) Sundays.

I could not miss my bonkers group of friends: João, Fábio, Martins, Carolina, Daniel, Laura, Cajó, Ana, Marcelo and Pedras, who, despite the distance, make me believe that home will, invariably, always be home. Thanks to Di and Falâncio who give meaning to the premise "Os amigos da Faculdade são para sempre" (If you're friends in Uni, you'll be forever friends). A massive thanks to Sofia and Anabela, the sisters from another mother who were always, always there.

Lastly, I want to thank my family, from the very north to the very south of little Portugal, ranging from aunts, uncles, cousins, grandparents and great-grandparents who shaped me into who I am today and always fully supported and encouraged my decisions.

The very final and most special thanks goes to my mom Paula, my dad Luís and my siblings Manuel and Mariana.

PS: I'm definitely forgetting people…

Table of Contents

Lay summary

"Flu" is a respiratory infectious disease caused by influenza A viruses (IAV).

IAV circulate in aquatic birds where they mainly cause mild or asymptomatic infections. However, through adaptation, these viruses are able to infect other avian and mammalian species such as poultry, pigs, and humans, causing severe clinical symptoms and high mortality rates, leading to losses in food production and economic burden. Moreover, the unpredictable occurrence of human pandemics could result in the deaths of millions of people worldwide. Given the current lack of a definitive prevention method, it is vital to fully understand how IAV replicates and causes disease.

Similar to humans, mammals, and indeed every other living organism, viruses also possess a genome - coding for several proteins which they need to replicate. The IAV genome is composed of eight segments. Gene overlapping is widely employed by these viruses to generate genetic novelty while retaining a small genome size, meaning that the same genomic sequence encodes for more than one protein. Therefore, from a small genome, IAV is capable of expressing not only their ten essential proteins, but also an additional ten accessory proteins which have also been identified in different IAV isolates/strains. Although not crucial for virus propagation, many of these accessory proteins have been shown to counteract the host immune response, halt the host protein synthesis, or increase cell death, contributing to a more severe viral pathogenesis and faster disease progression.

In this work, we have identified two additional accessory proteins, PB1-N92 and PB1-N111, which are expressed from IAV segment 2. Mutant viruses lacking these peptides induced a stronger innate immune response (interferon response) and struggled to replicate in cell lines, in embryonated hen's eggs, and in mouse models. However, when the innate immune response was weakened, the mutant viruses recovered their replication. Moreover, these proteins were individually expressed separately from the virus and were able to counteract the interferon response by themselves.

Bioinformatic analyses predicted the likely expression of these peptides in the large majority of IAV isolates, and research into human pandemic, seasonal, and swine strains corroborated the importance of PB1-N92 and PB1-N111 in IAV infection. However, deleting the two proteins in the context of a duck virus did not affect virus replication nor innate immunity induction in mammalian cells, but reduced the growth of this virus in avian cells, showing a possible species specificity in the function of PB1-N92 and PB1-N111.

Therefore, the data described in this study suggest the existence of two additional proteins coded in IAV segment 2 which are interferon antagonists. Further studies on segment 2 should have their coding regions taken into consideration.

Abstract

Influenza A viruses (IAV) are a major group of pathogens that infect a broad range of mammalian and avian species and in humans, cause of annual epidemics and occasional pandemics. IAVs are orthomyxoviruses containing an 8 segment negative-sense single-stranded RNA genome encoding 10 core polypeptides essential for virus replication. Alternative translation events that produce additional viral polypeptides have been shown to be significant in IAV biology.

IAV genome segment 2 is a virulence determinant known to encode PB1, PB1-F2 and PB1-N40 proteins, starting from AUG codons 1, 4 and 5 respectively. Work in this thesis investigated the expression of two additional polypeptides, arising from translation initiation at AUGs 10 and 11 of segment 2. These codons are highly conserved in IAV and direct the translation of two N-terminally truncated versions of the primary PB1 product (PB1-N92 and -N111 respectively).

Mutation of AUGs 10 or 11 in the background of the A/PR/8/34 strain had minor effects on virus replication kinetics despite giving elevated levels of IRF3 phosphorylation and type I IFN secretion compared to the WT virus. However, simultaneous mutation of AUGs 10 and 11 severely decreased viral fitness. Similar patterns of defective replication and elevated innate signalling were seen when mutating AUGs 10 and/or 11 in other mammalian virus isolates. The propagation deficit of the PR8 ΔAUG10,11 mutant recovered in IFN-deficient models, including IFN α/β receptor (IFNAR) knockout bone marrow-derived macrophages and *in vivo*

in IFNAR-/- mouse lungs. Moreover, expression of PB1-N92 or –N111 polypeptides blocked poly I:C- and TBK1-, but not IRF3-induced activation of the IFN-β promoter in transfected cells, suggesting the polypeptides blocked innate immune signalling downstream of RIG-I-like receptor signalling but upstream of IRF3 phosphorylation. Consistent with this, addition of a TBK1/IKKε inhibitor increased growth of the mutant viruses.

In conclusion, IAV segment 2 expresses two previously undescribed N-terminally truncated versions of PB1 which play a role in antagonising the host IFN response, most likely at the stage of the TBK1/IKKε complex.

Abbreviations

Abbreviation	Full name
bp	Base pair
BSA	Bovine serum albumin
BX-795	N-[3-[[5-Iodo-4-[[3-[(2-thienylcarbonyl)amino]propyl]amino]-2-pyrimidinyl]amino]phenyl]-1-pyrrolidinecarboxamide
cDNA	Complementary deoxyribonucleic acid
CFP	Cyan fluorescent protein
cRNA	Complementary ribonucleic acid
Ct	Cycle threshold
CSF1	Colony Stimulating Factor 1
DAPI	4',6-Diamidino-2-phenylindole
DIP	Defective interfering particles
DMEM	Dulbecco's modified Eagle's medium
DMSO	Dimethyl sulphoxide
DNA	Deoxyribonucleic acid
dpi	Days post infection
dsRNA	Double-stranded ribonucleic acid
EC_{50}	Half maximal effective concentration
eIF2	Eukaryotic initiation factor 2
ELISA	Enzyme-linked immunosorbent assay
EOP	Efficiency of plaquing
FBS	Foetal bovine serum
FRET	Forster resonance energy transfer
GFP	Green fluorescent protein
hpi	Hours post infection

IAV	Influenza A viruses
IC_{50}	Half maximal inhibitory concentration
IF	Immunofluorescence
IFITM	Interferon-induced transmembrane proteins
IFN	Interferon
IFNAR	Interferon-α/β receptor
IL	Interleukin
IMD0354	N-(3,5-Bis-trifluoromethylphenyl)-5-chloro-2-hydroxybenzamide
IRES	Internal ribosome entry site
IRF	Interferon regulatory transcription factor
IRSE	Interferon stimulated response element
ISG	Interferon stimulated genes
JSH-23	4-Methyl-N1-(3-phenyl-propyl)-benzene-1,2-diamine
kDa	Kilo Dalton
LB	Luria-Bertani
LGP2	Laboratory of genetics and physiology 2
MAVS	Mitochondrial antiviral-signalling protein
MCS	Multiple cloning site
MDA-5	Melanoma differentiation-associated protein 5
MDCK	Madin-Darby canine kidney
MOI	Multiplicity of infection
mRNA	Messenger ribonucleic acid
MyD88	Myeloid differentiation primary response 88
M1	Matrix protein
M2	Matrix-2 ion channel
NA	Neuraminidase
NBF	Neutral buffered formalin

NES	Nuclear export signal
NF-κB	Nuclear factor kappa B
NLS	Nuclear localisation signal
NMR	Nuclear magnetic resonance
NOD	Nucleotide oligomerisation domain
NP	Nucleoprotein
NPC	Nuclear pore complex
NS1	Non-structural protein 1
NS2/NEP	Non-structural protein 2/Nuclear export protein
ORF	Open reading frame
PA	Polymerase acidic protein
PAMP	Pathogen-associated molecular pattern
PBS	Phosphate-buffered saline
PB1	Polymerase basic protein 1
PB2	Polymerase basic protein 2
PCR	Polymerase chain reaction
PFU	Plaque forming units
PHE	Public Health England
pIRF3	Phosphorylated IRF3
PKR	Protein kinase R
Poly I:C	Polyinosinic:polycytidylic acid
PRR	Pattern recognition receptor
qPCR	Quantitative polymerase chain reaction
RIG-I	Retinoic acid-inducible gene I
RIPLET	RIG finger proteins leading to RIG-I activation
RIP1	Receptor interacting protein 1
RLR	RIG-I-like receptors

RNA	Ribonucleic acid
RNA PolII	RNA polymerase II
RNP	Ribonucleoprotein
RPMI	Roswell Park Memorial Institute
SA	Sialic acid
SDS-PAGE	Sodium dodecyl sulphate polyacrylamide gel electrophoresis
SDM	Site-directed mutagenesis
SEAP	Secreted embryonic alkaline phosphatase
SFM	Serum free media
ssRNA	Single-stranded ribonucleic acid
STAT	Signal Transducer and Activator of Transcription
TBK1	TANK-binding kinase 1
TEMED	Tetramethylethylmediamine
TLR	Toll-like receptor
TNFα	Tumour necrosis factor α
TPCK	N-tosyl-L-phenylalanine chloromethyl ketone
TRAF	TNF receptor-associated factor
TRIF	TIR-domain-containing adapter-inducing interferon-β
TRIM	Tripartite motif-containing protein
UTR	Untranslated region
vRNA	Viral RNA
vRNA2	Viral RNA of segment 2
vRNA8	Viral RNA of segment 8
WHO	World Health Organisation
WT	Wild-type

List of Figures

CHAPTER 1:

CHAPTER 2:

CHAPTER 3:

CHAPTER 4:

CHAPTER 5:

CHAPTER 7:

CHAPTER 8: MATERIALS AND METHODS

List of Tables

Chapter 1

Introduction: Influenza A viruses, accessory proteins and innate immunity

1.1. General Introduction to Influenza A viruses

Influenza A viruses (IAV) are members of the *Orthomyxoviridae* family and possess an 8-segment negative-sense single-stranded RNA genome. Additional genera within *Orthomyxoviridae* include: influenza viruses B, C and D, *Thogotovirus*, *Isavirus* and *Quaranjavirus*. IAV is known to cause acute febrile respiratory illness in several species and is responsible for seasonal infections or outbreaks with high morbidity and mortality, being therefore a substantial economic burden to society.

Hospitalization occurs mainly among high risk groups. Nevertheless, worldwide, annual Influenza epidemics are estimated to result in 3 to 5 million cases of severe illness, and between 290,000 and 650,000 respiratory deaths (World Health Organisation, 2019). In the most recent season (winter of 2018/2019), 5,505 IAV-positive people were reported hospitalised in a network of 24 trusts in England. Across

all of the United Kingdom, 3,157 people were admitted to an Intensive Care or High Dependency Unit as a result of confirmed Influenza, of whom 312 deceased. Overall the 2018/19 season resulted in an estimated 1,692 deaths associated with IAV (Public Health England, *Surveillance of influenza and other respiratory viruses in the UK Winter 2018 to 2019*).

1.1.1. Taxonomy and nomenclature

In order to be better catalogued, IAV can be serologically subtyped, according to the antigenic properties of their glycoproteins haemagglutinin (HA) and neuraminidase (NA). So far, 16 HAs and 9 NAs have been identified circulating in the avian reservoir but only H1N1, H1N2, H2N2 and H3N2 subtypes are known with certainty to have circulated in humans. More recently H17N10 and H18N11 subtypes were also found in bat species (Tong *et al.* 2012; Tong *et al.* 2013). Conventionally, influenza virus isolates are titled according to their type (A, B, C or D), host, location, strain identifier, year of isolation and HA and NA subtype. Therefore, an H5N2 isolate from a Pennsylvanian chicken in 1983, strain number 1370 would be named A/chicken/Pennsylvania/1370/1983 (H5N2). In human cases, the species designation is omitted.

1.1.2. Ecology and host adaptation

IAV has waterfowls from Anseriformes and Charadriiformes orders as its natural host and reservoir for the majority of the isolated subtypes (Webster *et al.*

1992). In these hosts IAV primarily replicates in gut epithelium-lining cells, often asymptomatically, leading to virus spread via the faecal-oral route (Webster *et al.* 1978). Moreover, in addition to bird-to-bird transmission, the virus can undergo adaptive mutations, acquiring zoonotic and epizootic potential, allowing infection of a variable group of mammalian and avian hosts including human, canine, equine, swine, galliform birds, migratory birds and a small number of sea mammals such as seals (Joseph *et al.* 2017).

1.1.3. Antigenic shift and antigenic drift

IAV is fast-evolving. Although its adaptation to and efficient transmission between new hosts usually involves multifactorial genetic changes, rapid gain of these attributes have often been associated with antigenic shift. Given the segmented nature of the IAV genome antigenic shift is possible upon coinfection of individual cells within a single organism with two or more antigenically distinct IAVs. As a result of the segmented genome, virus replication will originate progeny virions that incorporate mixtures of genome segments from the different parental strains; something termed reassortment (Steel and Lowen 2014). This dramatic change can allow the emergence of novel viral serotypes and facilitate crossing of species barriers. In fact, various reassortants between pig, human and/or avian strains are thought to be the cause of several of the human pandemics which occurred in the last century (Smith *et al.* 2009; Scholtissek *et al.* 1978).

In contrast to antigenic shift, antigenic drift refers to less drastic changes in the antigenicity of circulating strains within an individual host species. These changes are

associated with the lack of proof-reading mechanisms of the viral RNA polymerase, leading to point mutations in several segments (Drake 1993). Functional changes in HA (and to a lesser extent NA) result in structurally distinct antigenic regions which can no longer be recognised by established adaptive immune responses: neutralising antibodies (Boni 2008).

1.1.4. Prevention strategies against IAV: Diagnostics, Vaccination and Antivirals

In order to prevent and monitor disease and host transmission, several clinical strategies are put in place. Diagnosis of influenza is mostly based on clinical presentation and epidemiological likelihood of infection. However, for management of individual patients, and public health surveillance reasons, nasopharyngeal swabs, nasal wash or a combination of both can be sent for confirmation. Diagnostic assays vary in sensitivity, cost and time and include virus culture, qRT-PCR, and antigen testing (reviewed in Krammer *et al.* 2018).

Aiming to elicit an adaptive immune response against IAV and further limit infection and symptoms, vaccines are also used as a preventive measure (Salk and Salk 1977). The membrane-distal end of the surface of HA constitutes the main humoral antigen of IAV. Therefore, inactivated virus, or live-attenuated virus are the vaccine types currently in use. These types are usually tetravalent and contain two IAV subtypes, a H1N1 2009 pandemic and a currently circulating H3N2 strain, as well as two influenza B strains. In some cases, trivalent vaccines only containing one B strain are still used. Inactivated virus vaccines are the most commonly used. These are

generally developed in embryonated hen's eggs, after which the viruses are purified, formaldehyde-inactivated and treated with a non-ionic detergent (Wong and Webby 2013). This type of vaccine is also in place for poultry. Avian influenza vaccines are often monovalent, containing either H5 or H7 strains (Swayne *et al.* 2014). However, a bivalent H5 and H7 vaccine has recently been used to great effect (reviewed in Wei and Cui 2018). Vaccine efficacy was analysed by large-scale surveillance in poultry markets and farms before and after vaccine administration where a 95% reduction in the number of H7N9 occurrences was observed (Shi *et al.* 2017; Shi *et al.* 2018).

Despite the effectiveness of vaccination, HA evolution and the emergence of new subtypes reduces its efficacy. Therefore, antivirals are used as a rapid response to IAV infection. The current IAV antiviral repertoire is dominated by neuraminidase inhibitors. These inhibit the later stages of infection by diminishing NA activity and preventing virus spread (Colman 1994).

Another class of anti-IAV drugs to be developed, the adamantanes, are blockers of the M2 ion channel, acting at early stages of the virus life cycle by avoiding acidification of the virion and the subsequent release of RNPs in the cytoplasm (Cady *et al.* 2010). However, due to the emergence and spread of resistant strains, adamantanes are now clinically obsolete (Zaraket *et al.* 2010; Furuse *et al.* 2009).

A novel class of polymerase inhibitors targeting the cap-dependent endonuclease activity of both influenza A and B viruses has been approved by the FDA in 2018 to use in cases of uncomplicated influenza and adolescents (Hayden *et al.* 2018).

1.2. Influenza A virion structure

1.2.1. Virion morphology

Influenza virus particles are pleomorphic, being able to assume spherical, bacilliform or filamentous morphologies. The classical IAV representation, spherical particles, have a diameter of approximately 120nm and are observed in lab-adapted strains (Figure 1.1A). However, bacilliform particles of ~ 95 nm diameter but 250nm length and similar or slightly smaller diameter filaments reaching 30µm lengths (Figure 1.1 B and C) are also frequently found in clinical and veterinary isolates (Mosley and Wyckoff 1946; Cox *et al.* 1980; Calder *et al.* 2010). A more recent cryotomography study showed the formation of viral filaments with bulbous heads (Archetti bodies) (Figure 1.1C.V), many of which seem to lack any genomic content (Vijayakrishnan *et al.* 2013; Archetti 1955). Studies have suggested that the filamentous strains have higher neuraminidase activity and are more readily transmitted but the role of this morphological type of virion in the influenza virus infectious cycle remains poorly determined (Campbell *et al.* 2014; Dadonaite *et al.* 2016).

1.2.2. Virion composition

All forms of influenza virions obtain their bilayer phospholipid envelope from the host cell membrane during viral budding (Shaw *et al.* 2008). This envelope is decorated by incorporation of the viral transmembrane glycoproteins: the trimeric HA and tetrameric NA in a ratio of 4:1, making HA the main surface antigen (Webster and Pereira 1968)Also embedded within the envelope is the ion channel M2, which is

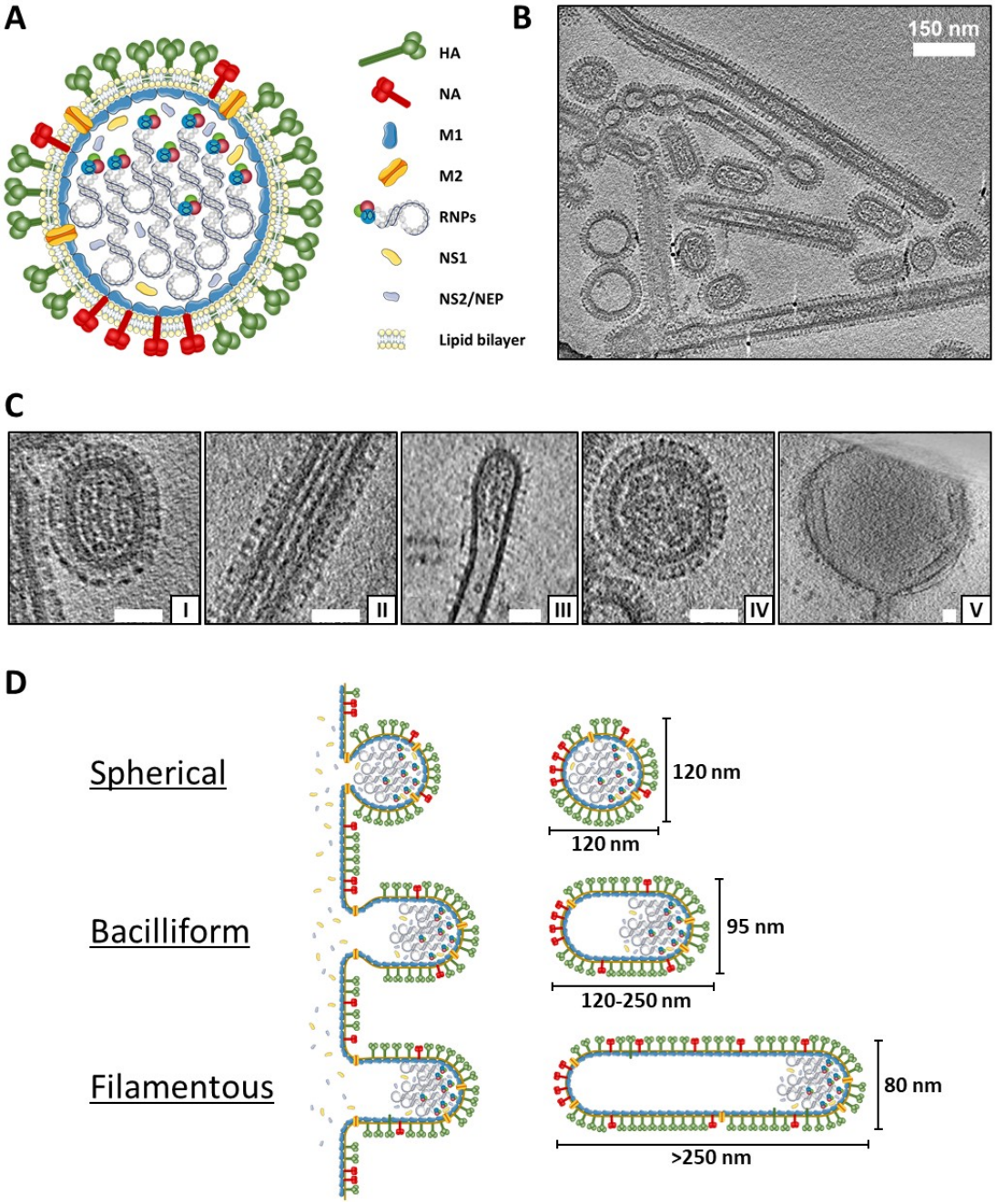

Figure 1.1: IAV virion structure. (A) Schematic representation of a spherical IAV virion. (B) Tomography of filamentous and spherical influenza virions: Overall representation of purified A/Udorn/307/1972 virions. (C) Distinct IAV morphologies: (I) bacilliform, (II and III) filaments, (IV) spherical and (V) Archetti body. Scale bars represent 50nm. (D) Diagram of budding of different virion morphologies. Micrographs were taken and/or adapted from Prof Paul Digard, Vijayakrishnan *et al*. 2013 and Dadonaite *et al*. 2016.

present in smaller quantities (Pinto *et al.* 1992). The envelope is structurally supported by an underlying matrix protein 1 (M1) oligomer and filled with 8 individual viral ribonucleoproteins (vRNP; considered in more detail below) which, by electron microscopy studies, were shown to present a 7+1 rearrangement, suggesting a specific packaging mechanism (Noda *et al.* 2006).

Additional constituents of the viral particle include two proteins originally thought to be non-structural: NS2 (also known as nuclear export protein or NEP) and NS1, but now known to be low abundance components of IAV virions (Richardson and Akkina 1991; Hutchinson *et al.* 2014). Membrane-bound and cytoplasmic host cell proteins such as tetraspanins CD9 and CD81 and annexins A1 and A2 have also been reported to be included in virus particles (Hutchinson *et al.* 2014; Shaw *et al.* 2008). Of note, these studies have largely been carried out on spherical particles as filamentous viruses are more difficult to purify; therefore less is known about inclusion of host proteins in filamentous IAV.

1.2.3. RNP structure and composition

Representations of RNP structures are shown in Figure 1.2. Each segment of negative-sense, single-stranded genomic RNA is bound to nucleoprotein (NP) monomers with high affinity at approximately 24 nucleotides per NP molecule. This NP-RNA binding is known to occur through the phosphate backbone and therefore in a relatively sequence unspecific-manner (Scholtissek and Becht 1971; Compans *et al.* 1972; Ortega *et al.* 2000).

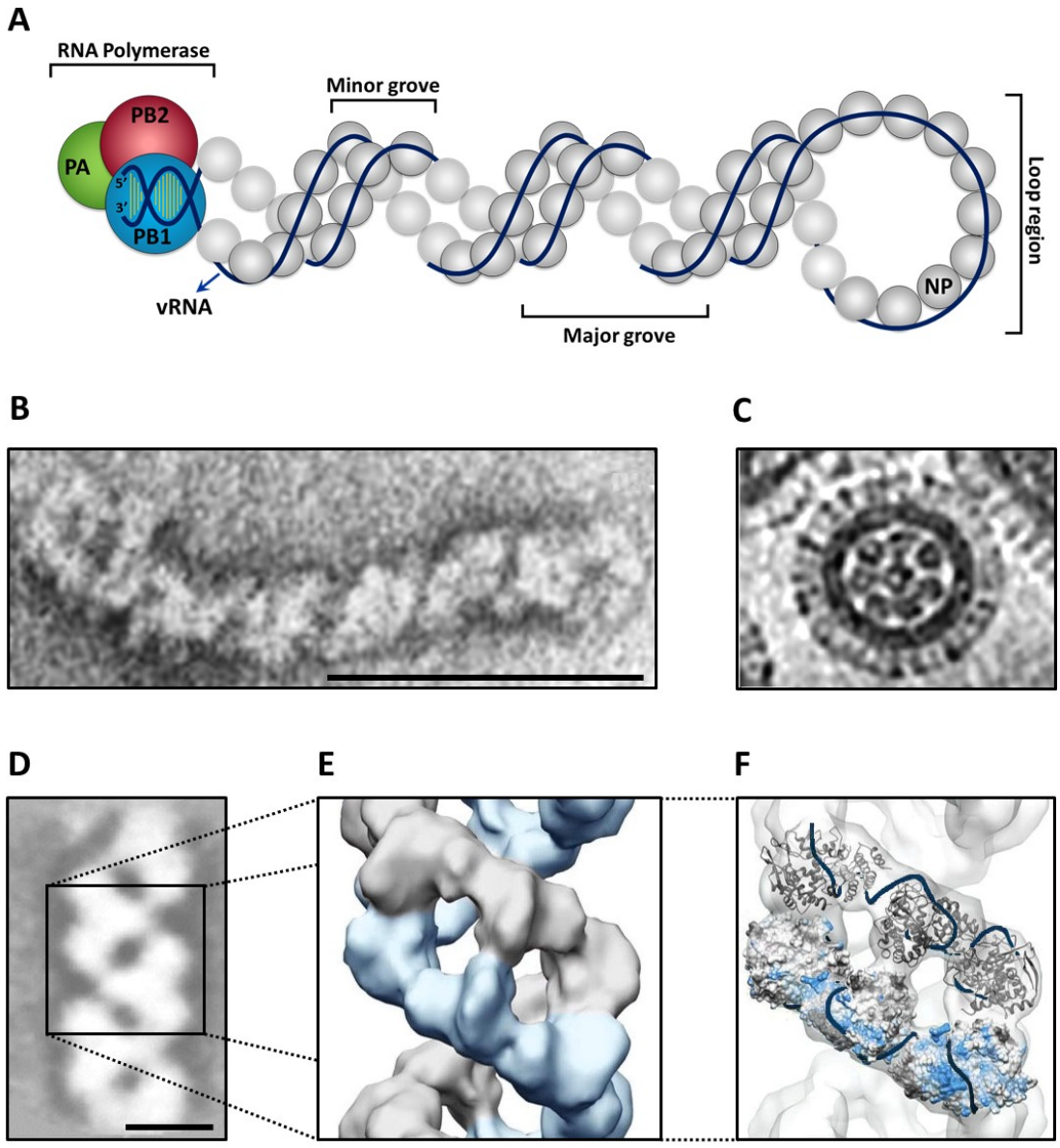

Figure 1.2: Structural models of the IAV ribonucleoprotein complex. Schematic representation (A – adapted from Prof Paul Digard) and negatively stained electron micrograph (B) of a vRNP showing its shape and structural components. Viral RNA is linked to the heterotrimeric RdRp complex by its 5' and 3' ends and associated with NP monomers. (C and D) Electron micrograph and cartoon showing the antiparallel double helix organisation of internal vRNA regions. (E) Detail of the association of vRNA with NP monomers (Arranz *et al.* 2012; Hutchinson and Fodor 2013; Coloma *et al.* 2009).

Electron microscopy studies have revealed an overall antiparallel double helical arrangement of RNP molecules (Figure 1.2D-F), which is kept by intra-RNP NP interactions (Wu *et al.* 2009; Compans *et al.* 1972; Jennings *et al.* 1983; Arranz *et al.* 2012). The 5' and 3' ends of vRNP ends share partial Watson-Crick base-paring and form a panhandle-shaped duplex structure (Desselberger *et al.* 1980; Hsu *et al.* 1987), which is in turn bound by the RNA-dependent RNA polymerase.

1.2.3.1. The heterotrimeric RNA polymerase

The viral polymerase is a trimeric complex consisting of polymerase basic protein 1 (PB1), polymerase basic protein 2 (PB2) and polymerase acidic protein (PA) subunits (Skehel and Hay 1978; Digard *et al.* 1989; Detjen *et al.* 1987). Initial biochemical studies suggested an N-terminal to C-terminal linear interaction arrangement between the subunits: C terminus of PA interacts with the N terminus of PB1 (Perez and Donis 1995), the C terminus of which binds to the N terminus of PB2, with an apparent lack of interaction between PA and PB2 (Digard *et al.* 1989; Gonzalez *et al.* 1996; Perez and Donis 1995; Toyoda *et al.* 1996). However, more recent 3D-imaging acquired from electron microscopy and crystallisation followed by X-ray diffraction studies have revealed the globular structure of the polymerase and the intrinsic interactions between the three subunits (Pflug *et al.* 2014; Reich *et al.* 2014; Moeller *et al.* 2012; Coloma *et al.* 2009). Transcription and replication functions of the viral polymerase will be further described in section 1.4.4 and the crystal structure of the viral polymerase can be found in Figure 2.10.

1.3. IAV genome organisation and protein coding strategies

In total, the IAV genome is ~13.6kb, comprised of 8 segments with lengths ranging from 0.89 to 2.3kb, which encode all the viral polypeptide products. Following genome transcription to positive sense mRNAs, polypeptide expression can occur through different translation mechanisms: canonical translation of unspliced or spliced mRNA transcripts produce 10 long-established "core" proteins, but further differential splicing events as well as ribosomal frame-shifting and alternative translation initiation events also occur, leading to the expression of additional accessory polypeptides (summarised in Table 1.1 and Figure 1.3).

1.3.1. Canonical translation to produce the essential IAV gene products

All IAV vRNAs contain a long antisense coding region flanked by shorter untranslated regions (UTRs). Each segment contains a principal (generally the longest) coding region which is translated from the first AUG codon into the primary gene product of the segment. This mechanism leads to expression of the three elements of the heterotrimeric viral RNA-dependent RNA polymerase (PB2, PB1 and PA from segments 1, 2 and 3, respectively), the glycoproteins (HA from segment 4 and NA from the 6th segment), the RNP constituent nucleoprotein (NP from segment 5), M1 and NS1 from segments 7 and 8 respectively (Figure 1.3, dark blue bars).

Unlike many other RNA viruses, IAV RNA synthesis occurs in the host cell nucleus, giving access to the cellular mRNA splicing machinery. mRNA splicing has

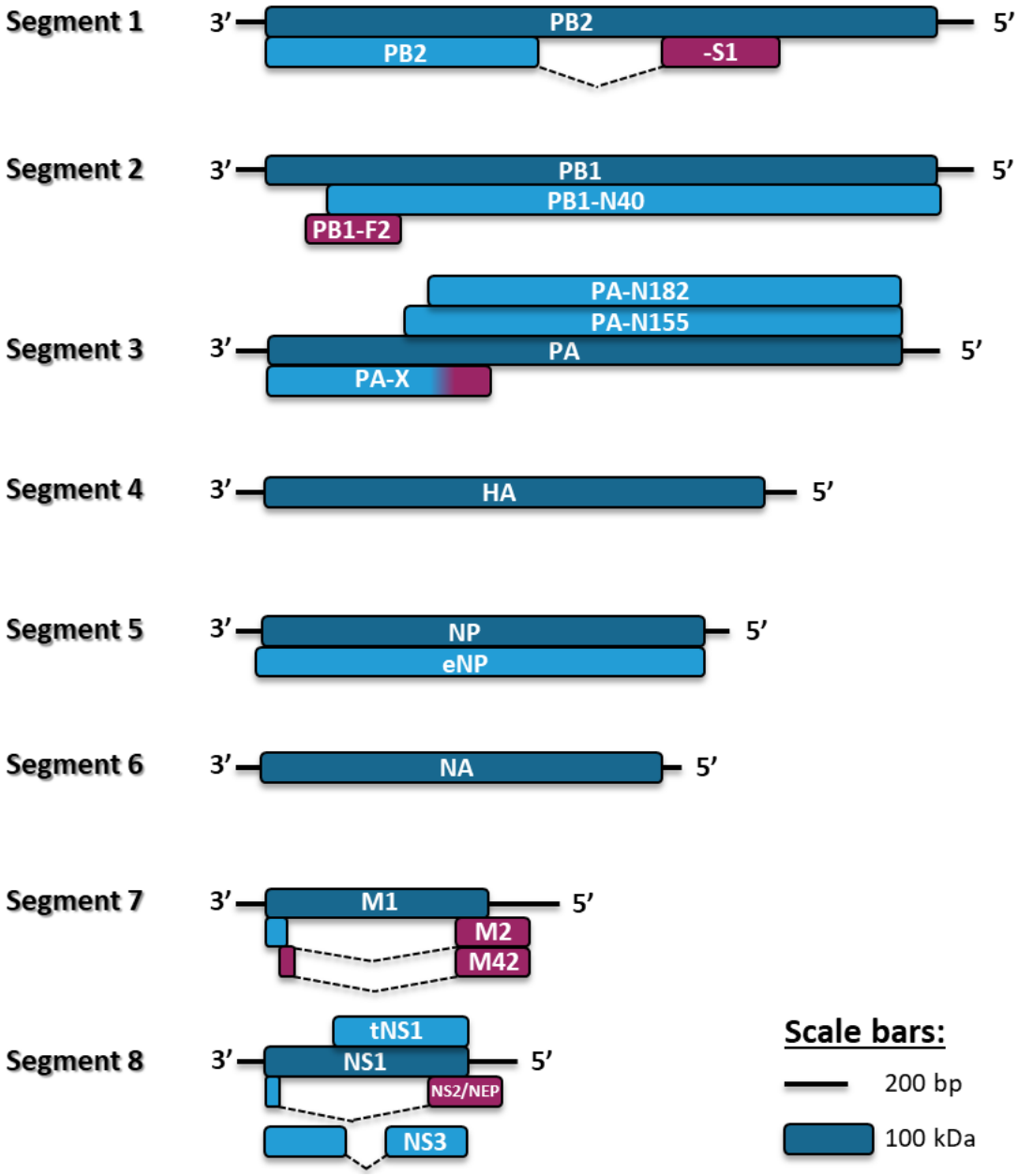

Figure 1.3 IAV gene products. mRNAs from the 8 segments are symbolised by horizontal black lines. Coding regions are represented by boxes with colours defining different reading frames (dark blue: primary products, frame 1; light blue: secondary products, frame 1; magenta: secondary products, frame 2). mRNA splicing in segments 1, 7 and 8 is denoted by dashed deflected lines connecting two coding regions.

Table 1.1: IAV gene products and respective expression mechanism and functions. *Segment and protein sizes were based on A/Puerto Rico/8/1934 (H1N1)

Segment	Segment length (bp)*	Protein products	Expression mechanism	Length (aa)*	Molecular mass (kDa)*	Main function
1	2341	**PB2**	Canonical translation initiation	759	85.7	Component of the heterotrimeric viral RdRp. Promotes viral RNA expression through 5' end host mRNA binding and "cap-snatching".
		PB2-S1	mRNA splicing	508	55	Inhibitor of the RIG-I signalling pathway.
2	2341	**PB1**	Canonical translation initiation	757	86.6	Component of the viral RdRp. Involved in elongation.
		PB1-N40	Alternative AUG initiation (translation reinitiation)	718	82.4	Unknown. It's known to interact with the viral polymerase.
		PB1-F2	Alternative AUG initiation (leaky scanning)	87	10.5	IFN antagonist. Pro-apoptotic activity.
3	2233	**PA**	Canonical translation initiation	716	84.2	Component of the viral RdRp. Viral RNA endonuclease responsible for cleaving host pre-mRNAs to produce capped primers.
		PA-X	Ribosomal frameshift	252	29	Exhibits endonuclease activity, contributing to host cell shut-off
		PA-N155	Alternative AUG initiation	562	62	Unknown
		PA-N182	Alternative AUG initiation	535	60	
4	1778	**HA**	Canonical translation initiation	566	61.5	Trimeric surface glycoprotein. Mediates receptor binding, virus entry and budding.
5	1565	**NP**	Canonical translation initiation	498	56.1	Encapsidation of vRNA (to form vRNP complexes). Required for transcription activity and vRNP nuclear import.
		eNP	-	504	56.8	Virulence factor for H1N1 IAVs (Wise, Gaunt *et al.*, unpublished).
6	1413	**NA**	Canonical translation initiation	454	50.1	Heterotrimeric surface glycoprotein. Exhibits sialidase activity allowing release of virus progeny from the cell surface.
7	1027	**M1**	Canonical translation initiation	252	27.8	Matrix protein. Known to interact with RNPs and glycoproteins. Involved in genome nuclear export, virus assembly and budding.
		M2	Canonical translation initiation followed by mRNA splicing	97	11	Acts as proton ion channel. Required during virus entry (uncoating) and for membrane scission at the budding stages of infection.
		M42	mRNA splicing and leaky scanning	99	13	Variant of M2 with common functions
8	890	**NS1**	Canonical translation initiation	230	26.8	Broad-spectrum IFN antagonist.
		NS2/NEP	Canonical translation initiation followed by mRNA splicing	121	14.2	Involved in nuclear export of vRNPs.
		NS3	Canonical translation initiation followed by mRNA splicing	187	21	Unknown
		NEG8	-	-	-	Unknown. Protein expression bioinformatically proposed, but yet not experimentally detected.
		tNS1	Alternative AUG initiation	150/152	17	Involved in inhibition of IRF3

long been known to occur for transcripts from segments 7 and 8, giving rise to mRNAs encoding the M2 and NS2/NEP proteins respectively (Lamb and Lai 1980; Lamb *et al.* 1981). These polypeptides are also produced by canonical translation initiating at the first AUG codon in the mRNA, while the splicing event directs translation into an alternative reading frame downstream of the splice junction (Figure 1.3). M2 and NS2/NEP are produced by every strain of IAV and, outside of specialised laboratory settings, are considered to be essential for virus replication; these two polypeptides therefore complete the suite of the 10 core virus proteins. However, the IAV proteome is further elaborated in a virus strain-dependent fashion by the expression of further polypeptide species that tend to be low abundance and non-essential for virus replication. These "accessory" proteins are produced by further minor mRNA splicing events and/or examples of non-canonical translation, including leaky ribosomal scanning and frameshift events. The following sections will describe the essential and accessory peptides coded in overlapping reading frames which are produced by these and other mechanisms, and their function within the IAV life cycle.

1.3.2. PB2-S1

Identified in 2016, PB2-S1 is the result of expression from a spliced mRNA from segment 1 in which the region corresponding to nucleotides 1513 to 1894 of the PB2 mRNA is deleted and the mRNA continues in the +1 frame to encode the S1 ORF (Figure 1.3) (Yamayoshi *et al.* 2016). Despite being highly conserved among pre-2009 human H1N1 virus isolates, the splice donor and acceptor site nucleotide sequences which allow the expression of PB2-S1 are not present in human H1N1pdm09 and

H3N2 viruses. Localisation of PB2-S1 is mainly mitochondrial and occurs via an N-terminal mitochondrial localisation signal shared with PB2 (Carr *et al.* 2006; Graef *et al.* 2010). This polypeptide was shown to inhibit the retinoic acid-inducible gene I (RIG-I)-dependent/ mitochondrial antiviral-signalling protein (MAVS) interferon signalling pathway and interact with the PB1 subunit of the viral polymerase, negatively interfering with its activity. Nonetheless, abrogation of expression of PB2-S1 did not alter virus fitness *in vitro* nor its virulence in murine *in vivo* systems (Yamayoshi *et al.* 2016).

1.3.3. PB1-F2

PB1-F2 is an 87-101 amino acid polypeptide first identified as a short-half-life protein that interacted with mitochondria and postulated to be responsible for induction of apoptosis in immune cells (Chen *et al.* 2001). Further studies revealed that PB1-F2 translocated into mitochondria via Tom40 channels and that it contained a C-terminal region responsible for interaction with two other mitochondrial proteins, VDAC3 (inner membrane) and ANT1 (outer membrane), both of which are part of the permeability transition pore and play important roles in apoptosis stimulation (Gibbs *et al.* 2003; Yoshizumi *et al.* 2014; Belzacq *et al.* 2002; Zaid *et al.* 2005). A more recent study has related these PB1-F2-mitochondria interactions to a reduction of mitochondrial inner membrane potential leading to oxidative stress deregulation and contributing to the early stages of IAV replication cycle (Shin *et al.* 2015). PB1-F2 has also been shown to interact with the immune response modulator MAVS (mitochondrial antiviral signalling protein), blocking its function and therefore leading

to an indirect inhibition of type I IFN induction (Varga *et al.* 2012). PB1-F2 expression is thought to occur by leaky ribosomal scanning from the fourth initiation codon in segment 2 (Chen *et al.* 2001; Wise *et al.* 2011; Wise *et al.* 2009), although more recent studies have suggested further regulation of PB1-F2 expression from sequences located downstream of the AUG codon (Buehler *et al.* 2013).

Despite thorough molecular characterisation *in vitro*, elucidation of the roles of PB1-F2 *in vivo* have at times given conflicting results, possibly reflecting viral strain- and host-dependent effects (reviewed by Kosik *et al.* 2013). Consistent with this, not all IAV strains possess a full-length (≥ 87 codon) ORF; in general, avian strains of IAV tend to have full length genes while human and swine viruses often do not (Kamal *et al.* 2017). For example, PB1-F2 sequences from 2009 pandemic H1N1 strains have an early stop codon at position 11 and studies confirmed its minimal impact on virulence in mouse models (Hai *et al.* 2010). Conversely, PB1-F2 truncations are not only rare in avian isolates but in experimental infections of chickens with H5N1 and H9N2 strains, lead to an attenuation of virulence, accompanied by prolonged virus shedding (Leymarie *et al.* 2014; James *et al.* 2016).

1.3.4. PB1-N40

PB1-N40 corresponds to an N-terminally truncated version of the main segment 2 product PB1 (Wise *et al.* 2009). The absent first 39 amino acids include the primary PA interaction site (Perez and Donis 1995; Pflug *et al.* 2014; He *et al.* 2008) and therefore PB1-N40 lacks heterodimerisation function and consequently, nuclear import and transcriptase functions (Wise *et al.* 2009). It nevertheless retains some

ability to interact with PB2 and the polymerase trimer, as well as with a variety of cellular proteins (Wang *et al.* 2019; Wise *et al.* 2009). Despite its AUG codon (codon 5 in segment 2) being highly conserved in IAV isolates, PB1-N40 function remains to be clarified. Single knockout of PB1-N40 expression (by mutating its AUG codon, with consequent mutation of the full-length PB1 protein) slightly reduced viral fitness of the H1N1 A/Puerto Rico/8/34 (PR8) laboratory strain *in vitro*. However, double deletion of PB1-N40 and PB1-F2 resulted in WT-like virus propagation (Wise *et al.* 2009). Moreover, regardless of its lack of viral polymerase activity, overexpression of PB1-N40 lead to increased vRNA production and an increase in genome:PFU ratios of released virus particles (Tauber *et al.* 2012).

1.3.5. PA-N155 and PA-N182

PA-N155 and PA-N182 are translated from the 11th and 13th AUG codons, respectively, of segment 3 mRNA (Muramoto *et al.* 2013). The mechanism by which these AUG codons are accessed by ribosomes has not been elucidated. These initiator codons are highly conserved among IAV sequences and are present in isolates from different host species. The precise roles of these truncated PA polypeptides within the IAV life cycle have not yet been elucidated. Recent studies on these polypeptides from an H5N1 virus suggested interactions of -N155 and -N182 with (chicken) cellular proteins involved in RNA processing, protein transport and various cellular signalling pathways (Wang *et al.* 2018). Many, if not most of these interactions might be common to the full length PA protein and their significance is unclear. Nonetheless, mutant H1N1 A/Wilson-Smith Neurotropic/33 (WSN) laboratory strain viruses unable to

express PA-N155 and/or -N182 following mutation of the relevant AUG codons showed delayed virus replication *in vitro* and reduced virulence in mouse models (Muramoto *et al.* 2013). As with PB1-N40 mutants however, it must be borne in mind that the strategy used to ablate expression of the accessory proteins also mutates the primary gene product of the segment.

1.3.6. PA-X

PA-X expression occurs through a ribosomal frame shift event, driven by a rare arginine codon next to a sequence that facilitates tRNA realignment, leading to the production of a fusion peptide containing the first 191 amino acids of the PA endonuclease domain and a variable strain-specific C-terminal domain translated from the +1 reading frame of segment 3 mRNA (the X-ORF; Figure 1.3) (Jagger *et al.* 2012; Firth *et al.* 2012). The frameshift site is highly conserved amongst IAV strains, but the length of the X-ORF varies, with common polymorphisms being either 41 or 61 codons long (Shi *et al.* 2012; Rash *et al.* 2014). Expression of PA-X is not required for *in vitro* and *in ovo* virus replication (Jagger *et al.* 2012; Hussain *et al.* 2018). Nonetheless, this protein is known to selectively destroy host RNA polymerase II (pol II)-derived mRNA transcripts and contribute to host cell shut-off through the activity of the endonuclease domain shared by PA (Jagger *et al.* 2012; Khaperskyy *et al.* 2016; Desmet *et al.* 2013).

In mouse models of IAV infection using H1N1 and H5N1 strains, the absence of PA-X resulted in augmented clinical disease and immune responses (Jagger *et al.* 2012; Gao *et al.* 2015b; Hu *et al.* 2015; Rigby *et al.* 2019). Conversely, infection with

wild type (WT) and PA-X-deficient H9N2 avian viruses resulted in opposite phenotypes, suggesting that in this viral context, the presence of PA-X increases virulence *in vivo* (Gao *et al.* 2015c). In other host species, such as chickens (adult or the *in ovo* model using embryos), ducks and swine, mutation of PA-X mostly but not always increased pathogenicity (Hussain *et al.* 2018; Nogales *et al.* 2017). In addition, *in vitro* studies of PA-X activity found that the length of the X-ORF-derived sequence (specifically the 41-61 polymorphism) influenced endonucleolytic activity of the protein (Bavagnoli *et al.* 2015). This 20 amino acid-truncation is commonly observed in swine and canine isolates and viruses harbouring truncated PA-X products were shown to enhance virulence and transmissibility in pigs (Xu *et al.* 2016). Conversely, other studies on H1N1 2009 pandemic viruses have suggested that the additional C-terminal 20 amino acids are beneficial to PA-X shut-off activity and increase virulence in murine models (Lee *et al.* 2017; Gao *et al.* 2015a). Therefore, as seen for other accessory proteins, PA-X also exhibits virus strain- and host-specific functions.

1.3.7. M2, M42 and other segment 7 gene products

In addition to the primary unspliced transcript which encodes M1, segment 7 is known to produce up to three other transcripts originated from alternative splicing: mRNAs 2-4. These splice variants use a common splice acceptor site but use different splice donor sequences (reviewed by Dubois *et al.* 2014). Virus strain-dependent variations in the sequences of these splice donor sites leads to variability in their use. As discussed above, mRNA2 is produced by virtually all strains of IAV and encodes the ion channel, M2. The M2 ORF has the initiator codon and the first 9 codons in

common with M1 but the C-terminal 88aa are coded in the +1 ORF (Lamb and Choppin 1981).

mRNA3 is known to be produced from the most 5'-proximal splice donor site, but lacks obvious protein-coding potential (encoding a 9 amino acid peptide in its 5'-proximal ORF) Lamb *et al.* (1981). Production of mRNA3 has however been proposed to negatively regulate segment 7 protein expression at early stages of infection (Shih *et al.* 1995). However, its presence is non-essential for virus growth *in vitro* and protein expression from the mRNA has also not been detected (Shih *et al.* 1995; Chiang *et al.* 2008; Jackson and Lamb 2008). Production of mRNA3 has become enshrined in influenza text books through its early discovery (Lamb *et al.* 1981), but it is not clear if all strains of IAV produce it; the PR8 strain for example, accumulates far lower quantities of mRNA3 than other human strains of IAV (Wise *et al.* 2012).

A small fraction of IAV strains produce appreciable amounts of a third splice variant, mRNA4 (Shih *et al.* 1995; Wise *et al.* 2012; Dubois *et al.* 2014). This mRNA is predicted to express a 90 amino-acid long internally deleted version of M1 from the first AUG codon, but no protein product has been detected yet. However, in the PR8 strain, the transcript has been shown to express a variant form of the ion channel, M42 (Wise *et al.* 2012). M42 shares the same C-terminal domain as M2, but is initiated from a different AUG codon in a +1 frame downstream of segment 7 AUG1. M42 can functionally replace M2 during virus replication, despite having a different cellular localisation (Wise *et al.* 2012).

There is also evidence for further potential gene products from segment 7, produced not by differential splicing but by non-AUG initiation at CUG codons in the + 1

reading frame (Yang *et al.* 2016). Evidence for this comes from readily detectable expression of a well-defined T cell epitope, artificially engineered into the M2 ORF. Expression of this peptide could not be blocked by the small molecule inhibitor of splicing, spliceostatin A, but was abrogated by mutation of M2 codons Leu59 and 96 (Yang *et al.* 2016). Translation initiation at Leu59 in a WT virus would produce a 40 amino acid C-terminal M2 fragment; this has not been detected however, and any functional significance to virus replication remains unknown.

1.3.8. NS2, NS3 and tNS1

Similarly to segment 7, the NS segment is also known to be differentially spliced to express NS2/NEP (Lamb *et al.* 1978; Lamb and Choppin 1979; Lamb *et al.* 1980). This 121 amino acid protein shares its N-terminal 10 residues with NS1. However, the remaining C-terminal region is expressed from the +1 reading frame. All strains of IAV produce NEP as it is required to ensure the export of vRNPs from the nucleus and therefore essential in the virus life cycle (O'Neill *et al.* 1998; Neumann *et al.* 2000).

An additional spliced mRNA from segment 8 has been defined as encoding the NS3 protein, which constitutes an internally truncated version of NS1 missing amino acids 126-168 (Selman *et al.* 2012). Activation of NS3 expression by the alteration of its splice donor site (along with nonsynonymous M124I and D125G changes in the NS1 ORF) resulted in increased virus propagation in murine but not human cell lines. Despite this gain-of-function phenotype, the function of NS3 within the IAV life cycle is still not fully understood. As with segment 7 mRNA 4, production of NS3 is likely

to occur in only a small minority of IAV strains, but it has been proposed to be a feature particularly associated with viral adaptation to a new host species (Selman *et al.* 2012).

More recently, N-terminally truncated versions of NS1 have also been identified (Kuo *et al.* 2016). These "tNS1" polypeptides are expressed from the 2nd and/or 3rd AUG codons of segment 8, lacking the first 79 or 81 amino acids of NS1. A mutant PR8 virus lacking these AUG codons induced higher levels of IRF3 phosphorylation and hence greater IFN-β induction (Kuo *et al.* 2016). *A priori*, this could be due to the non-synonymous mutation of NS1, and/or failure to express the tNS1 polypeptides. However, exogenously expressed tNS1 polypeptides displayed differential localisation (cytoplasmic versus nuclear) to the WT protein and were able to antagonise IRF3 activation, supporting the suggestion that loss of their expression contributed to the phenotype.

1.4. The Influenza A Virus Life cycle

IAV replication occurs mainly in respiratory and gastrointestinal (depending on the host) epithelial cells. Mathematical modelling from an H1N1 human *in vivo* infection suggested that it takes only 6 hours between infection of target cells and virion release (Baccam *et al.* 2006). Nevertheless, experimental data showed that, in permissible cell lines, it takes 8-10 hours for the replication cycle to reach its full completion (Gaush and Smith 1968). The life cycle of IAV can divided into the following stages: receptor binding and entry, fusion and uncoating, RNP nuclear import, replication and transcription of the viral genome, genome nuclear export,

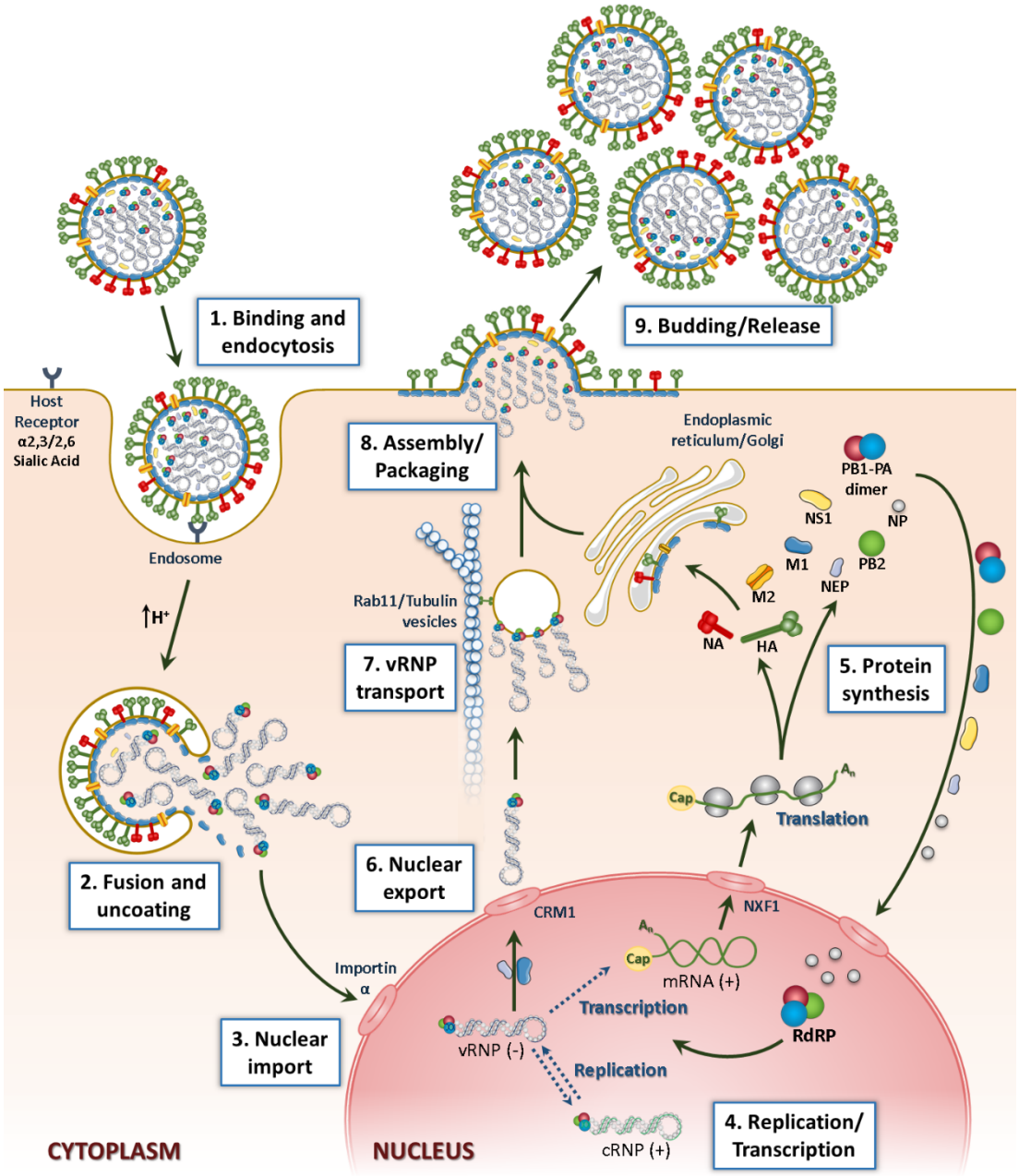

Figure 1.4: The IAV life cycle. Virions enter the host cell through receptor-mediated endocytosis after attachment of HA to sialic acid (1). Endosome acidification triggers fusion of the viral envelope with the endosome membrane and the release of vRNPs into the cytoplasm (2). The RNPs undergo nuclear import (3) where the preformed trimeric viral RdRp initiates viral transcription (4). Newly synthesised viral mRNA is processed and translated to produce viral polypeptides which will constitute novel RNPs in the nucleus (5). Progeny RNPs are exported to the cytoplasm (6), trafficked to the apical plasma membrane (7) and assembled into offspring viral particles (8) which are released from the cell surface (9). Cellular and viral structures are not to scale.

packaging, budding and release. A schematic representation of IAV life cycle is shown in Figure 1.4.

1.4.1. Receptor binding and internalisation

The life cycle initiates with the attachment of IAV to the host cell. The primary receptor for influenza viruses is N-acetylneuraminic acid, also called sialic acid (SA), which is recognised and bound by the receptor binding pocket of the viral glycoprotein HA (Johnson *et al.* 1964; Gottschalk 1959). SA is attached to its underlying galactose ring by either α2,3 or α2,6 linkages. It is well established that α2,3 linkage SA predominates in avian species and avian IAV strains preferentially use this isoform as a receptor. In contrast, human IAV strains generally have a higher receptor specificity for the α2,6 conformation, as this form predominates in the human upper respiratory tract (Weis *et al.* 1988; Connor *et al.* 1994). The "HA"s of the recently-found bat H17 and H18 IAV strains do not bind to sialic acid (Sun *et al.* 2013); the receptor for these viruses has recently been identified as MHC class II molecules (Karakus *et al.* 2019). Interactions between HA and sialic acid are believed to be low affinity. However, multiple HA molecules are used to bind several glycoproteins, resulting in high-avidity binding to the cell surface (Sauter *et al.* 1989). Upon receptor binding, spherical virus particles are internalised by dynamin-dependent clathrin-mediated endocytosis (Matlin *et al.* 1981) whilst filamentous virions have been suggested to use micropinocytosis (Rossman *et al.* 2012). This internalisation process may involve triggering of cellular receptor tyrosine kinase signalling (Eierhoff *et al.* 2010).

1.4.2. Fusion and uncoating

Once engulfed within the endosome the virion requires the release of its genome into the cytoplasm. To do so, the inactive precursor HA (HA_0) molecule must previously have undergone proteolytic cleavage by host cell proteases into HA_1 and HA_2 domains. While HA_1 mediates endocytosis via its receptor-binding site, the new N terminus of HA_2 liberated by the cleavage event contains a highly conserved 14 amino acid-long fusion peptide, required to mediate fusion (Nobusawa *et al.* 1991; Stegmann 2000). The low pH environment of late endosomes induces the HA conformational changes which expose and position this fusion peptide towards the endosomal membrane (Maeda and Ohnishi 1980; Carr and Kim 1993). The fusion peptide is then inserted into the target membrane, while further HA conformational rearrangements bring the two membranes into close proximity, which results in their integration and the formation of a fusion pore (Tsurudome *et al.* 1992; Spruce *et al.* 1989; Melikyan *et al.* 1993). At the same time, the ion channel M2 allows entry of positively charged hydrogen ions, acidifying the viral core, disrupting M1 protein-protein interactions and permitting the release of vRNP complexes into the cytoplasm through the HA-mediated formed pore (Bui *et al.* 1996).

1.4.3. RNP nuclear import

Upon release from the late endosomes, vRNPs are translocated from the cytoplasm into the nucleus, where viral genome transcription and replication takes place (Herz *et al.* 1981; Shapiro *et al.* 1987). vRNPs are thought to diffuse through the cytoplasm with no input from either microtubules or actin filaments (Martin and

Helenius 1991b), but the peri-nuclear localisation of late endosomes may reduce the distance needed for travel (Lakadamyali *et al.* 2003). Given the large size of vRNPs, they are not able to passively diffuse through the nuclear pore complex (NPC). Nonetheless, all protein components of the vRNP complex possess nuclear localisation signals (NLS; reviewed in Hutchinson and Fodor 2013) Moreover, the pH-induced dissociation of M1 from vRNA leads to the exposure of the NLS contained within the first 13 amino acids of NP, allowing their active import via the cellular classical karyopherin import pathway (Stewart 2007; Cros *et al.* 2005; Wang *et al.* 1997). These NLS regions are recognised by importin-α which in turn binds to importin-β to allow nuclear import (O'Neill *et al.* 1995). Once in the nucleoplasm, importins-α and β are dissociated from vRNPs by exportin CSE1L, after which importins can be recycled back to the cytoplasm (Kutay *et al.* 1997).

1.4.4. Viral genome transcription and replication

Within the nucleus the heterotrimeric viral RNA polymerase transcribes the vRNA into 5'capped and 3'polyadenylated mRNAs which are exported to the cytoplasm to be translated by cellular ribosomes into newly synthesised proteins. However, the viral polymerase is also responsible for the replication of vRNA to create new copies of the virus genome. This is performed by the formation of an intermediate uncapped and non-polyadenylated "complementary RNA" specimen (cRNA) which serves as template for the production of new vRNAs (reviewed by Fodor 2013). Transcription and replication are functionally and temporally distinct (Figure 1.5A): expression of mRNA peaks earlier while synthesis of vRNA-like molecules

predominate later in infection (Hay *et al.* 1977; Smith and Hay 1982). The mechanisms behind the shift between transcription and replication are still to be fully elucidated. Nonetheless, newly synthesised NP has been suggested to account for the differential levels of the three RNA types, since free NP is required for full-length cRNA synthesis and NP mutations have be shown to affect cRNA and mRNA levels (Beaton and Krug 1986; Medcalf *et al.* 1999). Moreover, the levels of the three viral RNA species at different times post infection suggest that the switch between transcription and replication relies on the stability of cRNPs, which is only possible after the accumulation of newly synthesised NP monomers and polymerase trimers (Vreede and Brownlee 2007). Nevertheless, overexpression of NP does not seem to alter transcription or replication activities (Mullin *et al.* 2004) and additional studies have suggested that the switch is regulated by the concentrations of the vRNA 5' termini (Olson *et al.* 2010), while others have proposed a stochastic nature of switching between transcription and replication (Mondal *et al.* 2015).

The next sections will describe in detail the processes by which the polymerase performs genome transcription and replication.

1.4.4.1. Cap snatching, transcription of vRNA and polyadenylation

As described in section 1.2.3, the incoming RNPs are already associated with a viral polymerase complex. This allows the immediate transcription of vRNA. Transcription is primed by a "cap-snatching" mechanism (Figure 1.5B). This requires a 5' fragment of a 7-methyl guanosine (m^7GpppX^m)-capped pre mRNA from the host cell transcriptome which is recognised by and bound to the cap-binding domain of PB2

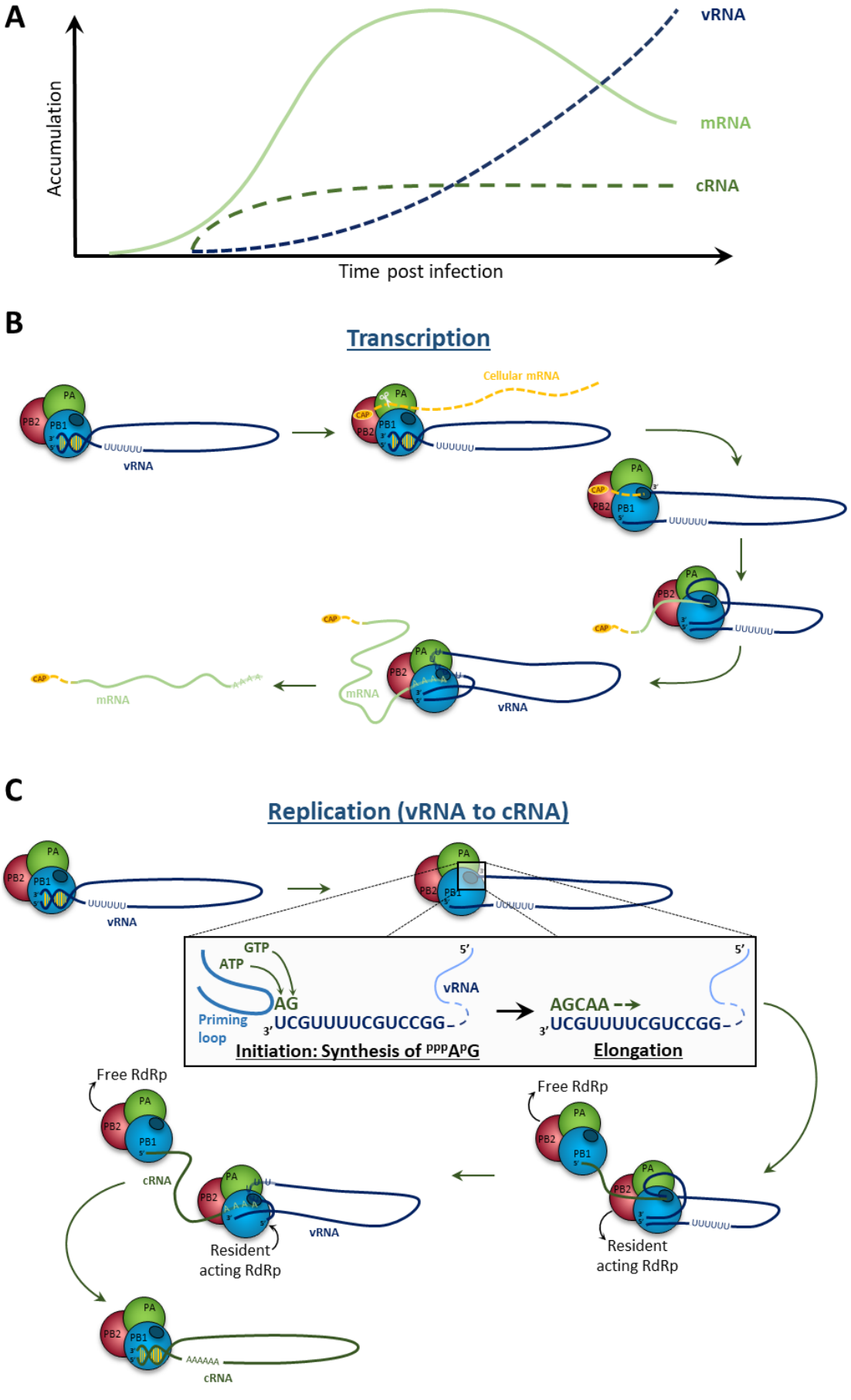
A
Accumulation
vRNA
mRNA
cRNA
Time post infection
B
Transcription
Cellular mRNA
PA
PB2
PB1
CAP
vRNA
mRNA
C
Replication (vRNA to cRNA)
GTP
ATP
Priming loop
AG
UCGUUUUCGUCCGG
Initiation: Synthesis of pppApG
AGCAA
Elongation
Free RdRp
Resident acting RdRp
cRNA

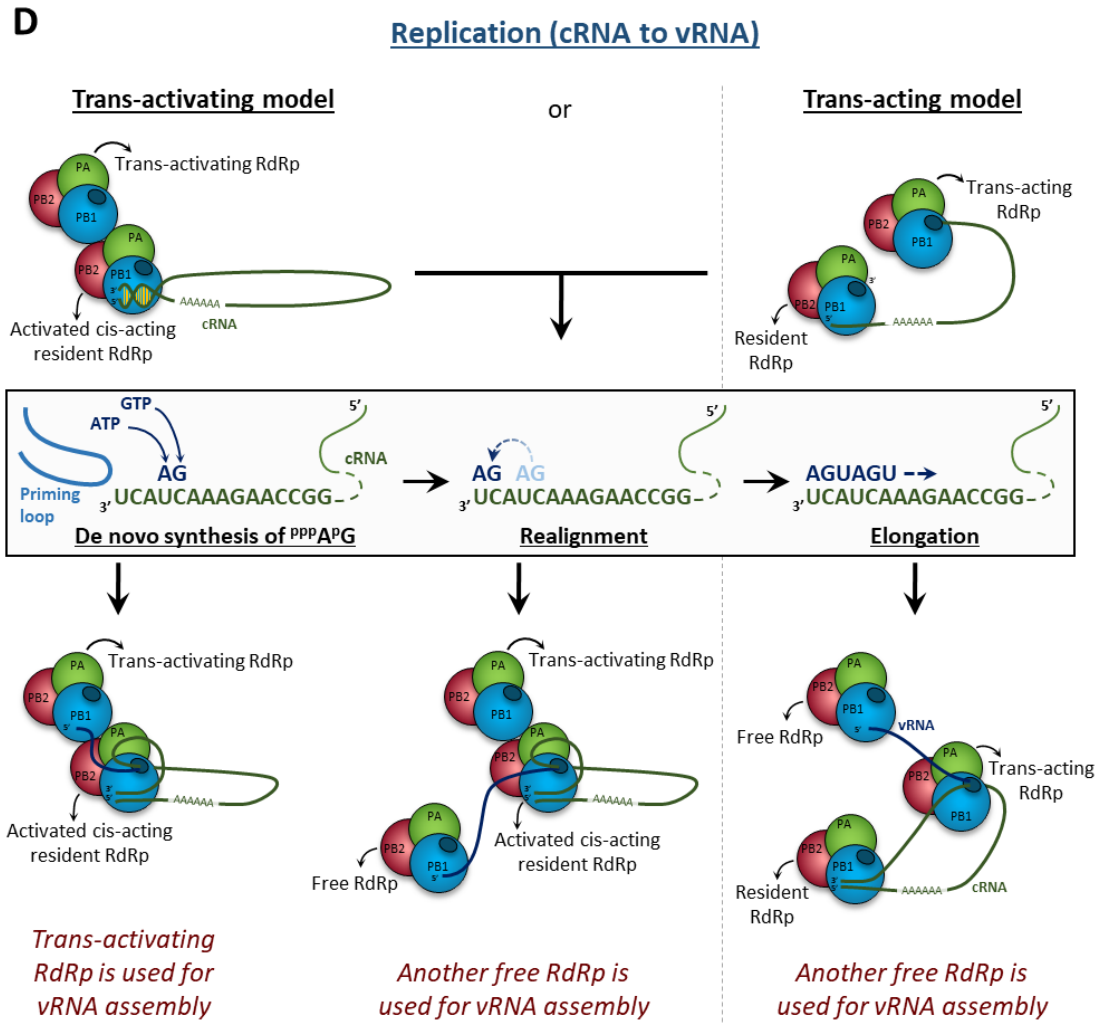

Figure 1.5: Transcription and replication of vRNA: (A) Kinetics of viral mRNA, cRNA and vRNA accumulation in a single infectious cycle. Adapted from Prof Paul Digard. (B) Schematic representation of vRNA transcription. (C) Schematic representation of the first step of vRNA replication. Evens in the light grey boxes represent the inside of the polymerase active site. In all illustrations vRNA is represented in dark blue, cRNA in dark green and mRNA in light green lines and/or letters. NP monomers in vRNPs and cRNPs are omitted. Adapted from Lo *et al.* 2018 and Fodor 2013.

(Blaas *et al.* 1982), followed by the cleavage of a 10-14 nucleotide fragment mediated by the endonuclease domain of the PA subunit (Plotch *et al.* 1981; Dias *et al.* 2009). This fragment is then used as a primer by the PB1 subunit to initiate transcription of the vRNA template (Braam *et al.* 1983).

Transcription elongation proceeds until reaching a conserved 5-7 nucleotide polyuridine stretch located 15-17 nucleotides upstream of the 5' end of the vRNA template (Robertson *et al.* 1981). Given that the 5' end of the vRNA template is proposed to remain bound to PB1 (Tiley *et al.* 1994), once reaching the U-rich sequence the polymerase cannot proceed further given the steric hindrance imposed by the persistence of the 5'end-PB1 interaction. Therefore, the template slips, effectively producing a sequence of repeated U nucleotides which results in a poly(A) tail (Poon *et al.* 1999).

1.4.4.2. Processing of viral mRNA

Due to the presence of the m^7GpppX^m cap and the poly-A tail, viral mRNAs derived from vRNA transcription resemble mature host mRNAs and this allows them to be exported from the nucleus and translated by the cellular protein expression machinery (York and Fodor 2013). Nuclear export of many but perhaps not all of the viral mRNAs is facilitated by the primary cellular mRNA nuclear export factor 1 - NXF1 (Hao *et al.* 2008; Read and Digard 2010; Herold *et al.* 2000; Erkmann and Kutay 2004). In addition, IAV gene expression is temporally regulated, with NP and NS1 being regarded as "early" genes, the M1, HA, NA and the spliced gene products M2 and NEP as "late" genes, while the polymerase subunits are expressed at lower abundance

throughout infection (Skehel 1973, 1972; Hay *et al.* 1980; Shapiro *et al.* 1987; Chua *et al.* 2013). This temporal distinction is not as marked as with some viruses (*e.g.* the large DNA viruses) and the mechanisms behind it remain ill-defined.

1.4.4.3. Mechanisms of vRNA replication

In contrast to transcription, IAV genome replication requires a full-length positive-sense RNA intermediate which will constitute the template for the formation of progeny vRNAs. Thus, replication occurs in two independent steps: replication of vRNA into cRNA (Figure 1.5C) and then copying of the newly synthesised cRNA back to vRNA. The replicative intermediate cRNA does not include a 5' cap nor 3'-poly(A) tail, and therefore requires primer-independent initiation and termination mechanisms that are distinct from the viral mRNA expression (Hay *et al.* 1980).

Biochemical studies have suggested the formation of cRNA by the preformed/resident polymerase (Vreede and Brownlee 2007; York *et al.* 2013).

The first replication step initiates by the translocation of the 3' end of vRNA into the PB1 active site, followed by unprimed terminal initiation - the synthesis of a AG dinucleotide complementary to the vRNA 3'end (Deng *et al.* 2006). Elongation then proceeds as in mRNA synthesis. However, in contrast with transcription, the 5' end of the vRNA template is released from the PB1 subunit, assuring that it is copied without stuttering on the preceding poly(U) stretch. As cRNA is formed, its 5' end is bound to an additional polymerase trimer. The second polymerase recruits NP molecules which translocate through the surface of the polymerase to associate with cRNA (Vreede and Brownlee 2007; Vreede *et al.* 2004). Subsequent NP monomers

are recruited through groove and tail-loop interactions (Ye *et al.* 2006; Shen *et al.* 2011) between NP monomers and form new cRNP complexes (Turrell *et al.* 2013; Ye *et al.* 2006). These are also double-helical vRNP-like structures (York *et al.* 2013; Lo *et al.* 2018).

In the second replication stage, the newly formed cRNA acts as template for vRNA synthesis (Figure 1.5D). Copying of vRNA from a cRNA template occurs by internal initiation on residue U4 followed by transcription of C5 to form an A^{p}G dinucleotide. This acts as a primer after being re-aligned with the terminal U^{p}C residues of the cRNA 3'-end, enabling transcriptional elongation into a full-length vRNA (Deng *et al.* 2006). This step is dependent on the recruitment of a trans-active or trans-activating polymerase trimer (York *et al.* 2013). In order to explain the requirement for this additional polymerase complex, two independent models of this second replication step have been suggested:

- One suggests that considering the optional catalytic activation of the second polymerase, this fulfils a trans-activating, rather than a trans-acting role (York *et al.* 2013). A recent study has shown that, despite the ability of purified vRNPs to perform mRNA and cRNA synthesis *in vitro*, purified cRNPs cannot synthesise vRNA either *de novo* or in the presence of an ApG primer. However, the addition of purified RdRp to purified cRNPs results in synthesis of vRNA (York and Fodor 2013), suggesting the requirement of a second catalytically-active polymerase. Therefore, this model proposes that the trans-activating RdRp induces a conformational rearrangement within the active/resident polymerase, favouring the transfer of the 3'-end of cRNA to the active site or/and favouring initiation at this terminus. Moreover, it hypothesises that the trans-activating polymerase will

constitute the *de novo* assembled vRNP complexes and recruit NP in a similar fashion to that observed in the first stage of cRNP formation (Te Velthuis and Fodor 2016).

- An alternative model involves a catalytically active trans-acting RdRp which gains access to the cRNA 3'-end, which enters its active site where cRNA to vRNA replication is carried out. In this model, a third polymerase complex is proposed to bind to the 5'-terminus of nascent vRNAs to assemble new vRNPs. This trimer of polymerase complexes has been seen in cryo-EM studies (Jorba *et al.* 2009; Moeller *et al.* 2012).

1.4.4.4. Regulation of transcription and replication by viral factors

In addition to the potential contributions of NP in the switching between genome transcription and replication described earlier in section 1.4, other viral proteins have been suggested to play important roles in IAV gene expression and replication. NS1 and NS2/NEP have also been suggested to regulate transcription and replication. NS1 interacts with NP during mRNA synthesis and splicing (Garaigorta and Ortin 2007; Robb and Fodor 2012; Marion *et al.* 1997). In addition to mediating the nuclear export of newly synthesised vRNA (further developed in section 1.4.5), NS2/NEP, has been shown to have roles in regulating vRNA synthesis (Robb *et al.* 2009; Manz *et al.* 2012; Bullido *et al.* 2001).

1.4.4.5. Regulation of transcription and replication by cell host factors

Given the occurrence of IAV transcription and replication in the nucleus, specific interactions between vRNPs and cellular nuclear-localised proteins have been proposed to also contribute to viral RNA synthesis. These can broadly be broken down into those that support viral transcription and those that support genome replication. Only a subset of the better characterised factors are described here, further information has been previously reviewed (Josset *et al.* 2008; Watanabe *et al.* 2010).

Transcriptional support factors include chromatin remodellers CHD1 (chromodomain-helicase-DNA binding proteins 1), nuclear matrix protein 2 and the pol II modulator CLE (Marcos-Villar *et al.* 2016; Rodriguez *et al.* 2011). These are thought to target vRNPs to the nuclear matrix and chromatin nuclear compartments where viral transcription and replication are proposed to take place (Mayer *et al.* 2007; Bortz *et al.* 2011; Jackson *et al.* 1982). Moreover, to access nascent capped host mRNA, the viral polymerase is known to directly interact with the serine-5 phosphorylated C-terminal domain of pol II (Martinez-Alonso *et al.* 2016; Engelhardt *et al.* 2005). Moreover, this interaction also likely contributes to bringing newly synthesised viral mRNA to sites of high concentration of splicing factors. Of these factors, SFPQ (proline-glutamine rich splicing factor) has been shown to bind to vRNPs and increase the efficiency of viral mRNA polyadenylation, while the RED-SMU1 complex (SMU1: suppressor of mec-8 and unc-52 1; RED: named after a region rich in arginine (R)/glutamic acid (E) or arginine/aspartic acid (D) repeats) has also been shown to be recruited by the viral polymerase to control viral mRNA splicing (Fournier *et al.* 2014; Landeras-Bueno *et al.* 2011; Te Velthuis and Fodor 2016).

Although being a cellular helicase involved in DNA replication, the minichromosome maintenance complex (MCM) is known to interact with the pol II C-terminal domain to stimulate IAV vRNA replication. Moreover, the MCM also binds to PA to induce the transition of *de novo* transcription initiation to elongation on the vRNA template (Kawaguchi and Nagata 2007). Proteins belonging to the ANP32 family have also been associated with viral genome replication. Recent findings suggest that ANP32A contributes to the recruitment of the second trans-acting/trans-activating polymerase to the cRNP-bound polymerase, and thereby facilitates vRNA synthesis (Sugiyama *et al.* 2015; Long *et al.* 2016). Notably, the identification of this support factor also resolves the long-standing question of why viral polymerases with a glutamate residue at PB2 position 627 generally do not function well in mammalian cells (Subbarao *et al.* 1993), as a length variation in ANP32A between chickens and mammals prevents a successful functional interaction between the viral polymerase and the longer mammalian support factor (Long *et al.* 2016).

1.4.5. Nuclear export and trafficking of vRNPs

Upon the formation of newly synthesised vRNPs, these are exported from the nucleus and moved to the apical plasma membrane where they are assembled into new virions (Shapiro *et al.* 1987; Rodriguez-Boulan and Sabatini 1978; Rodriguez-Boulan *et al.* 1983). RNP nuclear export happens via the nuclear pores through the Ran-GTP-powered cellular β-exportin chromosome maintenance region 1 (CRM1)-dependent pathway in which M1 and NS2/NEP also play important roles (O'Neill *et al.* 1998; Paterson and Fodor 2012; Martin and Helenius 1991a). IAV NS2/NEP contains two

separate nuclear export signals (NES), both in its N-terminal domain, lying between amino acids 12-21 and 31-40. The first NES constitutes the predominant CRM1 interaction point whilst the second one has been shown to bind to cellular chromodomain-helicase-DNA-binding protein 3 (CHD3) which aids recruitment of RNPs to chromatin and exposure to CRM1 (Neumann *et al.* 2000). Direct interactions between NEP and vRNPs have not been identified. However, M1 is known to directly bind to vRNPs whilst its N-terminal region interacts with NEP (Yasuda *et al.* 1993; Akarsu *et al.* 2003; Shimizu *et al.* 2011; Noton *et al.* 2009). Therefore, it is thought that M1 works as a bridge between vRNPs and NS2 in a proposed "daisy chain" interaction model (vRNP-M1-NEP-CRM1) which is responsible for nuclear export of vRNP complexes.

Originally, RNP nuclear export was held to be specific for vRNPs, with cRNPs remaining in the nucleus (Shapiro *et al.* 1987). This requires the discrimination of vRNPs from cRNPs, a step thought to take place in the nucleus by somehow sensing differences in the terminal panhandle RNA structure (Tchatalbachev *et al.* 2001). However, more recent studies have shown that cRNP complexes are also exported to the cytoplasm, but in a CRM1-independent manner (Chaimayo *et al.* 2017). Although both RNP complex types are present in the cytoplasm, the same study also suggested that the vRNP/cRNP segregation (thus avoiding packaging of cRNPs) occurs through specific interactions with M1 during viral assembly.

Following arrival in the cytoplasm, vRNP complexes disassociate from the CRM1-RanGDP dimer and accumulate by the perinuclear microtubule organisation centre (MTOC) from where they are transported to the cell surface to be packed into progeny virions. This concentration is aided by interactions between the RNPs and the

cellular protein YB-1 (Kawaguchi *et al.* 2012). Diffusion of the RNPs towards the cell membrane has been reported (Babcock *et al.* 2004). Nevertheless, more rapid trafficking of vRNPs to the apical membrane is believed to occur via Rab11- and microtubule-dependent vesicular transport, where the interaction between PB2 polymerase subunit and Rab11 mediates the "piggy-backing" of vRNPs on Rab11-containing vesicles (Amorim *et al.* 2011; Bruce *et al.* 2010; Eisfeld *et al.* 2011; Momose *et al.* 2011). A further refinement of this transport model suggests that rather than the Rab11-positive membrane structures being derived from the recycling endosome, they are actually tubulated membranes derived from the endoplasmic reticulum (de Castro Martin *et al.* 2017).

1.4.6. Virion assembly, budding and release

Assembly of IAV progeny occurs at the apical membrane of polarised cells (Rodriguez Boulan and Sabatini 1978). To achieve virion assembly, the essential virion constituents are required at the budding site: these are the membrane-associated HA, NA, M2 and M1 polypeptides, as well as the internal virion components of the genomic RNPs along with minor components, NS1 and NEP. HA, NA and M2 are translated at, and undergo oligomerisation in, the rough endoplasmic reticulum (Doms *et al.* 1993). HA and NA undergo glycosylation here and in the Golgi apparatus, after which all three viral proteins are specifically transported to the apical plasma membrane (Kundu *et al.* 1996; Hughey *et al.* 1992). Here, HA and NA accumulate in cholesterol- and sphingolipid-rich regions – so called lipid rafts (Scheiffele *et al.* 1999; Zhang *et al.* 2000), while M2 congregates at the edge of these structures (Leser and Lamb 2005). M1 may reach the apical plasma membrane by binding to the cytoplasmic

domains of HA and NA and following them through the exocytic pathway (Ali *et al.* 2000).

In order to form an infectious particle, the packaging of all eight genomic vRNPs is also necessary. Both random and specific mechanisms have been hypothesised to explain the packaging of viral RNPs. However, the observed ratio of infectious versus incomplete virus particles in the overall population of released virions is significantly higher than what is statistically predictable by the random method, if only 8 segments are incorporated per virion (Donald and Isaacs 1954; Hutchinson *et al.* 2008). Instead, much evidence suggests that specific packaging of one copy of each of the segments happens by virtue of packaging signals consisting of conserved sequence regions in the 5' and 3' termini of each vRNA (Gog *et al.* 2007; Fujii *et al.* 2003; Duhaut and McCauley 1996). The specific mechanism by which 8 segments are preferentially packaged is yet to be fully elucidated, but it is presumed to comprise a network of RNA-protein and/or RNA-RNA interactions, with recent studies favouring the RNA-RNA interaction model (Gerber *et al.* 2014; Dadonaite *et al.* 2019).

Once at the correct site, all viral membrane-associated proteins have been suggested to drive the budding process, which requires a network of interactions between these and the other structural viral complex of the RNPs (Rossman and Lamb 2011). M1 is likely to be a major driver of budding (Gomez-Puertas *et al.* 2000), because it not only interacts with the cytoplasmic tails of the glycoproteins (Ali *et al.* 2000; Zhang *et al.* 2000) and M2 (McCown and Pekosz 2006), but also with the vRNPs (Zvonarjev and Ghendon 1980; Ye *et al.* 1999; Noton *et al.* 2009), being therefore a crosslink between all the structural components. In addition, all three viral

transmembrane proteins probably cause some degree of membrane curvature which aids the formation of a viral bud containing the collected vRNPs (Rossman *et al.* 2010; Dou *et al.* 2018) from which newly assembled virions emerge with a compact fringe of HA trimers. In particular, the raft-edge accumulation of M2 is thought to concentrates M2 tetramers at the neck of budding virions to mediate virion scission by pinching off the neck of progeny virions (Rossman *et al.* 2010). Finally, once membrane scission has proceeded, NA mediates the cleavage of sialic acid therefore preventing the binding of virus-associated HA to the receptor and thus allowing the detachment of progeny virions from the cell membrane (Palese *et al.* 1974).

1.5. Innate immune responses against influenza A viruses

Innate immune responses represent an early barrier to IAV infection. Interferons (IFNs), vital constituents of this response, are a group of secreted cytokines which elicit diverse antiviral effects (reviewed by Randall and Goodbourn 2008). These next sections will explore the molecular mechanisms underlying the induction and signalling of IFN (particularly type I) upon IAV infection, ways by which it leads to inhibition of infection, and countermeasures developed by IAVs to prevent and avoid these effects.

1.5.1. Interferons

IFNs are cytokines which were firstly discovered in the 1950s (Isaacs and Lindenmann 1957) and can be divided in three classes: type I, II and III, each with

different structural homologies and class-specific receptors (reviewed in Platanias 2005; Wack *et al.* 2015). Type II IFN has only one member: (IFN-γ), which is secreted by natural-killer cells and is also known to contribute to innate antiviral defence (Iwasaki and Pillai 2014). Type III IFNs (which includes IFN-λ1, 2, 3 and 4) are also induced in direct response to viral infection (Ank *et al.* 2006) and share pathway components with type I IFN (Onoguchi *et al.* 2007). Type I IFNs in human include IFN-α, -β, -ω, -ε, -τ, -δ and -κ, the first two being the better characterised ones and which will be the ones referred to by "type I IFN" from now onwards. An overview of the induction and signalling of type I IFN can be found in Figure 1.6.

1.5.2. RNA sensing and type I interferon induction

The innate immune system detects viral infections by the recognition of pathogen associated molecular patterns (PAMPs) by pattern recognition receptors (PRRs). IAV can be detected by Toll-like receptors (TLRs), retinoic acid-inducible gene I (RIG-I)-like receptors (RLRs) and nucleotide oligomerisation domain (NOD)-like receptors (Sabbah *et al.* 2009). Each of these types of receptors are located in different cell compartments and are activated by different PAMPs.

1.5.2.1. Intracellular viral RNA

Cytoplasmic IAV vRNAs can, at least in theory, be detected by RLRs such as RIG-I, melanoma differentiation-associated protein 5 (MDA-5) and laboratory of genetics and physiology 2 (LGP2). Amongst all these, RIG-I is thought to be the

predominant sensor for IAV single-stranded 5′-triphosphate RNAs (Pichlmair *et al.* 2006; Rehwinkel *et al.* 2010), despite the fact that MDA-5 has also been reported to be involved in ISG upregulation against the virus (Benitez *et al.* 2015). In contrast, overexpression of LGP2 has been shown to decrease IAV-driven IFN-β induction in cells infected with H3N2 viruses (Malur *et al.* 2012). For full activity, RIG-I requires ubiquitylation, which is mediated by the cellular tripartite motif-containing protein 25 (TRIM25) (Gack *et al.* 2007), RIG finger proteins leading to RIG-I activation (RIPLET) (Oshiumi *et al.* 2009; Cadena *et al.* 2019), or Mex-3 RNA binding family member C (MEX3C) (Kuniyoshi *et al.* 2014). Upon activation, RIG-I recruits and activates mitochondrial antiviral signalling protein (MAVS) – also known as CARD adaptor inducing IFN-β (Cardif), virus-induced signalling adaptor (VISA) or IFN-β promoter stimulator protein 1 (IPS-1) (Seth *et al.* 2005; Xu *et al.* 2005; Hiscott *et al.* 2006). Once engaged, MAVS interacts directly with tumour necrosis factor (TNF) receptor-associated factor 6 (TRAF6) (Xu *et al.* 2005) which recruits receptor-interacting proteins 1 (RIP1) (Seth *et al.* 2005). Once recruited, TRAF6 ubiquitylates itself and RIP-1 (Chen 2005) and the polyubiquitin chains are recognised by TAK-binding proteins 2 and 3 (TAB2 and 3) which recruits transforming growth factor β-activated kinase 1 (TAK1) to the TRAF6-RIP1-TAB-TAK complex. In association, TAK1 directly phosphorylates the IKKβ subunit of the IKK complex (Wang *et al.* 2001), resulting in the downstream phosphorylation, ubiquitylation and eventually degradation of IκB, leading to the nuclear intake of NF-κB and the subsequent upregulation of IFN-β and pro-inflammatory cytokines (Kim and Maniatis 1997; Liu *et al.* 2017). At the same time, MAVS is thought to also recruit TRAF3, which directly interacts with TRAF family member-associated NF-κB activator (TANK)

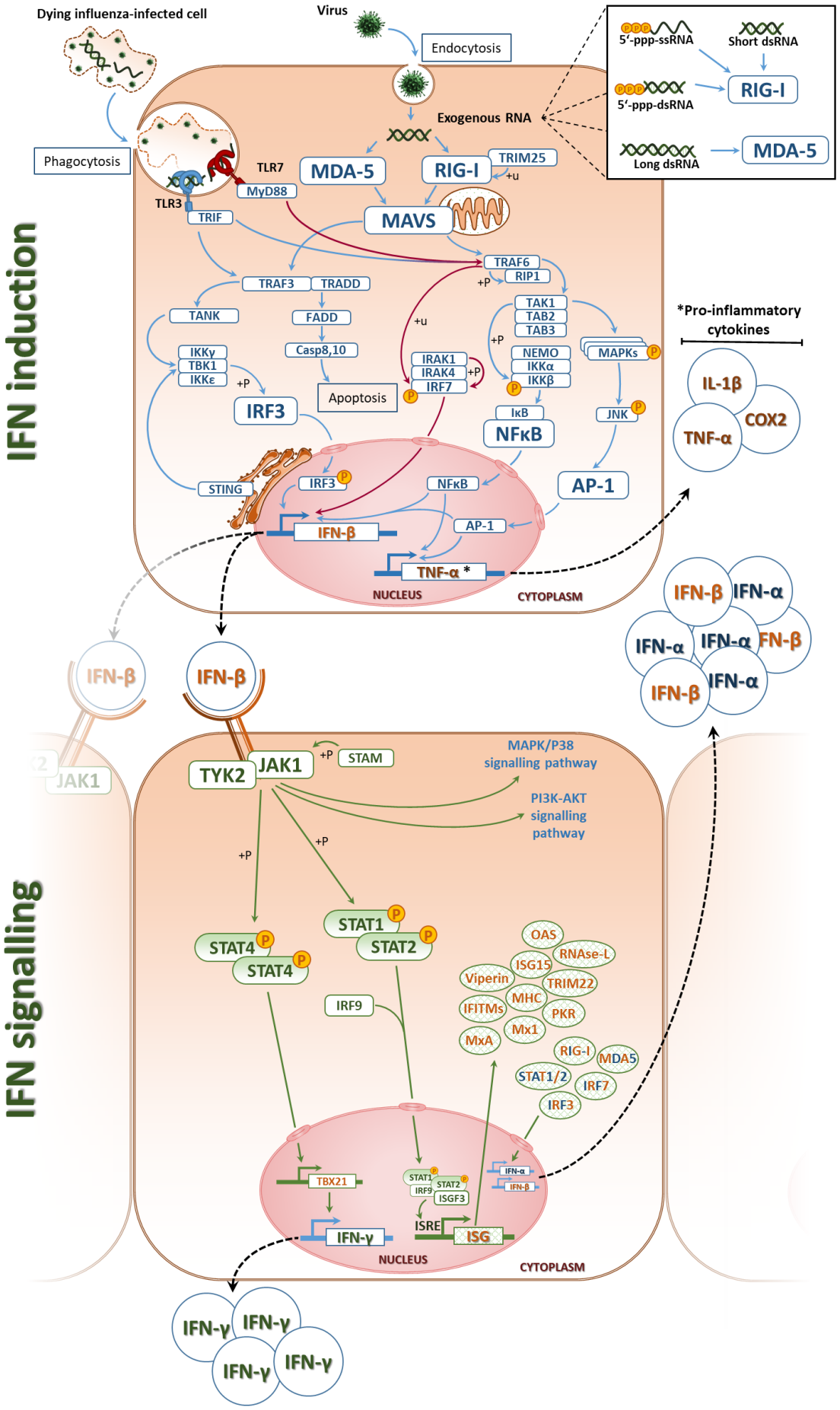
IFN induction
IFN signalling
Dying influenza-infected cell
Virus
Endocytosis
Phagocytosis
Exogenous RNA
5'-ppp-ssRNA
Short dsRNA
5'-ppp-dsRNA
RIG-I
Long dsRNA
MDA-5
TLR7
TLR3
MyD88
TRIF
MDA-5
RIG-I
TRIM25
+u
MAVS
TRAF6
RIP1
+P
TRAF3
TRADD
TANK
FADD
Casp8,10
Apoptosis
IKKγ
TBK1
IKKε
IRF3
STING
IRAK1
IRAK4
IRF7
TAK1
TAB2
TAB3
NEMO
IKKα
IKKβ
IκB
NFκB
MAPKs
JNK
AP-1
*Pro-inflammatory cytokines
IL-1β
COX2
TNF-α
IRF3
NFκB
IFN-β
AP-1
TNF-α *
NUCLEUS
CYTOPLASM
IFN-β
IFN-α
IFN-α
IFN-α
FN-β
IFN-β
IFN-β
IFN-β
JAK1
TYK2
JAK1
+P
STAM
MAPK/P38 signalling pathway
PI3K-AKT signalling pathway
+P
+P
STAT4
STAT4
STAT1
STAT2
IRF9
OAS
RNAse-L
ISG15
Viperin
TRIM22
MHC
IFITMs
PKR
Mx1
MxA
RIG-I
MDA5
STAT1/2
IRF7
IRF3
TBX21
IFN-γ
STAT1
STAT2
IRF9
ISGF3
ISRE
ISG
IFN-α
IFN-β
NUCLEUS
CYTOPLASM
IFN-γ
IFN-γ
IFN-γ
IFN-γ

Figure 1.6: Innate immune recognition and the interferon system. Schematic representations type I IFN induction and signalling pathways in the context of IAV infection. IAV dsRNA are recognised by cytoplasmic RIG-I and MDA-5 and endosomal TLRs 3 (blue arrows) and 7 (red arrows). A panoply of signalling cascades takes place to ultimately result in the activation of transcription factors IRF3, NF-κB and AP-1 which upregulate IFN-β expression. Secreted IFN-β functions in an auto-paracrine fashion, being recognised by IFNAR and activating the JAK/STAT signalling pathway which leads the phosphorylation and dimerisation of STAT1/2, the formation of the STAT/1/2/IRF9 trimeric complex and the resulting regulation of ISRE promoters and the expression of ISGs (green arrows). "+u" and "+P" represent ubiquitylation and phosphorylation, respectively.

(Li *et al.* 2002). TANK associates with TANK-binding kinase 1 (TBK1) (Pomerantz and Baltimore 1999)which along with IKKε interact with and phosphorylate IRF3 (Fitzgerald *et al.* 2003). Phosphorylated IRF3 monomers undergo dimerisation followed by nuclear import where it acts as a transcription factor to upregulate several genes (Grandvaux *et al.* 2002), including IFN-β.

In the context of intracellular RNA signalling, NEMO (a component of the IKK complex) interacts with TANK (Zhao *et al.* 2007), being therefore an adapter for both NF-κB and IRF3 activation.

1.5.2.2. dsRNA or ssRNA delivered through endosomes

RLR-dependent RNA sensing in IAV infection is common in most cell types. However, phagocytes such as plasmacytoid dendritic cells and macrophages use TLRs 3 and 7 to detect IAV RNA (Kawasaki and Kawai 2019). Detection of dsRNA and ssRNA in endosomes or phagosomes is mediated by TLR3 and 7, respectively.

Binding of TLR3 to dsRNA is initiated with the dimerisation and phosphorylation of TLR3 (Sarkar *et al.* 2004) as well as the recruitment of its adapter Toll-interleukin-1-resistance domain-containing adaptor inducing IFN-β (TRIF) (Yamamoto *et al.* 2003). Similarly to RLR RNA recognition, engagement of TRIF signals the activation of both NF-κB and IRF3 through the recruitment of TRAF6 and RIP1 (Hacker *et al.* 2006) as well as TRAF3 (Oganesyan *et al.* 2006) and both pathway arms develop as described in section 1.5.2.1.

Contrary to dsRNA, if recognised from endosomes, ssRNA is detected by TLR7 (Diebold *et al.* 2004). The mechanism of IFN-β induction following from TLR7 activation show some differences compared to TLR3-driven IFN expression. TLR7 uses myeloid differentiation factor 88 (MyD88) as its adapter. In turn, MyD88 recruits a trimeric complex formed by the kinases interleukin-1 receptor-associated kinase 4 (IRAK4), IRAK1 and TRAF6 (Hacker *et al.* 2006). The recruitment of TRAF6 activates NF-κB through the already described TAK1-TAB2-TAB3 complex. In contrast to the IRF3 activation observed from TLR3 induction, given the constitutive expression of IRF7 in dendritic cells, TLR7 engagement has been suggested to occur. In this case, the MyD88-IRAK1-IRAK4-TRAF6 complex directly interacts with IRF7 (Honda *et al.* 2004; Kawai *et al.* 2004) which is polyubiquitylated by TRAF6 and phosphorylated by IRAK1 in a TBK1/IKKε-independent fashion. Upon phosphorylation, the entire complex of IRAK1-TRAF6-MyD88-IRF7 is translocated to the nucleus where it stimulates transcription of IFN-β (Honda *et al.* 2005).

1.5.3. Signalling responses to type I interferon

Once translated and secreted, IFN-β acts in an auto-paracrine manner via a common heterodimeric receptor: Interferon-α/β receptor (IFNAR), composed of IFNAR1 and IFNAR2 (reviewed by (Randall and Goodbourn 2008). While the IFNAR1 subunit is associated with tyrosine kinase 2 (Tyk2), IFNAR2 is bound to tyrosine Janus/just another kinase 1 (JAK1) and signal transducer and activator of transcription 2 (STAT2). Ligand-induced dimerisation of the receptor induces conformational changes, leading to tandem phosphorylation cascades which result in

the phosphorylation and consequent dimerisation of STAT1 and 2. The STAT1/2 dimer associates with IRF9 monomers to form the heterotrimeric interferon stimulated gene factor 3 (ISGF3). This complex is imported into the nucleus where it is acetylated (Tang *et al.* 2007) and binds to the IFN-stimulated response element (ISRE) to regulate the transcription of IFN-stimulated (ISGs) and repressed (IRGs) genes.

1.5.4. Interferon-stimulated genes

As previously described, the induction and recognition of type I IFN results in the transcriptional stimulation of hundreds of ISGs (Shaw *et al.* 2017), some of which restrict viral propagation through distinct mechanisms. The following sections will list some of the ISGs which have been found to be antiviral against IAV.

1.5.4.1. Myxovirus resistance proteins

Mx1 is a nuclear-localised mammalian guanosine triphosphatase (GTPase) and was the first ISG protein found to restrict IAV replication (Haller *et al.* 1980; Staeheli *et al.* 1986b). Moreover, a follow up study further correlated the susceptibility of BALB/c and CBA/J mice to IAV infection with large deletions or a nonsynonymous mutation in the Mx1 gene (Staeheli *et al.* 1988; Staeheli *et al.* 1986a). Murine Mx2 is also an ISG. However, Mx2 is cytosolic and has no antiviral activity against IAV (Zurcher *et al.* 1992).

The human Mx1 orthologue, MxA, is also known to inhibit a large variety of viruses, including IAV (Haller *et al.* 2009; Netherton *et al.* 2009). Studies on MxA

have suggested that its oligomerisation around RNPs prevents their nuclear import and thus blocks viral replication (von der Malsburg *et al.* 2011; Turan *et al.* 2004). Inhibition of IAV by Mx1 is also thought to be mediated by the disruption of NP-PB2 interactions, resulting in reduced vRNP assembly and abrogated polymerase activity (Verhelst *et al.* 2012). A more recent study has suggested that MxA also has an indirect antiviral affect in IAV inhibition by positively regulating the induction of type I IFN (Schattgen *et al.* 2016). The murine Mx2 and its human orthologue MxB are cytoplasmic and, in spite of inhibiting other RNA viruses such as HIV-1, they present no antiviral effects against IAV (Goujon *et al.* 2013).

1.5.4.2. 2' 5'-oligoadenylate synthetases

The 2' 5'-oligoadenylate synthases (OAS) act alongside ribonuclease L (RNase L) in order to degrade cytosolic-localised viral RNA (reviewed in Silverman 2007). OAS is enzymatically activated by dsRNA binding, converts ATP into 2'-5'-oligoadenylate which activates latent RNase L, leading to the cleavage of viral and cellular RNA and the cessation of viral infection (Chakrabarti *et al.* 2011). Moreover, RNase L-cleaved products have been shown to activate RIG-I in a positive feed-back to enhance IFN secretion (Malathi *et al.* 2007). The importance of the OAS1/RNAse L pathway to IAV has been shown by large reduction of IFN-β-mediated inhibition in RNase L knock-down and knockout cells (Min and Krug 2006).

1.5.4.3. Protein kinase R

Although ubiquitously expressed, protein kinase R (PKR) is upregulated by type I IFN (Shaw *et al.* 2017). PKR is activated by dsRNA, resulting in auto-phosphorylation. Upon activation, PKR phosphorylates the alpha subunit of eukaryotic initiation factor 2 (eIF2α), increasing its affinity to eIF2β and rendering it inaccessible for subsequent initiation events and thus contributing to a general translational block and reduced viral protein synthesis (Pindel and Sadler 2011; de Haro *et al.* 1996; Gale and Katze 1998). PKR also targets IκB, which further activates NF-κB and induces IFN expression, resulting in a positive loop of ISG activation (Kumar *et al.* 1994).

1.5.4.4. Interferon-induced transmembrane proteins

Interferon-induced transmembrane proteins (IFITMs) are a family of dispanins which have a common double transmembrane domain configuration (Sallman Almen *et al.* 2012). IFITM1, 2, 3, 5 and 10 have been identified in humans and of these, the first three are known to have antiviral functions against multiple viruses (Zhang *et al.* 2012; Perreira *et al.* 2013). While IFITM1 localises to the cell surface and early endosomes, IFITM2 and 3 are enriched in late endosomes and lysosomes (Mudhasani *et al.* 2013) and are thought to prevent IAV viral entry (Brass *et al.* 2009; Feeley *et al.* 2011). Additionally, IFITM3 has been identified as important in restricting mortality and morbidity against IAV in man and *in vivo* models of infection (Everitt *et al.* 2012). IFITMs seem to be specific inhibitors of viruses which take advantage of the endosomal pathway to ensure entry (Huang *et al.* 2011), suggesting a block in viral fusion in the endosome, potentially by interfering with HA fusion activity.

Nevertheless, the exact mechanism by which this takes place has not yet been fully elucidated.

1.5.5. Interferon induction by IAV infection

As reviewed above, IFN induction in the context of IAV infections results from detection of PAMPs through RLRs and TLRs. The next subchapter will review the two main IAV IFN inductors: the RNA "panhandle" and defective interfering particles.

1.5.5.1. Induction of RIG-I by the IAV "panhandle"

As previously mentioned in this chapter, the 5' and 3' termini of IAV genome segments respectively contain 13 and 12 nucleotide highly conserved sequences (Desselberger *et al.* 1980; Robertson 1979). These sequences have partial complementarity with the potential to form a "panhandle" structure which acts as the vRNA promoter and is involved in the initiation of transcription (Fodor *et al.* 1994; Tiley *et al.* 1994). This structure has been shown to form a stable partial duplex of approximately 15bp in length between the conserved termini through Watson–Crick and non-Watson–Crick base pairing - Figure 1.7A - (Cheong *et al.* 1996). Therefore, by virtue of the 5'ppp being directly adjacent to a small stretch of partially dsRNA, this panhandle is a potent RIG-I ligand (Killip *et al.* 2015; Liu *et al.* 2015). Moreover, observations of RIG-I activation by RNA extracted from IAV-infected cells, from purified virions, or from RNP reconstitution assays also provides evidence of panhandle-dependent IFN induction (Pichlmair *et al.* 2006; Rehwinkel *et al.* 2010).

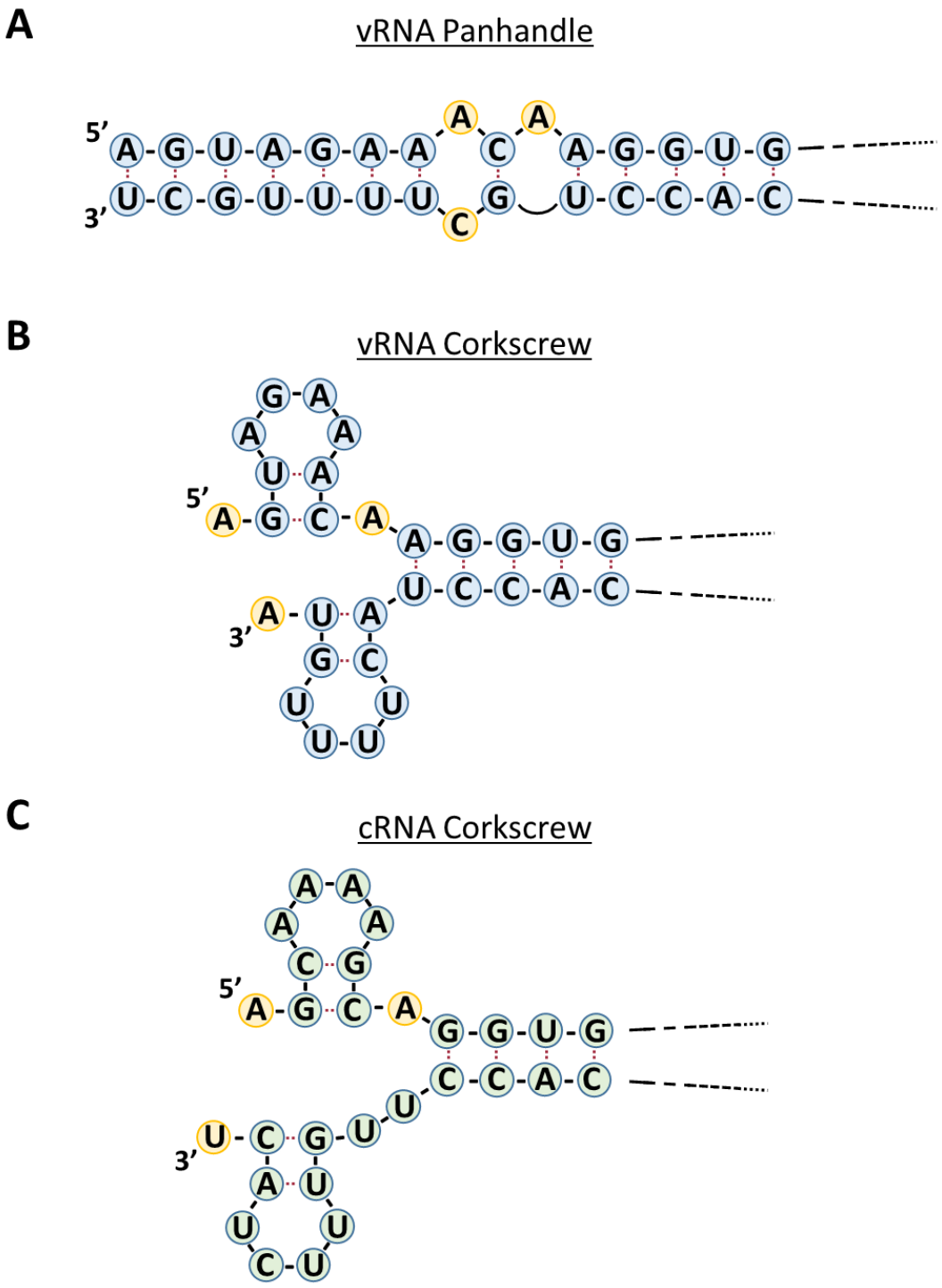

Figure 1.7: vRNA and cRNA promoter conformations. Schematic representation of the (A) vRNA "panhandle" and vRNA and cRNA "corkscrew" secondary structures. Adapted from (Ferhadian *et al.* 2018).

Despite the formation of this dsRNA region in naked vRNA, studies have shown that, when encapsidated by the viral RdRp, its structure is altered. RdRp binding to the vRNA termini leads to the formation of a 'forked' or "corkscrew"-like secondary structure which is critical for viral polymerase activity (Tomescu *et al.* 2014; Killip *et al.* 2015). Besides, this polymerase-dependent conformational switch allows a smaller number of inter-strand base pairs, making this RNA region potentially therefore less likely to be detected by RIG-I, as the RNA extremities do not engage in binding and dsRNA is not formed (Flick and Hobom 1999) (Figure 1.7B).

1.5.5.2. Defective genomes and defective interfering particles

These were first identified in the 1940s as incomplete viruses capable of inhibiting the replication of a wild-type virus (Gard and von Magnus 1947). Defective viral genomes (DVGs) were identified upon serial passage of the virus in embryonated chicken eggs at high multiplicity and described as 'incomplete' non-infectious viruses derived from full-length genome segments (von Magnus 1951a, 1951b). Defective interfering particles (DIPs) were defined as a viral particle which contained the standard structural components but possess a DVG (Huang and Baltimore 1970).

IAV DVGs have been shown to have suffered loss of long internal sequences that still preserve the vRNA terminal regions (Duesberg 1968; Davis *et al.* 1980; Davis and Nayak 1979; Nayak 1980). These preserved terminal sequences tend to include approximately 200bp at the 3' end and 250bp at the 5' end (Duhaut and Dimmock 2000; Duhaut and Dimmock 2002), which includes the segment-specific packaging signals. Given their smaller size, coupled with the ability to be packaged and replicated

by the viral polymerase, these DVG segments can outcompete the full-length segments. Several studies have shown that these deletions are particularly associated with the largest IAV segments - segments 1, 2 and 3 (Sivasubramanian and Nayak 1983; Nayak *et al.* 1982) – where the size advantage of the DVG RNA is proportionally greater and that furthermore, the defective segments specifically compete with the parent segment at the stage of incorporation into virions (Duhaut and McCauley 1996; Odagiri and Tashiro 1997; Ueda *et al.* 1980).

For a long time, the generation of DIPs was considered a tissue culture-associated artefact of virus preparations, as serial passage resulted in the generation and accumulation of high number of DVGs (Perez-Cidoncha *et al.* 2014). However, more recent studies have suggested the importance of DIPs in naturally occurring IAV infections. DVGs with internal deletions have been identified as occurring in experimentally infected mice (Tapia *et al.* 2013) and humans (Saira *et al.* 2013). Additional studies on DIPs in IAV pathogenesis supported that the presence of DIPs negatively correlates with increased lung pathology in a mouse model (Rabinowitz and Huprikar 1979). In this study, mouse infections with DIP-enriched viral preparations presented decreased numbers of inflammatory cells infiltrated in lungs, compared with wild-type virus, leading to the assumption that DIPs protect against viable virus particles. In contrast, the presence of DIPs in H1N1 2009 pandemic infections in humans have been correlated with severe clinical outcomes (Vasilijevic *et al.* 2017; Saira *et al.* 2013).

Evidence that DIPs are involved in IFN induction has accumulated over the years. Studies have shown that IFN-inducing particles are not productively infectious (Marcus *et al.* 2005). Conversely, DVG RNA was directly implicated in a stronger

RIG-I recognition and subsequent IFN induction, in contrast to full-length genomes which are not bound to RIG-I during infection (Baum *et al.* 2010).

1.5.6. IFN antagonism and prevention by IAV

Like every virus, IAV has evolved several mechanisms to counteract and circumvent the IFN response. It is likely that some of these strategies involve masking viral PAMPs. First, if IAV genome replication took place in the cytoplasm, vRNA and cRNAs could constitute cytoplasm-localised RIG-I and MDA-5 ligands and lead to the activation of an IFN-driven antiviral response. Therefore, unlike most other negative-strand RNA viruses which replicate in the cytoplasm, IAV RNA synthesis takes place in the nucleus (previously described in the chapter) and it is possible that this makes these RNA species inaccessible to detection by RLRs. However, recent studies have suggested the presence of nuclear-resident RIG-I which binds to vRNPs in the nucleus (Liu *et al.* 2018; Liu *et al.* 2019). Nevertheless, synthesis of cRNA and vRNA is closely coupled with the incorporation of NP monomers and RNA encapsidation (Ye *et al.* 2006; Vreede *et al.* 2004).

A second strand of IAV IFN evasion mechanisms involve active interference with the sensing and response systems of the IFN pathway. These evasion mechanisms arise because the IAV genome encodes proteins which antagonise the IFN system (reviewed in Garcia-Sastre 2011). The major protein responsible for this is NS1. However, in addition, several other viral proteins have been associated with inhibiting the IFN response, such as PB1-F2 and PA-X (described above), HA and the viral polymerase.

1.5.6.1. NS1

Despite more recent discoveries of accessory proteins with IFN antagonism activity, NS1 still remains the main IAV blocker of IFN induction, for which it has evolved multiple mechanisms (reviewed by Hale *et al.* 2008; Engel 2013; Krug 2015). Although often acting in a strain-specific manner, NS1 has been shown to inhibit the induction of IFN-β by directly targeting multiple components of the IFN induction cascade and/or by generally inhibiting host gene expression.

Activation of key transcription factors such as IRF3, NF-κB and AP-1 have been shown to be inhibited by NS1, leading to the reduction of IFN-β expression (Talon *et al.* 2000; Wang *et al.* 2000; Ludwig *et al.* 2002). Position 196 of NS1 has been associated with the ability of NS1 to inhibit IRF3 activation, as viruses containing E196 were apparently more efficient at blocking IRF3 phosphorylation than strains with K196 (Kuo *et al.* 2010). However, direct interactions between NS1 and these transcription factors have not been described. Instead, NS1 prevents IFN induction by acting upstream of IRF3, NF-κB and AP-1 transcription factors (Krug 2015). Direct interactions between NS1 and RIG-I have been described (Mibayashi *et al.* 2007). Additional binding of NS1 to the factors involved in RIG-I activation, TRIM25 (Gack *et al.* 2009; Koliopoulos *et al.* 2018) and RIPLET (Rajsbaum *et al.* 2012) have also been identified. Additionally, NS1 binds to PACT, another cellular protein important for RIG-I activation (Tawaratsumida *et al.* 2014; Brisse and Ly 2017). In each case, these interactions are thought to inhibit RIG-I ubiquitylation and activation and thus the following IFN-β transcription.

NS1 is also known to bind to dsRNA, preventing RLR recognition (Hatada and Fukuda 1992). For this, the positive charge on NS1 residue R38 in the N-terminal RNA-binding domain has been shown to be essential, but adjacent basic amino acids also make strong contributions to the affinity of binding, *i.e.* K41 (Wang *et al.* 1999). Point mutations of these amino acids results in RNA binding deficits, increased IFN-β induction and virus attenuation in a murine model (Donelan *et al.* 2003). In addition to limiting RIG-I activation, the dsRNA-binding function of NS1 has also suggested to impair the function of ISGs which have been shown to have direct antiviral functions against IAV, such as the OAS/RNase L duo (Min and Krug 2006) and PKR (Min *et al.* 2007; Bergmann *et al.* 2000).

In addition to the above specific effects on the innate immune response, NS1s from many strains of IAV also have a general inhibitory effect on cellular gene expression. Various points of inhibitory interaction between NS1 and the cellular splicing machinery have been proposed over the years (Fortes *et al.* 1995; Qiu *et al.* 1995; Wang and Krug 1998; Wolff *et al.* 1998), but while these may contribute to overall host protein shut-off, they may contribute towards regulation of viral mRNA splicing (Tsai *et al.* 2013). NS1-mediated inhibition of cellular mRNA export has also been proposed to play a role in limiting antiviral gene expression (Satterly *et al.* 2007), though this proposal is not easily reconcilable with much evidence indicating that many of the viral mRNAs use the same cellular pathway for nuclear export (Hao *et al.* 2008; Read and Digard 2010; Wang *et al.* 2008) and that interactions between NS1 and this machinery have a positive role for export of the viral late gene mRNAs (Pereira et al 2017). What is less contentious, is the establishment that many, but not all, NS1s potently repress cellular gene expression by inhibiting processing and

polyadenylation of the 3'-end of cellular mRNAs (Nemeroff *et al.* 1998). This mechanism, mediated by inhibitory interactions between NS1 and both cleavage and polyadenylation specificity factor 30 (CPSF30) and poly(A)-binding protein II (PABPII) achieves specificity for host gene expression because, as described above, the mechanism by which viral mRNAs are polyadenylated is totally separate. However, not all strains of IAV use this approach; for example the laboratory strain PR8 and pdm09 viruses do not (Kochs *et al.* 2007; Hale *et al.* 2010).

1.5.6.2. Viral polymerase

The role of the viral polymerase in IFN inhibition has been suggested by systems biology analysis (Shapira *et al.* 2009) as well as partial UV inactivation studies (Marcus *et al.* 2005). The mechanism of cap-snatching performed by the polymerase contributes to a general host mRNA shut down (Schmolke and Garcia-Sastre 2010) and consequent restraint of the expression of IFN-β, RLRs and ISGs. Moreover, virus strains with higher polymerase efficiency present an increased replication speed and are able to outrun the IFN response (Grimm *et al.* 2007). However, in addition, to mechanisms related to polymerase RNA synthesis, both the individual components and the overall trimeric polymerase complex have been shown to directly inhibit aspects of the IFN pathway. Direct interactions between the polymerase and RIG-I have been identified. However, the association of each individual virus polymerase component with RIG-I failed to significantly affect dsRNA- or 5' triphosphate RNA-elicited IFN induction and IRF3 phosphorylation (Li *et al.* 2014). However, another study has again suggested an interaction of RIG-I with the polymerase of incoming

vRNPs. (Liedmann *et al.* 2014b). This interaction was dependent on amino acids 398E, 524S and 536I of PB1 and 351E of PA (the ESIE motif) and was proposed to be responsible for inhibiting IFN induction at very early stages of infection. These specific PB1 and PA residues had also been identified as determinants of IFN inhibition and virulence of IAV (Liedmann *et al.* 2014a).

Counteraction of IFN stimulation by individual subunits of the polymerase have also been described, as PB2 from some strains of IAV has been shown to localise to mitochondria (Carr *et al.* 2006) and this has been linked to inhibition of RLR-signalling through MAVS (Graef *et al.* 2010; Iwai *et al.* 2010).

1.5.6.3. Haemagglutinin

The HA conserved fusion peptide has been shown to interact with STING, and reduce STING-driven IFN induction (Holm *et al.* 2016). However, this proposed function of the HA fusion peptide is inconsistent with the localisation of both HA fusion peptide and STING. Although both proteins can be found in membranes of the Golgi apparatus, STING faces the cytoplasm whilst the fusion peptide in kept in the lumen (reviewed in Sriwilaijaroen and Suzuki 2012). Moreover, HA of a lab adapted H1N1 strain has also been suggested to interact with IFNAR, leading to IFNAR ubiquitylation and its subsequent degradation (Xia *et al.* 2015), resulting in limited induction of ISGs.

1.6. Aims and approaches

As introduced in section 1.3, several accessory peptides have been shown to be encoded by the IAV genome in overlapping and/or alternately initiated open reading frames. Several of these IAV accessory peptides, although not necessarily crucial for virus replication, have been shown to modulate cellular responses and affect IAV virulence. The overall goal of this dissertation was to assess the expression of alternative polypeptides from segment 2 of IAV with special attention to AUG codons 10 and 11 in the PB1 reading frame and any functions of these polypeptides in the IAV replication cycle.

Chapter 2 describes assessment of the translation initiation potential of segment 2 AUG codons 10 and 11, using plasmid-based reporter constructs and mutant viruses made in the background of a laboratory adapted IAV strain, and the effects of mutating these start codons on viral fitness *in vitro* and *in ovo*. A more detailed phenotypic characterisation of the mutant viruses is presented in Chapter 3, where the interplay between virus and the type I IFN system was considered. Chapter 4 includes murine *in vivo* studies of an AUG mutant virus. Chapter 5 describes studies of the individual proteins that arise from AUGs 10 and 11 and their effects on the IFN system. Finally, Chapter 6 is dedicated to the analysis of the sequence conservation of these segment 2 AUG codons and their importance in a broader panel of IAV strains. Concluding remarks and future research directions are discussed in Chapter 7, and the materials and methods used in this study are given in Chapter 8.

Chapter 2

Segment 2 AUG codons 10 and 11 and their effects on viral fitness *in vitro*

2.1. Background and Aims

Influenza A virus virulence is multidimensional and has been shown to be dependent on both viral and host features. Determinants of virulence are regulated in a polygenic manner in which segment 2 plays an important role (Baigent and McCauley 2003; Basler and Aguilar 2008; Kawaoka *et al.* 1989).

Segment 2 is known to encode three different proteins; PB1, PB1-F2 and PB1-N40. As reviewed in Chapter 1, PB1 is the primary product of segment 2. It complexes with two other subunits (PB2 and PA) to form the viral RdRp and is therefore indispensable for virus replication. PB1-F2 and PB1-N40 proteins are expressed from alternative AUG codons. PB1-F2 is a small accessory protein, initiated from the fourth AUG codon in segment 2 (in frame 2), which acts as a mitochondria-localised innate immune inhibitor and is also known to induce cell death (Varga and Palese 2011).

PB1-N40 (or simply N40) was first described in 2009 and consists of an N-terminally truncated version of PB1 lacking the first 39 amino acids, the region required for the binding to the PA polymerase subunit (Wise *et al.* 2009). N40 translation initiates from the fifth segment 2 AUG codon (in frame 1) by ribosomal reinitiation (Wise *et al.* 2011). Although it is known to localise in the cytoplasm, PB1-N40 function remains unclear, although it has been associated with altered production of vRNA (Tauber *et al.* 2012).

Examination of the 5' end of segment 2 of the A/PR/8/34 (PR8) strain further revealed that, in addition to the AUG codons which initiate expression of PB1, PB1-F2 and N40, a number of other AUG codons are found (Figure 2.1):

- Frame 1: AUG codons 10 and 11
- Frame 2: AUG codons 2, 3, 7, 8 and 9
- Frame 3: AUG 6.

Studies on PB1-F2 expression *in vitro* also suggested the expression of a PB1-F2 C-terminal fragment from subsequent frame 2 AUG codons; one or more of AUGs 7, 8 and 9 (Zamarin *et al.* 2006; Kamal *et al.* 2015). Given that these potential PB1-F2 initiation codons are in medium strength Kozak consensus settings while AUG codons 10 and 11 are in strong contexts (Figure 2.1), the potential for protein expression from these latter AUGs was also considered. Accordingly, this chapter aimed to investigate possible protein translation initiation from segment 2 AUG codons 10 and 11. Furthermore, the importance of these AUG codons for IAV biology was assessed by measuring the replicative fitness of mutants of the lab adapted PR8 strain lacking these AUG codons in several *in vitro* and *in ovo* systems.

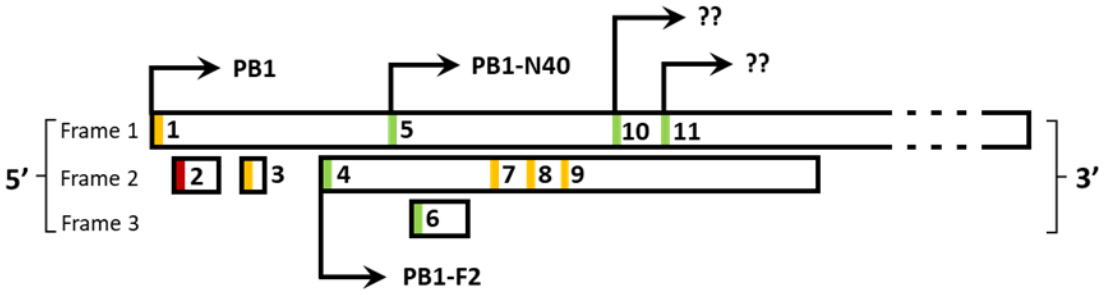

Figure 2.1. Diagram of the 5′ end of segment 2 mRNA. Open reading frames from the three frames are indicated by boxes. AUG codons are colour-coded according to the relative strength of their Kozak consensus: green-strong (-3A/G and +4G), amber-intermediate (-3A/G or + 4G), red-weak (-3U, +4U). Characterised AUG initiation codons and respective products are indicated by arrows (PB1, PB1-F2 and PB1-N40). Adapted from Wise *et al.*, 2009.

2.2. Results

2.2.1. Translation initiation from segment 2 AUG codons 10 and 11

Initially, protein expression from AUGs 10 and 11 was examined in the context of plasmid transfection. In order to do this, the first 380bp of PR8 segment 2 cDNA were cloned into a green fluorescent protein (GFP) expression plasmid, so that the reporter gene was positioned into frame with AUG codons 1, 5, 10 and 11 (Figure 2.2A). This recombinant construct (termed WT), was used as a template to mutate frame 1 AUG codons by site-directed mutagenesis as described in Table 2.1. These constructs were generated by Dr Helen Wise (Wise *et al.*, 2011 and unpublished data). After confirmation by DNA sequencing, the panel of WT and mutated constructs were individually transfected into 293T cells and after 48 hours, the expression of GFP-fused products was investigated by SDS-PAGE and western blot for GFP and tubulin as a loading control. All samples contained similar amounts of tubulin (Figure 2.2B), confirming equivalent loading. As a negative control, a sample from mock transfected cells was included, which did not contain detectable GFP peptides (Figure 2.2B, lane 1). The detection system was validated by the transfection of a GFP-only plasmid positive control, where a major polypeptide product was seen at 27kDa, the expected molecular mass for GFP (lane 2). When transfected with WT PB1-GFP plasmid, cells expressed fusion peptides corresponding to PB1 and PB1-N40, detectable by the presence of the expected 41 and 36kDa products (lane 3) which were absent after the mutation of AUGs 1 and 5 respectively (lanes 4 and 5). WT plasmid-transfected cells also expressed two smaller peptides whose sizes corresponded to proteins initiating at AUGs 10 and 11 (30 and 28kDa). Furthermore, the 30kDa product was no longer

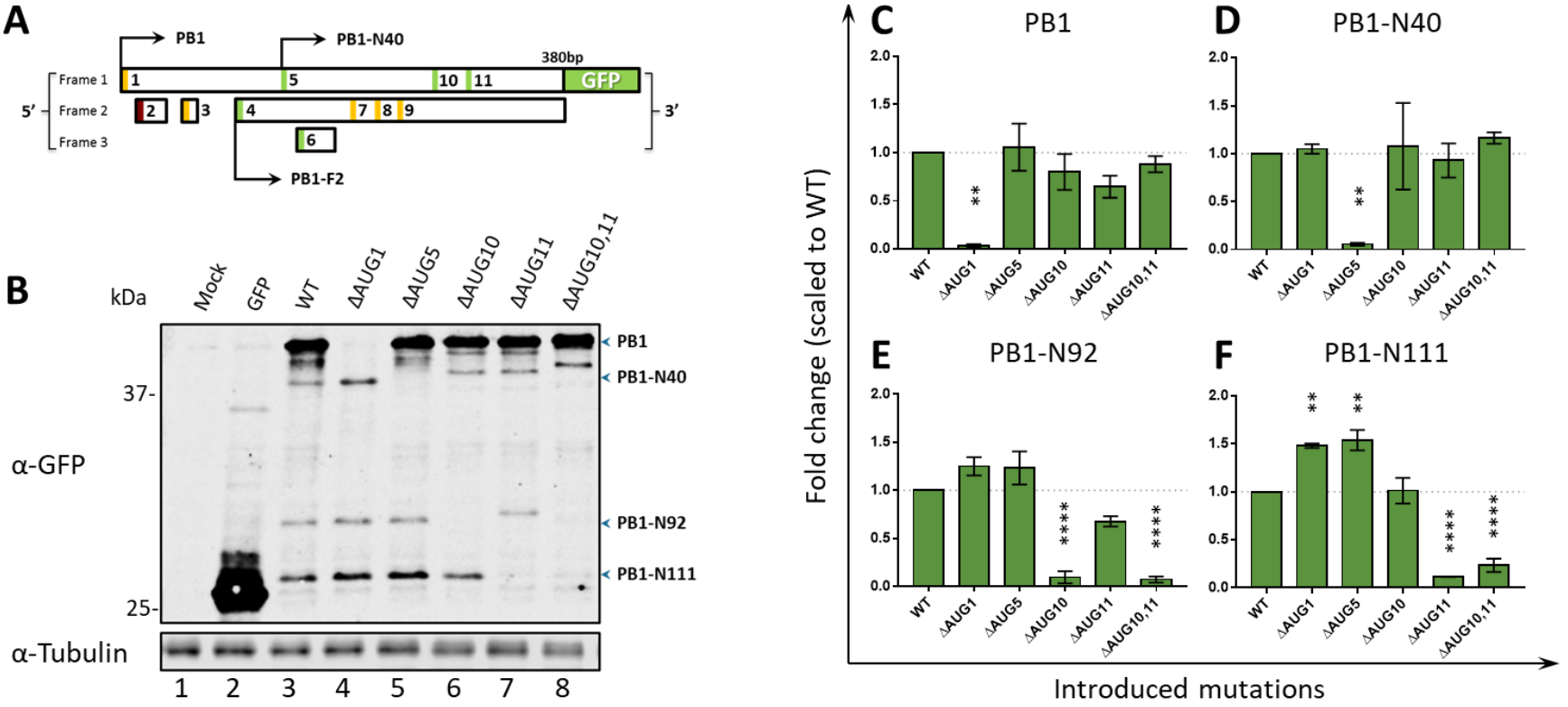

Figure 2.2. Expression of PB1 related species cDNA in transfected cells. 293T cells were transfected with a panel of GFP-fusion plasmid for 48 hours. (A) Diagram of the AUG codon and ORF structure of the 5' end of PR8 segment 2 mRNA with GFP fused into frame 1. The position of molecular mass markers (in kDa) is indicated on the left. (B) Lysates from cells transfected (or mock transfected) with the indicated panel of plasmids were analysed by western blot with anti-GFP serum; α-tubulin was used as loading control. Quantification of the relative expression of the different PB1-related products, PB1 (C), N40 (D), N92 (E) and N111 (F), was performed by densitometry following single technical repeats from three independent experiments. Statistic annotations are the result of an ordinary one-way ANOVA test. *p-value <0.05, **p-value <0.01, ****p-value <0.0001.

Table 2.1. Summary of segment 2 frame 1 mutants. Nucleotide, codon and amino acid changes resulting from the mutations in each construct are given, as well as a prediction of the expressed polypeptides.

Construct	Nucleotide changes	Codon changes	Predicted frame 1 products			
			PB1	PB1-N40	PB1-N92	PB1-N111
ΔAUG1	A25U	AUG- UUG	Null	WT	WT	WT
ΔAUG5	A142U	AUG-UUG	M40L	Null	WT	WT
ΔAUG10	A298G	AUG-GUG	M92V	M53V	Null	WT
ΔAUG11	A355G	AUG-GUG	M111V	M72V	M20V	Null

expressed when AUG 10 was mutated (lane 6). Likewise, the 28kDa product largely disappeared when AUG 11 was deleted (lane 7) and the amounts of both polypeptides were markedly reduced after the simultaneous deletion of AUGs 10 and 11 (lane 8). These data suggested that protein expression was initiated from AUGs 10 and 11. Consistent with previous nomenclature, the AUG 10 and 11 initiated polypeptides were named PB1-N92 and PB1-N111 respectively, considering the predicted omission of the first 91 and 110 amino acids of WT PB1, respectively.

Quantification of the individual peptide species by densitometry from this and replicate experiments showed that the above pattern was reproducible (Figures 2.2 C-F), further supporting the conclusion that AUGs 10 and 11 directed translation initiation. The amounts of the remaining PB1 fusion products were not generally affected by mutation of another start codon, except for a small but statistically significant increase in PB1-N111 accumulation after mutation of AUGs 1 or 5 (Figure 2.2F).

2.2.2. Generation of PR8 segment 2 mutant viruses

After detecting the expression of further N-terminally truncated PB1 polypeptides from transfected DNA, we asked if the same products could be detected in virus-infected cells and if so, whether loss of their expression would have an impact on viral fitness. To address these questions, reverse genetics was used to create segment 2 mutant viruses in the PR8 background. 293T cells were co-transfected with eight PR8 pDUAL plasmids individually encoding a different IAV segment

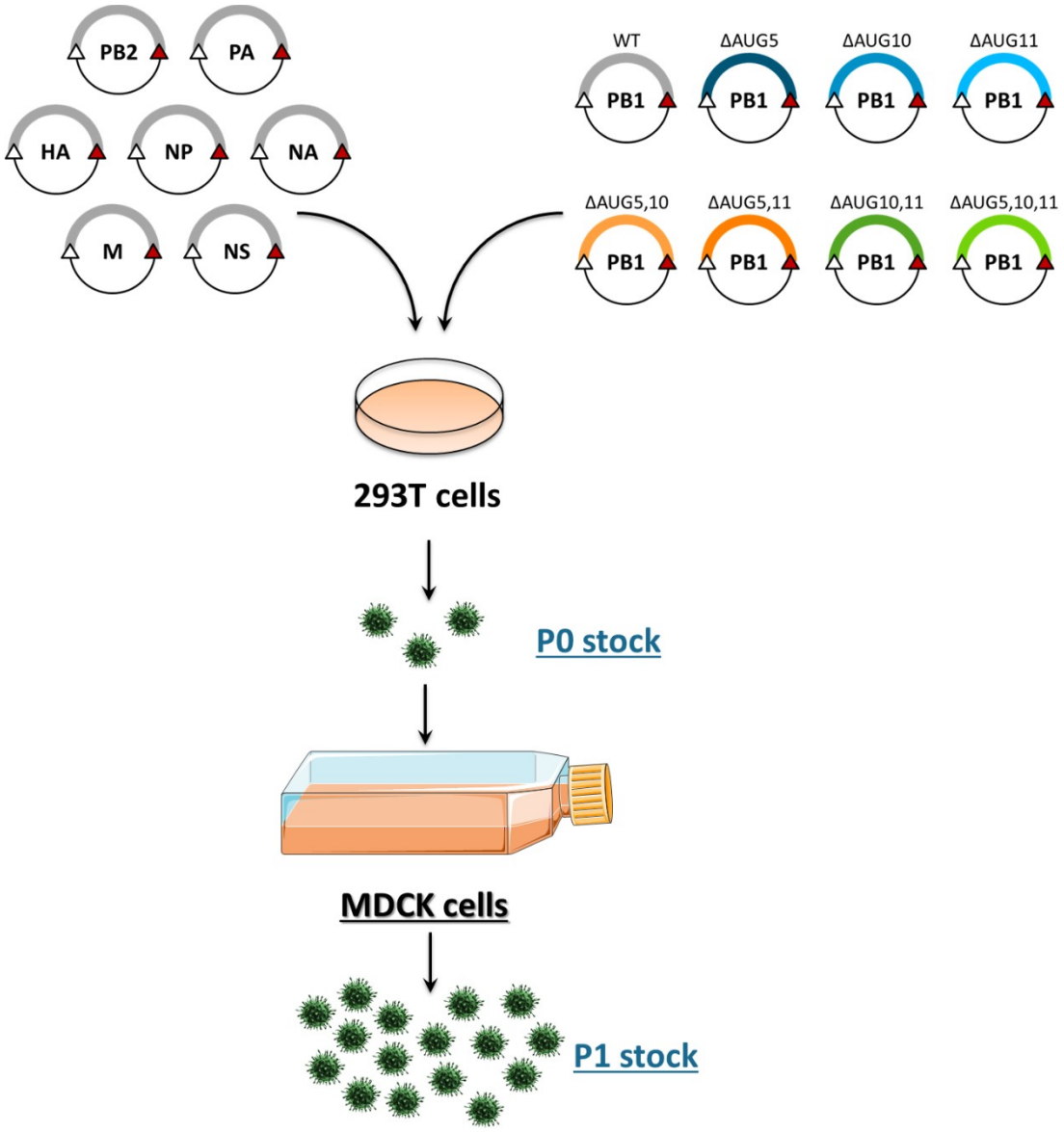

Figure2.3. Scheme of reverse genetics system. 293T cells were co-transfected with 8 pDUAL plasmids, each driving the production of mRNA and 'vRNA-like' RNA from pPolII (△) and pPolI (▲) promoters, respectively from each segment of the IAV genome.

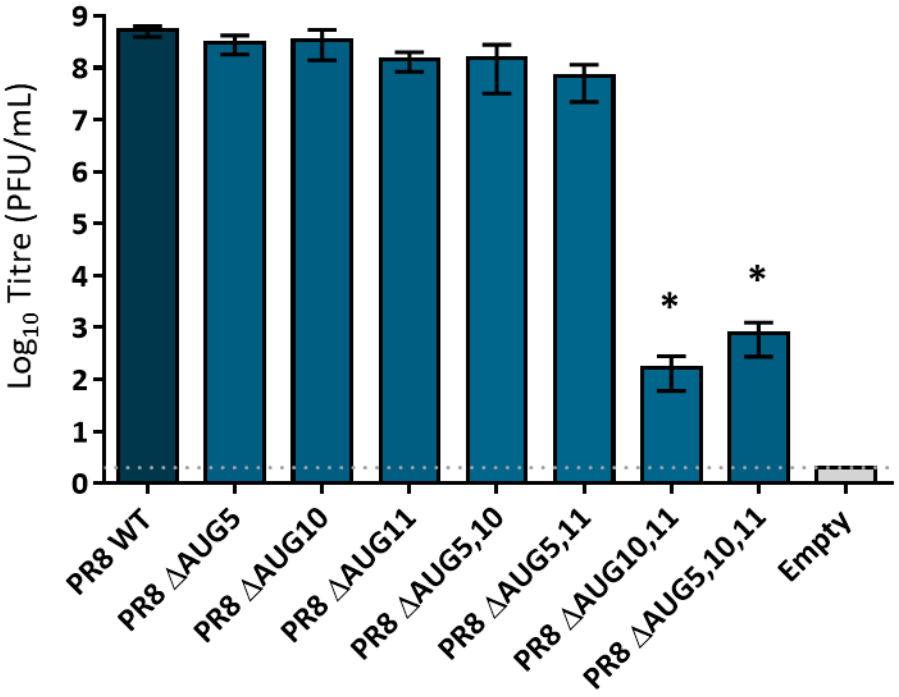

Figure 2.4. Growth of PR8 segment 2 mutant viral stocks. MDCK cell monolayers were infected at low MOI (<0.01). Supernatants were cleared, stored and titrated by plaque assay at 48 hpi. Data represent the mean ± SEM of at least two independently rescued virus stocks. Statistic annotations are the result of an ordinary one-way ANOVA test. *p-value <0.05.

(de Wit *et al.* 2004). These plasmids contain both RNA polymerase II (polII) and RNA polymerase I (polI) promoters, which facilitate the expression of mRNA (leading to IAV protein translation) as well as the production of 'vRNA-like' RNA, essential for genome replication (Hoffmann *et al.* 2000). Mutant segment 2 plasmids harbouring 'ΔAUG' mutations in which start codons were changed to leucine or valine codons (Table 2.1) were generated by site-directed mutagenesis and used to replace the WT segment 2 plasmid. These mutant plasmids included ones with individual AUG alterations (ΔAUG5, ΔAUG10 and ΔAUG11), three with double mutations (ΔAUG5,10, ΔAUG5,11 and ΔAUG10,11) and a triple mutant (ΔAUG5,10,11). A negative control transfection was included where segment 2 was replaced by an empty pDUAL plasmid vector and which therefore should have been unable to generate viable virus particles. Wild-type PR8 plasmids were used as a positive control and to generate a comparator WT virus. Forty-eight hours after transfection, cell supernatants were collected. These were termed 'P0 stocks' (Figure 2.3). These stocks were used to infect MDCK cells at low MOI (<0.01) and propagated for an additional 48 hours to generate P1 stocks which were clarified, titrated by plaque assay and used for subsequent experiments. In independent (including the virus rescue stage) replicate experiments the empty plasmid negative control did not produce detectable levels of virus (the limit of detection was 2 PFU/mL), while PR8 WT replicated to an average titre of over 10^8 PFU/mL (Figure 2.4). Individual mutation of AUG codons 5, 10 or 11 did not alter the levels of virus output compared to the WT virus. Comparable, although slightly lower titres were also seen for the double mutant viruses ΔAUG5,10 and ΔAUG5,11. However, the simultaneous mutation of AUG codons 10 and 11 resulted in a severe (~10^6-fold) reduction of the P1 viral titres to around 10^3 PFU/mL.

The same drop in titre was seen with the triple mutant ΔAUG5,10,11 (Figure 2.4). These results provided the first evidence for a role for AUG codons 10 and 11 in determining viral fitness.

In parallel, RNA extractions were performed on P1 supernatants followed by RT-PCR and Sanger DNA sequencing of segment 2, which confirmed the presence of AUG mutations (data not shown). The produced virus stocks were not plaque purified and therefore can be considered a mixed population. Nevertheless, stocks were only passaged once from the respective P0, the performed Sanger sequencing didn't show any additional mutations than the ones purposefully introduced, and plaque assays performed showed uniform, size-consistent plaques.

2.2.3. Viral protein synthesis in infected mammalian cells

In order to determine whether PB1-N92 and PB1-N111 were expressed in the context of virus replication, the WT and the majority of the mutant viral stocks were used to infect MDCK cells at a MOI of 10. The ΔAUG10,11 and ΔAUG5,10,11 mutants were not tested because the stock titres were too low to carry out high MOI infections. Seven hours post infection (hpi), the cells were pulsed with ^{35}S-methionine and at 8 hours, cell lysates were collected and fractionated by SDS-PAGE followed by autoradiography. No viral components were detected in mock-infected samples (Figure 2.5A, lane 1), whereas all infected samples showed expression of the major viral components: the RdRP, HA, NP, M1 and/or NS1 (lanes 2-7). Expression of these proteins was comparable between PR8 WT and the various segment 2 mutants.

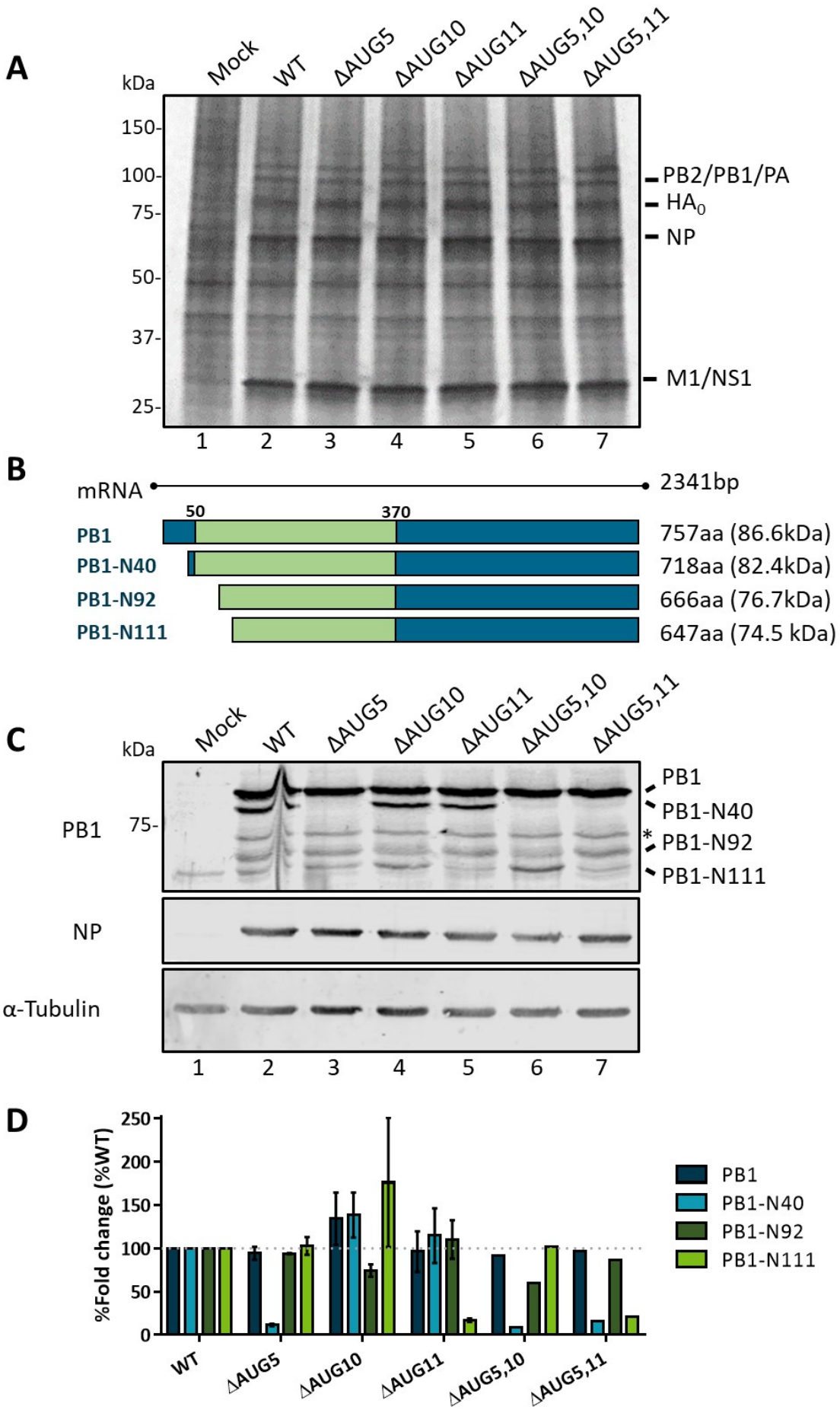
A
Mock
WT
ΔAUG5
ΔAUG10
ΔAUG11
ΔAUG5,10
ΔAUG5,11
kDa
150-
100-
75-
50-
37-
25-
PB2/PB1/PA
HA0
NP
M1/NS1
1 2 3 4 5 6 7
B
mRNA
2341bp
50
370
PB1
PB1-N40
PB1-N92
PB1-N111
757aa (86.6kDa)
718aa (82.4kDa)
666aa (76.7kDa)
647aa (74.5 kDa)
C
Mock
WT
ΔAUG5
ΔAUG10
ΔAUG11
ΔAUG5,10
ΔAUG5,11
kDa
PB1
75-
NP
α-Tubulin
PB1
PB1-N40
*
PB1-N92
PB1-N111
1 2 3 4 5 6 7
D
%Fold change (%WT)
250
200
150
100
50
0
WT
ΔAUG5
ΔAUG10
ΔAUG11
ΔAUG5,10
ΔAUG5,11
PB1
PB1-N40
PB1-N92
PB1-N111

Figure 2.5. Protein synthesis by PR8 WT and mutant viruses in mammalian cells. (A) A549 cells were infected at a MOI of 10, metabolic labelling was performed using ^{35}S protein labelling between 7 and 8 hpi after which cell lysates were collected. Lysates were subjected to SDS-PAGE and radiolabelled proteins were detected by autoradiography. (B) Schematic of the expression and respective sizes of PB1-related peptides. mRNA and proteins are represented by lines and blue rectangles, respectively. Green areas represent the potential V19 antibody binding region (from residues 50 to 370 of PB1). (C) The lysates used in (A) were used to detect PB1-related polypeptides by western-blot. NP was blotted as an infection control and alpha tubulin was used as a loading control. (D) Densitometric quantification of the different PB1-related polypeptides from infected cells. Bands were quantified in ImageJ and background levels from the mock-infected sample were subtracted from the original values, before scaling to WT values. Data represent the mean of single technical repeats of two independent experiment for WT and single mutant viruses or simply one for the double mutants ΔAUG5,10 and ΔAUG5,11. In cases where two independent experiments are plotted, error bars represent SEM.

The same lysates were also subjected to western blot analysis using an anti-PB1 serum raised against amino acids 50-370 of PB1 - V19 (Digard *et al.* 1989). As the majority of the epitope residues are common to PB1 and the family of shorter products (Figure 2.5B), V19 would be expected to detect all of them. Additional controls included the detection of α-tubulin as loading control, and NP was blotted to confirm infection. As earlier observed in Figure 2.5A, NP levels were consistent throughout all the segment 2 mutants. Blotting with the α-PB1 V19 antibody revealed similar expression of the main product, PB1, for all the viruses (Figure 2.5C. PB1-N40 (82.4kDa) was also strongly detected in WT virus-infected cells but absent in samples in which its initiator codon, AUG5, was mutated (lanes 3, 6 and 7). Also visible on the blot was a pattern of shorter polypeptides migrating faster than the 75 kDa molecular mass marker two of which were clearly virus-specific and one (the fastest migrating) which was also present in lower abundance in the mock-infected sample. The amount of the largest of these polypeptide species (marked with an asterisk on Figure 2.5C) was unaffected by any of the AUG mutations. However, the band pattern for the middle species (labelled as PB1-N92, predicted molecular mass of 76.7kDa) showed a subtle reduction following AUG10, mutation while the smallest band (PB1-N111, predicted molecular mass of 74.5kDa) showed a rather clearer lowering of staining intensity in samples from viruses lacking AUG11.

Densitometric analysis of replicate blots provided a more quantitative confirmation of this visual assessment (Figure 2.5D). Given the presence of a background product migrating similarly to PB1-N111 in mock-infected cell samples, the density of this band was subtracted from the values for PB1-N111 bands from infected samples. This analysis showed predictable fluctuations in the heights of the

various peaks according to which AUG codon had been mutated. However, while the deletion of AUGs 5 and 11 resulted in an 80-90% reductions in PB1-N40 and PB1-N111 expression respectively, mutation of AUG10 led to a weaker reduction (~ 30-50%) in accumulation of the putative PB1-N92 polypeptide.

Overall, data from this section suggested that segment 2 AUG11 was used for translation initiation in the context of virus infection. However, evidence for use of AUG10 was more equivocal.

2.2.4. Propagation of segment 2 mutant viruses in mammalian cells

To better understand the impact of mutating AUGs 10 and 11 on viral fitness in mammalian systems, growth kinetic analyses were performed. MDCK cells were infected with the panel of viruses at a MOI of 0.001, samples were collected at several times post infection and titrated by plaque assays. No virus was detected in mock infected controls (data not shown). In MDCK cells, PR8 WT reached titres of 10^8 pfu/mL by 24 hpi and then plateaued, and individual mutation of AUGs 5, 10 or 11 did not affect viral replication at any point post infection (Figure 2.6A). The double mutant ΔAUG5,10 virus also showed a WT-like growth pattern, while the ΔAUG5,11 virus showed a statistically significant attenuation at 24 hpi, but nevertheless reached WT-like titres by 36 hpi (Figure 2.6B). In contrast, both the PR8 ΔAUG10,11 and the triple mutant ΔAUG5,10,11 viruses grew only slightly more slowly than WT virus until 8-12 hpi but then showed a strongly attenuated phenotype with ~1000-fold reductions in titre between 24-48 hpi (Figure 2.6C).

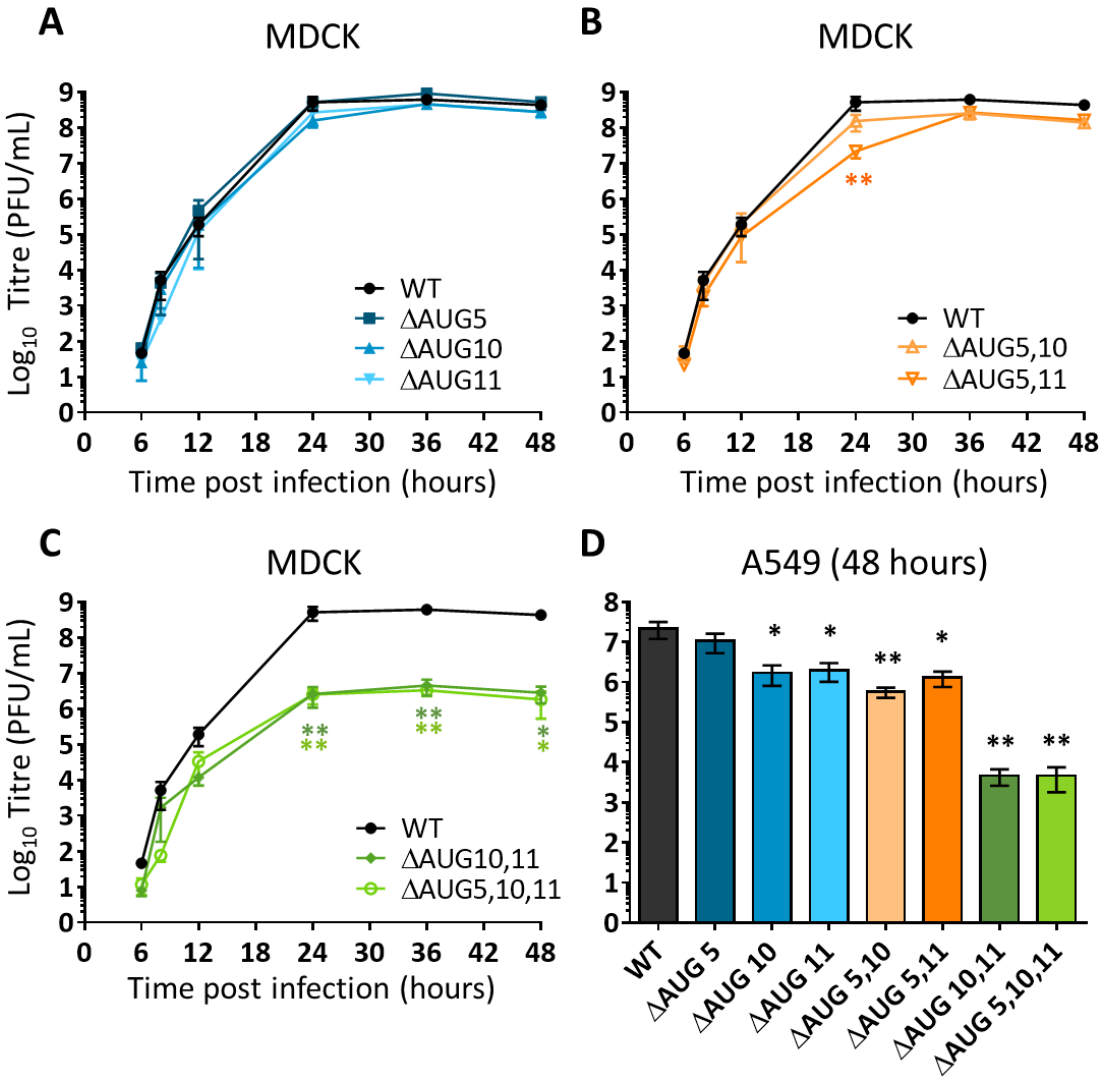

Figure 2.6. Growth kinetic analyses of PR8 WT and mutant viruses in mammalian cells. MDCK and A549 cells were infected at a MOI of 0.001 and samples were collected at the indicated times post infection. PR8 WT results are duplicated between panels A-C for comparison. Data represent the mean ± SEM of single technical repeats of three independent experiments. Statistic annotations are the result of an ordinary one-way ANOVA test (performed individually for each time-point). *p-value <0.05, **p-value <0.01.

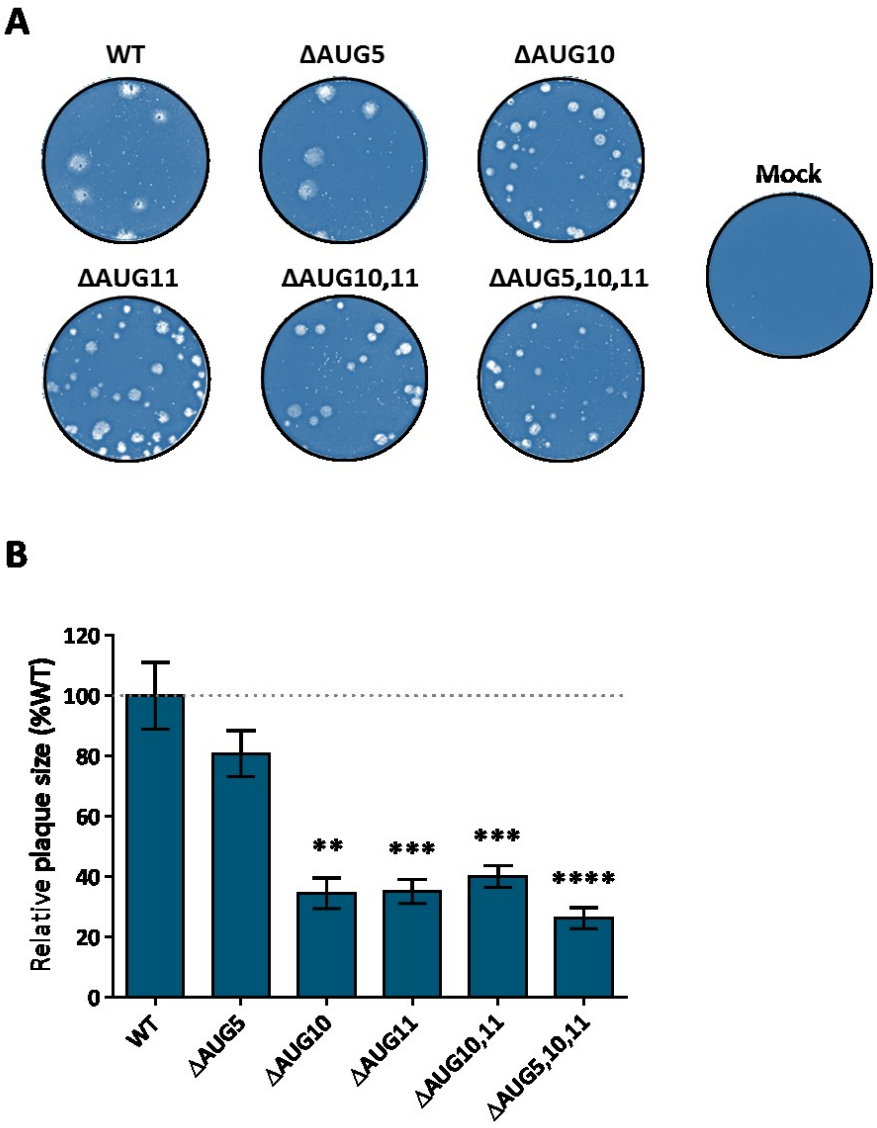

Figure 2.7. Plaque morphologies of PR8 WT and mutant viruses. Representative images of PR8 WT and mutant virus plaque phenotypes in MDCK cells (A) and quantitative measurements of the plaque area for each virus (B). A minimum of 50 plaques from two independent experiments were measured for each mutant virus. Statistic annotations are the result of an ordinary one-way ANOVA test. Multiple comparisons were performed against PR8 WT. **p-value <0.01, ***p-value <0.001, ****p-value <0.0001.

As a further test of virus fitness in mammalian cells, growth in A549 cells was assessed at 48 hpi. In this cell line, PR8 WT titres reached 10^7 PFU/mL and although the single mutant ΔAUG5 did not quite reach this value, it was not significantly lower (Figure 2.6D). However, in this system, discrete ΔAUG10 and ΔAUG11 mutations led to 10-fold reductions in viral titre. A comparable 10-fold attenuation was also observed for the ΔAUG5,10 and 5,11 mutant viruses. Similarly to the MDCK growth kinetic analysis, double mutant ΔAUG10,11 and the triple mutant ΔAUG5,10,11 showed a 1000-fold decrease in viral titre at 48 hpi.

To further characterise the capacity of the mutant viruses to spread, virus propagation was assayed by assessing their ability to form lytic plaques within a cell monolayer. MDCK cells were infected with 10-fold serial dilutions of P1 viral stock and incubated under a semi-solid overlay medium. 48 hpi, cells were fixed and plaques visualised by toluidine blue staining. Plates were scanned and cell-absent areas were measured in ImageJ. WT PR8 virus gave the largest plaque size (Figure 2.7A). Plaques produced by the PR8 PB1-N40 knockout virus (ΔAUG5) appeared similar in size. However, single mutation of AUG10 or AUG11 produced an obviously smaller, although somewhat variable plaque phenotype compared with WT PR8. The same level of reduction was also found in the double (ΔAUG10,11) and triple (ΔAUG5,10,11) mutants. These observations were confirmed by quantification of the plaque size, which showed that, with the exception of ΔAUG5, the mutant viruses produced statistically significantly smaller plaques than the WT virus (Figure 2.7B).

Overall, growth kinetics and plaque phenotype data confirmed the importance of segment 2 AUG codons 10 and 11 in supporting PR8 virus replication *in vitro*.

2.2.5. Fitness of segment 2 mutant viruses in avian systems

The PR8 strain used in this study is a descendant of the National Institute of Biological Standard and Control's vaccine strain that had been passaged six times in MDCK cells before cloning (de Wit *et al.* 2004). However, prior to that, the virus had had a long history of adaptation to growth in embryonated hens' eggs. In this setting, viral progeny is largely a result of replication in the chorioallantoic membrane, mostly composed of endothelial and mesenchymal cells (Ribatti 2016). Therefore, to test the effects of mutating segment 2 AUG codons on virus replication in this *in vivo* avian system, 100 PFU of each virus was introduced into 10-day old eggs. Studies of IAV growth in eggs have typically been measured at 48 hpi (Wise *et al.* 2009; James *et al.* 2016). However, in initial experiments using this time point, plaque phenotype and subsequent sequence analyses showed that reversion of the mutated AUG10 and AUG11 codons (particularly AUG11) from GUG back to AUG had occurred (data not shown). Accordingly, to reduce the likelihood and/or impact of such reversion events, in subsequent experiments both allantoic fluids and embryos were harvested and virus titres measured at 24 hpi. At this time point, instances of reversion were greatly reduced and the majority of the egg-grown viruses did not show restoration of altered AUG codons (data not shown). In cases where reversion was detected, samples were excluded from the analysis.

When grown in eggs, PR8 WT reached average titres of 3×10^9 PFU/mL in allantoic fluid, and 7×10^5 PFU/mL in macerated embryos, albeit with a wide range of variation between individual eggs (Figure 2.8). PR8 ΔAUG5 replicated to comparable titres to the WT virus in allantoic fluids (Figure 2.8A), consistent with previous data

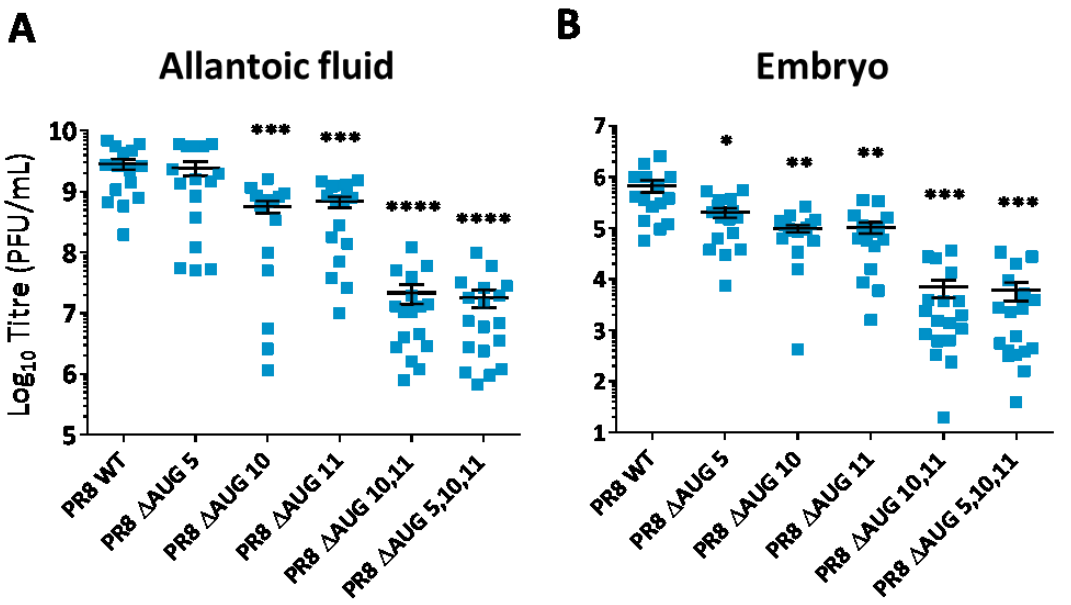

Figure 2.8. Viral fitness *in ovo*. Ten day old hen eggs were infected with 100 PFU of PR8 WT or mutant viruses and viral titres of the allantoic fluids (A) and embryos (B) were acquired by plaque assay 24 hpi. Data points represent titres for each individual egg as well as mean ± SEM. Three independent experiments were performed with 4-6 eggs infected with each virus. Statistic annotations are the result of an ordinary one-way ANOVA test. Multiple comparisons were performed against PR8 WT. *p-value <0.05, **p-value <0.01, ***p-value <0.001, ****p-value <0.0001.

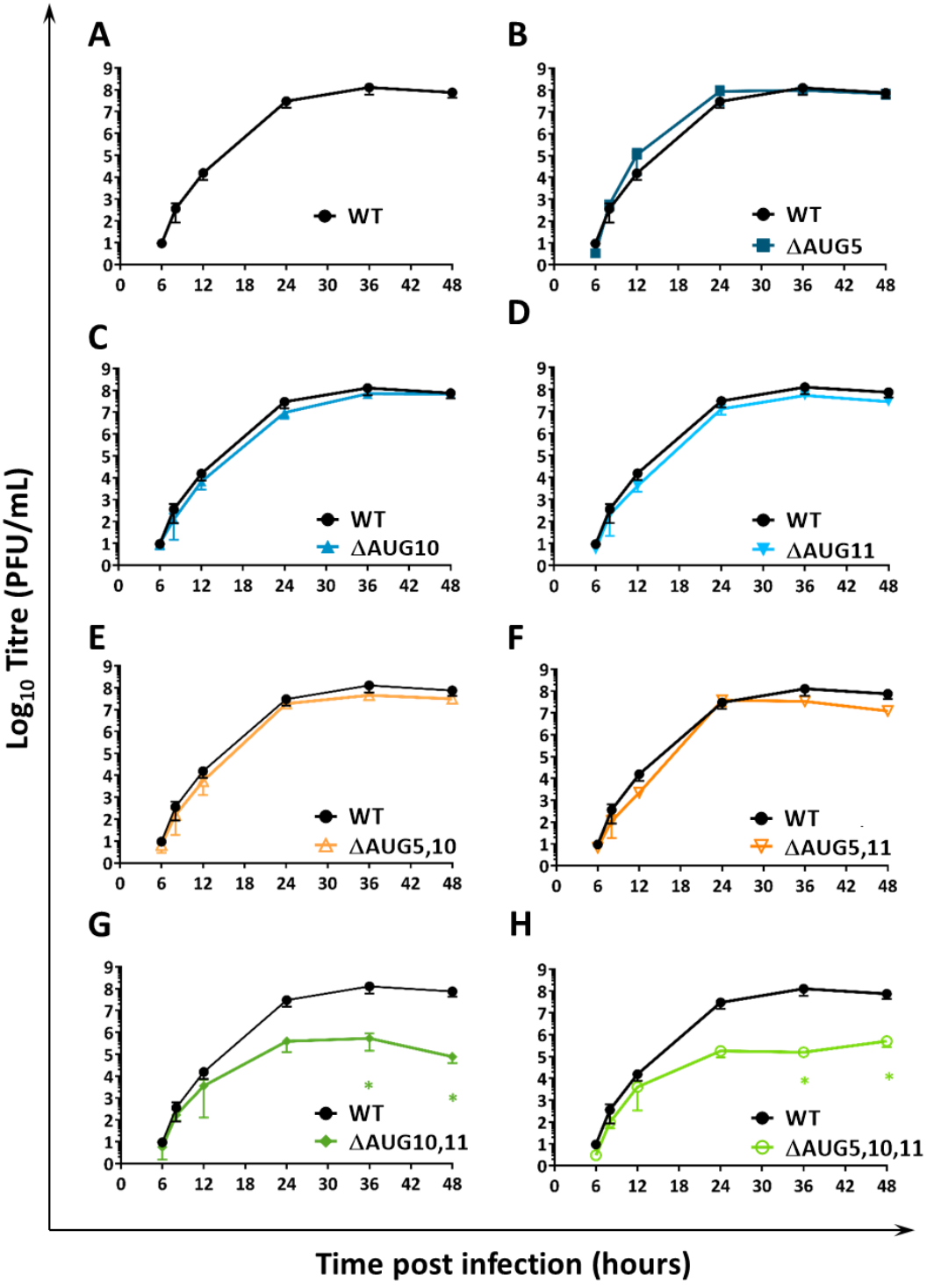

Figure 2.9. Growth kinetic analyses of PR8 WT and mutant viruses in QT-35 cells. Cells were infected at a MOI of 0.001 and samples were collected at the indicated times post infection. Data are mean ± SEM of single technical repeats of four independent experiments. PR8 WT results are duplicated across panels for comparison. Statistic annotations are the result of an ordinary one-way ANOVA test (performed individually for each time-point). *p-value <0.05.

from 48 hpi (Wise *et al.* 2009). However, replication of this mutant in embryos was marginally but significantly reduced, reaching an average titre of 2×10^5 PFU/mL (Figure 2.6B). In contrast to results obtained in MDCK cells, but similar to the A549 multicycle system (Figure 2.6A and B), the single AUG mutants PR8 ΔAUG10 and ΔAUG11 were attenuated in both allantoic cavity and embryos compared with WT PR8. The double and triple mutants PR8 ΔAUG10,11 and PR8 ΔAUG5,10,11 also showed lower levels of replication, producing 2-2.5 $\log_{10}$ less virus than WT PR8. Thus mutation of segment 2 AUG10 and/or 11 also led to a loss of virus fitness *in ovo*.

Given the pattern of gradually decreased titres from infected eggs and mammalian cells with the deletion of sequential segment 2 AUGs, it was hypothesised that this effect would be host species-independent and therefore also seen in avian cell lines. Accordingly, kinetic analyses were performed in quail fibroblast (QT35) cells. Confluent cell monolayers were infected at a MOI of 0.001, supernatants were collected at 6, 8, 12, 24, 36 and 48 hpi and titrated by plaque assay. Both PR8 WT and ΔAUG5 showed similar growth kinetics, reaching a maximum of 2×10^8 PFU/mL at 36 hpi (Figure 2.9A, B). Contrary to the observation in egg allantoic fluid and homogenized chick embryos, the single mutants PR8 ΔAUG10 and PR8 ΔAUG11 did not show any attenuation in quail fibroblasts, reaching similar titres to PR8 WT (panels C, D), and nor did their combination with ΔAUG5 affect virus growth (panels E, F). On the other hand, consistent with all the replication models tested so far, the double deletion of AUGs 10 and 11 conferred a significant loss of replication fitness on the PR8 strain (panels G, H). Thus, although the sequential decrease in viral fitness from mutating increasingly 3'-wards AUG codons in segment 2 was not seen in quail

fibroblasts, attenuated viral replication was observed when both AUGs 10 and 11 were removed.

Overall, endpoint and kinetic data acquired from hen's eggs and quail fibroblasts supported the results from mammalian systems and reinforced the importance of segment 2 AUG codons 10 and 11 to virus fitness. Moreover, the genetic reversion of AUG 10 and/or 11 mutations detected in hen's eggs further implied a critical role for these PB1 methionine codons in the IAV life cycle.

2.2.6. Evaluation of the polymerase function of mutant PB1 proteins

As shown in both mammalian and avian systems, simultaneous mutation of segment 2 AUG codons 10 and 11 led to a severe decrease in viral fitness. Two possible explanations for this were considered next:

1. The proteins whose translation is initiated at AUG codons 10 and 11 play important roles during the IAV life cycle and their cumulative loss leads to a deficit in viral fitness.
2. Alteration of AUG codons 5, 10 and 11 required the introduction of amino acid mutations within the PB1 protein: namely mutation of methionine at position 40 to a leucine as well as methionine residues 92 and 111 to valines (Table 2.1). As PB1 is the core subunit of the trimeric RdRp, these mutations could lead to altered polymerase transcription or replication activities and thus result in the observed deficits in viral propagation.

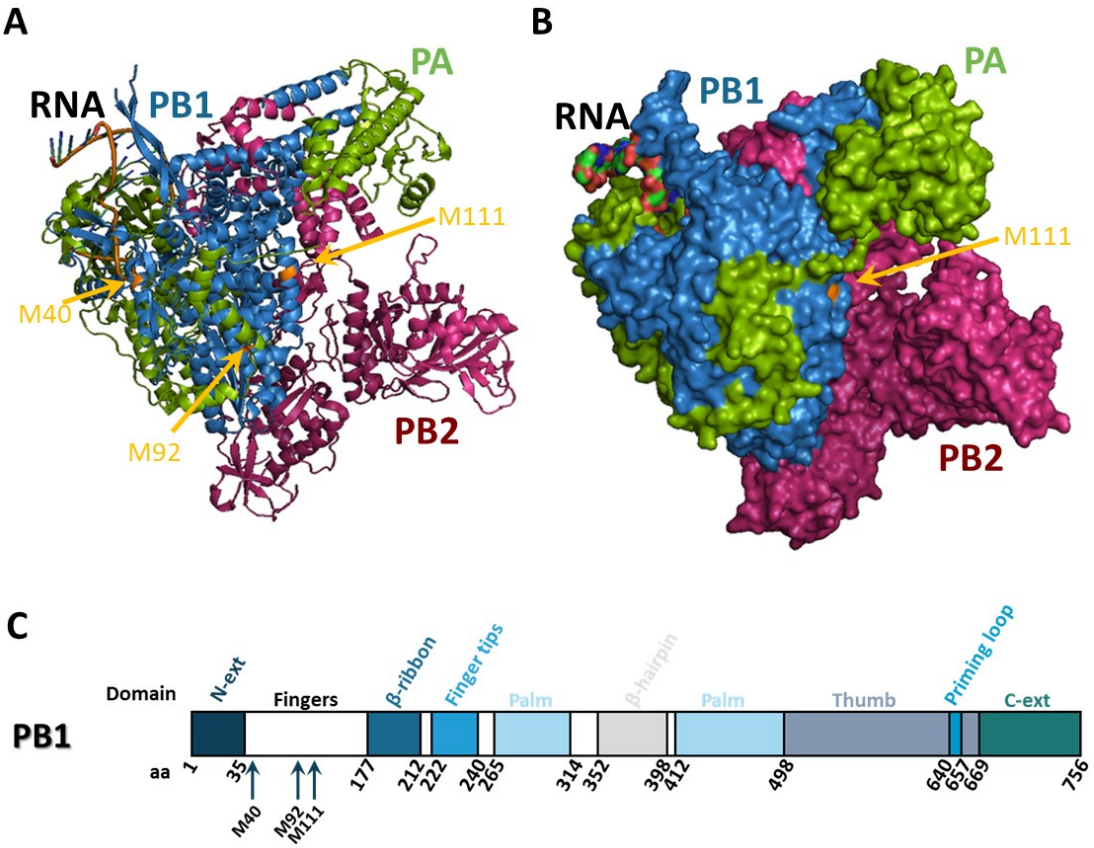

Figure 2.10. Polymerase structure and PB1 domain organisation. The structure of the trimeric IAV RdRp with vRNA promoter is depicted as ribbon (A) and surface (B) representations. The three polymerase subunits are colour coded: PB1-blue, PB2-magenta, PA-green. In (A), spirals represent α-helices and arrows represent β-sheets. Amino acids M40, M92 and M111 are also mapped on the structure and annotated in amber. (C) A diagram of the domain organisation of PB1 with annotated residue positions is also shown (Pflug *et al.* 2014). Influenza virus PB1 core subunit displays a typical viral RdRp domain organisation possessing, among others, 'fingers', 'palm' and 'thumb' regions. 'N-ext' and 'C-ext' represent the N- and C-ends of the protein, respectively. Amino acids M40, M92 and M111 are also annotated and belong to the first "fingers" region.

The crystal structure of a complete heterotrimeric bat influenza A polymerase bound to the vRNA promoter has been published, revealing similarities between the influenza RdRp and previously published viral polymerase structures (Pflug *et al.* 2014). In particular, the PB1 central region (residues 21-669) shows a close resemblance to the typical right-handed RdRp fold which has been observed for other single-stranded RNA viruses such as hepatitis C or Norwalk viruses. This structure comprises fingers, fingertips, palm and thumb domains. PB1 methionine residues 40, 92 and 111 were mapped on this RdRp crystal structure and were shown to localise to the PB1 fingers domain, with M111 being present at the surface of the enzyme (Figure 2.10). Thus, alteration of any or all of the AUGs 5, 10 or 11 could be functionally important for PB1 function.

As described in chapter 1, IAV genome replication and transcription occur in the host cell nucleus and require the formation of the RNP complex, constituted by the heterotrimetric polymerase in conjunction with the nucleoprotein and viral RNA (Portela and Digard 2002; Huang *et al.* 1990). Therefore, in order to determine whether the introduced mutations affected PB1 polymerase activity, RNP reconstitution reporter assays were performed. Plasmids encoding PR8 segment 2 mutants were introduced into highly transfectable 293T cells along with the wild type PB2, PA and NP segments as well as synthetic vRNA (containing negative–sense firefly luciferase or GFP coding regions flanked by the IAV UTRs) reporter plasmids (Lutz *et al.* 2005) (Figure 2.11 A-C). In these systems, measurement of luciferase expression or fluorescence levels are assumed to be directly related to viral mRNA levels and thus polymerase transcription activity. When using the GFP reporter plasmid, an empty eGFP-N1 plasmid was used as a positive control which consistently produced strong

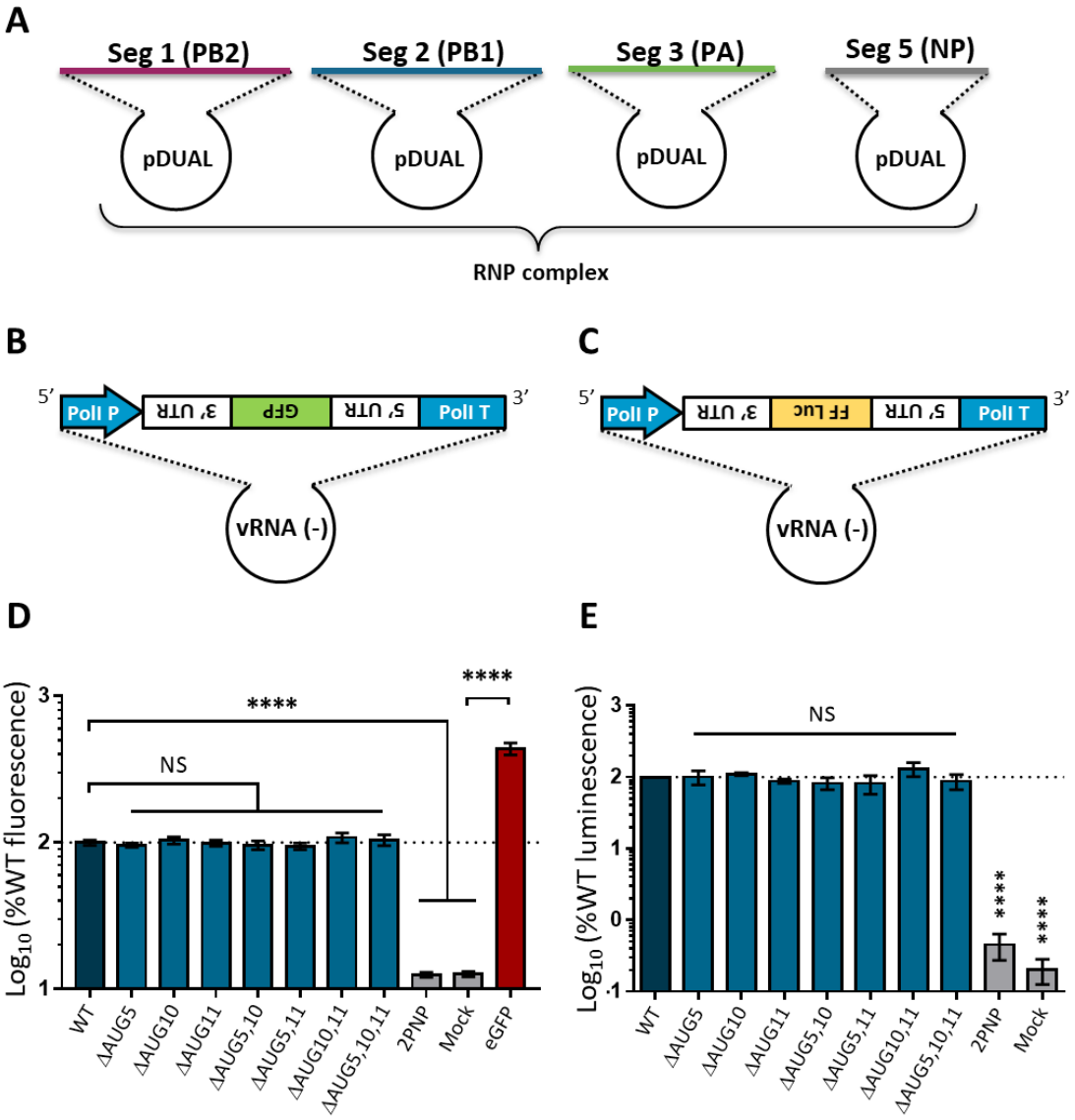

Figure 2.11. Mutant PB1s transcription activity. 293T cells were co-transfected with pDUAL PR8 plasmids expressing the protein components of the vRNP complex: PB2, PB1, PA and NP (A) alongside PolI driven reporter plasmids expressing negative strand vRNA-like GFP or firefly luciferase RNA (B and C; PolI T indicates an PolI transcription terminator sequence) to measure polymerase transcription activity (D and E). Fluorescence or luciferase activity were measured 48 hours post-transfection. In D, eGFP-N1 empty plasmid was used as a positive control. Data represent the mean ± SEM of three technical repeats from at least three independent experiments. Statistic annotations are the result of an ordinary one-way ANOVA test. ****p-value <0.0001.

fluorescence values (Figure 2.11D). A transfection control such as a plasmid overexpressing *Renilla* luciferase was not included, once the components of the polymerase have protein shut-off activity which could skew the ratios between the measurements.

In the presence of WT RNP proteins, there was high level expression of fluorescence or luciferase (Figure 2.11D, E respectively), to which all the other measurements were scaled to. In the absence of PB1 segment (2PNP), there was a statistically significant decrease in reporter gene expression to background levels. However, regardless of the reporter plasmid system used, none of the PB1 mutants showed a significant difference in gene expression activity compared to WT PB1.

As these assays were carried out with a single dose (50ng) of PB1 plasmid which could have potentially saturated the system, the same type of analysis was performed in a PB1 plasmid dose-dependent manner. In order to achieve this, the amounts of PB2, PA, NP and reporter plasmids were kept unchanged, but the PB1 plasmid was titrated and the output luciferase expression values were fitted to a variable slope dose-response model. Luciferase measurements of samples of the 50ng dose of PB1 plasmids was used as maximum control (Figure 2.2A). The resulting curve for WT PB1 showed a plateau phase which reached 1 ng (suggesting that the original experimental setup could indeed have had saturating amounts of PB1), after which luciferase readings decreased with the reduction of added PB1 plasmid. Luciferase activity of the lowest dose of PB1 plasmid represented 0.1% of the original 50ng dose. The curve for the AUG5 mutant virtually overlapped that of the WT enzyme (Figures 2.12A), while when AUG10 or 11 were mutated, the mutant curves

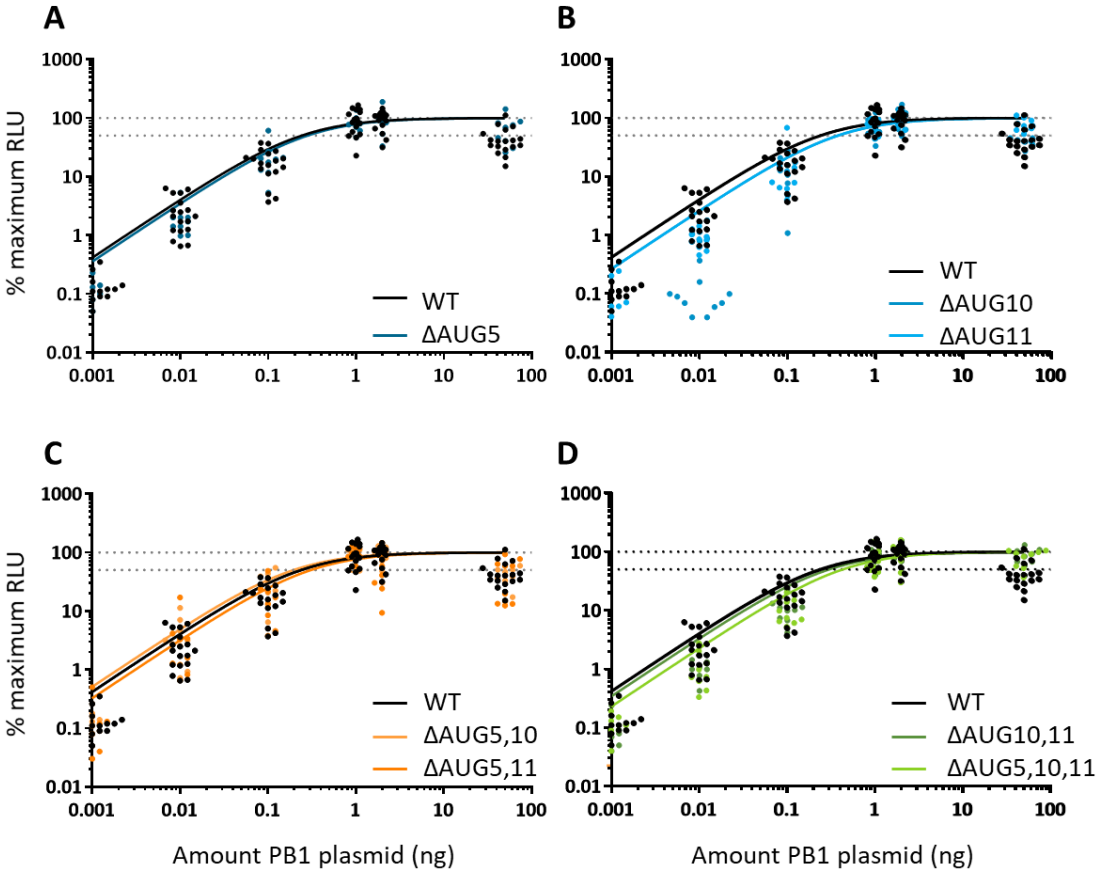

Figure 2.12. Measurement of dose-dependent transcription activity. Luciferase activity was measured from RNP reconstitution assays in which the PB1 plasmid was titrated and all other plasmids kept constant. Normalisation was performed to the maximum luminescence within each individual titration set. Grey dashed lines indicate 100% and 50% of the maximum of each individual data set. PB1 WT results were duplicated for comparison. Data points represent individual measurements, while lines are minimum squares curve fits. At least four independent experiments were performed each one with three technical repeats.

were shifted only slightly to the right of WT (Figures 2.12B). Small shifts were also observed when either AUG10 or AUG11 were mutated in combination with AUG5 (Figure 2.12 C). Notably, the ΔAUG10,11 double mutant and the triple ΔAUG5,10,11 mutant also gave curves that were very similar to that of WT PB1 (Figure 2.12D). The half maximal effective concentrations (EC_{50}) values for the various PB1 plasmids were estimated from the curve fits, showing that all constructs were less than 2-fold different to the WT, including the most defective (in terms of overall virus fitness) ΔAUG5,10,11 enzyme (Table 2.2). None of these differences were statistically significant, with wide overlaps of the 95% confidence intervals. However, variability in the replicate data points led to overall low R^2 values for the curve fits, so although the conclusion that any of the mutants differed from the WT protein with regards to transcriptional activity could not be drawn, the possibility of small differences remained.

To further probe the function of the mutant PB1 polypeptides, the same RNP reconstitution assays were performed using a firefly luciferase cRNA-like reporter plasmid (Figure 2.13A). In this version of the assay, viral mRNA can only be produced after the input cRNA molecules have been replicated to provide a vRNA template, so the system interrogates genome replication as well as transcription. Cells were transfected with the RNP components as before, lysed 24 hours later and luciferase expression levels measured. As expected, transfection with WT PR8 components resulted in high levels of luciferase expression, around 5000-fold greater than compared to the 2PNP negative control lacking PB1 (Figure 2.13B). However, all the segment 2 mutants had a WT-like polymerase phenotype in this system.

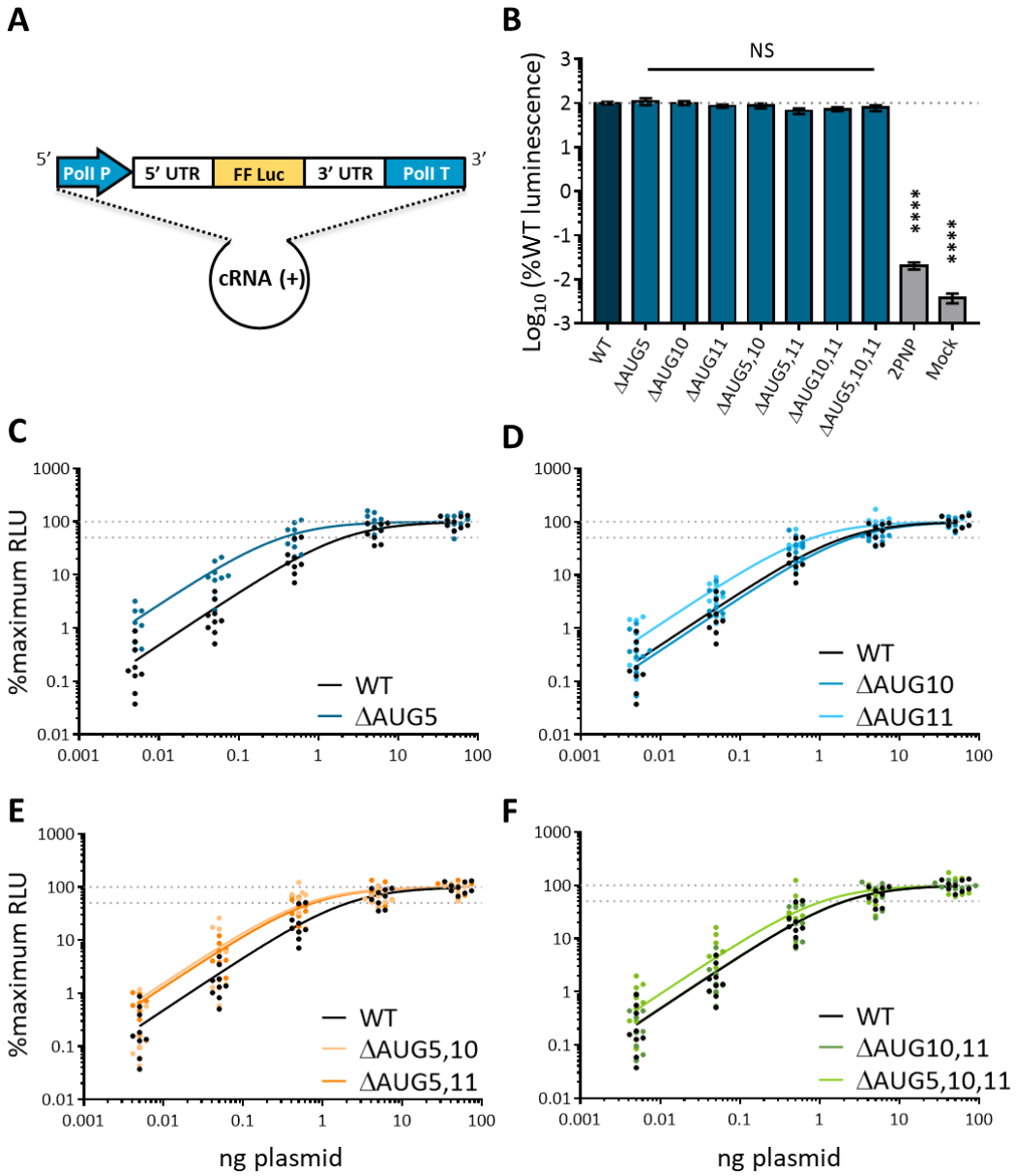

Figure 2.13. Measurement of mutant PB1s replication activity. 293T cells were co-transfected with pDUAL PR8 plasmids expressing the protein components of the vRNP alongside a PolI reporter plasmid expressing positive strand cRNA-like firefly luciferase RNA (Shown diagrammatically in (A)). (B) Luciferase activity was measured 24 hours post-transfection. Data represent the mean ± SEM of four independent experiments performed in triplicate. Statistic annotations are the result of an ordinary one-way ANOVA test. ****p-value <0.0001. (C-F) A dose-dependent titration of the PB1 plasmid was performed using the cRNA-like reporter. Normalisation was performed to the maximum luminescence within each individual titration set. Grey dashed lines indicate 100% and 50% of the maximum of each individual data set. Data are individual points of three independent experiments performed in triplicate and a minimum squares curve fit. Values relative to WT PR8 RNP reconstitution were repeated from C to F to allow comparison.

Table 2.2. Replication and transcription activities of mutant PR8 PB1 subunits. Titration curves were used to calculate EC_{50}, 95% Confidence Intervals and R^2 values. Calculations were performed in Excel and GraphPad Prism software.

PB1 construct	Replication			Transcription (Firefly Luciferase)		
	EC_{50} (ng)	95% CI (ng)	R^2	EC_{50} (pg)	95% CI (pg)	R^2
WT	2.086	1.42 to 3.04	0.87	239.7	148.1 to 383.2	0.49
ΔAUG5	0.357	0.21 to 0.60	0.80	279.2	143.5 to 529.7	0.60
ΔAUG10	2.942	1.76 to 4.69	0.82	372.9	196.3 to 675.5	0.53
ΔAUG11	0.833	0.52 to 1.33	0.82	383.6	233.2 to 610.6	0.72
ΔAUG5,10	0.642	0.35 to 1.26	0.74	196.0	91.6 to 413.4	0.40
ΔAUG5,11	0.760	0.48 to 1.22	0.83	309.4	139.0 to 665.1	0.34
ΔAUG10,11	2.038	1.35 to 3.05	0.86	288.7	179.5 to 456.1	0.77
ΔAUG5,10,11	1.095	0.52 to 2.54	0.68	442.2	262.7 to 717.9	0.71

Plasmid saturation was also considered for the RNP reconstitution replication analysis. Therefore, to provide a more sensitive examination of PB1 replication activity, the amount of segment 2 plasmid was titrated and the luciferase expression values were fitted to a variable slope enzyme kinetic dose-response model. In this system, maximal activity with the WT plasmid was only reached at the highest dose tested (50ng; figure 2.13C). The dose-response curves for the PB1 mutants were reasonably similar to that of the WT enzyme, with the mutants generally being shifted leftwards to slightly lower plasmid concentrations (Figure 2.13C-F). In this assay, the R^2 values of the curve fits were generally satisfactory (mostly > 0.7) and several of the mutants had estimated EC_{50} values whose 95% confidence limits did not overlap with that of the WT plasmid, suggesting statistical significance (Table 2.2). However, with the exception of PB1 ΔAUG5, where the difference in EC_{50} was ~ 5-fold, the rest were within 2- to 3-fold of the WT plasmid, indicating, at most, only minor changes in activity.

Although not shown in this dissertation, PB1 transcription and replication activity in an infection context was analysed by performing single cycle infections. MDCK cells were infected at a MOI of 5, virus was adsorbed for 1h at 37ºC and cells were subjected to an acid wash and media change. Every-two-hour time points were collected up to 12 hpi, and supernatants were titrated by plaque assay. Preliminary results from the single mutant viruses showed no differences in viral titre at any points post infection between WT PR8 or any mutant virus (data not shown).

Overall, this section did not show evidence for a deleterious effect of the PB1 amino acid mutations M92V and M111V on viral genome transcription and replication activity; a finding consistent with the apparently normal viral gene expression seen in previous experiments (Figures 2.5A and C).

2.2.7. Analysis of the genome packaging efficiency of segment 2 mutant viruses

Several regions of segment 2 that contribute to vRNA packaging signals have been identified. However, these have mainly been located at the 3' and 5' ends of vRNA (Liang *et al.* 2005; Wise *et al.* 2011; Marsh *et al.* 2008). Nonetheless, packaging efficiency of the segment 2 mutants was analysed. MDCK cells were infected at a multiplicity of 0.001. Forty-eight hpi, supernatants were clarified by centrifugation and viral titres were quantified by plaque assay. In parallel, vRNA was extracted from the same supernatants. In order to ensure consistent RNA extractions between samples, the lysis buffer was spiked with a consistent amount of porcine reproductive and respiratory syndrome virus (PRRSV; kindly provided by Dr Christine Tait-Burkard). RT-qPCR was then performed to detect 4 different RNA species: PRRSV genomic RNA and IAV segments 2, 5 and 7. Following this, the PRRSV Ct (cycle threshold) values were similar, varying between 17.69 and 19.88, giving confidence that the RNA extraction had been performed consistently (Figure 2.14A). The Ct values acquired for IAV segments 2, 5 and 7 were transformed into copy number using a standard curve and genome/PFU ratios were calculated based on the infectious viral titres (Figure 2.14B). Assuming that each virion contains a single copy of individual segments (Hutchinson *et al.* 2010), these values could be considered as an estimate of the particle/PFU ratio. The values obtained for WT PR8 varied between 15 and 33 (Figure 2.14B), which is in accordance with previous estimates of 10-100 particle:PFU measurements (Donald and Isaacs 1954; Hutchinson *et al.* 2008; Hutchinson *et al.* 2010; Nakajima *et al.* 1979) As a positive control, a known packaging mutant was used. This mutant virus harbours synonymous mutations in the 5'-ends of HA (in

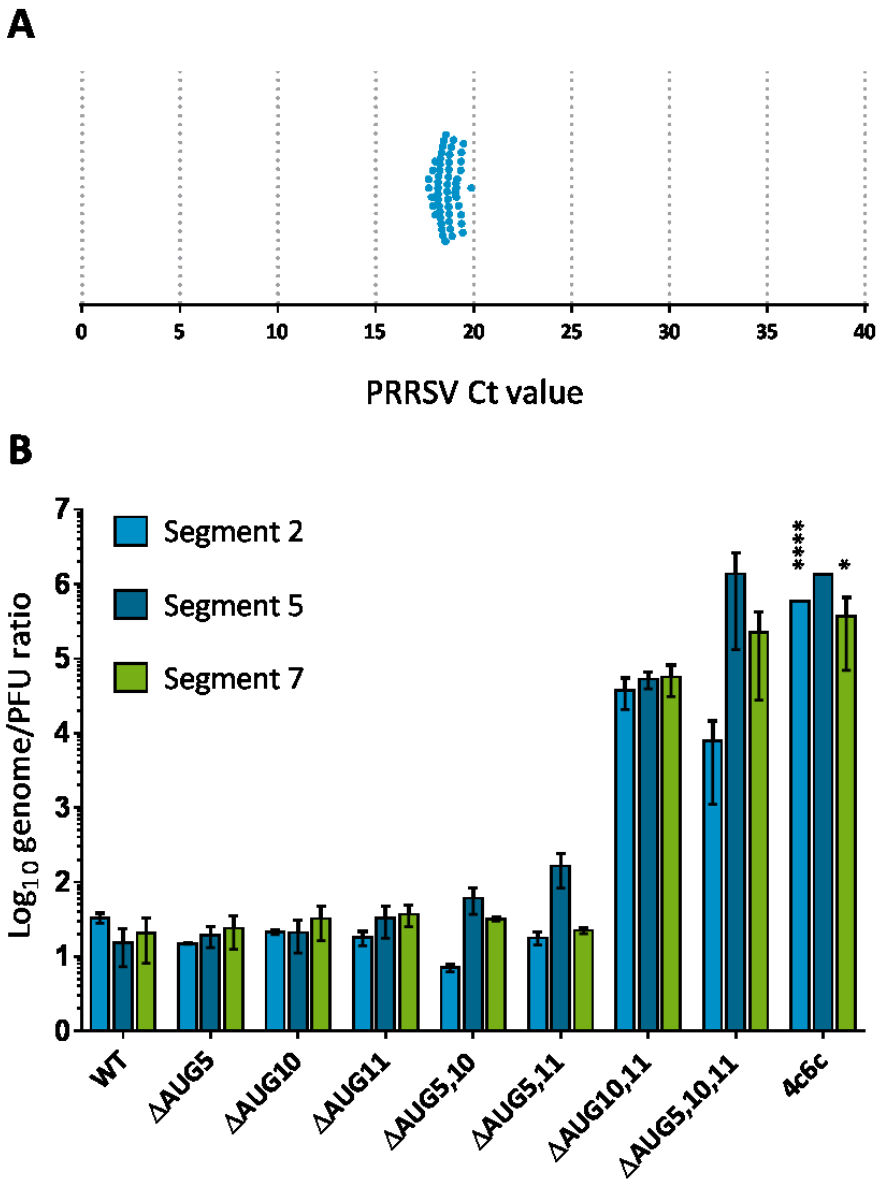

Figure 2.14. Genome copy/PFU ratios of segment 2 mutant viruses. PR8 virus stocks were grown in MDCK cells, titrated by plaque assay and (in parallel) vRNA extracted after spiking with aliquots of PRRSV as an extraction control. (A) qPCR analysis for PRRSV showed comparable extraction efficiencies of the samples. (B) qRT-PCR analysis for segments 2, 5 and 7 was performed and IAV genome copy numbers derived in comparison to standard curves for each of the indicated segments. Genome/PFU values were then calculated. Data represent mean ± SEM of at least 2 independently generated virus stocks which were analysed in duplicated in a single qPCR reaction (with exception with the 46c6 mutant which segments 2 and 5 were only analysed from one virus stock). Statistical annotations are the result of a two-way ANOVA test. Multiple comparisons were made against the WT virus. *p-value <0.05, ****p-value <0.0001.

codons L546-A548) and NA (S451-D453) vRNA segments (Kudryavtseva 2014). This mutant showed an overall 10,000-fold increase in particle:PFU ratio. The segment 2 single AUG mutant viruses showed an essentially WT-type phenotype, while double mutants ΔAUG5,10 and ΔAUG5,11 showed a slight augmentation in the genome/PFU ratio, with up to a 10-fold increase seen in segment 5 values. However, the highly attenuated mutants ΔAUG10,11 and ΔAUG5,10,11 had very poor particle:PFU ratios, with a 1000-fold or greater increases in genome copy number when compared to the number of infectious particles. These data suggested that, although not altering PB1 polymerase activity, the ΔAUG mutations led to the production of virus particles with severely decreased infectivity, potentially associated with a modification of the packaging efficiency of the virus progeny.

2.3. Discussion

Previous work has shown that segment 2 of IAV expresses the accessory proteins PB1-F2 and PB1-N40 in addition to the canonical gene product PB1 (Wise *et al.* 2009; Wise *et al.* 2011; Chen *et al.* 2001). These non-essential minor gene products are translated from internal AUG codons 4 and 5 which, unlike the PB1 AUG1, are set in strong Kozak translation initiation contexts. Following the identification of PB1-F2, a first approach to knocking out its expression (to probe its biological significance) involved the deletion of its initiator codon (AUG 4) and the introduction of a stop codon at its 8th amino acid position (Chen *et al.* 2001). However, this second mutation led to a non-synonymous change in PB1 codon 40 of M to I and, as was subsequently shown (Wise et al., 2009), the ablation of PB1-N40 expression, thus further

complicating interpretation of the mutant phenotype. A further study showed that this double PB1-F2/PB1-N40 knockout mutant was not attenuated for growth *in vitro*, but showed diminished virulence and mortality in a mouse model (Zamarin *et al.* 2006). However, as this knockout virus had simultaneous deletion of two accessory proteins and a non-synonymous change in PB1, the basis of the phenotype cannot be unequivocally determined. Moreover, a more recent study that examined both PB1-F2 and PB1-N40 showed that individual ablation of either protein was not disadvantageous for the virus, but the double deletion of PB1-F2 and PB1-N40 results in an attenuated phenotype *in vivo* (Tauber *et al.* 2012). These studies highlight the importance of accounting for potential protein expression from other AUG codons when designing knockout strategies in RNA regions encoding overlapping accessory proteins.

In this chapter, evidence for the expression of two additional polypeptides species from IAV segment 2 AUG mRNA was presented. These proteins, here named PB1-92 and PB1-N111, are N-terminally truncated versions of the primary product, PB1 arising from translation initiation at AUG codons 10 and 11 respectively (codons 92 and 111 in the mRNA), which are both in strong Kozak signalling contexts. This evidence was first obtained from the observation of two lower-molecular-weight peptides produced by plasmids containing a gene fusion between the 5'-end of segment 2 and GFP whose expression levels altered predictably according to the presence or absence of AUGs 10 and 11 in this DNA-based setting. Given the caveats originating from the PB1-F2 knockout strategy studies discussed above, in order to minimise the changes within overlapping segment 2 ORFs, AUG 10 and 11 mutations were designed to solely affect frame 1 proteins.

GFP-tagged transcripts are useful to identify alternative translation start sites in a given mRNA. Nevertheless, mRNA expressed from the peGFP-N1 plasmid is under the control of the CMV promoter, which results in higher levels of transcription compared to the ones detected in infected cells. In addition to better expressed, the polypeptides expressed from GFP-tagged plasmids are shorter and easier to detect in a western-blot.

Further evidence of translation initiation from AUG codons 10 and 11 came from western blotting experiments for PB1 polypeptides produced in cells infected with mutant PR8 viruses lacking either AUG10 or 11. Although background reactivity of the anti-PB1 serum with cellular and/or other viral polypeptides was a problem, mutation of AUG11 clearly led to loss of expression of a polypeptide of the expected molecular weight for PB1-N111. Weak evidence for production of PB1-N92 was also obtained, but the presence of a probable background species running at the same position prevented a clear conclusion from being drawn. Multiple attempts at detecting PB1-N92 and -N111 by immunoprecipitation of radiolabelled cell lysates were also made, but although expression of PB1-N111 could be detected (data not shown), the presence of PB1-N92 was either obscured by a background band or alternatively, insensitive to mutation of AUG10. On balance, given that previously published work (Wise *et al.* 2009; Wise *et al.* 2011) and the data shown here show good agreement between the effects on protein expression of mutating segment 2 AUGs 4, 5 and 11 in the background of the GFP reporter plasmid and the virus itself, it seems most likely that PB1-N92 is expressed by PR8, but that it cannot be detected by the approach tried here.

The fitness of segment 2 AUG mutant viruses was evaluated in a variety of different models. PR8 with PB1-N40 knocked out was able to replicate to WT-like levels in all replication systems used, in the exception of chicken embryos. Single mutation of AUGs 10 or 11 resulted in growth kinetics similar to WT PR8 in the MDCK and QT35 cell lines. These single mutations resulted in a minor, but statistically significant attenuation in A549 cells and embryonated hen's eggs and allantoic fluids. However, the simultaneous deletion of AUGs 10 and 11 led to a severely attenuated phenotype in all the models tested, reinforcing the importance of these AUG codons during infection.

The mutation of frame 1 AUG codons leads to the inevitable introduction of point mutations within the PB1 ORF (Table 2.1). Within the PB1 structure, these mutations sit in the fingers domain of the core polymerase. Although no function has been specifically associated with this domain in IAV, studies on HCV have established a critical role of this domain in the transition from *de novo* initiation with GTP to the elongation of the growing primer-template RNA (Mosley *et al.* 2012). Various mutational analyses on PB1 transcription and replication activities have been described (Chu *et al.* 2012; Biswas and Nayak 1994). However, these studies have mainly been focused of the SSDD motif and surrounding areas (residues 303 to 482), not including the area affected by the deletion of the AUG codons. In addition, PB1 M111 is located at the surface of the polymerase structure. This could potentially compromise the interaction between PB1 and other viral and host factors, for instance the formation of PB1-driven polymerase-polymerase associations, leading to a decrease in RNA synthesis activity (Digard *et al.* 1989). Therefore, the introduction of mutations in PB1 could potentially alter overall viral gene expression and/or

replication and explain the attenuated phenotype of the double and triple mutants (ΔAUG10,11 and ΔAUG5,10,11). Therefore, genome replication and transcription activities of mutant PB1 specimens were assessed using cRNA- and vRNA-like reporter plasmids in RNP reconstitution systems. Fixed dose and dose-dependent assays showed no major differences in polymerase activity for any of the reporter systems, suggesting that the introduced changes were not detrimental for either PB1 transcription or replication activities. These data are in agreement with the apparently normal levels of expression of viral proteins in cells infected with the AUG mutant viruses (Figure 2.5A, C) which further support a WT-like function of the mutant PB1 polypeptides as well as indicating that RNP function is not dependent on the shorter PB1 peptides. Nonetheless, the ΔAUG5 data reported here does not recapitulate the replication deficit in the PB1-N40 knockout system previously shown by Tauber *et al*. 2012. However, that study was developed only using the A/Wilson Smith Neurotropic /1933 (H1N1) virus (WSN), while our data originated from the PR8 strain, which could potentially explain the discrepancy between the two studies.

PB1 interacts with the PA polymerase subunit though its N-terminal domain. This region is not present in PB1-N40 which has previously been shown to lack detectable transcription function (Wise *et al.* 2009). Therefore the further loss of functionally important sequences in PB1-N92 and -N111 would strongly predict that these would also be non-functional as polymerase subunits. However, these polypeptides share the PB1 C-terminal PB2 interaction site (Poole *et al.* 2007; Toyoda *et al.* 1996; Ohtsu *et al.* 2002; Gonzalez *et al.* 1996; Pflug *et al.* 2014). Moreover, studies on segment 2 accessory proteins have shown that the absence of PB1-N40 expression also has a negative effect on the viral polymerase (Tauber *et al.* 2012),

making it possible to hypothesise the potential association of PB1-N92 and/or -N111 with polymerase functions. Nevertheless, transcription and replication activity of the polymerase in the absence of the initiation codons of these peptides is not altered, therefore discarding this hypothesis.

Apart from amino acid changes, the introduced mutations involved the alteration of the vRNA. In addition to containing essential sequences for viral transcription and genome replication initiation, conserved vRNA motifs have been suggested to be functionally important as packaging signals and to be involved in RNA-RNA interactions (Kobayashi *et al.* 2016; Marsh *et al.* 2008; Gog *et al.* 2007; Cobbin *et al.* 2014; Liang *et al.* 2005; Liang *et al.* 2008). The 3' and 5' ends of segment 2 vRNA (vRNA2) have been widely shown to be highly conserved and essential for adequate packaging of vRNPs (Liang *et al.* 2005; Liang *et al.* 2008; Cobbin *et al.* 2014). Although AUGs 10 and 11 are not included within these packaging signals, they are highly conserved (Gog *et al.* 2007; Gong *et al.* 2014). Furthermore, functional sequence-specific interaction analysis between genomic vRNA segments showed inter-vRNA interactions of nucleotides 125-384 in vRNA2 (region which include both AUGs 10 and 11 codon) and 256-435 of segment 8 vRNA (vRNA8), suggesting the co-packaging of these two segments. Moreover, this interaction is of an almost perfect complementarity with vRNA8 between nucleotides 289-309 of vRNA2, which includes AUG 10 (Gavazzi *et al.* 2013). Viruses harbouring mutations in these regions presented a packaging defect and lower viral titres in comparison to their WT counterpart. However, this study was conducted using an avian H5N2 virus (A/Finch/England/2051/91). In PR8, complementarity between vRNA2 289-309 and the supposedly equivalent region in vRNA8 was seen in solely between 3 nucleotides

which are not included in the AUG10 codon (data not shown). Accordingly, measurements of genome copy:PFU ratios of the single mutant PR8 ΔAUG10 suggested a WT-like packaging efficiency. Unexpectedly, a dramatically increased genome copy:PFU ratios were seen in the double and triple mutants; similar to those seen with a *bona fide* packaging mutant created by deliberate mutation of conserved segment terminal sequences thought to be likely candidates for segment-specific packaging signals (Gog *et al.* 2007; Kudryavtseva 2014). However, the "4c6c" packaging mutant contains a total of 9 nucleotide substitutions across 2 segments that act synergistically to create a highly defective virus (Kudryavtseva 2014). For a genome packaging defect to explain the results obtained here with the segment 2 mutations would require that the two nucleotide changes required to mutate both AUGs 10 and 11 to act synergistically, as the phenotype was not strongly present in the single ΔAUG 10 or 11 mutants or in the double mutants ΔAUG5,10 and ΔAUG5,11. Another possible explanation could be the surface-exposed change of PB1 amino acid M111, which could lead to the diminished interaction of PB1 with other viral proteins involved in genome packaging. However, again, the largest increase in genome to PFU ratios was seen in the double and triple mutants ΔAUG10,11 and ΔAUG5,10,11 and not in the ΔAUG11 single mutant. Therefore it is unlikely that the surface M111 amino acid is the cause of the packaging deficiency of the mutants ΔAUG10,11 and ΔAUG5,10,11. Alternatively, it is possible that the defect in genome copy:PFU ratio seen here for the segment 2 mutants is not the result of a packaging defect, but instead represents a deficit in efficiency of plaquing (EOP) arising from some other mechanism. Additional thoughts on packaging deficiency will be discussed in following sections.

Overall, the data described in this section adds an additional polypeptide to the list of IAV accessory proteins. Functional studies of these peptides in the context of *in vitro* and *in vivo* infections and their conservation in IAV field isolates will be explored in the following chapters.

Chapter 3

Type I interferon in response to segment 2 mutant viruses

3.1. Background and aims

As described in the previous chapter, AUGs 10 and 11 in IAV segment 2 constitute translation initiation sites and lead to the expression of PB1-N92 and PB1-N111. Moreover, viruses harbouring mutations that simultaneously ablated expression of these two peptides showed significantly attenuated viral fitness, despite the WT-like RNA replication and transcription activities of the altered PB1 proteins. However, as shown in Figures 2.6 and 2.9, although diminished at later time points, propagation of the PR8 ΔAUG10,11 and ΔAUG5,10,11 viruses was comparable to WT PR8 at 6-12 hpi. Previous studies have detected IFN-β mRNA expression induction as early as 4 hours after polyinosinic:polycytidylic acid (poly I:C) treatment (Abe *et al.* 2012) and IFN secretion and STAT1 phosphorylation have been detected at 8 hpi following IAV infection (Liedmann *et al.* 2014b). Therefore we hypothesised that the attenuated viruses might either lack an IFN counteraction mechanism or provoke stronger IFN

induction; both of which could result in the observed phenotype of attenuated virus replication at later times.

Hence, this second chapter aimed to determine other reasons behind the severely attenuated phenotypes of viruses with the ΔAUG10,11 lesions, bearing in mind the biphasic pattern of multicycle replication kinetics and thus focusing on host type I IFN responses. IFN sensitivity and IFN induction by the segment 2 mutant viruses were assessed. PB1-related defects which could be associated with an IFN response were also be approached. Moreover, IFN-defective systems were used to assess viral fitness in the absence of a fully established type I IFN response.

3.2. Results

3.2.1. Quantification of type I IFN production during infection with segment 2 mutant viruses

As a first test of the hypothesis that the severely attenuated phenotype of segment 2 mutant viruses resulted from a failure to control cellular innate immune responses, the levels of active type I IFN secreted during infection with WT and mutant viruses were measured. To do so, a reporter cell line (HEK-Blue IFN-α/β cells) was used. These cells express human secreted embryonic alkaline phosphatase (SEAP) under the control of the ISG54 promoter (https://www.invivogen.com/hek-blue-ifn-ab) (Bluyssen *et al.* 1994). Therefore, SEAP expression can be detected upon JAK/STAT signalling and ISRE activation which is induced by exogenous type I IFN.

The experimental design involved the infection of the human IFN-competent A549 cell line at a range of multiplicities (3, 0.3, 0.03 and 0.003). Twenty-four hpi, cell supernatants were collected and half was UV-treated in order to inactivate infectious viral particles. Treated and untreated supernatants were then added to HEK-Blue reporter cells and after a 24 hour incubation, the levels of secreted SEAP were measured by absorbance at 600nm following addition of substrate (summarised in Figure 3.1A). To test the success of the original infection rates, cells were fixed, permeabilised and immunostained for the presence of NP at 24 hpi. Mock-infected cells showed no NP-positive staining, while at MOI 3, the majority of the cells were positively stained (Figure 3.1B). Approximate 10-fold drops in infection levels were observed for MOI 0.3 and the two lower multiplicities, thus verifying the variable MOIs of infection. The success of the UV-treatment was also tested. Pre- and post-UV treatment cell supernatants were titrated by plaque assay. Mock-infected cells showed no detectable titre (Figure 3.1C) while MOI 3 infections produced viral titres of 10^7 PFU/mL. As observed for the proportion of infected cells, the titres of released virus also showed approximate 10-fold reductions between each multiplicity step. In contrast to the non-treated supernatants, the infectious particle load for UV-treated samples was below detectable levels, confirming an efficacious inactivation.

Once the assay foundations had been established, the levels of type I IFN induction upon infection with the panel of the different PR8 segment 2 mutants were quantified. Experimental design was performed as in Figure 3.1A. Varying concentrations of universal type I IFN were also incubated with the HEK-Blue cells to create a standard curve (Figure 3.2). SEAP secretion levels increased with IFN concentration, demonstrating that the HEK-Blue cells were responding to exogenous

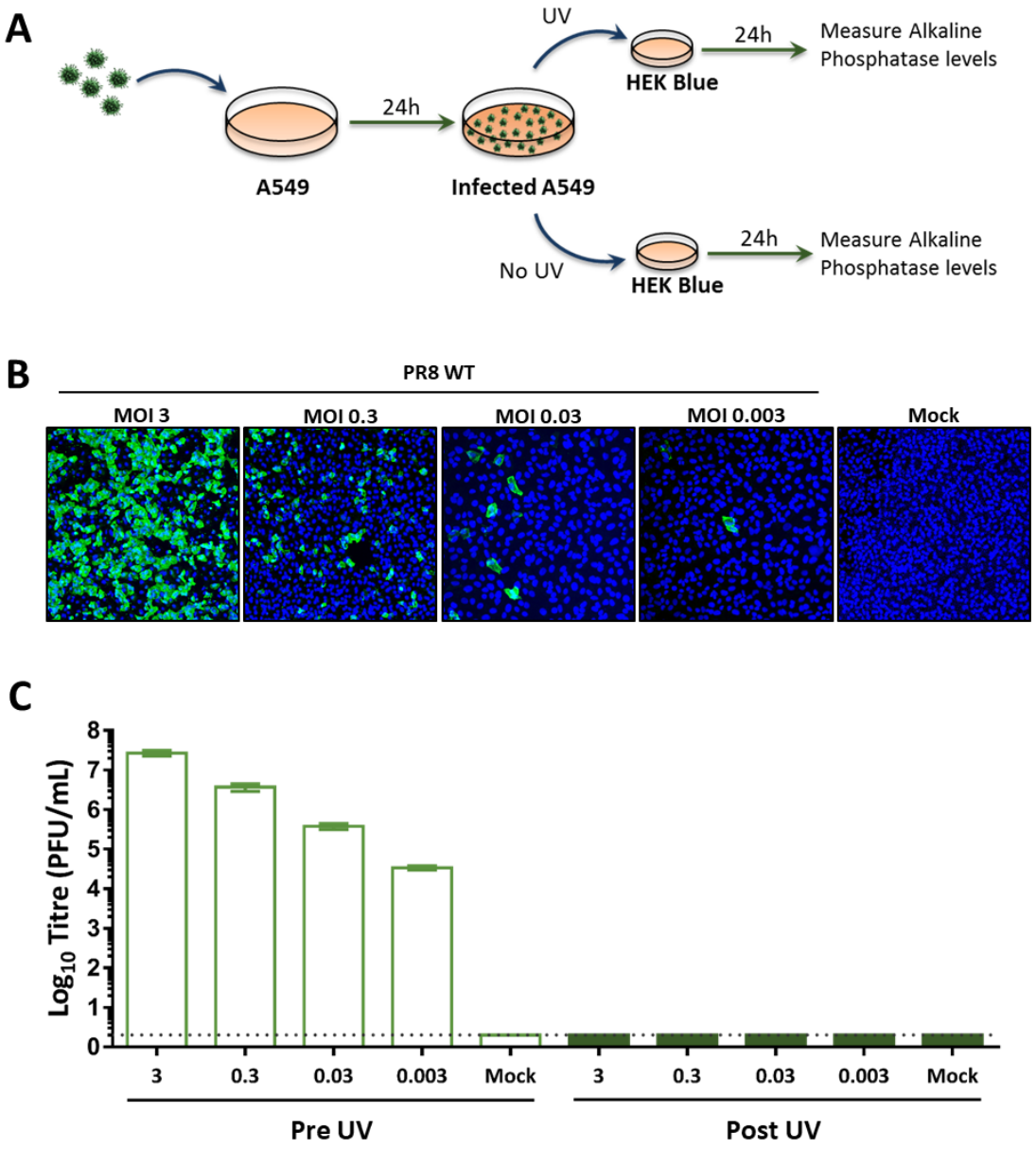

Figure 3.1: Establishment and validation of the HEK-Blue cell type I interferon reporter assay. (A) Schematic diagram of the protocol. (B) A549 cells were infected at decreasing multiplicities. Twenty-four hpi cells were fixed and immunofluorescence against viral NP was used to test the success of infection. Nuclear staining was achieved by DAPI staining which is shown in blue. Micrographs shown are a representation of one of the independently performed experiments. (C) Cell supernatants from the previous infection were collected and one half was UV-treated to inactivated infectious virions. Effective inactivation was assessed by plaque assay. Viral titres pre- and post-UV inactivation for PR8 WT infections for the different MOIs used are shown. Data represent mean ± SEM of at least three independent experiments with single technical repeats and the dotted line represents the assay limit of detection (2 PFU/mL).

type I IFN. Negative controls included supernatants from mock-infected A549 cells, HEK-Blue cells only and SEAP assay substrate only which set the background levels of the assay; approximately equivalent to 5 U/mL of the universal type I IFN. A549 cells infected with PR8 WT did not produce IFN above this background level, regardless of the MOI. As a positive control, a PR8 NS1 RNA-binding mutant virus was used - NS1 residues R38 and K41 were mutated to alanines (R38K41A - mutagenesis performed by Dr Helen Wise) - which is known to be deficient in IFN antagonism (Talon *et al.* 2000; Newby *et al.* 2007; Gack *et al.* 2009; Turnbull *et al.* 2016). As expected, a strong type I IFN induction was observed when A549 cells were infected with this virus, at MOI 3, 0.3 and 0.03, while infection at MOI of 0.003 only resulted in background IFN levels. In general, levels of IFN induction were higher in the non-UV treated samples for all mutant viruses and MOIs (compare figures 3.2A and B). In the absence of UV treatment, all viruses with mutated AUG codons induced statistically significant higher IFN levels than the WT virus after infection at MOI 3, with a gradient of ΔAUG5,11 > ΔAUG5,10 ~ ΔAUG11 > ΔAUG10 > ΔAUG5. However, for UV-treated samples, this increased induction was only statistically significant for the double mutants ΔAUG5,10 and ΔAUG5,11 when compared to WT PR8 (Figure 3.2A). High multiplicity infections with the double and triple mutants ΔAUG10,11 and ΔAUG5,10,11 were not possible due to the low titres of the P1 stocks (as described in the previous chapter). Therefore, infections with these viruses could only be performed at MOI of 0.003. Nevertheless, for these infections a stronger IFN induction was also observed when compared to PR8 WT infections at the same multiplicity (Figure 3.2A). Similarly to the remaining mutants, a more pronounced (and statistically significant) difference was also observed in non-treated samples

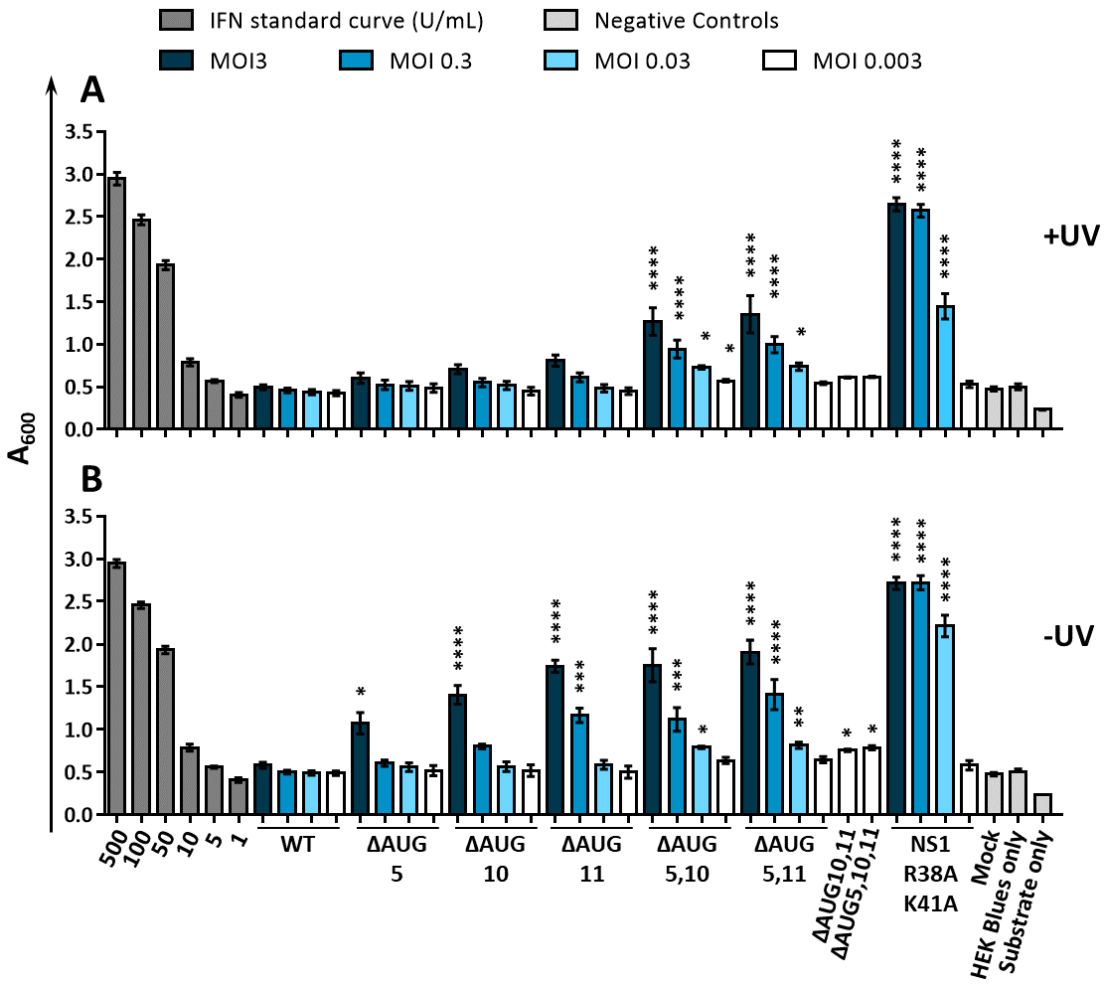

Figure 3.2: Measurement of Type I IFN induction during infection. HEK-Blue cells were treated with supernatants from A549 cells infected with the PR8 segment 2 mutant virus set or PR8 NS1 R38K41A at MOIs of 3, 0.3, 0.03 and 0.003. Twenty-four hpi, cell supernatants were inactivated and incubated with HEK-Blue cells for a further 24 hours, after which SEAP activity was measured by measuring absorbance at 600nm (A_{600}). A_{600} for inactivated (A) and non-inactivated (B) supernatants are shown. Data represent mean ± SEM of at least four independent experiments performed in duplicates. Statistical symbols represent individual one-way ANOVA tests performed between mutant viruses used at the same MOI. Dunnett's multiple comparison tests were performed having WT PR8 as control. *p-value <0.05, **p-value <0.01, ***p-value <0.001, ****p-value <0.0001.

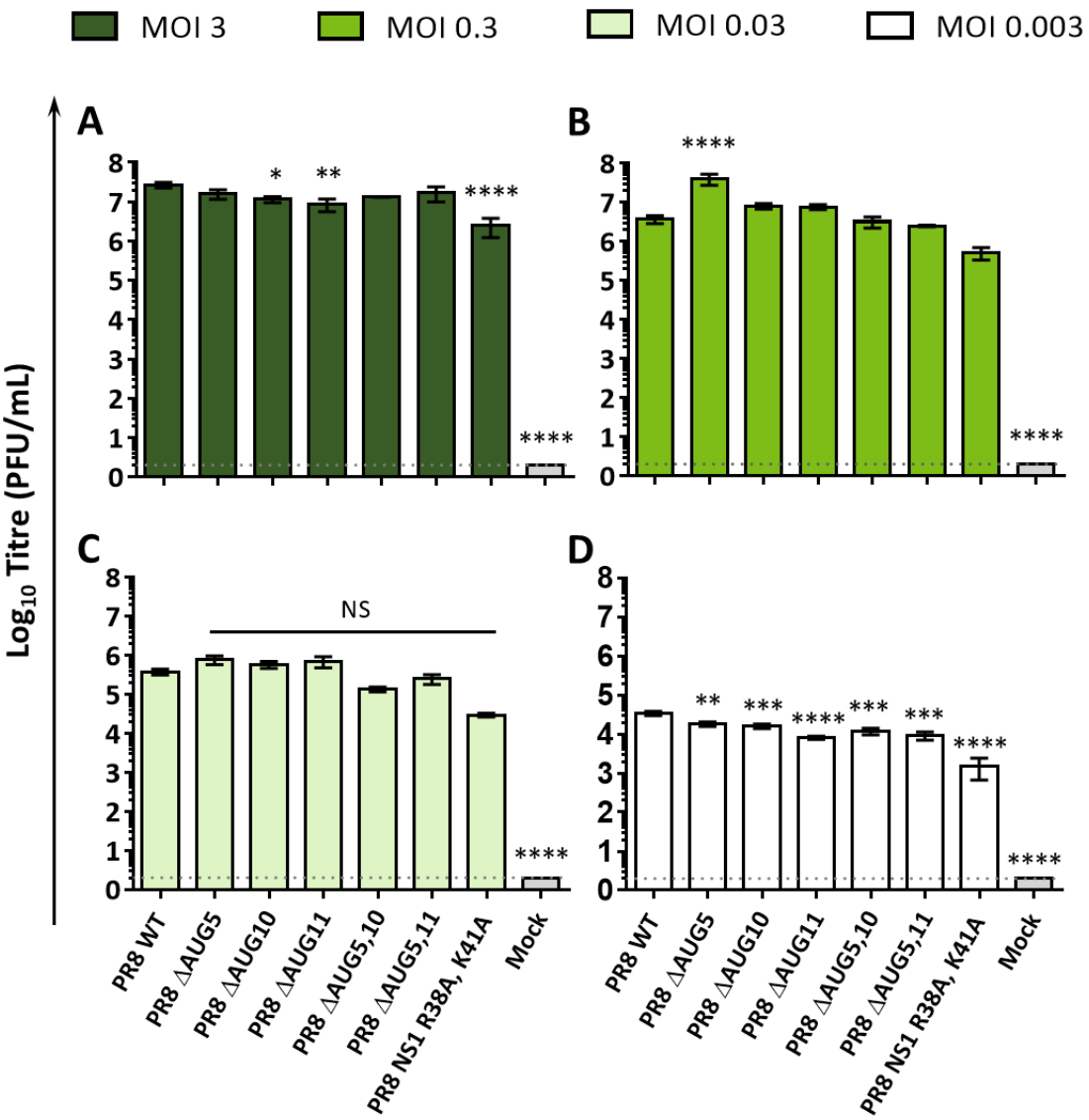

Figure 3.3: A549 virus titres pre-UV treatment. Supernatants collected from the different MOI A549 infections (from Figure 3.3) were titrated by plaque assay. Data represent mean ± SEM of four independent experiments performed in duplicates and the dotted line represents the assay limit of detection. Statistical symbols represent one-way ANOVA tests performed within each MOI. Multiple comparison tests were performed with WT PR8 as control. *p-value <0.05, **p-value <0.01, ***p-value <0.001, ****p-value <0.0001.

(Figure 3.2B).

As noted above, non-UV treated samples gave an overall stronger response compared to the treated supernatants. However, the increased levels of SEAP by HEK Blue cells could potentially be explained by the accumulation of type I IFN secreted by A549 cells and additional IFN being expressed by HEK Blue cells when infected by infectious viral particles released from the previous A549 infection. Therefore, supernatants from the A549 infection were titrated, to assess if such a mechanism might have skewed the outcome because of major differences in virus titre (Figure 3.3). Mock-infected cells did not show detectable infectious particles (the limit of detection was 2 PFU). WT PR8 titres ranged from ~ 10^7 down to ~ 10^4 PFU/ml, decreasing around 10-fold with each 10-fold reduction of MOI. When infected at MOI 3, concordant with previous infections in A549 cells, the segment 2 mutants produced slightly reduced viral titres (Figure 3.3A). At the other MOIs, with the exception of the ΔAUG5 virus at MOI 0.3 (Figure 3.3B), all mutants showed equivalent or lower titres than WT PR8, despite showing equal or higher type IFN induction levels. Therefore, with exception of the ΔAUG5 mutant, it was possible to associate the increased levels of IFN induction to deficiencies in the mutant viruses and not to greater stimulation of the reporter cell line by higher amounts of infectious viral particles.

In global terms, this set of data allowed the conclusion that segment 2 mutant viruses provoked a stronger induction of the type I IFN response in comparison to their WT counterpart.

3.2.2. Ability of segment 2 mutant viruses to replicate under established antiviral conditions

Given the increased IFN induction in ΔAUG mutant virus infection, we next evaluated whether these mutant viruses would replicate in the presence of an established IFN response, using cells that had already been stimulated with type I IFN. A549 cells were preincubated for 20 hours with different concentrations of universal type I IFN prior to a 48-hour infection at a MOI of 0.001 with PR8 WT and the different segment 2 mutant viruses. Virus titres of infected cell supernatants were determined by plaque assay, and titres were scaled to those from the no IFN control (Figure 3.4A-D). The replication of most viruses was unaffected by IFN concentrations of 10U/mL and below while high concentrations of universal IFN preincubation (300 U/ml and above) inhibited virus replication by several orders of magnitude, relative to the no-IFN control samples. In general, the single ΔAUG mutants and the double ΔAUG5,10 and 5,11 mutants appeared more sensitive than WT virus and fitting of dose-inhibition curves showed shifts to the left of WT (Figures 3.4A-C). Within these mutants, although not substantially different, the most pronounced shift was observed for PR8 ΔAUG11, followed by the ΔAUG10 and ΔAUG5 viruses. Similar shifts were observed with the double mutants ΔAUG5,10 and ΔAUG5,11 (Figure 3.4C). The ΔAUG10,11 and ΔAUG5,10,11 mutants showed a comparable magnitude but surprising rightwards shift compared to WT PR8, especially at higher IFN concentrations (Figure 3.4D). From the fit curves, half maximal inhibition concentrations (IC_{50}) values were estimated. These varied between 12.3 and 19.8U/mL, with a trend towards lower values for the viruses lacking AUGs 10 and 11 (Figure 3.4E). However, due to the variability of the data, differences

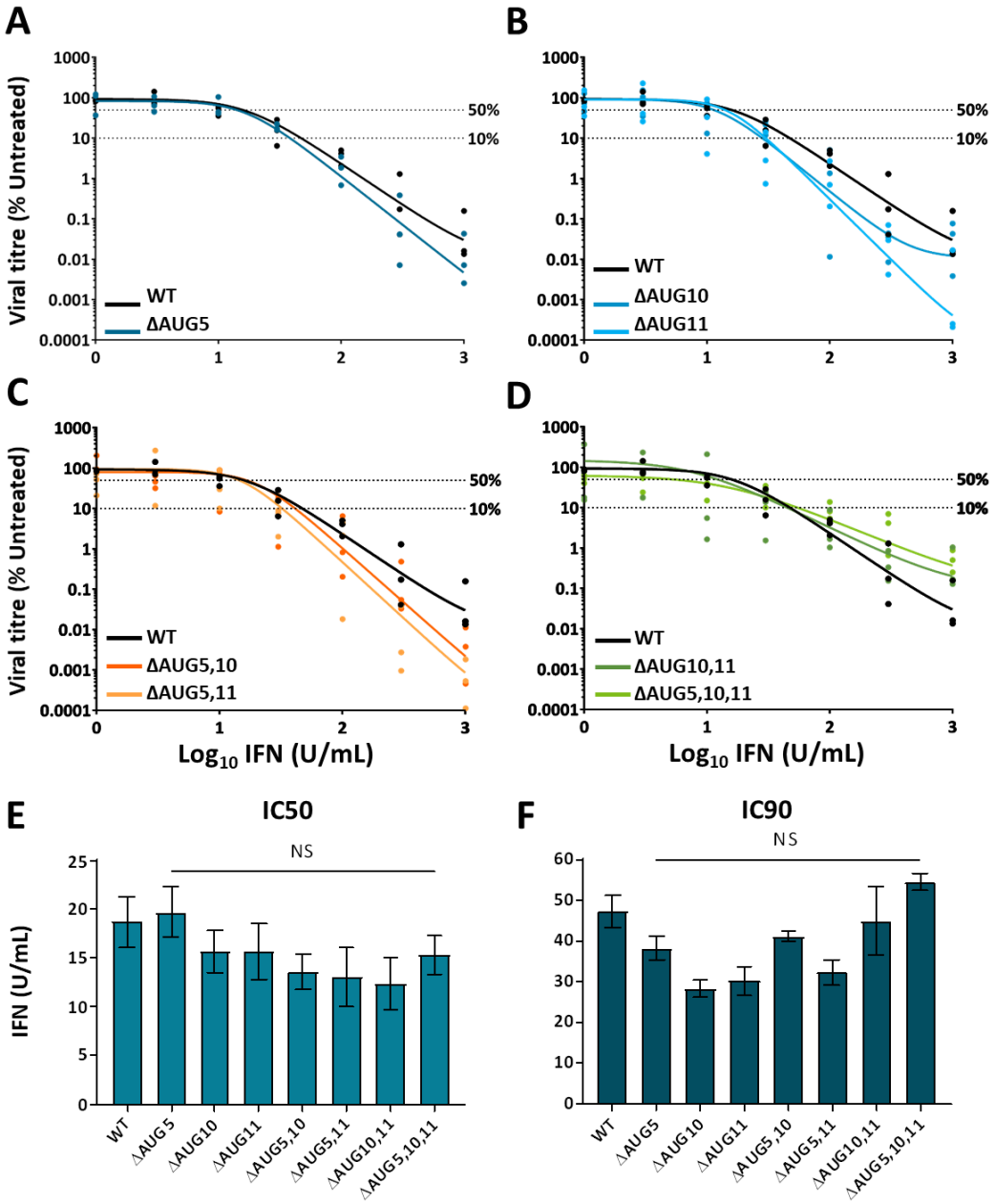

Figure 3.4: Ability of viruses to replicate in the presence of pre-established antiviral conditions. (A-D) A549 cells were pre-treated with the plotted concentrations of universal type I IFN for 20h followed by infection with PR8 WT and mutant viruses at MOI 0.001 for 48 hours. Virus in the supernatant was titrated by plaque assay. Plotted data are percentage of the no-IFN control for each virus of single technical repeats from three independent experiments. Dashed lines indicate 50 and 90% inhibition levels. WT PR8-relative data is repeated between panels for comparison. Data represent individual data points and respective curve fits. (E and F) From curve fits, IC50 and IC90 values were calculated. Plotted data are mean ± SEM of the three independent experiments performed with a single technical repeat. Multiple comparison (one-way ANOVA) tests were performed using WT PR8 as control. NS: Non-significant.

between WT and segment 2 mutant, viruses were not statistically significant. IC_{90} values were also calculated, but again with no statistically significant differences found between the different mutant viruses (Figure 3.4F). Therefore, although inducing stronger type I IFN levels, these data did not indicate that the segment 2 mutant viruses were less able to replicate in the presence of a pre-established ISG response.

3.2.3. Assessment of innate immune recognition of mutant vRNPs

As described in chapter 1, the IAV panhandle has been suggested to act as a potent RIG-I ligand, supported by (for instance) the induction of IFN by transcriptionally active RNPs reconstituted in cells through plasmid transfection (Rehwinkel *et al.* 2010). This 5'ppp RNA PAMP is normally hidden by the polymerase trimer (Klumpp *et al.* 1997). Given that PB1 binds to vRNA (Gonzalez and Ortin 1999; Pflug *et al.* 2014), point mutations in PB1 were hypothesised to potentially jeopardise this role, resulting in an increased number of exposed panhandle RNA structures, a stronger RIG-I stimulation and the observed type I IFN induction. To test this, RNP reconstitution assays were performed and the levels of IFN induction examined. Various amounts (ranging from 10 to 50ng) of pDUAL plasmids encoding the RNP components were transfected into 293T cells. Forty-eight hours post transfection, the supernatants were removed from cells and incubated with HEK Blue cells for 24 hours, after which the levels of SEAP were measured (Figure 3.5). Mock transfected and HEK Blue-only conditions showed low absorbance levels and were used to determine the background of the assay (< 50 IFN U/mL). The negative control where the PB1-coding plasmid was replaced by an empty pDUAL plasmid (2PNP) resulted in

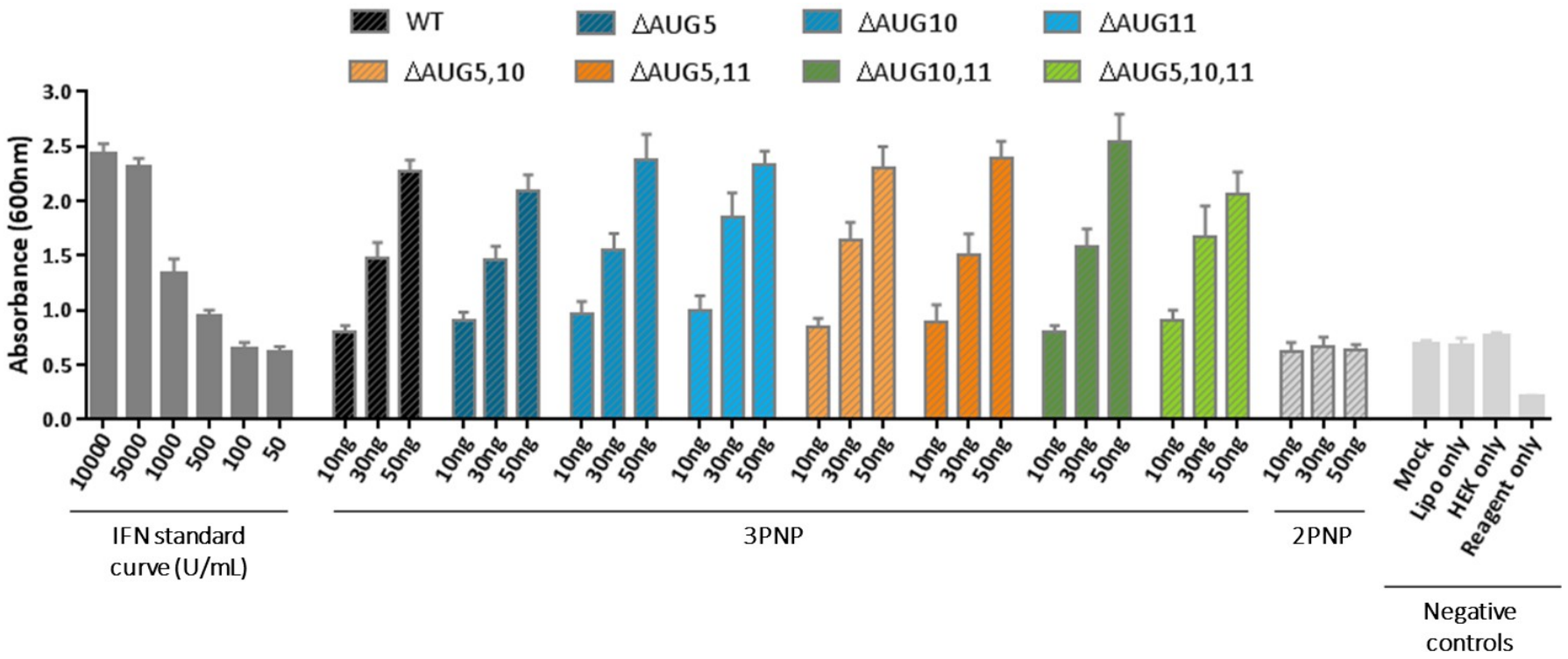

Figure 3.5: Assessment of IFN induction triggered by WT and mutant RNPs. 293T cells were transfected with 10, 30 or 50ng of each pDUAL plasmids encoding the individual components of the RNP complex alongside 4, 12 and 20ng of reporter vRNA-like plasmid, respectively. Forty-eight hours post transfection, IFN levels were measured using the HEK Blue cell assay. Data represent mean + SEM of at least 3 independent experiments performed in triplicates.

background levels of IFN induction, confirming as expected (Rehwinkel *et al.* 2010) that the levels of 5'-ppp-containing vRNA produced by RNA Pol I transcription of the pDUAL plasmids was not enough to provoke an IFN response. In contrast, all active RNP (3PNP)-containing samples showed a dose-dependent IFN induction that increased with the amount of transfected plasmid (50ng>30ng>10ng). However, comparison of IFN induction between WT and mutant RNP reconstitutions did not show any statistically significant differences at any of the plasmid doses tested. These data did not support the hypothesis of a stronger detection of the RNA "panhandle" associated with the mutant PB1 subunits.

3.2.4. Fitness of segment 2 mutant viruses in IFN-defective systems

Given the pronounced IFN induction by segment 2 mutant viruses and their reduced propagation in INF-competent *in vitro* systems, it was hypothesised that mutant viruses might recover fitness in IFN defective systems. The first IFN-defective system investigated was embryonated chicken eggs at early stages of development. Chick embryos lack many mechanisms required to recover from viral infections such as the production of antibodies and delayed type sensitivity (Simonsen 1957; Trnka and Riha 1959). Furthermore, IFN inducibility and responsiveness only develop from day 8 and become stronger from then onwards (Isaacs and Baron 1960). Moreover, a correlation between the lethality of viral infections and the absence of a developed IFN system in early development chicken eggs has been noted (Baron and Isaacs 1961).

Here, it was aimed to assess whether the attenuated viruses ΔAUG10,11 and ΔAUG5,10,11 propagated better in chicken eggs at an earlier developmental stage.

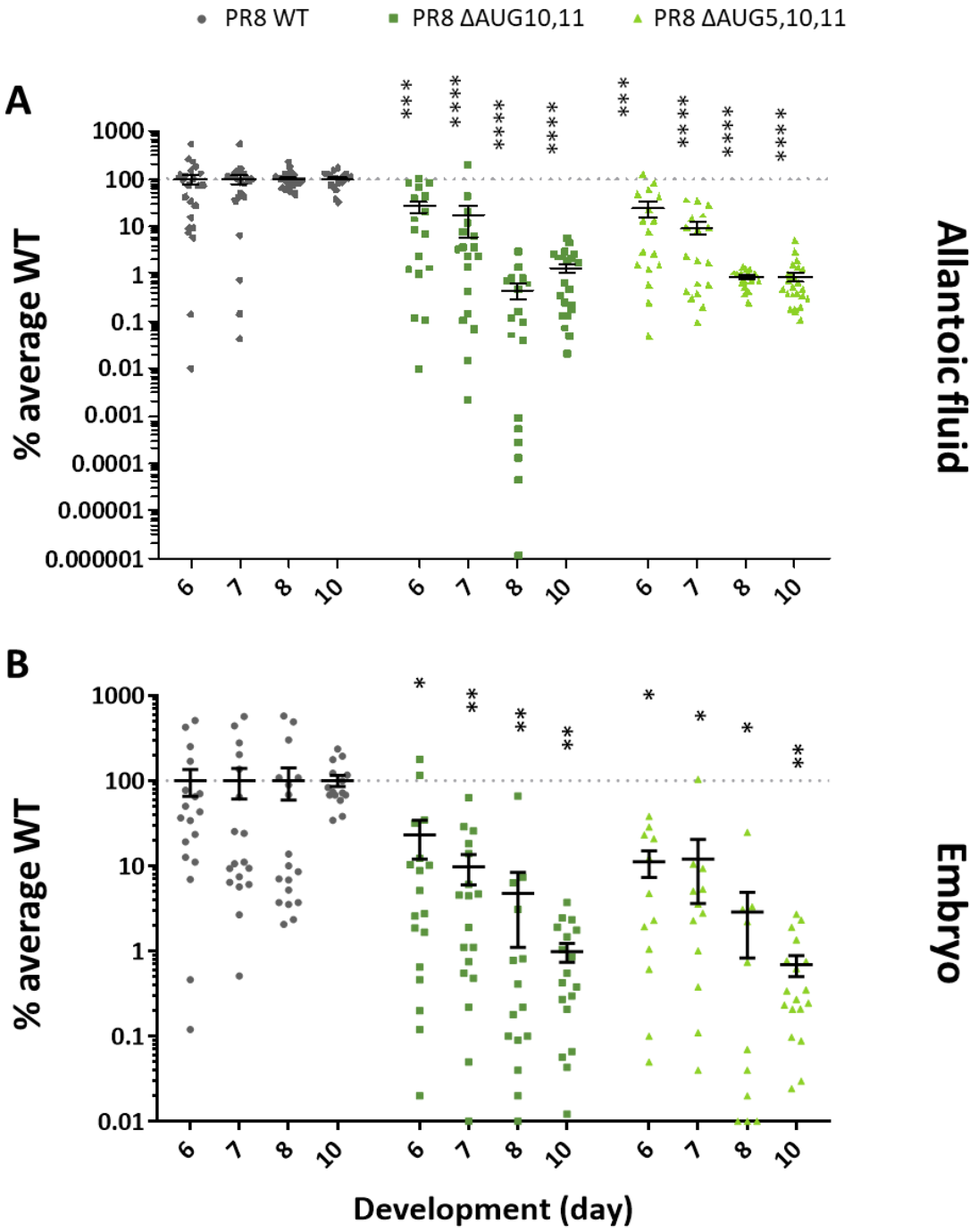

Figure 3.6: Virus growth in early development hen's eggs. Eggs at development days 6, 7, 8 and 10 were infected with 100 PFU of PR8 WT, ΔAUG10,11 or ΔAUG5,10,11. Twenty-four hpi, allantoic fluids (A) and embryos (B) were collected and viral titres were measured by plaque assay. Data represent individual viral titre data points scaled to WT PR8 from 3 independently performed experiments (total number of data points varies between 18 and 24). Statistical annotations represent the result of a two-way ANOVA test. Multiple comparisons were performed against WT. *p-value <0.05, **p-value <0.01, ***p-value <0.001, ****p-value <0.0001.

The allantoic cavity of 6, 7, 8 and 10 day old eggs was infected with WT, ΔAUG10,11 and ΔAUG5,10,11 PR8 viruses. Twenty-four hpi, eggs were humanely killed by overnight 4ºC incubation. Allantoic fluids and embryos were collected, the latter macerated and both titrated by plaque assay. WT PR8 replicated to titres of 10^9 and 10^7 PFU/mL in allantoic fluid and embryos, respectively, showing no relationship to the egg development stage (data not shown). The average of these titres (within each independent experiment) was used to scale the titres for PR8 ΔAUG10,11 and ΔAUG5,10,11 egg infections at the different days of development (Figure 3.6). In contrast to WT PR8, the replication of the mutant viruses was egg development stage-dependent. As shown in section *2.2.5. Fitness of segment 2 mutant viruses in avian systems*, allantoic fluid titres of PR8 ΔAUG10,11 and ΔAUG5,10,11 were significantly reduced in comparison to WT PR8 in 10 day-old eggs, replicating, on average, to approximately 1% of the WT virus titre (Figure 3.6A). A similar outcome was observed when these mutant viruses were used to infect 8-day eggs. The double mutant ΔAUG10,11 presented slightly (but not statistically significant) lower titres in 8-day old allantoic fluids, while the triple mutant showed an equivalent phenotype when compared to 10-day old infections. However, higher titres of these two viruses were observed when infecting pre-day 8 eggs. An at least 10-fold increase in titre was seen when comparing viral titres from 7- with 8-day old allantoic fluids from eggs infected with either mutant virus. An additional, not as pronounced, increase in viral titre was also observed between 7- and 6-day old allantoic fluids. Similarly to in section *2.2.5.*, embryo viral titres were also acquired from these infections (Figure 3.6B). These titres were more variable than the ones obtained from the allantoic fluids. In this case, WT PR8 replicated to 10^7 PFU/mL in 6-day old eggs, but only to 10^6

PFU/mL in 10-day old eggs (data not shown). Nonetheless, given the variability of the data, this difference was not statistically significant. After scaling the viral titres of the mutant viruses to those of PR8 WT, the expected growth pattern was observed for the embryo titres of the mutant viruses; a 100-fold reduction in comparison to WT PR8 in 10-day old embryos. Overall, although still statistically significantly diminished in comparison to PR8 WT, an increased replicative fitness of the attenuated viruses was observed in all egg ages under 10-days old. However, unlike what was observed in allantoic fluid titres, a 10-fold increase in virus fitness was seen in 8-day old embryos. Similarly to in allantoic fluids, this fitness increase also progressed in 7- and 6-day old eggs.

The second IFN-defective system used was type I IFN receptor knockout ($IFNAR^{-/-}$) bone marrow-derived macrophages (BMDM) as described in section *8.3.3. Isolation of bone marrow-derived macrophages*. The suitability of macrophages as a model cell type to access *ex vivo* IAV infection is arguable as IAV primarily targets airway and alveolar epithelial cells and the use of those could have constituted a more clinically relevant cell type. However, the main objective was to compare naïve and $IFNAR^{-/-}$ conditions. BMDMs were mainly chosen given the existence of an already established extraction and differentiation protocol available in the laboratory and the fact that they were previously known to be susceptible to PR8 infection. BMDMs were prepared from the femurs of female 129Sv/Ev and $IFNAR^{-/-}$ mice (Muller *et al.* 1994) and infected at a multiplicity of 0.001. Supernatants were collected at different points post infection and titrated by plaque assay (Figure 3.7). WT PR8 replicated with similar kinetics in WT and $IFNAR^{-/-}$ BMDMs, with the exception of a non-statistically significant 1 $\log_{10}$ difference observed at 24 hpi, reaching titres of 10^7 PFU/mL in both

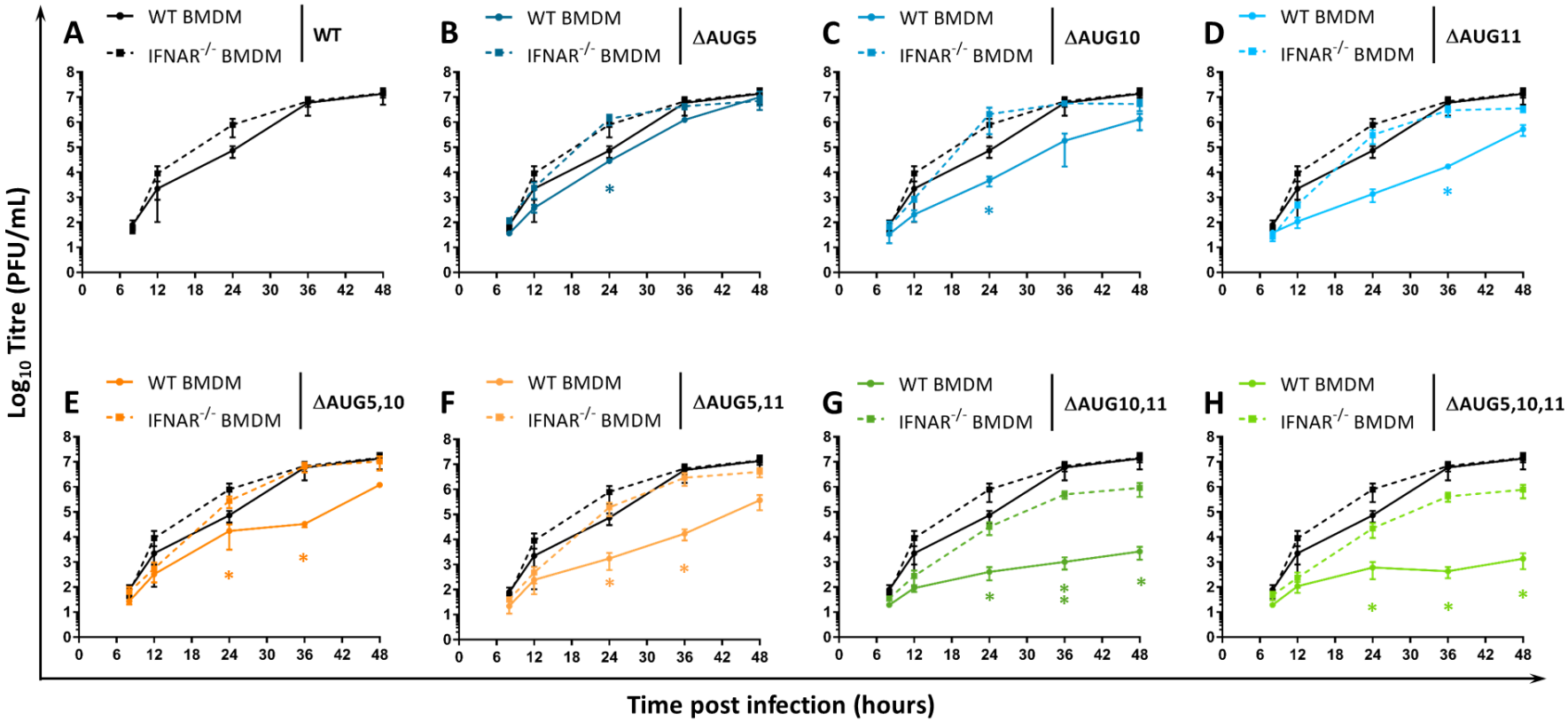

Figure 3.7: Growth kinetics of PR8 WT and segment 2 mutants in bone marrow-derived macrophages. WT and IFNAR$^{-/-}$ BMDM were infected at a MOI of 0.001. Supernatants were collected at various times post infection and viral titres were determined by plaque assay. Data relative to WT PR8 is repeated between panels to allow comparison. Data represent mean ± SEM of two technical repeats from at least 3 independent experiments (each experiment was performed with an independently extracted and differentiated batch of BMDMs). Statistic annotations are the result of t-tests performed individually for each time-point and WT and mutant virus between WT and IFNAR$^{-/-}$ BMDM. *p-value <0.05, ** p-value <0.01.

cell types (Figure 3.7A). In this system, single mutation of AUG5 gave comparable end-point titres to the WT virus but showed a 2-$\log_{10}$ attenuated growth at 24 hpi in WT macrophages, which was fully restored by the IFNAR knockout (Figure 3.8B). Single mutants ΔAUG10 and ΔAUG 11 replicated less throughout the entire span of infection in WT macrophages, with 1000-fold reductions in titres at 24 and 36 hpi and a 10-fold lower end-point titre (Figure 3.7 C and D). Like PR8 ΔAUG5, this attenuation was not present in IFNAR$^{-/-}$ BMDMs, with both viruses reaching WT-like titres at 24, 36 and 48 hpi. Similar behaviour was seen for the double mutants ΔAUG5,10 and ΔAUG5,11 (Figure 3.7 E and F), although it was noticeable that the ΔAUG11 containing mutants were slightly more attenuated than their ΔAUG10 counterparts. Replication of PR8 ΔAUG10,11 and ΔAUG5,10,11 in WT BMDMs was especially attenuated throughout the entire course of the growth curve, reaching peak titres more than 10,000-fold lower than WT PR8 at the 48 hpi end point. However, in the IFNAR$^{-/-}$ cells, replication of the ΔAUG10,11 and ΔAUG5,10,11 was much improved, with both viruses achieving end-point titres of ~10^6 PFU/mL (Figure 3.7 G and H). Nevertheless, this recovery was not complete, with these mutant viruses showing 10-fold lower viral titres than WT PR8 in the knockout cells at any given timepoint post-infection. Thus overall, the ΔAUG mutant viruses showed replication defects in the BMDMs that were either not present or substantially less severe when the cells were unable to respond to type I IFN.

Globally, the improved growth fitness of segment 2 mutant viruses in the IFN-defective systems tested: early development eggs and IFNAR$^{-/-}$ BMDMs, was consistent with the previous data showing their increased IFN induction and supported

the hypothesis that the mutations rendered the viruses less able to cope with innate immune responses.

3.3. Discussion

Having identified novel translation products from IAV segment 2, the function of said peptides became the next question. The use of an engineered cell line allowed the measurement of type I IFN induction from WT- and the ΔAUG- infected cells. These assays showed increased levels of IFN secreted from cells infected with ΔAUG5, 10, and most pronouncedly with ΔAUG11-containing viruses. However, these mutant viruses didn't seem to be more sensitive to IFN treatment which might indicate a problem with IFN induction rather than aggravated sensitivity to particular ISGs.

The attenuated phenotype of ΔAUG10 and/or 11 viruses seen in data from recovery experiments described in chapter 2, has now the caveat that virus stocks themselves contain varying levels of type I IFN, which may have effects on the subsequent infection of fresh cell monolayers. However, the viral stocks were prepared from canine cells and much of the growth kinetics presented in chapter 2 as well as all the IFN-related experiments described in this chapter were performed in human cells which are not responsive to canine IFN (data not shown).

Stronger IFN induction generally correlates with increased upregulation of hundreds of ISGs, some of which have well known antiviral properties. An example of one is BST2/tetherin which has been shown to restrict the release of several viruses

by retaining newly-formed enveloped viruses at the cell surface. However, the inhibitory effects of tetherin against IAV infection has not been fully elucidated, with disagreement between different studies (Gnirss *et al.* 2015; Watanabe *et al.* 2011). However, an additional ISG involved in the late stages of infection is CIG5/viperin. Viperin was shown to perturb lipid rafts and inhibit IAV packaging/release (Wang *et al.* 2007). Moreover, serpin1 was also shown to modify the extracellular environment and prevent IAV maturation (Dittmann *et al.* 2015). Hence, one can speculate that the observed upregulation of type I IFN upon infection with PR8 ΔAUG10,11 and ΔAUG5,10,11 can lead to the overexpression of these three ISGs, which combined affect may contribute to the packaging-deficient phenotype of these double and triple mutants, previously described in section 2.2.7.

The increased IFN induction by ΔAUG mutant viruses could be attributed to different reasons:

1. As previously mentioned earlier in chapter 2, the introduction of ΔAUG mutations translates into single amino acid mutations within the PB1 protein. Therefore, the observed IFN induction could be due to PB1-related defects such as greater sensing of the viral RNA panhandle by RIG-I due to a mutated PB1. However, data presented in this chapter suggested that IFN induction from mutant vRNPs was unaltered when compared to WT vRNPs. However, detection of panhandle from mutated cRNPs was not assessed and further assays to fully determine the implications of the detection of viral RNA could be tested by using RIG-I knockout cell lines.
2. The mutated polymerase can result in greater DVG formation and lead to the increased IFN induction. This hypothesis is consistent with the high genome/PFU

ratios described in section 2.2.7, once the oligonucleotides used to measure the number of genomes were designed against the 3' end of vRNA which has been shown to be present in both DVGs and complete vRNAs (Gog *et al.* 2007; Nayak 1980; Nayak *et al.* 1982). However, specific measurement of DVGs in segment 2 of other segments was not performed and a more detailed qPCR and or sequence analysis would be necessary to fully address this theory.

3. Mutations introduced in PB1 jeopardise its IFN antagonist function. As described in chapter 1, studies on the polymerase and the IFN response have suggested that the viral polymerase complex exhibited an inhibitory activity on IFN-β promoter activation through the interaction of PB2 with MAVS (Iwai *et al.* 2010) or the interaction of the PB1-PA dimer of incoming vRNPs with RIG-I at the very first stages of infection (Liedmann *et al.* 2014b). Although not inducing a stronger IFN response (according to results in section 3.2.3), the mutant vRNPs can potentially also be defective in this pre-packaged IFN inhibition mechanism.
4. The shorter forms of PB1 hold IFN antagonist function and their ablation hinders that control. Considering the lack of expression of PB1-N92 and –N111 from the ΔAUG10 and ΔAUG11 viruses, the over induced type I IFN expression can also be associated with these two polypeptides. Given the sequence overlap of PB1 and its shorter products, PB1 mutations downstream of amino acids 91 and 111 are also present in PB1-N92 and/or PB1-N111. Recent genome-wide studies showed that the point amino acid mutation in PB1 L155H is associated with IFN sensitivity (Du *et al.* 2018). The WT leucine is a highly conserved amino acid (although coded by varied codons) and is shared by ORFs of all four PB1-related polypeptides (Gog *et al.* 2007). However, mutation of this residue in the

background of WSN did not lead to increased levels of IFN-β, compared to its WT counterpart (Du *et al.* 2018).

To further correlate the increased IFN induction with the attenuated phenotype of segment 2 mutants, viral fitness was assessed in IFN defective systems (embryonated eggs under development day 8 and murine IFNAR$^{-/-}$ BMDM) where, in general terms, there was a better propagation of the mutant viruses, in comparison to the IFN competent counterpart. The obtained recovery in underdeveloped eggs correlated with previous studies of influenza B virus (IBV) NS1 which involved the use of 6, 8 and 11day old eggs to assess viral fitness. In these, wild-type IBV replicated to high titres in embryonated eggs regardless of their development age. In contrast, the growth of IBV ΔNS1 virus gradually declined with the increasing age of the eggs (Dauber *et al.* 2004).

Overall, this chapter revealed reasons behind the attenuation of the segment 2 AUG mutants – a stronger induction of type I IFN. The implications of this over induced presence of type I IFN in an *in vivo* system will be assessed in the following chapter.

Chapter 4

In vivo studies with segment 2 mutant viruses

4.1. Background and aims

The previous chapters characterised the segment 2 mutants *in vitro*, concluding that the ablation of PB1-N92 or/and PB1-N111 expression by the mutation of their initiator codons, lead to the attenuation of virus replication in several model systems. Moreover, these mutant viruses were shown to more strongly induce the type I IFN response, compared to their WT counterpart. Furthermore, replication of the attenuated mutants recovered in IFN-defective systems.

In vivo studies in murine models have been used to characterise important roles of IAV accessory proteins in pathogenesis, disease progression and viral fitness (Yamayoshi *et al.* 2016; Wise *et al.* 2012; Jagger *et al.* 2012). Therefore, since it was possible that the phenotype of the ΔAUG mutants resulted from loss of an accessory gene product, this chapter assessed whether:

- The discrepancy in viral replication and the recovery of the attenuated mutant in an IFNAR$^{-/-}$ context was also seen in an *in vivo* model;
- The attenuated replication of the ΔAUG10,11 virus was reflected in its virulence;
- Cytokine profiling in the context of viral infection corroborated the differences found in the viral titres and observed pathology.

To answer these questions, 129Sv/Ev WT and IFNAR$^{-/-}$ mice were infected with WT or ΔAUG10,11 PR8 viruses. These mice lack the type I IFN receptor and therefore do not respond to IFN α or β (Muller *et al.* 1994). Weight loss was measured at two different infection doses, while virus replication and IFN-β expression were assessed from infected lung tissues and histopathology analysis was carried out on H&E stained sections. Finally, innate immune and cytokine responses were also assessed by analysis of lung homogenates.

4.2. Results

4.2.1. Weight loss of infected 129Sv/Ev WT and IFNAR$^{-/-}$ mice

To first assess the ability of the segment 2 mutant virus to cause disease *in vivo*, weight loss was measured during infection of 129Sv/Ev WT and IFNAR-lacking mice. To test a suitable infectious dose (*i.e.*: not overly severe) for both types of mice, a small-scale pilot study was performed in which groups of 2 WT and 2 IFNAR$^{-/-}$ mice were infected with 200 PFU of WT PR8 under anaesthesia, through the intranasal route in a 40μL droplet. Mice were weighed at the same time each day and clinical scores

(based on marked piloerection, hunched position, moderate to marked staining around eyes and/or nose, greatly reduced spontaneous activity, poor response to external stimuli, or clinically-apparent dehydration) were also recorded. Both WT and IFNAR$^{-/-}$ mice showed weight loss from day 3 post infection but the IFNAR$^{-/-}$ exhibited more weight loss than WT mice (Figure 4.1A). By 6 dpi IFNAR$^{-/-}$ mice had lost an average of 22% of the initial weight while WT mice had only lost 12%. The severity of clinical symptoms correlated with weight loss, with IFNAR$^{-/-}$ mice presenting with more ruffled coats, lethargy, trembling and hunching (data not shown). Due to the overall severe clinical score of IFNAR$^{-/-}$ mice, this pilot study was halted at day 6 post infection.

To investigate the extent to which IAV pathogenesis varied depending on mutation of segment 2 AUG codons 10 and 11, having the pilot study as reference, the 200 PFU dosage was used in a larger scale experiment. This time, cohorts of 2-5 seven-week old WT and IFNAR$^{-/-}$ mice were inoculated with 200 PFU of WT and ΔAUG10,11 PR8 viruses, or sham inoculated with PBS (Figure 4.1B and C). Once again, weights and clinical scoring were recorded daily. Mock-infected animals showed minimal weight loss and no clinical signs throughout the entire experiment. All WT PR8-infected mice showed weight loss from day 3 (Figure 4.1B), reaching a 12% weight loss at day 5 post infection. PR8 ΔAUG10,11-infected WT mice, although non-statistically significant, showed a delay in weight loss, which was only observed from day 4 post infection. However, these mice reached equivalent levels of percentage weight loss by the 5th day post infection to PR8 WT-infected WT mice. Similar to the pilot study, IFNAR$^{-/-}$ mice showed a more rapid progression of clinical symptoms, reaching 21% weight loss at day 5 post infection (Figure 4.1C). A

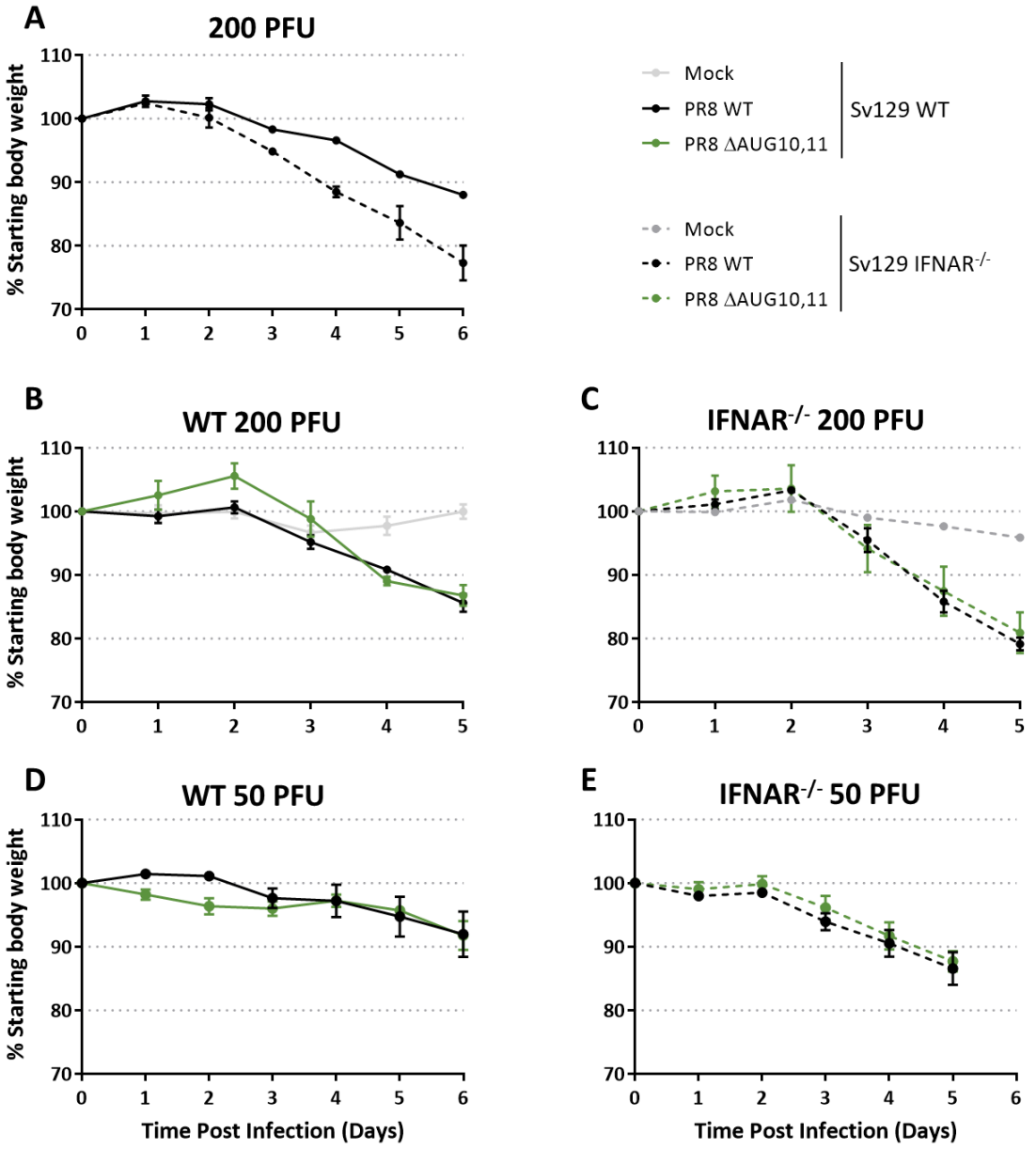

Figure 4.1: Weight-change of infected 129Sv/Ev mice. (A) Groups of two WT and IFNAR$^{-/-}$ mice were infected intranasally with 200 PFU of WT PR8 virus. Weight was monitored daily and mice were euthanised at day 6 post infection. Data represent mean ± SEM of one independent experiment. (B and C) Cohorts of WT and IFNAR$^{-/-}$ mice were infected with 200 PFU of PR8 WT or ΔAUG10,11, or mock inoculated with PBS. After 5 days of monitoring, mice were euthanised at day 5 post infection. Experiment was performed once with the following mouse numbers: WT/mock n=2, WT/WT n=2, WT/ΔAUG10,11 n=5, IFNAR$^{-/-}$/mock n=1, IFNAR$^{-/-}$/WT n=2, IFNAR$^{-/-}$/ΔAUG10,11: n=5. Data represent mean ± SEM. (D and E) As in B and C but mice were infected with 50 PFU of each virus. Experiment was performed once with the following mouse numbers: WT/WT n=5, WT/ΔAUG10,11 n=4, IFNAR$^{-/-}$/WT n=5, IFNAR$^{-/-}$/ΔAUG10,11: n=5. Data represent mean ± SEM.

comparable phenotype was seen for IFNAR$^{-/-}$ mice infected with PR8 ΔAUG10,11. At this time mice were euthanised for ethical reasons, given the severe clinical scoring of IFNAR$^{-/-}$ mice.

The 200PFU dose caused severe symptoms in the animals but without showing a statistically significant difference in weight loss between ΔAUG10,11 and WT PR8 viruses in WT or IFNAR$^{-/-}$ mice. Therefore, a lower infectious dose was administrated to test if this might separate the WT and ΔAUG10,11 weight loss curves. Groups of 5 five-week old mice were inoculated with 50 PFU of either virus and weight-loss was monitored daily (Figures 4.1D and F). With this dose, WT mice exhibited a delayed and less accentuated weight loss compared to the 200 PFU virus dose, with no change in weight until day 4 post infection and only reaching 8% weight loss at infection day 6. Animals infected with the mutant virus showed an immediate weight loss, which merged into the WT PR8 weight loss curve from day 3 post infection. Similarly to the results for the high dose study, IFNAR$^{-/-}$ mice were more susceptible to infection, starting to lose weight at day 3 and reaching an average 13% of weight loss at day 5 post infection, but as observed with the 200 PFU infection, there were no weight loss differences between WT and mutant virus-infected animals throughout the entire course of infection. IFNAR$^{-/-}$ animals were culled at day 5 because of increasingly severe clinical signs. However, hoping to see possible differences emerging at later time points, WT animals were only culled at day 6. Nevertheless, although disease was minimal, there was no differences between WT and ΔAUG10,11-caused weight loss.

In summary the data presented here indicated that the mutation of segment 2 AUG codons 10 and 11 (and the predicted removal of N-terminally truncated PB1

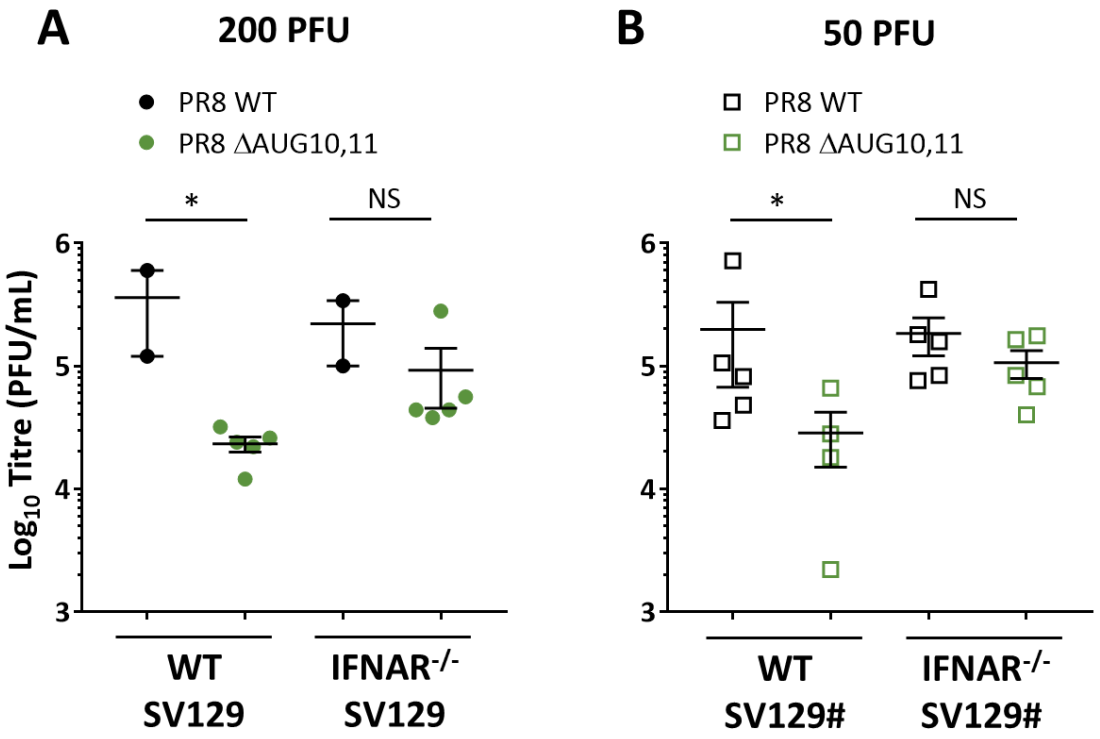

Figure 4.2: Virus titres from infected mouse lungs. Groups of at least 2 mice were infected with 200 (A) or 50 (B) PFU of virus. Five or six days post infection, mice were euthanised and the left lung was removed and homogenised in serum-free medium. Virus titres were measured by plaque assay. Data tagged with "#" correspond to an euthanasia and lung collection at day 6 post infection. Experiment was performed once. Data represent individual mouse data points as well as mean ± SEM. Statistic annotations are the result of t tests. *p-value <0.05.

products) in the background of PR8 did not affect weight loss *in vivo*, irrespective of the ability of the mice to respond to type I IFN. This was a surprising outcome in light of the strong attenuation of the ΔAUG10,11 virus *in vitro* and *in ovo*.

4.2.2. Virus fitness in 129Sv/Ev WT and IFNAR$^{-/-}$ mice

The replicative fitness of WT and mutant viruses was measured in infected mouse lungs. Mice infected with 200 or 50 PFU of each virus had been euthanised at 5 or 6-days post infection, as described above. Left lungs were extracted, homogenised and clarified by centrifugation, and infectious virus was quantified by plaque assay. Mock-infected mice did not have detectable (> 20 PFU/mL) levels of infectious virus (data not shown). Both inoculated viruses replicated *in vivo*, but the degree of replication varied significantly depending on the presence or absence of the segment 2 AUG codons (Figure 4.2). WT PR8 replicated to titres of ~ 10^5 PFU/mL in mice infected with either 200 or 50 PFU, regardless of the mouse type. However, PR8 ΔAUG10,11 grew to significantly lower titres in mice with an intact IFN system, reaching 10-fold less viral titre. This mirrored the *in vitro* findings in BMDMs (Figure 3.8). Further correlating with the *in vitro* replication findings, replication of PR8 ΔAUG10,11 recovered in IFNAR$^{-/-}$ mice such that there was no significant difference in titre between the two viruses.

Given the reversion of the ΔAUG10,11 virus previously seen in embryonated eggs, viral content from lung homogenates was sequenced. No reversions of the mutant virus were detected in any of the infected mice. Examination of potential revertant viruses was performed by Sanger sequence by which, for instance, a 1% reversion

would not be detected and therefore to have certainty of the absence of reversion, a more sensitive sequencing method could have been applied. However, as previously seen in section 2.2.4, a corresponding smaller plaque phenotype was also observed in ΔAUG10,11-infected viral samples, compared to lung homogenates from WT PR8-infected mice (data not shown).

Hence, although the attenuated virus caused similar weight loss in infected mice to WT virus, viral replicative fitness correlated with the *in vitro* data. PR8 ΔAUG10,11 replication was attenuated in WT mice and not in IFNAR$^{-/-}$ animals.

4.2.3. IFN-β induction in infected mouse lungs

Given the increased level of type I IFN induction seen in A549 epithelial cells (Figure 3.2) and the fact that IAV infection occurs mainly in epithelial cells in *in vivo* infections, we hypothesised that the same trend would be seen in infected mouse lungs. Therefore, the lung homogenates from a 200 PFU dose infection were used in an IFN-β ELISA test (Figure 4.3). Both WT and IFNAR$^{-/-}$ mock-infected samples gave assay background levels of IFN-β induction. PR8 WT infected mice had minor but statistically significant increased levels of IFN-β compared to mock-infected animals. However, in ΔAUG10,11-infected mice, the detection of IFN-β was higher in comparison to WT-infected mice. A similar IFN-β production pattern was observed for IFNAR$^{-/-}$ mice. These data corroborated those previously obtained in the *in vitro* system and showed that infection with segment 2 mutant viruses also resulted in increased induction of the type I IFN response *in vivo*.

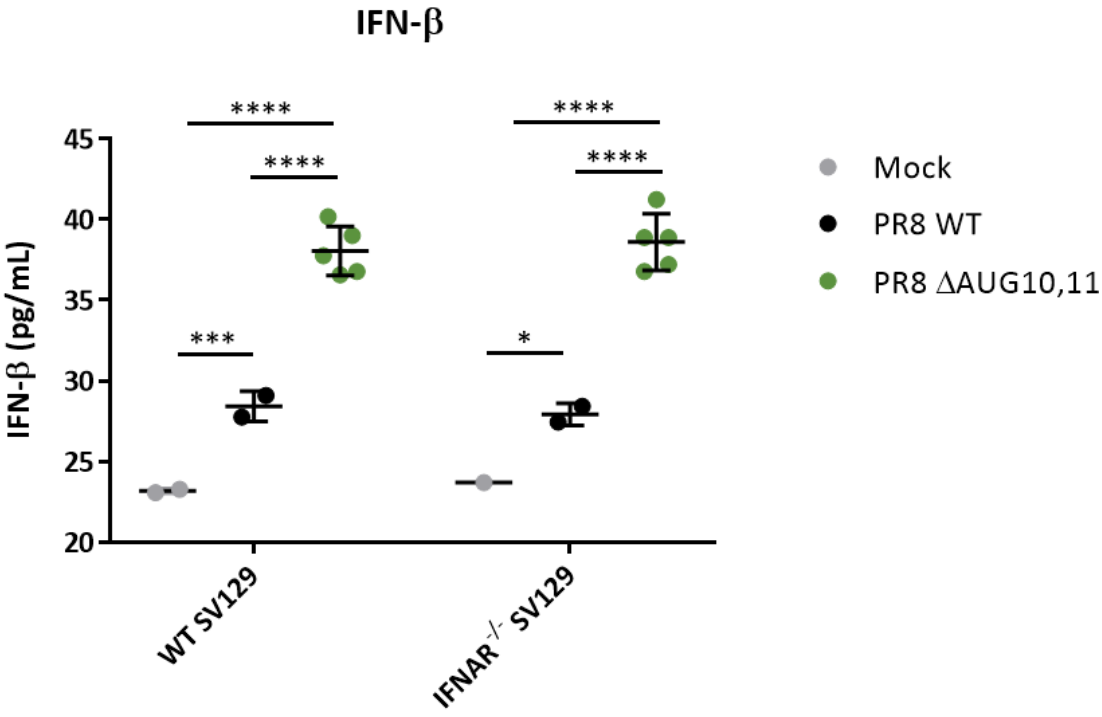

Figure 4.3: IFN-β induction from infected mouse lungs. Groups of mice were infected with 200 PFU of virus. Five days post infection, mice were euthanised and the left lung was removed and homogenised in serum-free media. IFN-β concentration was determined by ELISA plate and concentration of cytokine for each sample was performed based on a standard curve. Experiment was performed once with technical duplicates. Data represent individual mouse data points and mean ± SEM. Statistic annotations are the result of a two-way ANOVA test. *p-value <0.05, ***p-value <0.001, ****p-value <0.0001.

4.2.4. Histopathology of infected mouse lungs

To visualise the extent of the inflammatory response and compare the severity of tissue damage induced by WT PR8 and the attenuated ΔAUG10,11 mutant,histopathology of infected lungs was performed at 5 days post infection. Right lungs of infected mice were simultaneously inflated and fixed with a neutral buffered formalin solution. After embedding in paraffin wax, sections were cut and stained with haematoxylin and eosin (performed by the Easter Bush Pathology Unit), allowing pathology scoring by light microscopy. Samples were scored for epithelial cell degeneration and necrosis, peribronchial/peribronchiolar inflammation, perivascular inflammation, interstitial inflammation and interstitial necrosis as described in section 7.8.4, giving an overall score between 0 and 3 to represent the severity of pathology. Image acquisition and pathology scoring were performed blindly by Dr Philippa Beard (The Pirbright Institute, Surrey, UK). The following paragraph was adapted from the pathology report provided by Dr Beard.

Mock-infected samples showed no evidence of influenza infection, presenting only incidental changes (peracute multifocal mild haemorrhage and congestion with occasional mild crush artefact). The remainder of the images displayed evidence of histological changes consistent with murine influenza virus infection. The predominant changes identified were epithelial degeneration and necrosis accompanied by peribronchial and perivascular inflammation, and inflammatory cells within the alveolar airspaces with minimal necrosis of the alveolar walls. The inflammatory infiltrate surrounding blood vessels and airways varied from mixed (macrophages, lymphocytes and neutrophils) to predominantly lymphocytic. The

overall severity of the pathology was not particularly varied, however the specific pathology (such as the extent of inflammation of the interstitial tissues) did vary between images. In WT-infected lung samples, the pathology focused mainly on the airways and blood vessels with very little involvement of the alveoli or interstitium. In ΔAUG10,11-infected lung sections, there was a substantial number of mainly large foamy macrophages (and fewer lymphocytes and neutrophils) within the airspaces of alveoli with occasional necrotic intra-alveolar cells.

Graphical and statistical analyses of the tissue section cores provided by Dr Beard indicated that infection of IFNAR$^{-/-}$ mice with either WT or ΔAUG10,11 PR8 viruses did not result in statistically significant differences between the viruses in the overall score nor in any of the specific pathology scores (Figure 4.4). However, in WT mice, despite the lack of difference in the overall score between mutant and WT viruses, there was significantly reduced interstitial inflammation in ΔAUG10,11-infected mice in comparison to WT PR8. Comparison of specific pathology scores between virus/mice sample groups did not identify any statistical differences between WT and IFNAR$^{-/-}$ mice infected with PR8 WT. However, PR8 ΔAUG10,11 infection resulted in differences between WT and IFNAR$^{-/-}$ mice. IFNAR$^{-/-}$ mice infected with ΔAUG10,11 had more severe perivascular, peribronchial and interstitial inflammation and a higher overall pathology score compared to ΔAUG10,11-infected WT mice.

Thus overall, in WT mice, pathology did not correlate with virus titre, with the exception of interstitial inflammation, which was markedly lower in ΔAUG10,11 infected animals. However, the mutant virus provoked signifcantly more inflammatory damage in IFNAR$^{-/-}$ mice (where virus titre recovered) than WT mice, indicating that, consistent with the elevated IFN-ß levels, it might be intrinsically more inflammatory

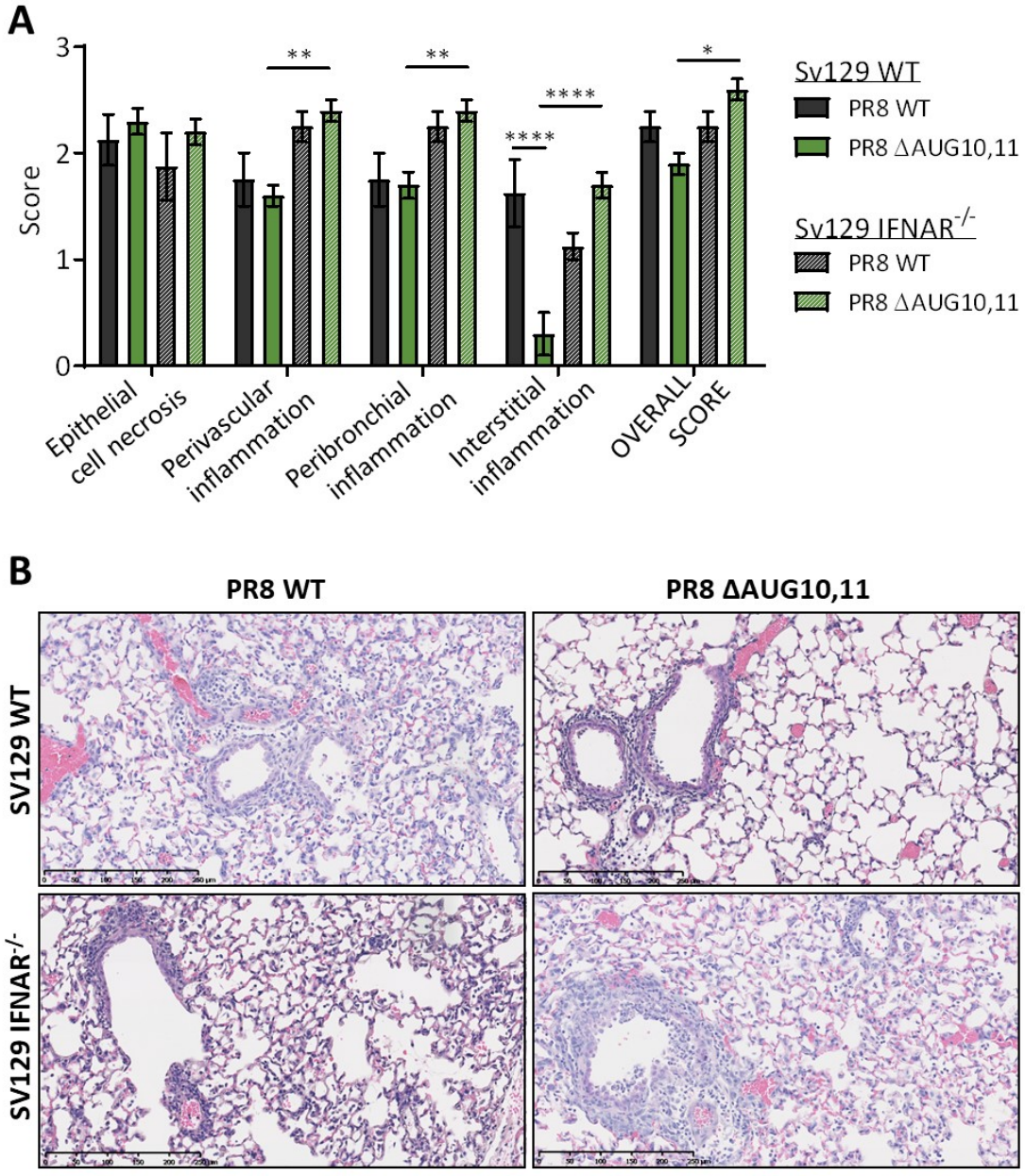

Figure 4.4: Histopathology of infected mouse lungs. Mice were infected with 200PFU of each WT or ΔAUG10,11 PR8 viruses. Five days post-infection, right mouse lungs were inflated, fix, processed and H&E stained. (A) Lung pathology severity was blindly assessed by Dr Philippa Beard and scored out of 3. Experiment was performed once with the following mouse numbers: WT/WT n=2, WT/ΔAUG10,11 n=5, IFNAR$^{-/-}$/WT n=2, IFNAR$^{-/-}$/ΔAUG10,11: n=5. Data are mean ± SEM. Statistical annotations are the results of a 2-way ANOVA test. *p-value <0.05, **p-value <0.01, ****p-value <0.0001. (B) Representative figures of the assessed pathology. Images were acquired and kindly provided by Dr Beard.

than WT PR8.

4.2.5. Cytokine and chemokine profiling of infected mouse lungs

To further explore the underlying reason behind the differences in pathology and viral titres but similar weight loss with WT and ΔAUG10,11 viruses, cytokine and chemokine profiles from mouse lungs were measured. Lung homogenates of 1-5 mice from day 5 post infection with 200PFU of virus were pooled and applied in a cytokine and chemokine immunoblot array as described in section 7.8.7. The number of mice used for each homogenate varied between conditions. Two mice per homogenate were used for PR8 WT-infected WT and IFNAR$^{-/-}$ animals infected while 5 mice of each background were used for ΔAUG10,11-infected mice. The spot intensities of two duplicate arrays were averaged and relative expression of each cytokine was scaled to its signal in the respective mock-infected sample. Cytokines were subdivided into 3 categories: proinflammatory agents, interleukins and chemokines. Fold-induction values were ranked in descending order of relative quantity of certain cytokine in the PR8 WT/WT mice sample values in each category and presented as a heat-map (Figure 4.5A, B). The majority of the cytokines measured were up-regulated in both WT and IFNAR$^{-/-}$ mice infected with either virus, compared to mock-infected mice, as expected. However, also visible was a general pattern of higher upregulation in animals of either genotype infected with the ΔAUG10,11 virus. All inflammatory markers (with the exception of siCAM-1 whose expression was unaltered in 3 of 4 conditions) were up-regulated in infected animals. The main examples of this were TIMP-1 and TREM-1 which were upregulated 8-fold in WT mice and 288-fold in the

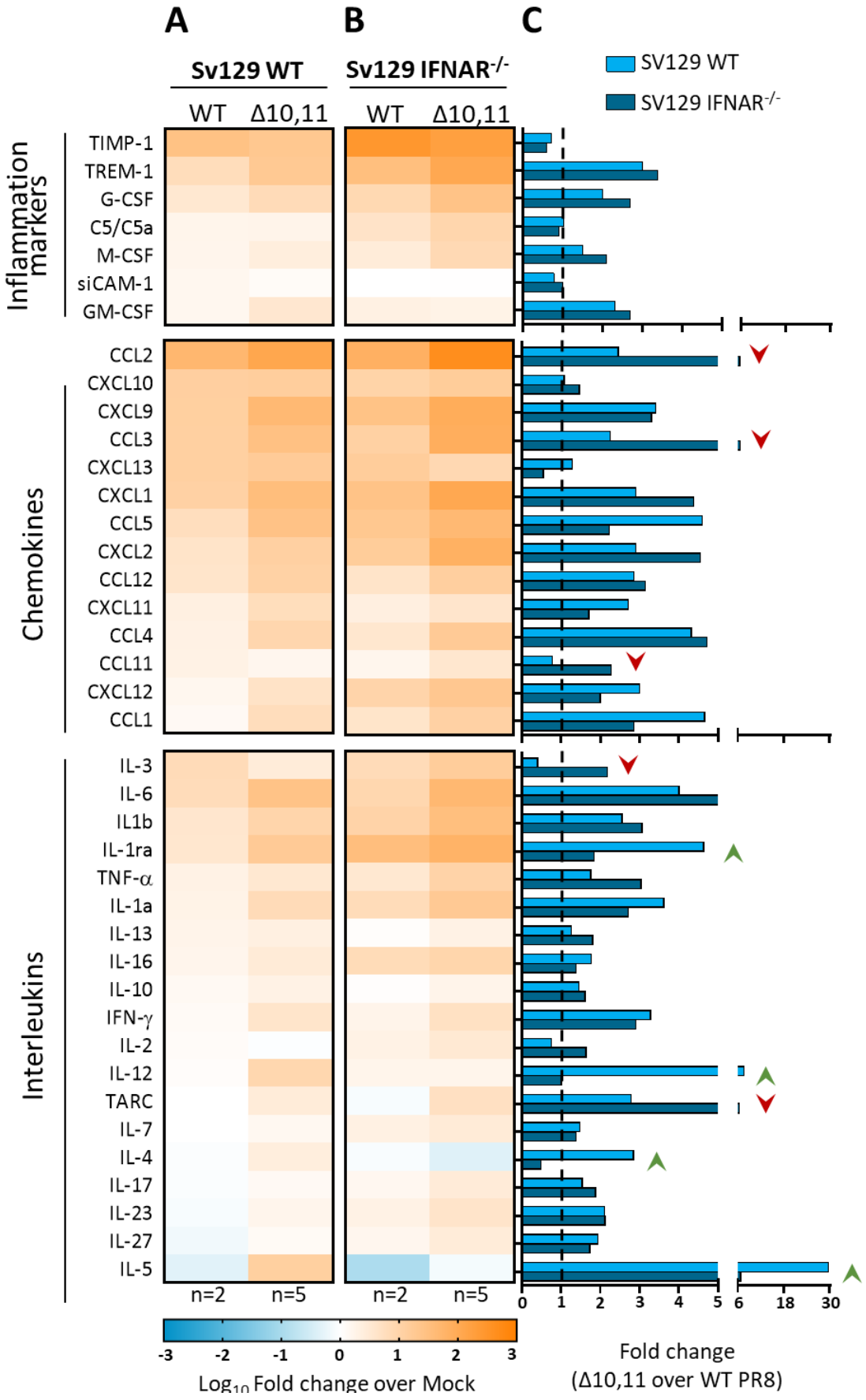
A
B
C
Sv129 WT
Sv129 IFNAR-/-
WT
Δ10,11
WT
Δ10,11
SV129 WT
SV129 IFNAR-/-
Inflammation markers
TIMP-1
TREM-1
G-CSF
C5/C5a
M-CSF
siCAM-1
GM-CSF
Chemokines
CCL2
CXCL10
CXCL9
CCL3
CXCL13
CXCL1
CCL5
CXCL2
CCL12
CXCL11
CCL4
CCL11
CXCL12
CCL1
Interleukins
IL-3
IL-6
IL1b
IL-1ra
TNF-α
IL-1a
IL-13
IL-16
IL-10
IFN-γ
IL-2
IL-12
TARC
IL-7
IL-4
IL-17
IL-23
IL-27
IL-5
n=2
n=5
n=2
n=5
-3
-2
-1
0
1
2
3
Log10 Fold change over Mock
0
1
2
3
4
5
6
18
30
Fold change
(Δ10,11 over WT PR8)

Figure 4.5: Cytokine and chemokine profiling of infected mouse lung. (A and B) The levels of various cytokines and chemokines were determined using an immunoblot spot array from pooled lung homogenates of mice infected with 200PFU of virus and culled at day 5 post infection. Values represent mean fold-induction relative to mock-infected samples and are plotted as a heat map. Experiment was performed once with technical duplicates with the following mouse numbers: WT/mock n=2, WT/WT n=2, WT/ΔAUG10,11 n=5, IFNAR$^{-/-}$/mock n=1, IFNAR$^{-/-}$/WT n=2, IFNAR$^{-/-}$/ΔAUG10,11: n=5. Values were ranked in descending order of relative abundance from the WT PR8/WT mice samples.(C) Ratios between ΔAUG10,11 and WT PR8 expression of each cytokine for each mouse background were calculated. Green upwards arrows indicate "overexpression hits" while red downwards arrows designate "underexpression hits" (see text).

IFNAR$^{-/-}$ counterpart mice, compared to the respective mock-infected animals (comparing the average of both viruses). Similarly, all the chemokines tested had increased expression in infected animals. The monocyte and NK cell chemotactic and pro-inflammatory cytokines CCL2, CXCL10 and CXCL9 were examples of this, presenting maximum fold induction ratios of 457.1, 15.1 and 87.1 over PBS-inoculated mice, respectively (Figure 4.5 A and B). WT PR8-infected WT mice showed a clear reduction in interleukin production when compared to the PR8 ΔAUG10,11 infection in the same type of mice (Figure 4.5A). However, this generic difference in interleukin induction between viruses was not as pronounced in the context of the IFNAR$^{-/-}$ (Figure 4.5B).

In order to better interrogate the differential cytokine expression by WT and ΔAUG10,11 viruses, we divided the cytokine induction levels of ΔAUG10,11 by the WT PR8-infection-related values (Figure 4.5C). This confirmed the visual impression from the heat maps that indeed, the majority of cytokines were upregulated more by infection with the ΔAUG10,11 virus than WT PR8 in either mouse strain. Exceptions were the inflammation markers TIMP-1, C5/C5a and siCAM-1. In addition, examination of the graphs highlighted specific cytokines that were differentially regulated by WT versus ΔAUG10,11 infection was performed.

A further ratio between the WT and IFNAR$^{-/-}$ mice was performed (here determined “double ratio”) (Tables 4.1 and 4.2). Cytokines whose double ratios were greater than 2 were considered “overexpression hits”. These hits represent cytokines where the ΔAUG10,11/WT ratio was considered higher in WT mice and therefore the potential cause of the ΔAUG10,11 attenuation. These over expression hits were entirely from the interleukin-related category: IL-12, IL-4, IL-5 and IL1ra. These are

Table 4.1: "Overexpression hits" between WT and IFNAR$^{-/-}$ mice. Description of the activation mechanisms and main role(s) of each cytokine are provided. Fold-change values represent the abundance of protein in ΔAUG10,11 infection relative to PR8 WT-infected sample. Double folds represent a further ratio between WT and IFNAR$^{-/-}$ mouse initial folds. $Double\ ratio = \frac{\left(\frac{\Delta 10,11}{WT}\right)\ of\ WT\ SV129}{\left(\frac{\Delta 10,11}{WT}\right)\ of\ IFNAR^{-/-}\ SV129}$.

Cytokine	Alternative name	Function	Reference(s)	ΔAUG10,11/WT PR8		Double ratio
				WT SV129	IFNAR$^{-/-}$ SV129	
IL-12	P70	Produced primarily by antigen presenting cells. Enhances proliferation and cytolytic activity of NK and differentiation of Th1 cells. Stimulates their IFNγ production.	(Trinchieri 1994)	7.62	1.01	7.57
IL-4	-	Regulator of Th cell differentiation into Th2. Regulator of cell proliferation, apoptosis and gene expression in lymphocytes, macrophages, fibroblasts and endothelial cells.	(Luzina *et al.* 2012)	2.85	0.5	5.71
IL-5	-	Major eosinophils maturation and differentiation factor	(Ikutani *et al.* 2012; Kouro and Takatsu 2009)	29.7	6.77	4.39
IL-1ra (interleukin-1 receptor antagonist)	-	Anti-inflammatory. Antagonises the IL-1 receptor, inhibiting IL-1α and IL-1β. Decreased expression of IL-1ra leads to uncontrolled systemic inflammation and polyarthropathy.	(Horai *et al.* 2000)	4.64	1.84	2.51

Table 4.2: "Under expression hits" between WT and IFNAR$^{-/-}$ mice. Description of the activation mechanisms and main role(s) of each cytokine are provided. Fold-change values represent the abundance of protein in ΔAUG10,11 infection relative to PR8 WT-infected sample. Double folds represent a further ratio between WT and IFNAR$^{-/-}$ mouse initial folds. $Double\ ratio = \frac{\left(\frac{\Delta 10,11}{WT}\right)\ of\ WT\ SV129}{\left(\frac{\Delta 10,11}{WT}\right)\ of\ IFNAR^{-/-}\ SV129}$.

Cytokine	Alternative name	Function	Reference(s)	ΔAUG10,11/WT PR8		Double ratio
				WT SV129	IFNAR$^{-/-}$ SV129	
CCL2 (chemokine (C-C motif) ligand 2)	JE, MCP-1 (monocyte chemoattractant protein 1), small inducible cytokine A2	Chemotactic for monocytes, memory T-cells NK cells to sites of inflammation.	(Deshmane *et al.* 2009)	2.45	6.46	0.38
CCL3	MIP1-α (macrophage inflammatory protein 1-alpha)	Pro-inflammatory. Activator of macrophages and CD8+ T-cells.	(Trifilo *et al.* 2003)	2.24	6.57	0.34
CCL11	Eotaxin, Eosinophil chemotactic protein	Selectively recruits eosinophils by inducing their chemotaxis.	(Jose *et al.* 1994; Ponath *et al.* 1996)	0.77	2.27	0.34
IL-3		Produced by T cells. Works alongside GM-CSF and IL-5 in the activation of myeloid cells. Involved in the production and activation of mast cell and basophil.	(Broughton *et al.* 2012)	0.41	2.19	0.19
TARC (thymus and activation regulated chemokine)	CCL17	Pro-inflammatory. Chemotactic for type II helper T-cells.	(Vestergaard *et al.* 2004)	2.79	6.40	0.44

mainly anti-inflammatory functions (with the exception of IL-12) and share functions such as lymphocyte and eosinophil maturation and differentiation. Important roles and activation mechanisms of each of these chemokines are described in Table 4.1. The same analysis was performed to determine "underexpression hits". These would have a double ratio of lower that 0.5 and would represent cytokines where differential expression between the two viruses was considered increased in IFNAR$^{-/-}$ mice. This increment could therefore be related to the higher pathology score of ΔAUG10,11-infected IFNAR$^{-/-}$ mice, compared with WT mice infected with the same virus (Figure 4.4). Underexpression hits included cytokines from the interleukins and chemokines groups: IL-3, CCL2, CCL3, CCL11 and TARC, which are all pro-inflammatory (Table 4.2).s

In general terms, these data show that infection with ΔAUG10,11 stimulated a stronger inflammatory response in the lung than WT PR8 in WT mice. Moreover, the differences between WT and IFNAR$^{-/-}$ mice cytokine responses correlated with the viral titres acquired from the same lungs and suggested that the overexpression of pro-inflammatory cytokines in IFNAR$^{-/-}$ mice was also responsible for the increased pathology score.

4.3. Discussion

The previous chapters 2 and 3 showed a fitness penalty adjacent with the double deletion of segment 2 AUG codons 10 and 11 in the background of PR8 virus, as well as the recovery of this attenuation in IFN-depletion conditions in *in vitro* systems such as IFNAR$^{-/-}$ murine bone marrow-derived macrophages. In this chapter,

given the complexity and the variety of the cellular environment of *in vivo* systems, PR8 WT and ΔAUG10,11 viruses were characterised in 129Sv/Ev WT and IFNAR$^{-/-}$ mouse hosts to further validate the conclusions taken from the previous sections.

WT and IFNAR$^{-/-}$ were infected with 200PFU of either WT or ΔAUG10,11 PR8 viruses and weight loss experiments were carried out over 5 days, in which IFNAR$^{-/-}$ mice consistently showed more severe clinical signs. These observations were consistent with previous studies where these mice were more susceptible to viral infections (Muller *et al.* 1994). In further correlation with the observed findings, previous studies on PR8 infection of IFNAR$^{-/-}$ mice resulted in altered recruitment of monocytes, translating into increased production of neutrophil chemoattractants and elevated numbers of neutrophils in the lung, resulting in the observed increased morbidity and mortality (Seo *et al.* 2011).

Previous *in vivo* studies on IAV viruses lacking IFN counteractive measures (WSN NS1 R38K41A) showed a decreased weight loss in naïve BALB/c mice compared to WT WSN (Donelan *et al.* 2003). Therefore, comparison of weight loss between WT and ΔAUG10,11 PR8 viruses was also performed where surprisingly no notable difference was found between the two viruses, despite the severe attenuation and the increased type I IFN induction of PR8 ΔAUG10,11 previously seen in *in vitro* systems. However, it is possible that the induced IFN levels led to a more severe cytokine storm which would result in the observed equal levels of clinical symptoms and weight loss between WT and ΔAUG10,11 viruses. Moreover, given the higher particle/PFU ratio of the attenuated mutant (previously shown in section 2.2.7), the dose of 200PFU of PR8 ΔAUG10,11 will have contained a higher number of viral particles (potentially DIPs), compared to the WT PR8 infection, which could also

contribute to a more severe weight loss than expected, considering the lower lung viral titres (Rabinowitz and Huprikar 1979).

In order to further support the results acquired from BMDM, lung viral titres were measured from euthanised mice. Regardless of the comparable weight loss between WT and ΔAUG10,11-infected WT and IFNAR$^{-/-}$ mice, viral titres at 5 days post infection supported the observations made in the previous chapters, showing the attenuation of the mutant virus in WT mice and its recovery in IFNAR$^{-/-}$ animals. This observation is also consistent with previous studies where IAV that are incapable of IFN counteraction (which harbour mutations, truncations or the deletion of the NS1 gene) replicate to lower titres in mice lungs (Donelan *et al.* 2003; Jiao *et al.* 2008). However, considering the stronger IFN induction of the mutant virus and given that viral titres were only assessed at one single point post infection, it is therefore not possible to distinguish if: a) the viral titres had not reached WT levels (which could also be related to its packaging deficiency) or b) the increased type I IFN levels induced an ISG/cytokine response which suppressed viral propagation and an earlier viral clearance in mouse lungs.

Lung histopathology was assessed from H&E stained tissue sections and concluded that WT PR8 caused comparable degrees of tissue damage in WT and IFNAR$^{-/-}$ mice, with small but non-statistically significant increase in perivascular and peribronchial inflammation in IFNAR$^{-/-}$ mice. This could explain the increased weight loss and more pronounced clinical symptoms observed in knockout animals. Moreover, PR8 ΔAUG10,11 infection also caused increased histopathology in IFNAR$^{-/-}$ mice.

Despite strong evidence demonstrating extensive antiviral properties of type 1 IFN, several studies also suggest pathogenic roles for IFN during influenza virus infection. Type I IFN signalling is known to be amplified by the production of several proinflammatory cytokines and chemokines. Studies on type I IFN in murine immunity to viral infections show its critical role in the control of secretion of innate and proinflammatory cytokines, including IL-12, TNF-α, IL-6, and IL-1 (Lousberg *et al.* 2010). Therefore, in order to further correlate the lung viral titres with observed histopathology, cytokine arrays were performed. WT PR8-infection elicited a general increment in abundance of proinflammatory cytokines in WT mice. Comparison between WT and ΔAUG10,11 viruses showed that the mutant virus was able to induce more cytokines, particularly interleukin-like proteins such as IL-12, IL-4, IL-17, IL-23 and IL-5. IL-23/IL-17 expression has been shown to occur through the NK-κB pathway, signalling which is common to the IFN-β induction pathway (Cho *et al.* 2006). Moreover, expression of IL-5 has been shown to be regulated by the transcription factor GATA3, which is also known to be activated by STAT4/STAT4 phosphorylation following JAK1-IFN-β interaction (Kaminuma *et al.* 2005). Therefore, augmented expression of type I IFN in the context of a ΔAUG10,11 infection correlated with the increased abundance of this interleukin.

Over- and underexpression "hits" were calculated as an attempt to explain the differences in ΔAUG10,11 between WT and IFNAR$^{-/-}$mice: the reduced viral titres in WT mice and the histopathology in the lungs of knockout mice. Elevated levels of some of these hits, (CCL2) was found in the serum of H5N1-infected patients compared to patients infected with less virulent strains and less severe clinical symptoms (de Jong *et al.* 2006; Peiris *et al.* 2004). The previously seen association of

CCL2 expression and increased pathology was also seen in our data set with the increased levels of histopathology of IFNAR$^{-/-}$ ΔAUG10,11-infected mice.

In general terms, proinflammatory cytokines were pinpointed as relevant in understanding these phenotypes. We therefore hypothesise that: in WT mice, the increased IFN induction caused by the mutant virus leads to a stronger induction of immune responses which results in a more efficient clearance of the virus and therefore reducing the severity of the observed histopathology in WT mice, particularly in interstitial inflammation.

IFNAR$^{-/-}$ mice infection resulted in equivalent lung viral titres for both viruses, similar IFN-β induction and comparable histopathology scores for either virus. Conversely, in these mice, there was still a substantial increase in cytokine and chemokine upregulation in ΔAUG10,11-infected mice, compared to WT PR8. However, in addition to IFN-β induction, the NF-κB arm of the IFN pathway is also involved in the expression of pro-inflammatory cytokines in the ΔAUG10,11 mutant. If the AUG 10 and/or 11 expressing peptides are IFN inhibitors, they might also counteract the activation of NF-κB, resulting in the observed upregulation of cytokines. On the other hand, the observed increased cytokine response can be due to the presence of non-infectious particles present in the ΔAUG10,11 viral preparations.

Given the augmented levels of genome/PFU ratios of the ΔAUG10,11 virus, since the submission of this dissertation until the date of its examination, additional *in vivo* experiments were performed in naïve and IFNAR$^{-/-}$ mice, comparing the behaviour of ΔAUG11 virus (which genome/PFU ratio is WT-like) in comparison to its WT counterpart. Groups of five naïve and IFNAR$^{-/-}$ 129Sv/Ev mice were infected

with 200PFU of WT and ΔAUG11 viruses or mock-infected, weight changes and clinical signs were monitored daily. Mice were euthanised at day 5 post infection and lungs were harvested for further histopathology examination, quantification of viral load and cytokine profiling.

As observed with the 200PFU infection with ΔAUG10,11 virus, IFNAR$^{-/-}$ infected mice lost more weight that their naïve counterpart. However, no differences in weight change were observed between PR8 WT and ΔAUG11 viruses in either type mouse. Nonetheless, consistently to what observed in the ΔAUG10,11 infection, an approximately 10-fold reduction in viral titre was observed in ΔAUG11 in comparison to WT PR8 in naïve mice. Difference which was lost in IFNAR$^{-/-}$ mice, were no statistically significant differences in lung viral titre were observed. However, in contrast to the ΔAUG10,11 infection, no substantial differences in cytokine expression were observed between WT and ΔAUG11 PR8 viruses in either WT or IFNAR$^{-/-}$ mice, potentially relating the differences of cytokine expression with the higher number of viral particles administrated in the ΔAUG10,11 infection.

Overall, this chapter supports the principle that modulation of type I IFN signalling/production required balancing in order to effectively control viral infections not promoting excessive inflammation, as seen by the comparable weigh loss between PR8 WT and ΔAUG10,11 viruses, despite the differences in IFN and cytokine induction. Moreover, these *in vivo* studies of PR8 WT and ΔAUG10,11 viruses supported the results acquired from growth kinetics in murine BMDM: virus propagation was impaired in IFN competent systems (WT mice) and recovered in IFN-defective conditions (IFNAR$^{-/-}$ mice). These data, in addition to the stronger expression of cytokines via the type I IFN-β pathway and/or upregulation in the

context of higher IFN levels provides further evidence that AUGs 10 and 11 are involved in IFN expression, perhaps with PB1-N92 and –N111 playing important roles in IFN counteraction during infection. These potential roles will be explored in the next chapter.

Chapter 5

Studies on the mechanisms of the inhibition of type I IFN induction by PB1-N92 and PB1-N111

5.1. Background and aims

In the previous chapters, the expression of PB1-N92 and –N111 was characterised. Viruses which lacked expression of these peptides were shown to be attenuated in *in vitro* and *in vivo* models, most likely due to the induction of a stronger IFN response. Data were presented suggesting that changes in RNP function were not the reason for this increased IFN induction. Therefore, it was hypothesised that the enhanced IFN production resulted from the absence of the shorter products, PB1-N92 and PB1-N111, and their potential involvement in IFN counteraction. The experiments described in this chapter therefore focused on testing and understanding the inhibitory effect of PB1-N92 and PB1-N111 on the IFN induction pathway. In order to test and better describe these functions, PB1-related peptides were assessed in transfection-

based assays. The peptides were expressed in mammalian cells and their abilities to interfere with activation of the IFN-β promoter assessed after stimulation of innate immune pathways. Moreover, IFN pathway steps which were inhibited by the PB1-related peptides were then assessed in the context of ΔAUG segment 2 mutant virus infection, including testing the effects of the inhibition of these cascades on viral replication.

5.2. Results

5.2.1. Expression and cellular localisation of PB1 shorter products

In order to understand the function of PB1 truncated peptides in counteracting the IFN induction and dissect the mechanisms behind the stronger IFN induction in their absence, full length PB1, N40, N92 and N111 ORFs were individually cloned into the pcDNA3.1 expression plasmid, commonly used in transient expression assays (Figure 5.1A). Although different in size, these proteins share the same C terminus and therefore can be detected by the same antiserum to PB1 (V19, Figure 2.5).

Aiming to test the expression of the different peptides, 293T cells were transfected with 500ng of each plasmid and PB1 polypeptide expression was assessed by western blot (Figure 5.1B). The cellular protein α-tubulin was used as a loading control and was detected at similar levels in the different lysates. No PB1 polypeptides were detected in cells transfected with an empty pcDNA construct (Figure 5.1, lane 1). Proteins of the expected size were expressed by all four plasmids (PB1: 86.6, PN1-

N40: 82.4, PB1-N92: 76.7 and PB1-N111: 74.5kDa), with all PB1 polypeptides being detected between 75 and 100kDa. Given the nested set nature of the ORFs, the PB1-

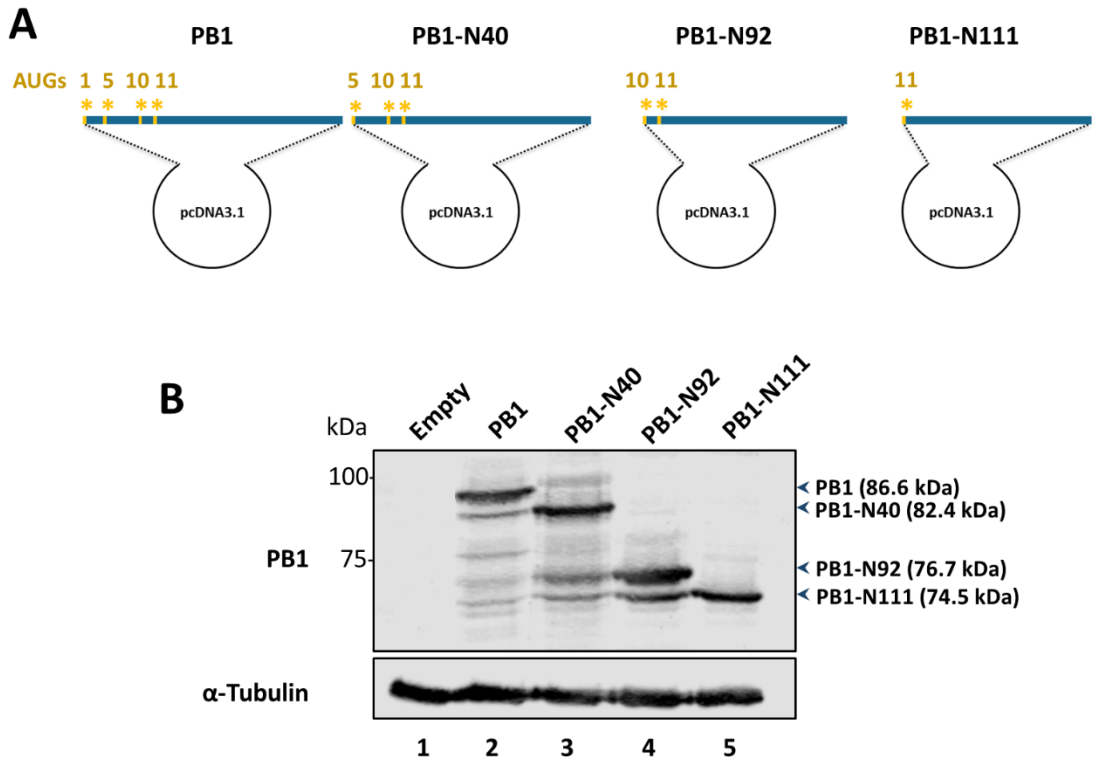

Figure 5.1.: Expression of PB1-related polypeptides from pPolII expression vectors. (A) Schematic representation of the individual cloning of PB1, PB1-N40, PB1-N92 and PB1-N111 coding regions (from AUGs 1, 5, 10 and 11, respectively) into the pcDNA3.1 plasmid. Asterisks represent AUG codons. (B) 293T cells were transfected with 400ng of each pcDNA. Expression of PB1 polypeptides was tested by western-blot using polyclonal antibodies against PB1 (V19) and α-tubulin was used as loading control.

expressing plasmid also expressed lower levels of the other three polypeptides PB1-N40, -N92 and -N111 (lanes 2). The same was also observed in the PB1-N40-expressing plasmid which, in addition to N40 also expressed N92 and N111 (lane 3); and the expression of N92 also resulted in the production of N111 (lane 4).

Since the various PB1-related peptides contain common sequences, it is not possible to differentiate their expression from the pcDNA plasmids by immunofluorescence. Therefore, in addition, constructs expressing N-terminal FLAG-tagged versions of PB1-related peptides were also created (Figure 5.2A). In order to assess the intracellular localisation of the PB1 proteins, FLAG plasmids were also constructed and transfected into 293T cells. Twenty-four hours post transfection, cells were fixed and stained using an αFLAG antibody and, to validate the FLAG detection and the structure of the tagged peptides, co-stained with an αPB1 antibody. DAPI was used to determine nuclear boundaries (Figure 5.2B). No staining with either primary antiserum was visible in cells transfected with empty vector plasmid, while in all other samples, strong staining was seen in which co-localisation of the FLAG tag (green) and the PB1 (red) antibodies was always present. Full-length PB1 localised in the cytoplasm, with minor evidence of nuclear staining. Although IAV transcription and replication take place in the nucleus in a PB1-dependent manner, PB1 nuclear translocation only occurs in the presence of PA (Nieto *et al.* 1992; Fodor and Smith 2004), which was absent in this system. PB1-N92 and –N111 also showed primarily cytoplasmic localisation.

Next, intracellular localisation of the shorter products in the presence of PA was examined. Like PB1-N40, PB1-N92 and -N111 also lack the sequences primarily

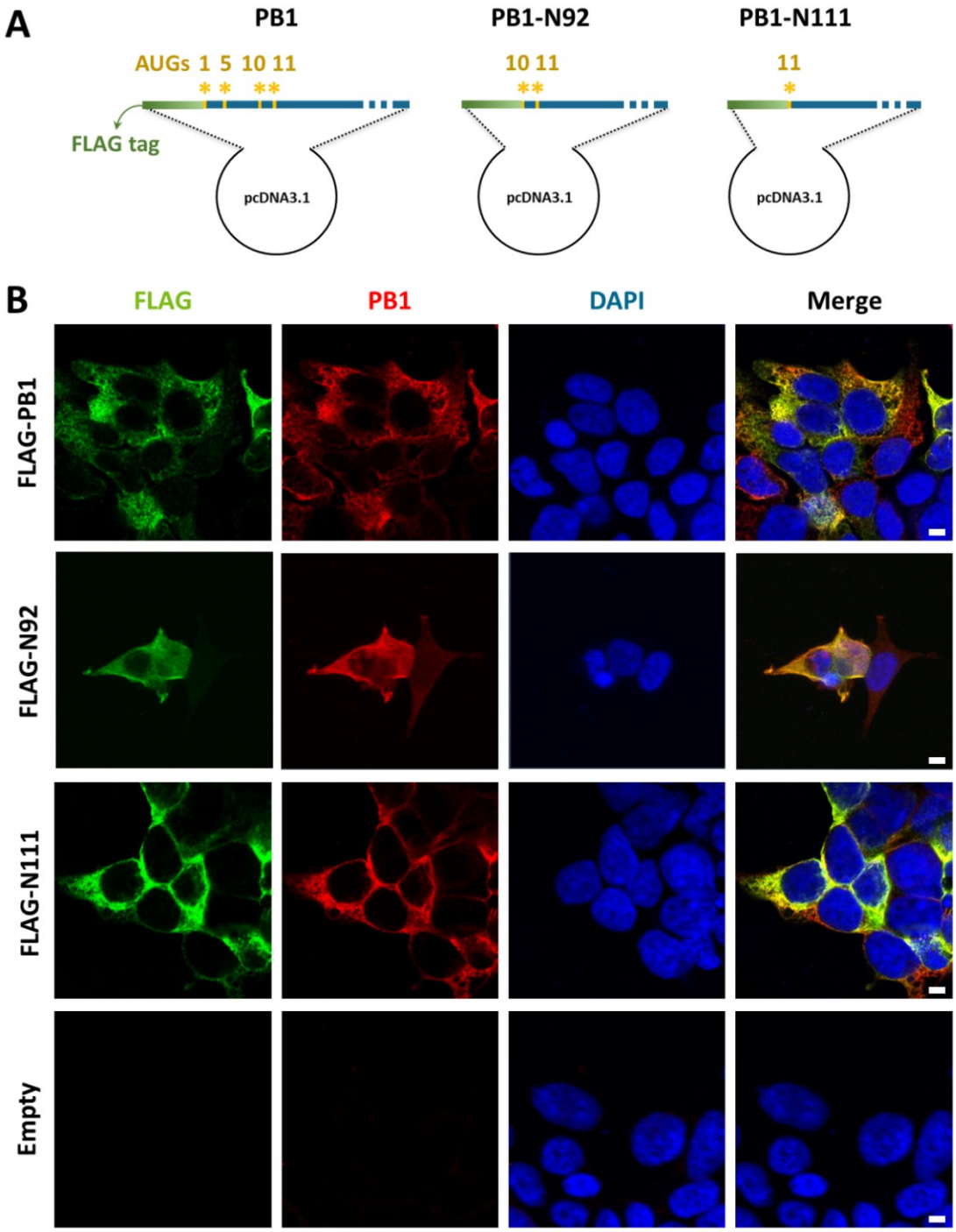

Figure 5.2: Cellular localisation of PB1 polypeptides: (A) Schematic representation of the N-terminal FLAG-tagged versions of PB1, PB1-N92 and PB1-N111. (B) 293T cells were transfected with 500ng of N-terminal FLAG-tag versions of PB1, PB1-N92, –N111 and empty pcDNA. Immunofluorescence staining was performed against FLAG (green) and PB1 (V19 antiserum, red). DAPI staining (blue) was used as nuclear marker. Image acquisition was performed with a Zeiss 710 confocal microscope using a 63x objective. Images are representative of two independent experiments performed with a single technical repeat. Scale bars represent 10µm.

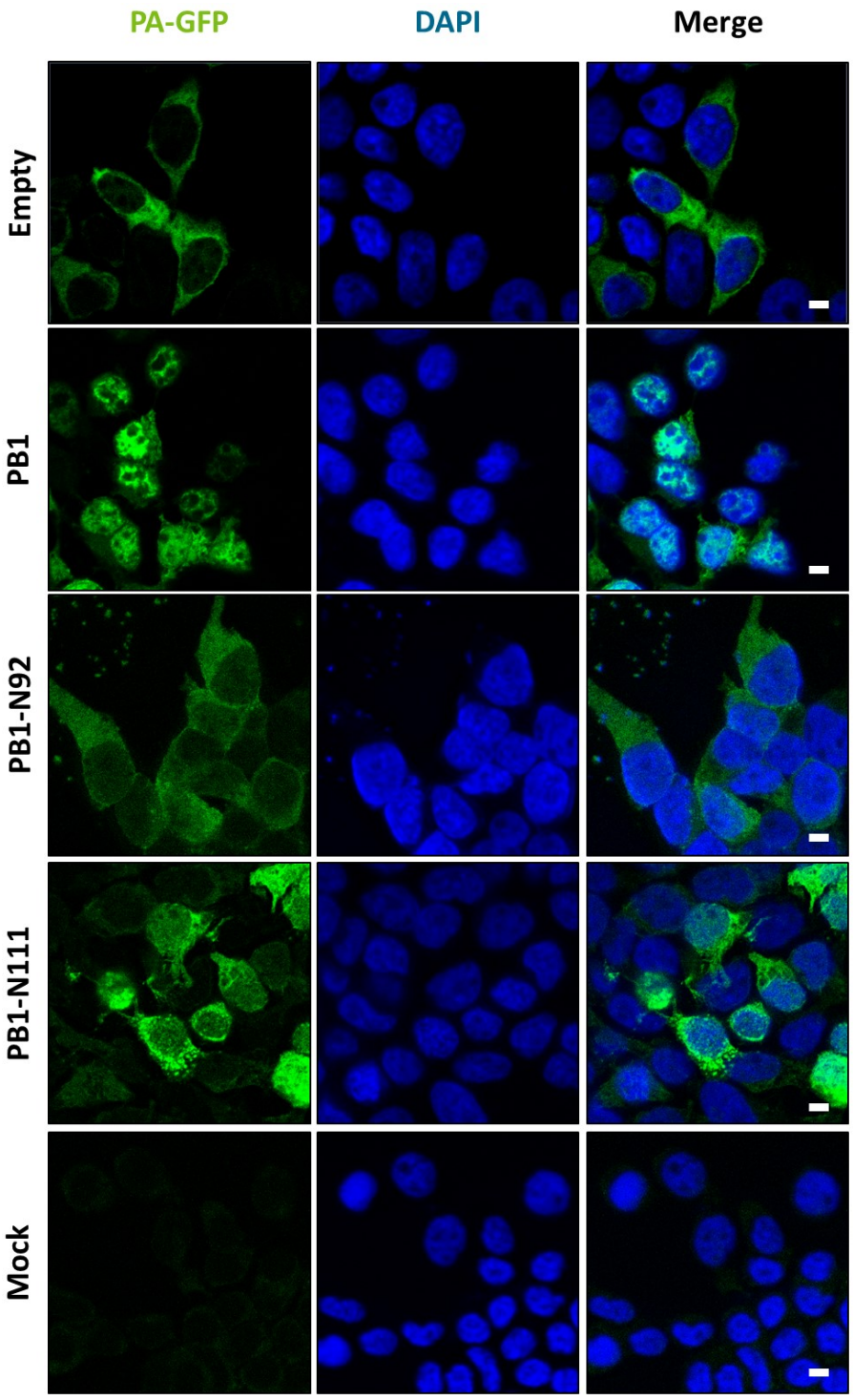

Figure 5.3: Ability of PB1 polypeptides to induce PA nuclear translocation. 293T cells were transfected with plasmids expressing the indicated PB1 products along with a GFP-tagged PA-expressing plasmid. Twenty-four hours post transfection, cells were fixed and imaged after staining with DAPI to delineate nuclei. Images were acquired in a Zeiss 710 confocal microscope with a 63x objective. Images are representative of two independent experiments performed with a single technical repeat Scale bars represent 10μm.

responsible for binding PA. As mentioned above, since PB1 and PA only undergo efficient nuclear import as a heterodimer, it was predicted that PA would not complete nuclear import in the presence of N92 or N111. To test this hypothesis, 293T cells were transfected with pcDNA plasmids expressing the full PB1 or its shorter versions, along with C-terminal GFP-tagged PA (PA-GFP) and monitored by fluorescence microscopy (Figure 5.3). Transfection of PA-GFP with an empty pcDNA plasmid resulted in the cytoplasmic localisation of PA. However, when expressed in combination with full-length PB1, PA-GFP was predominantly (but not exclusively) localised in the nucleus. In contrast, when PA-GFP was co-expressed with either N92 or N111, it remained mostly cytoplasmic. These observations are similar to the previously reported behaviour of PB1-N40 (Wise et al., 2009) and agree with the predicted inability of the shorter PB1 fragments to form a stable PA-PB1 heterodimer complex.

Overall, this section showed the successful expression of the PB1-related peptides from a mammalian expression plasmid. Moreover, it confirmed the prediction of their incapacity for PA nuclear co-translocation, and therefore their cytoplasmic intracellular localisation.

5.2.2. Suppression of IFN induction by PB1-related polypeptides

Once their expression in transfection assays had been confirmed, the ability of PB1-truncated polypeptides to inhibit the induction of IFN-β and ISRE promoters was assessed using IFN::Luc and ISRE::Luc reporter plasmids. (Figure 5.4A and B). These plasmids (kindly provided by Prof Richard Randall, The University of St Andrews,

UK) contain the firefly luciferase ORF under the control of the IFN-β promoter or four tandem repeats of the interferon stimulated response element (ISRE) region, respectively (King and Goodbourn 1994, 1998; Didcock *et al.* 1999; Hagmaier *et al.* 2006). Induction of these promoters was achieved by transfecting polyinosinic:polycytidylic acid (poly I:C), a synthetic mimic of dsRNA which is recognised by dsRNA sensors such as RIG-I and MDA-5, leading to IFN-β and consequent ISRE upregulation (Yoneyama and Fujita 2004; Kato *et al.* 2006) and, in this case, the expression of firefly luciferase. Therefore, luciferase levels are an indicator of the upregulation of either promoter. Moreover, by transfecting the PB1-related peptides expressing plasmids alongside the reporters, it was possible to measure the effects of their presence on IFN-β and ISRE induction. A plasmid expressing the NS1 from the isolate A/green-winged teal/Ohio/175/1986 (H2N1) (NS1 O175A) has been shown to be an effective inhibitor of IFN induction (Turnbull *et al.* 2016) and therefore was used as a positive control effector plasmid. As IAV NP is not known to influence the induction of either IFN-β or ISRE promoters, a plasmid encoding PR8 NP was used as a negative control.

293T cells were transfected with 50ng of either reporter plasmid and 400ng of PB1-related polypeptide or NS1 O175A or NP, here designated as "effector plasmids". Twenty-four hours post transfection, cells were stimulated or mock-stimulated by transfecting 5μg/well of poly I:C or by solely adding Lipofectamine, respectively. Twenty-four hours post stimulation, cells were lysed, and luciferase readings were taken. Additional negative controls included the mock-transfected cells as well as cells stimulated with poly I:C in the absence of luciferase reporter plasmid. Both of these controls gave luciferase readings several orders of magnitude lower that the reporter-

containing lysates (data not shown). Stimulated and non-stimulated samples were performed for each tested effector plasmid. Fold-stimulation values were calculated by the division of relative light units obtained from stimulated over non-stimulated cells. This way, potential differences in basal expression of luciferase between effectors was accounted for. Transfection of IFN-β or ISRE reporters with empty pcDNA plasmids followed by stimulation with poly I:C resulted in an upregulation of an average of 30-fold luciferase activity in comparison to non-stimulated cells (data not shown). These values were used to scale the remaining data set values to 100% (Figure 5.4 C and D). Transfection of PR8 NP as effector plasmid resulted in similar luciferase expression levels to the empty pcDNA negative control for both IFN-β and ISRE reporters. On the other hand, the use of the positive control effector NS1 O175A gave a highly significant reduction of luciferase induction down to 6.5 and 5.9% of the empty control induction, respectively for IFN-β and ISRE reporters. Transfections with any of the PB1-related peptides also led to a significant reduction of the stimulation of the IFN-β promoter (Figure 5.5C). A similar outcome was seen for the IRSE promoter using the same effector plasmids, although this phenotype was not as severe as seen when using the IFN-β reporter. For the ISRE reporter construct, there was a stronger inhibition in PB1-transfected cells which was progressively diminished by further truncation of N-terminal sequences (Figure 5.4D).

FLAG-tagged versions of the PB1-related peptides were also tested. These polypeptides also showed IFN-β and ISRE activation inhibition when compared to the empty control sample (Figure 5.4 E and F), although this was not as pronounced as seen for their untagged counterparts. In the case of the IFN-β promoter, there was an

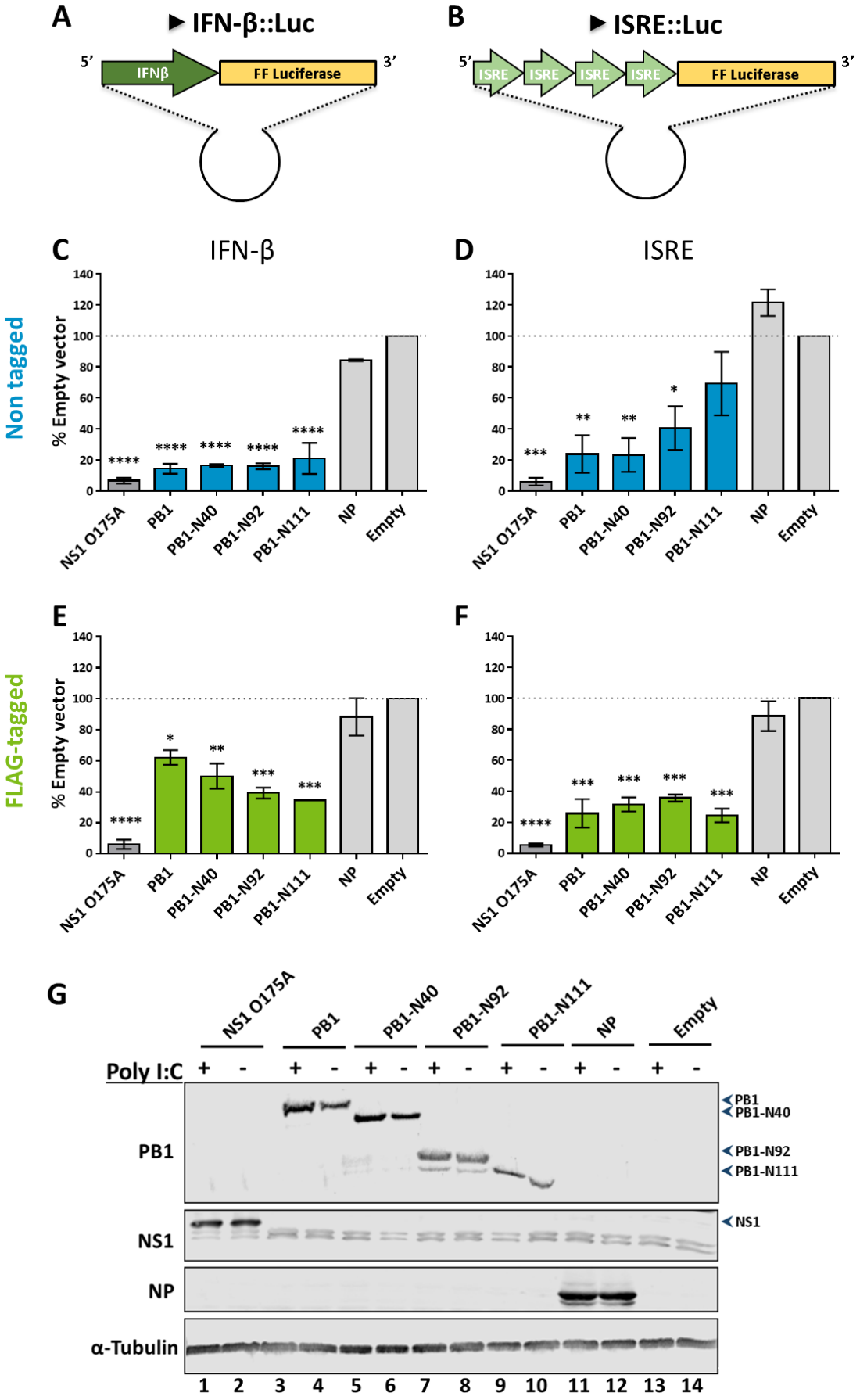
A
► IFN-β::Luc
5'
IFNβ
FF Luciferase
3'
B
► ISRE::Luc
5'
ISRE
ISRE
ISRE
ISRE
FF Luciferase
3'
C
IFN-β
D
ISRE
Non tagged
% Empty vector
NS1 O175A
PB1
PB1-N40
PB1-N92
PB1-N111
NP
Empty
E
F
FLAG-tagged
G
Poly I:C
PB1
NS1
NP
α-Tubulin
PB1
PB1-N40
PB1-N92
PB1-N111
NS1
1 2 3 4 5 6 7 8 9 10 11 12 13 14

Figure 5.4: Induction of IFN–β and ISRE promoters in presence of PB1 truncated products. 293T cells were co-transfected with one of the reporter plasmids IFN-β (A) or ISRE (B) alongside the different untagged (C and D) or FLAG-tagged (E and F) PB1 truncated proteins. Twenty-four hours post transfection, cells were stimulated by transfection with poly I:C and luciferase activity was measured after a further 24 hours. NS1 O175A and NP constructs were used as positive and negative controls, respectively. Data represent the mean ± SEM of three independent experiments performed with three technical repeats. Statistic annotations are the result of an ordinary one-way ANOVA test. *p-value <0.05, **p-value <0.01, ***p-value <0.001, ****p-value <0.0001. (G) Lysates from C were analysed by western blot using polyclonal antisera against PB1 (V19), NS1 (V29) and NP. Alpha-tubulin was used as loading control.

inhibitory effect with the deletion of N-terminal PB1 sequences while the ISRE inhibition was constant for all the FLAG-tagged PB1-related peptides. Similar to as previously explained in section 2.2.6, a transfection control such as a plasmid overexpressing *Renilla* luciferase was not included, once the positive control (NS1 A175A) is known to alter cellular proteins synthesis by its CPSF30 binding. Nevertheless, assessment of shut-off activity by the PB1'like specimens will be later described in this dissertation (sections 5.2.3).

The expression of PB1 polypeptides (untagged versions) and the used control effectors was tested by western immunoblot (Figure 5.4G). The cellular protein α-tubulin was used as loading control and was evenly detected in all samples. No specific bands were detected in cells transfected with empty pcDNA (Figure 5.4, lanes 13 and 14). For all the remaining samples, expression of the PB1 truncated products as well as control effectors was seen in equivalent amounts in the presence or absence of poly I:C. The expression of the positive and negative control effectors NS1 O175A (lanes 1 and 2) and NP (lanes 11 and 12) were detected for cells transfected with the respective plasmids. PB1 truncated products were detected using an αPB1antiserum. PB1 expression was detected in lanes 3 and 4, followed by PB1-N40 (lanes 5 and 6), PB1-N92 (lanes 7 and 8) and PB1-N111 (lanes 9 and 10). As previously seen in Figure 5.1, the transfection of PB1-N92 also results in smaller, but detectable expression of PB1-N111.

Despite some incongruences between the tagged and un-tagged PB1-related polypeptides, these data indicated that the PB1 shorter products were able to directly inhibit the activation of the IFN-β promoter and (perhaps) consequently minimise the induction of the ISRE promoter in poly I:C-stimulated cells.

5.2.3. PB1-related polypeptides and RNA polymerase II promoter activity

The inhibition of IFN-β and ISRE promoters seen in previous sections could be attributed to a) a specific obstruction of the IFN pathway or, b) a general restraint of host gene expression. Therefore, in order to determine whether the PB1-related peptides had a general shut-off activity, plasmid vectors containing constitutively active polymerase II promoters upstream of readily detectable reporter genes were used as targets. The first reporter plasmid contained the *Renilla* luciferase ORF under the control of the simian virus 40 (SV40) promoter, while the second one contained the gene for β-galactosidase enzyme (β-gal), the expression of which was controlled by a human RNA polymerase II (RNA PolII) promoter (Figure 5.5A and B, respectively). 293T cells were co-transfected with 100ng *Renilla* or 50ng of β-gal reporter plasmid with 400ng of effector plasmid. Forty-eight hours post-transfection, cells were lysed and levels of *Renilla* luciferase or β-gal were measured (as described in section 8.3.7). Background luminescence (luciferase) or A_{420} levels (ß-galactosidase) were measured from mock-transfected samples. These negative controls gave values orders of magnitude lower than the tested samples (Figure 5.5 C and D). As a positive control, the PA segment from A/chicken/Rostock/1934 (fowl plague virus or FPV) was used. In addition to PA, this segment also expresses FPV PA-X, which has a high shut-off activity against cellular gene expression (Jagger *et al.* 2012; Hussain *et al.* 2018). As negative controls, an empty pcDNA plasmid was used, as well as a temperature sensitive (ts) PA mutant, PA ts45. This mutant contains a single amino acid mutation in the PA endonuclease domain (F117C) which affects both PA and PA-X shut-off activity (Almond *et al.* 1979; Bell 2006). Transfections

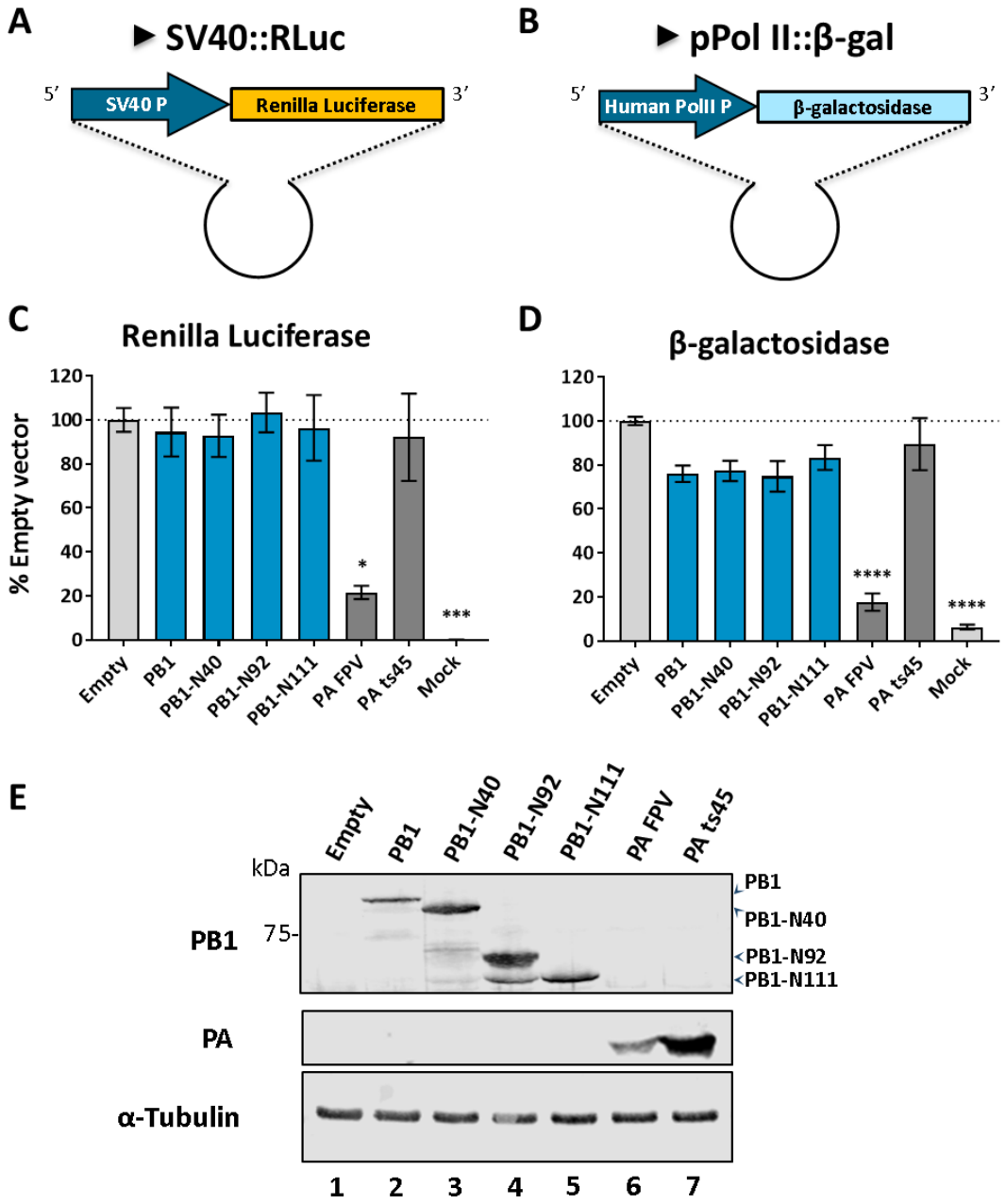

Figure 5.5: Shut-off activity of PB1 related polypeptides. 293T cells were with one of the reporter plasmids *Renilla* (A) or β-gal (B) alongside PB1 truncated proteins. *Renilla* luciferase (C) or β-galactosidase (D) readings were measured 48 hours post-transfection. FPV PA and ts45 PA-expressing constructs were used as positive and negative controls, respectively. Data represent the mean ± SEM of three independent experiments performed with three technical repeats. Statistic annotations are the result of an ordinary one-way ANOVA test. Multiple comparisons were performed in reference to the empty plasmid-transfected sample. *p-value <0.05, <0.01, ***p-value <0.001, ****p-value <0.0001 (E) Expression of PB1 shorter products and PA was assessed by western blot using V19 and V35 antisera, respectively. The cellular protein α-tubulin was used as loading control.

with the WT FPV plasmid resulted in a statistically significant ~5-fold reduction in both *Renilla* luciferase and β-gal expression, whereas the ts45 PA did not. Similarly, use of any PB1-derived polypeptide as an effector protein resulted in comparable levels of both *Renilla* and β-gal expression to the empty plasmid negative control, indicating a lack of inhibitory activity. To test for successful expression of the effector peptides, western blots were performed (Figure 5.5E). Alpha-tubulin expression, which was used as a loading control, was uniform in all tested samples. No polypeptides were detected from empty plasmid-transfected cells (lane 1). PB1-related peptides were detected with a αPB1 antibody (lanes 2-5), presenting the expected sizes, as well as the previously seen co-expression of N92 and N111 from the PB1-N92 plasmid. PA was also successfully detected using an αPA polyclonal antibody in lysates of cells transfected with PA FPV and PA ts45-expressing plasmids. Overall therefore, these data showed that unlike PA-X, the PB1-related peptides do not generally inhibit cellular RNA Pol II-mediated gene expression.

5.2.4. Identification of steps in IFN induction which are modulated by the PB1-related polypeptides

In section 5.2.2, the ability of PB1-truncated products to inhibit the induction of IFN-β promoter following poly I:C stimulation was demonstrated (Figure 5.4). Poly I:C mimics dsRNA, which activates the IFN pathway cascade from its very early stages (Field *et al.* 1967; Dauletbaev *et al.* 2015). However, the reporter assays used did not identify where in the pathway the PB1-truncated versions were having an effect. This section aimed to identify at what stage of IFN induction the PB1-related

peptides acted. To achieve this, instead of inducing IFN from the dsRNA detection phase, the pathway was stimulated by transfecting plasmids coding for various components of the signalling pathway whose overexpression activates IFN-β expression from specific points within the cascade. For example, transfection of a MAVS-encoding plasmid will bypass RIG-I activation and induce IFN-β expression from a forward step (Xing *et al.* 2012). These plasmids are here called "inducing plasmids". 293Ts were co-transfected with 50ng of IFN-β::Luc reporter plasmid, the same PB1 effector plasmids as in section 5.2.1 and 400ng of one of the inducing plasmids (kindly provided by Dr Andrew MacDonald, The University of Leeds, UK). Twenty-four hours post transfection, cells were lysed and levels of luciferase expression were measured. As in section 5.2.1, luciferase amounts were assumed to be proportional to the levels of IFN-β promoter induction. Background levels of firefly luciferase were set with mock- and IFN-β::Luc only-transfected cells. Co-transfection of IFN-β::Luc reporter with each of the inducing plasmids alone resulted in luciferase inductions of between approximately 25- and 2000-fold, depending on the induction plasmid (data not shown). Negative control effector plasmids included an empty pcDNA plasmid, to which all the remaining effector and control plasmids luciferase values were scaled. An effector plasmid expressing PR8 NS1 was used as a positive control when testing RIG-I and MAVS inducing plasmids. A plasmid expressing PR8 NP was used as negative control. RIG-I/MAVS activation is the immediate step following foreign RNA recognition. Induction of the IFN-β pathway from these two stages was unaffected by the negative control NP while transfection of the positive control, PR8 NS1, significantly reduced the levels of promoter activation (Figures 5.6A, B). Equivalent inhibition levels were also seen with the transfection of the PB1-

related peptides. RIG-I/MAVS activation leads to the stimulation of other signalling pathways. These can be largely divided into two main arms: IRF3 and NF-κB (as reviewed in Chapter 1, Figure 1.6). To induce the NF-κB cascade, plasmids encoding the kinase IKKβ (which conjugates with IKKα and NEMO to form the IKK complex) and two NF-κB subunits, RelA and P50, were used. IFN-β promoter induction using these plasmids was not inhibited by the negative control PR8 NP, or PR8 NS1. This lack of inhibitory activity was also shared by the PB1family of proteins (Figure 5.6 C-E). In addition to activation by RIG/MAVS, IFN-β induction has been shown to occur following triggering of TLR3 and/or 7, although TLR7 has been suggested to be dispensable for a full IAV-driven IFN induction (Wu *et al.* 2015; Jeisy-Scott *et al.* 2012; Barchet *et al.* 2005). These activation mechanisms were represented here by induction plasmids expressing the TLR1/2/5/6/7/8/9 ligand MyD88 and the TLR3 ligand TRIF (Kawasaki and Kawai 2014; Uematsu and Akira 2008) (Figure 5.6 F and G). IFN-β induction by MyD88 and TRIF was not supressed by PR8 NP or NS1. However, PB1, N40, N92 or N111-transfected cells all showed significantly reduced IFN-β activation upon the transfection of these two TLR adaptors. TRIF recruitment is followed by its association with TRAF3 together with TBK1 and IKKε complex, which subsequently promotes the phosphorylation, dimerisation and translocation of the transcription factor IRF3 into the nucleus (Sato *et al.* 2003; Fitzgerald *et al.* 2003). Aiming to test the effects of the PB1-related peptides in that cascade, inducing plasmids coding for TBK1, naïve IRF3 and a phospho-mimic of IRF3 (with serine amino acid residues 396 and 398 substituted to aspartic acid) were transfected into cells (Figure 5.6 H-J). As with the NF-κB root components, IFN-β induction by these plasmids was unaffected by the co-transfection of PR8 NP. Induction was also largely

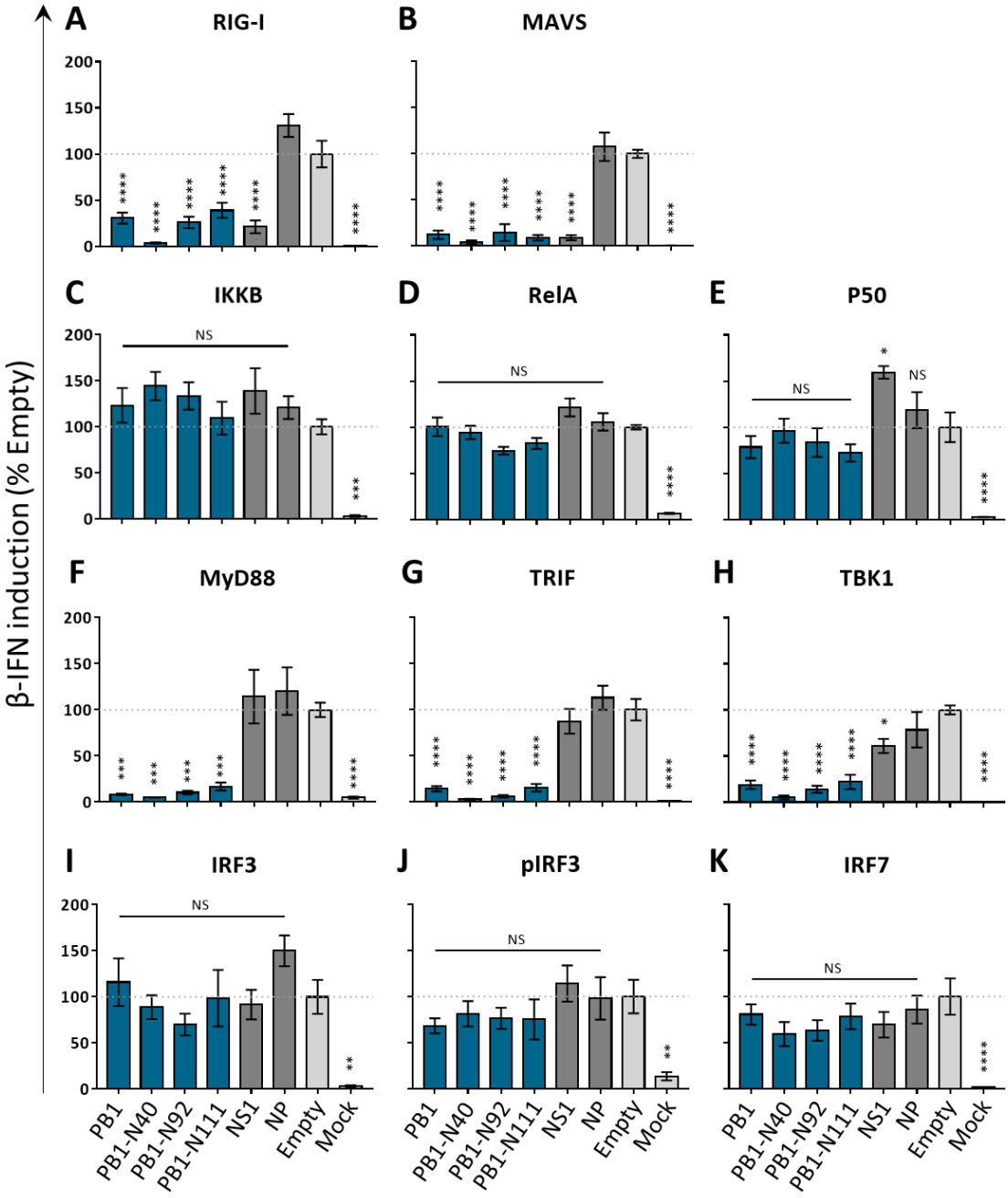

Figure 5.6: Counteraction of stimulation of the IFN-β promoter pathway at different stages. 293T cells were co-transfected with an IFN-β::Luc reporter plasmid, effector polypeptides (PR8 PB1, N40, N92, N111, NS1 or NP) and one of the various IFN pathway component proteins: (A) RIG-I, (B) MAVS, (C) IKKB, (D) RelA, (E) P50, (F) MyD88, (G) TRIF, (H) TBK1, (I) IRF7, (J) IRF3, (K) pIRF3. Twenty-four hours post transfection, cells were lysed and luciferase activity was measured. Data represent the mean ± SEM of three independent experiments performed with three technical repeats. Statistic annotations are the result of an ordinary one-way ANOVA test. Multiple comparisons were performed in reference to the empty plasmid-transfected sample. *p-value <0.05, ***p-value <0.001, ****p-value <0.0001.

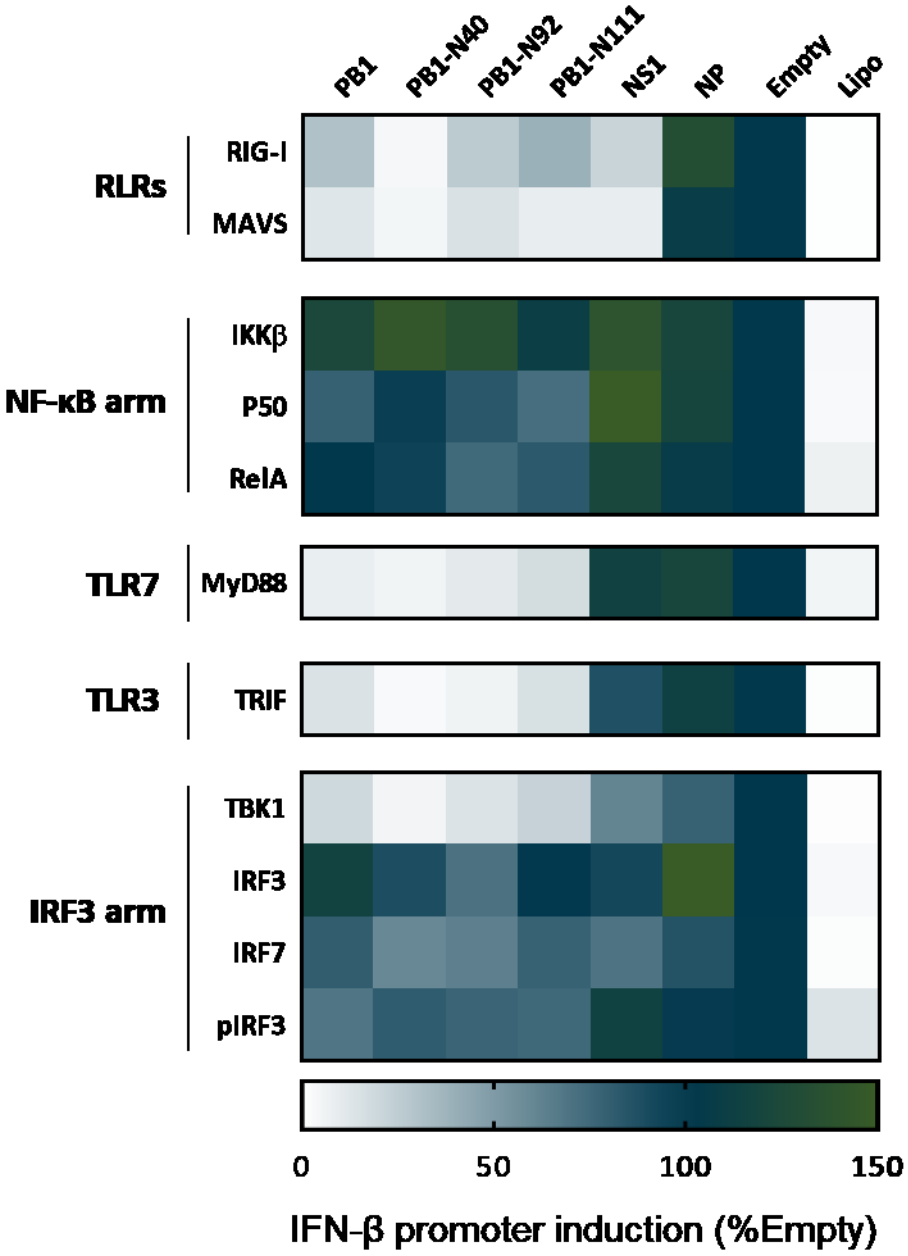

Figure 5.7: Heat map representation of the inhibition of the pathway leading to IFN-β expression by PB1-truncated proteins: 293T cells were co-transfected with IFN-β::Luc reporter plasmid, effector polypeptides (PR8 PB1, N40, N92, N111, NS1 or NP) and one of the induction plasmids. Twenty-four hours post transfection, cells were lysed and luciferase activity was measured. IFN-β promoter induction was scaled to the empty pcDNA control and plotted in a heat map. Colour saturation is associated with luciferase activity. Therefore, lighter colours represent a weak IFN-β induction, in contrast to dark colours which symbolise the lack of IFN-β counteraction. Induction plasmids were separated into different families/arms: RLRs, NF-κB arm, TLR7, TLR3 and IRF3 arm.

insensitive to NS1 co-transfection, although there was a small (less than 2-fold) but significant reduction of TBK1-induced expression (Figure 5.6 H). In contrast, the use of PB1-related peptides as effector plasmids led to substantial and highly significant reductions in IFN-β upregulation induced by TBK1. However, this attenuation was lost in IRF3 or pIRF3-stimulated cells (Figure 5.6 I and J). Phosphorylation and nuclear translocation of the regulatory factor IRF7 also occurs via TBK1 (Iwamura *et al.* 2001; Ning *et al.* 2011). However, similar to IRF3, an IRF7-induced IFN-β promoter response was not inhibited by the PB1-truncated peptides (Figure 5.6 K).

To aid visualisation and interpretation of these data, they were summarised in a heat map where strong IFN-β promoter induction is represented by dark shades, contrasted to weak promoter induction in light colours (Figure 5.7). No IFN-β induction was seen in mock-transfected cells in the absence of reporter. This diagram made it clear that transfection of NP did not negatively affect the induction of IFN-β promoter under any circumstances, while as expected (Turnbull 2017), expression of PR8 NS1 inhibited IFN-β promoter induction triggered by overexpression of RIG-I and MAVS. None of the effector plasmids affected IFN-β induction initiated at the stages of IKKβ, P50 or RelA/P65 (the NF-κB cascade). However, expression of PB1, N40, N92 or N111 supressed IFN-β activation with MyD88 or TRIF expression plasmids, but this repression was not shared by the positive control, NS1. Moreover, the same phenotype was observed when inducing the pathway at the stage of TBK1. This inhibition was lost when IFN-β activation was achieved by IRF3, pIRF3 or IRF7 overexpression. Thus, considering the flow of the IFN-β pathway, these data indicated that PB1-related peptides counteracted induction of the IFN cascade occurring via the IRF3 cascade at the stages of TBK1.

5.2.5. IRF3 phosphorylation in cells infected by segment 2 mutants

Given the ability of the PB1-related peptides to inhibit TBK1-induced IFN-β promoter activation, it was hypothesised that infection by viruses which did not express PB1-N92 and/or PB1-N111 would therefore result in increased levels of IRF3 phosphorylation. To test this hypothesis, A549 cells were infected with PR8 WT and segment 2 mutant viruses at a MOI of 5. Twenty-four hpi, cell lysis was followed by the detection of IRF3 naïve and phosphorylated forms by western immunoblot (Figure 5.8A). Infections with two further viruses were also used as controls: the PR8 NS1 RNA-binding mutant R38K41A virus which (unlike WT PR8) is known to induce increased levels of IFN and higher levels of IRF3 nuclear translocation (Talon *et al.* 2000; Turnbull *et al.* 2016), and the IAV strain A/Udorn/307/1972 (here abbreviated to Udorn) which is also known not to inhibit IRF3 phosphorylation (Kuo *et al.* 2016). As seen in chapter 3, infection with various segment 2 ΔAUG mutant viruses led to the upregulation of IFN expression. IFN functions in an auto-paracrinal fashion and leads to the upregulation of hundreds of ISGs, some among which are components of the IFN pathway such as RIG-I, TRIM25, TLR3 or MyD88 (Shaw *et al.* 2017) whose overexpression can induce IRF3 phosphorylation. Therefore, increased levels of IRF3 phosphorylation in ΔAUG mutant-infected cells could be a result of a generalised ISG response. In order to assess the looping effect of type I IFN in IRF3 phosphorylation, cells stimulated with type I IFN were included as a control. NP was also blotted for to confirm viral infection and α-tubulin was used as loading control. Mock-infected cells did not express detectable levels of pIRF3 (Figure 5.8A, lane 1). WT PR8 showed higher IRF3 phosphorylation levels compared to mock-infected cells (lane 2). Relative pIRF3 levels were quantified by densitometry from 3 independent experiments and all

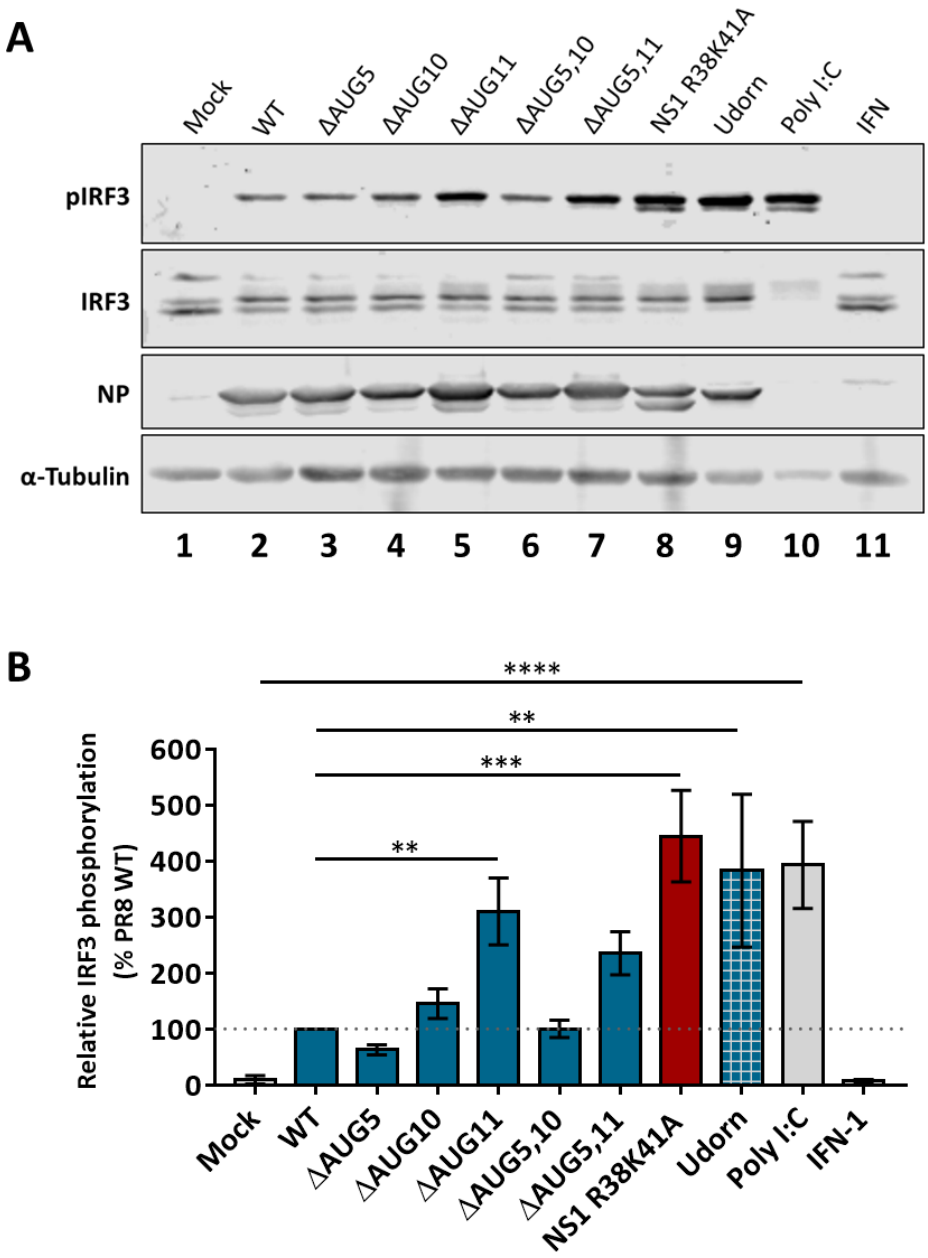

Figure 5.8: IRF3 phosphorylation levels in PR8 segment 2 mutant-infected cells. (A) A549 cells were infected at a MOI of 5 for 24 hours, after which cell lysates were collected. Lysates were subjected to SDS-PAGE followed by the detection of naïve and phosphorylated forms of IRF3 by western blot. Infection with PR8 NS1 R38K41A, poly I:C transfection and IFN incubation were used as controls. NP and α-tubulin were also detected to confirm infection and to act as a loading control, respectively. (B) Relative quantification of the phosphorylated IRF3 form was performed in ImageJ and scaled to the PR8 WT infection values. Plotted data are the mean ± SEM of three independent experiments performed with a single technical repeat. Statistic annotations are the result of an ordinary one-way ANOVA test. Statistical annotations are the result of multiple comparison tests. **p-value, <0.01, ***p-value <0.001, ****p-value <0.0001.

tested conditions were scaled to the WT PR8 pIRF3 values (Figure 5.8B). The positive control infections with PR8 NS1 R38K41A and Udorn, as well as poly I:C transfection gave 3-5-fold increased levels of IRF3 phosphorylation (lanes 8, 9 and 10). IFN-treated cells did not show detectable levels of IRF3 phosphorylation (lane 11), indicating that IFN induction by the mutant viruses could be discarded as the cause of increased IRF3 phosphorylation. Infection with segment 2 mutant viruses showed variable degrees of IRF3 phosphorylation dependent on the precise AUG codon that were mutated. Infections with ΔAUG5 and/or 10 viruses did not show a significant increase in IRF3 phosphorylation compared to WT PR8 (lanes 3, 4 and 6). However, ΔAUG11-containing virus infections resulted in a statistically significant 2-3-fold enrichment in levels of pIRF3 levels (lanes 5 and 7). Thus, these data partially supported the hypothesis that viruses unable to express PB1-N92 and/or -N111 would have defects in controlling IRF3 phosphorylation and were consistent with the results acquired in section 5.2.4, showing a correlation between the inhibitory effects of PB1-N111 and TBK1-induced IFN upregulation.

5.2.6. Effects of IRF3 phosphorylation inhibition on fitness of segment 2 mutant viruses

As levels of IRF3 phosphorylation were increased following infection with ΔAUG11 mutant viruses, we asked if the fitness of such mutants would alter in the presence of an IRF3 inhibitor. To test this, the aminopyrimidine compound BX-795 (Figure 5.9A), which was developed as an inhibitor of 3-phosphoinositide-dependent kinase 1 but was recently shown to be a potent inhibitor of the catalytic activity of the

A

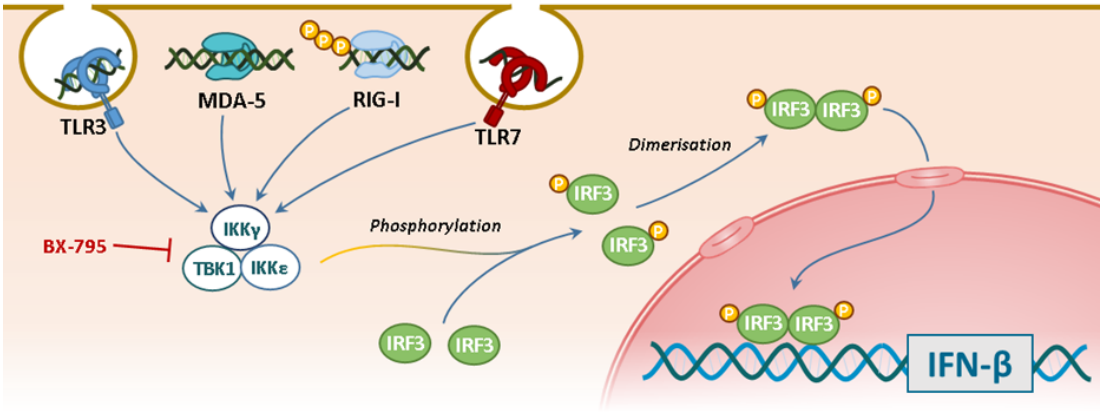
TLR3
MDA-5
RIG-I
TLR7
Dimerisation
IRF3
IRF3
IRF3
IRF3
IKKγ
BX-795
TBK1
IKKε
Phosphorylation
IRF3
IRF3
IRF3
IRF3
IFN-β

B

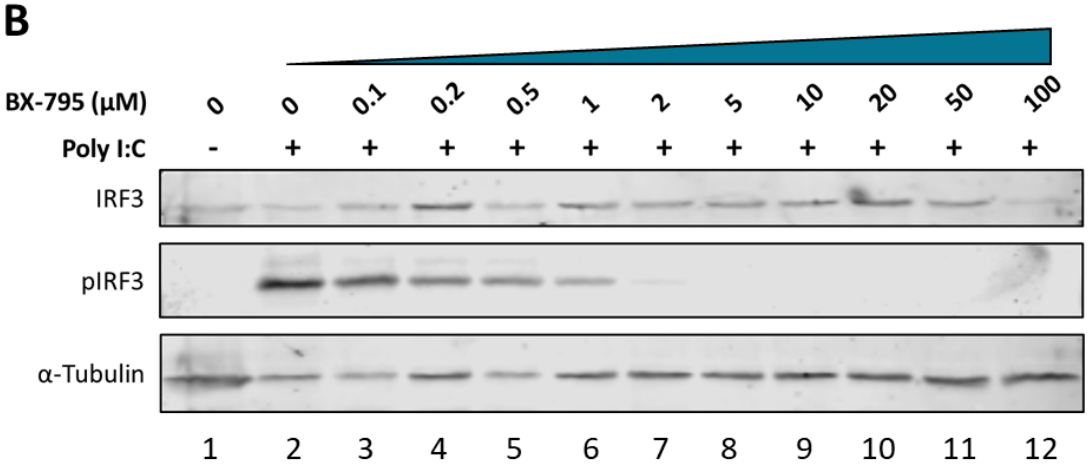
BX-795 (μM)
0
0
0.1
0.2
0.5
1
2
5
10
20
50
100
Poly I:C
-
+
+
+
+
+
+
+
+
+
+
+
IRF3
pIRF3
α-Tubulin
1
2
3
4
5
6
7
8
9
10
11
12

C

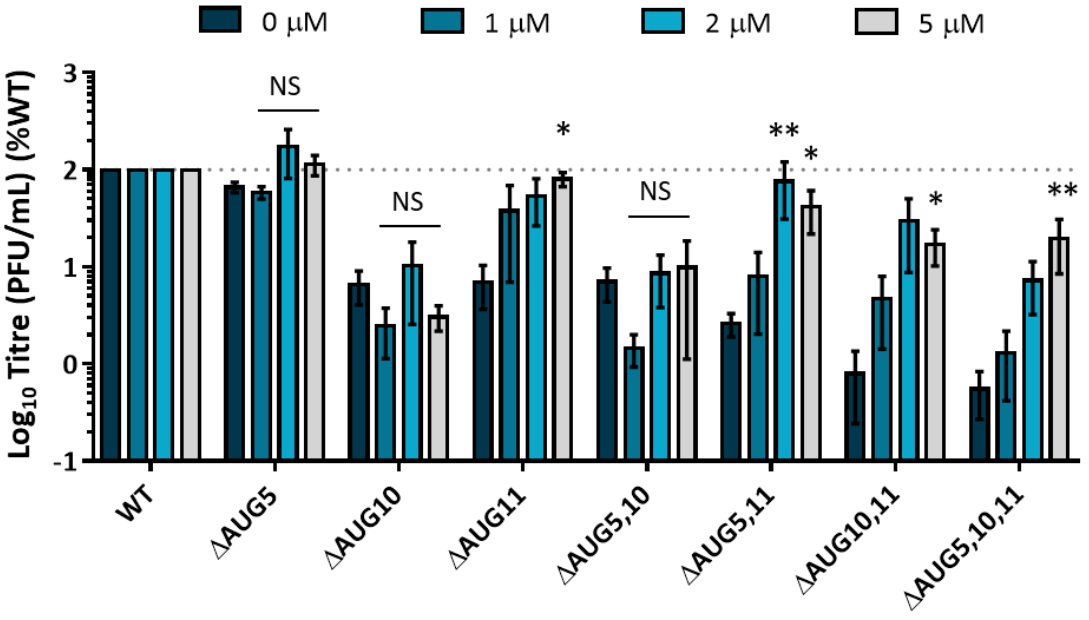
0 μM
1 μM
2 μM
5 μM
Log10 Titre (PFU/mL) (%WT)
3
2
1
0
-1
NS
NS
NS
*
**
*
*
**
WT
ΔAUG5
ΔAUG10
ΔAUG11
ΔAUG5,10
ΔAUG5,11
ΔAUG10,11
ΔAUG5,10,11

Figure 5.9: Replication of segment 2 mutant viruses in the presence of BX-795. (A) Simplified schematic representation of the IRF3 induction pathway and inhibitory mechanisms of BX-795. Upon stimuli such as TLR3, TLR7, RIG or MDA-5 activation, the IKKγ/TBK1.IKKε complex is formed and is responsible for the phosphorylation of IRF3. pIRF3 forms homodimers which translocate into the nucleus though nuclear pores where they act as a transcription factor to induce the expression of IFN-β. BX-795 prevents the formation of the IKKγ/TBK1/IKKε complex, therefore inhibiting the induction of IFN-β by pIRF3. (B) A549 cells were pre-treated with different concentrations of BX-795 and transfected with poly I:C. Twenty-four hours post stimulation, cells were lysed and levels of IRF3, phosphorylated IRF and α-tubulin were detected by western blot. Datum is a representative of two independent experiments performed with one single technical repeat. (C) A549 cells were mock-pre-treated or pre-treated with 1, 2 or 5μM of BX-795 and infected with segment 2 mutant viruses at a MOI of 0.001. BX-795 concentrations were kept during the entire time course of infection. Forty-eight hpi, viral titres were measured by plaque assay. Values were scaled to the PR8 WT titre of each drug concentration. Data are the mean ± SEM of three independent experiments performed with a single technical repeat. Statistical symbols represent the result of a two-way ANOVA test. Multiple comparison tests were performed within each mutant, having the 0μM concentration as control. *p-value <0.05, **p-value <0.01.

TBK1/IKKε complex by blocking their phosphorylation was used (Bai *et al.* 2015; Clark *et al.* 2009; Stewart *et al.* 2014).

First, to determine the concentration at which the drug best inhibited the IRF3 cascade, A549 cells were pre-treated with a range of concentrations of BX-795 for 2 hours after which they were transfected with poly I:C. After a further 24-hour incubation with poly I:C and BX-795, cells were harvested and pIRF3 was detected by western blot (Figure 5.9A). Naïve non-phosphorylated IRF3 was present in all samples, as well as the loading control, α-tubulin. Non-stimulated cells showed undetectable levels of pIRF3 (lane 1), in contrast to a robust detection of pIRF3 in stimulated cells in absence of BX-795 (lane 2). The amounts of phosphorylated IRF3 decreased with increased concentrations of the compound, being totally abrogated at 5μM (lanes 3-8). Based on these results, concentrations of 1, 2 and 5μM were chosen to use in infection experiments. At these concentrations, drug-induced cytotoxicity levels in A549 cells were insignificant (*section 8.3.4. Cytotoxicity assays*).

In order to assess the impact of this IRF3 inhibitor on replication of the ΔAUG segment 2 mutants, A549 cells were mock-pre-treated or pre-treated with 1, 2 or 5μM of BX-795 followed by infection at a MOI of 0.001. Forty-eight hpi, cell supernatants were collected, and viral titres were measured by plaque assay. Mutant virus titres from each drug concentration were scaled to the corresponding WT PR8 titre (Figure 5.9 C). Infections performed in the absence of BX-795 gave comparable results to those previously described: single and double mutants ΔAUG10/11 and ΔAUG5,10/11 showed titres at least 10-fold lower than WT PR8 while the double and triple mutants ΔAUG10,11 and ΔAUG5,10,11 replicated to at least 2 orders of magnitude less titre. Nevertheless, this panorama changed in the presence of the inhibitor. The ΔAUG5

and/or 10 viruses were insensitive to BX-795 treatment, giving titres that were not statistically different than those from the 0μM controls. However, ΔAUG11-containing viruses (PR8 ΔAUG11, ΔAUG5,11, ΔAUG10,11 and ΔAUG5,10,11) all showed a recovery in virus propagation in cells treated with BX-795. Moreover, this recovery was dose-dependent, with generally better titres with higher doses of BX-795. At 5μM BX-795, these viruses showed an at least 10-fold increase in viral titre, compared to those acquired from infections without the addition of inhibitor. Thus, viruses lacking AUG11 all replicated to higher viral titres when IRF3 phosphorylation was inhibited by BX-795, corroborating the results in the previous section which showed increased pIRF3 levels during AUG11 mutant virus infection. This strongly suggests that the PB1-N111 polypeptide expressed from AUG11 acts to counteract IRF3 phosphorylation.

5.2.7. Effects of TLR3 inhibition on viral fitness of segment 2 mutants

Studies have shown the requirement for TLR3 for maximum IFN-β induction in IAV infection (Wu *et al.* 2015; Leung *et al.* 2014; Le Goffic *et al.* 2007). TLR3 activation is followed by the binding of its adapter, TRIF (Takeda and Akira 2005). Results from section 5.2.4 showed the capacity of the PB1-related peptides to arrest TRIF-induced IFN induction (Figures 5.4 and 5.5). Therefore, to corroborate those data, viral replication in the presence of a TRIF inhibitory peptide was assessed.

The TRIF inhibitory peptide used is commercially available (TRIF Pepinh, InvivoGen) and contained the 14 amino acids that correspond to the sequence of the BB loop of TRIF (FCEEFQVPGRGELH) linked to the cell-penetrating 16-amino acid

A

Peptides	Amino acid sequence
TRIF inhibitor	RQIKIWFQNRRMKWKKFCEEFQVPGRGELH
Control inhibitor	RQIKIWFQNRRMKWKKSLHGRGDPMEAFII

B

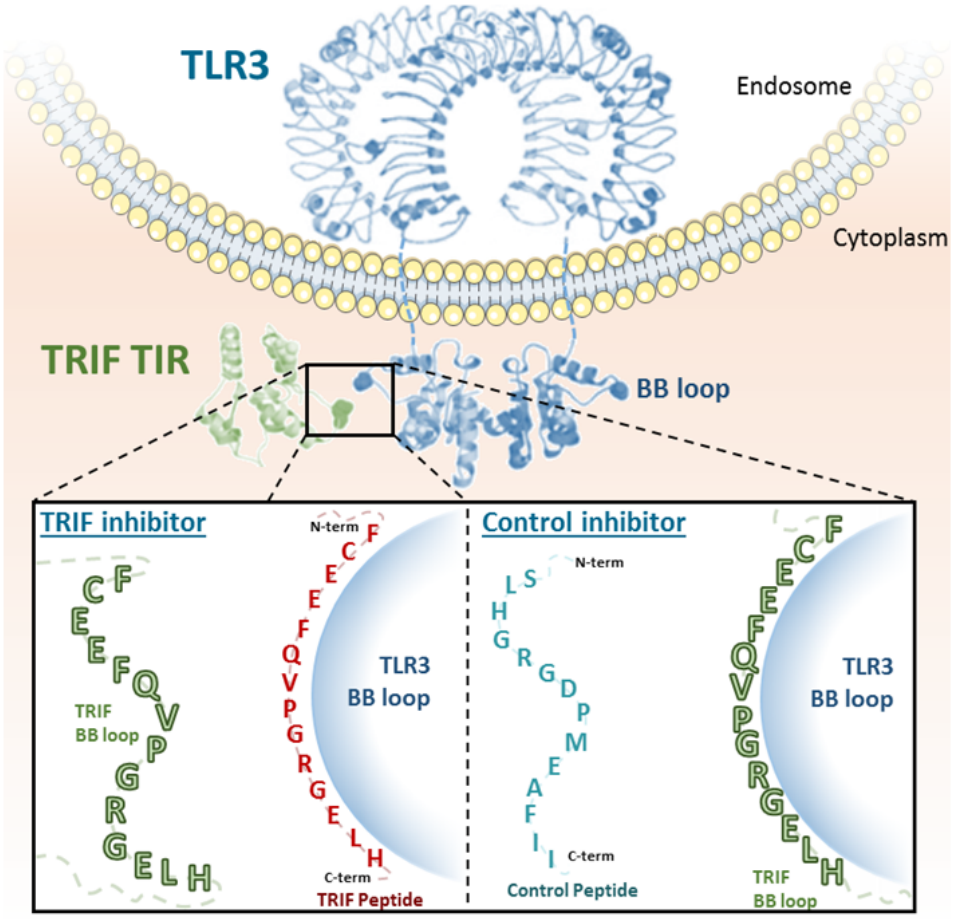

C

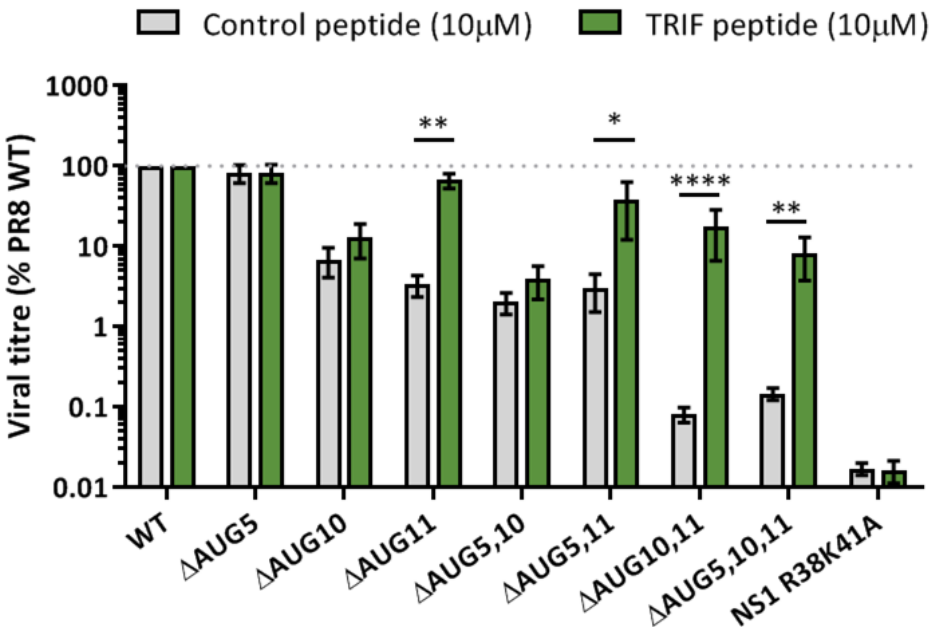

Figure 5.10: Virus propagation in the presence of a TRIF inhibitor. (A) Sequences of the used TRIF inhibitor and control peptides (InvivoGen). Underlined amino acid peptides represent the BB loop of TRIF and a size-equivalent random control sequence. (B) Schematic representation of the interaction between TLR3 TIR and TRIF BB loops and the binding of the used TRIF and control peptides. (C) A549 cells were pre-treated with 10μM of either TRIF or control peptide for 6 hours after which cells were infected at MOI 0.001 for 48 hours. Viral titres were acquired by plaque assay. Values were scaled to the PR8 WT titres for each peptide. Data are mean ± SEM from three independent experiments performed with one technical repeat. Statistical symbols represent the result of a two-way ANOVA test. Multiple comparison tests were performed within each mutant, having the 0μM concentration as control. *p-value <0.05, **p-value <0.01, ****p-value <0.0001.

sequence of the antennapedia homeodomain: RQIKIWFQNRRMKWKK. Addition of this domain enables translocation through the plasma membrane into the cytoplasm and nucleus of cells (Derossi *et al.* 1996; Derossi *et al.* 1998). In addition, a negative control peptide with a previously published random size-matching amino acid sequence was also purchased (Toshchakov *et al.* 2005) (Figure 5.10A). Thus, the TRIF inhibitory peptide will interact with the TLR3 TIR and prevent TLR3-driven IFN-β induction, while the control peptide will not (Figure 5.10B).

A549 cells were pre-treated with either TRIF inhibitor or control peptides for 6 hours at a concentration of 20μM. After pre-treatment, cells were infected with segment 2 AUG mutants and the NS1 R38K41A at a MOI of 0.001. Considering that R38K41A point mutation in NS1 confers an RNA-binding deficiency at the level of RIG-I recognition (Gack *et al.* 2009; Wang *et al.* 1999), the NS1 mutant virus used should therefore be a TRIF-insensitive control virus. Peptides were added to the infection overlay medium at the same concentration. Forty-eight hpi, virus titres were quantified by plaque assay (Figure 5.10C). WT PR8 virus reached titres of 10^8 PFU/mL in the presence of either control or TRIF inhibitory peptides, which were like the titres achieved from an A549 infection without the addition of any peptide (data not shown). The negative control NS1 R38K41A mutant showed a 500-fold reduction in viral titre in comparison to WT, which was not affected by the presence of the TRIF inhibitor peptide. In the presence of the control peptide, the PR8 PB1-N40 knockout virus showed a WT-type phenotype. PR8 ΔAUG10 and ΔAUG11 showed a 10-fold reduction in virus titre in comparison to WT in control peptide treated cells, as previously seen in A549 cells. This phenotype was shared by the PR8 ΔAUG5,10 and ΔAUG5,11 viruses, while PR8 ΔAUG10,11 and ΔAUG5,10,11 showed 100-1000-fold

reductions in titre. Similar to what was previously observed with the addition of BX-795, incubation of cells with TRIF-inhibitor affected only a subset of the ΔAUG mutants. ΔAUG5/10-containing viruses were insensitive to inhibition of TRIF. However, treatment with the TRIF inhibition peptide led to better virus propagation of mutant viruses containing ΔAUG11. Recoveries of at least 10-fold in viral titre were observed for the single and double mutants ΔAUG11 and ΔAUG5,11, while ΔAUG10,11 and ΔAUG5,10,11 showed an approximate 100-fold increase in viral titre. Overall, data reported in this section supported the hypothesis that loss of TBK1 complex antagonism was important to the IFN induction seen in ΔAUG11 mutant virus infections.

5.2.8. P65 (NF-κB) phosphorylation in segment 2 mutant infected cells

Despite not as well expressed as PB1-N111, the deletion of PB1-N92 initiation codon (ΔAUG10) in the context of PR8 infection also led to increased IFN induction (Figure 3.2). Moreover, as previously seen in this chapter, the overexpression of PB1-N92 and –N111 resulted in the inhibition of MyD88-driven IFN-β induction. MyD88 is the TLR7 ligand and acts via the TRAF6 complex, leading to NF-κB activation, cytokine secretion and the inflammatory response (Kawai *et al.* 2004). Moreover, as observed in the arrays performed in chapter 4 (section 4.2.5), stronger induction of inflammatory cytokines such as IL-6, IL-1, IL-1ra and CCL5/RANTES were strongly detected in lungs of PR8 ΔAUG10,11-infected mice and have been associated with increased levels of NF-κB(Son *et al.* 2008; Smith *et al.* 1994; Mori and Prager 1996;

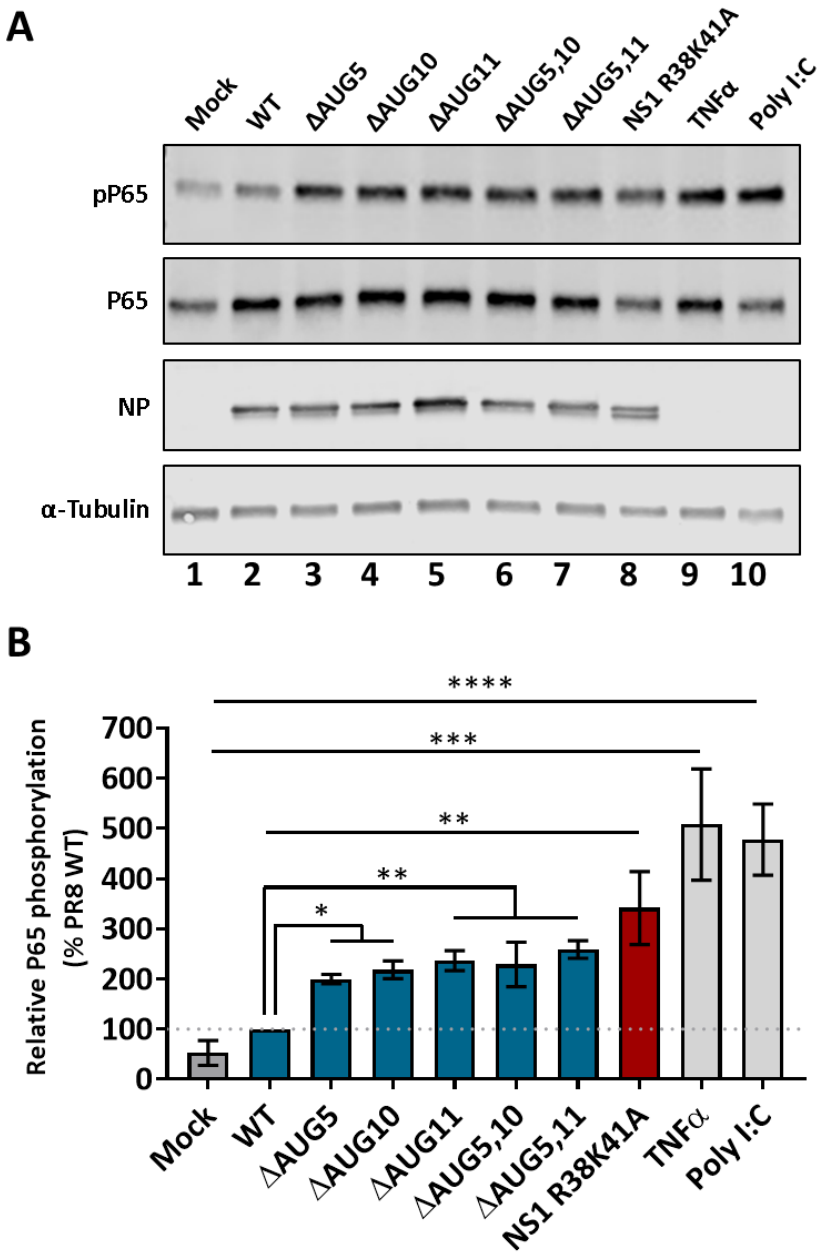

Figure 5.11: P65 phosphorylation levels in PR8 segment 2 mutant-infected cells. (A) A549 cells were infected at a MOI of 5 for 24 hours, after which cell lysates were collected. Lysates were subjected to SDS-PAGE followed by the detection of naïve and phosphorylated forms of P65 by western immunoblot. Infection with PR8 NS1 R38K41A, poly I:C transfection and TNFα incubation were used as positive controls. NP and α-tubulin detection were used to confirm infection and as loading control, respectively. (B) Relative quantification of the phosphorylated P65 form was performed in ImageJ and scaled to the PR8 WT infection values. Plotted data are the mean ± SEM from three independent experiments performed with one technical repeat. Statistic annotations are the result of an ordinary one-way ANOVA test. Multiple comparisons tests were performed against Mock and PR8 WT values. *p-value <0.05, **p-value <0.01, ***p-value<0.001, ****p-value <0.0001.

(Son *et al.* 2008; Smith *et al.* 1994; Mori and Prager 1996; Wickremasinghe *et al.* 2004). Studies on the links between the NF-κB transcription factor binding sites and IL-12 (also stronger expressed in ΔAUG10,11-infected mice in comparison to WT PR8) production have also been described (Murphy *et al.* 1995; Yoshimoto *et al.* 1997). Therefore, changes in the NF-κB P65 phosphorylation levels were assessed in the context of ΔAUG mutant virus infection *in vitro*.

A549 cell were infected at a MOI of 5 with the panel of WT, PB1- and NS1-mutant PR8 viruses. Twenty-four hpi, viral NP (to confirm infection), α-tubulin (as a loading control) and P65 naïve and phosphorylated forms were detected by western blot (Figure 5.11A). P65 species were quantified from replicate experiments (Figure 5.11B). Similarly to pIRF3 detection, infection with PR8 NS1 R38K41A was used as a positive control (Wang *et al.* 2000). Additional positive controls included cells stimulated with TNFα or poly I:C (Schutze *et al.* 1995). Mock-infected cells had the lowest P65 phosphorylation levels (lane 1), followed by WT virus-infected cells (lane 2). TNFα and poly I:C treated cells showed the strongest P65 phosphorylation, presenting 5- to 6-fold statistically increases over the mock-treated-cells (lanes 9 and 10). The NS1 mutant also showed increased levels of pP65 (on average a 3-fold induction) in comparison to PR8 WT. Mutation of AUGs 5, 10 and/or 11 resulted in statistically significant 2-3-fold increase of P65 phosphorylation over their WT counterpart. However, in contrast to the IRF3 phosphorylation experiments, pP65 levels were rather consistent between the different segment 2 mutant viruses.

Overall, increased P65 phosphorylation was consistently augmented in all mutant viruses. Unlike IRF3, P65 phosphorylation was not strongly associated with a

particular AUG codon. Instead, the presence of pP65 was associated with all AUG codons 5, 10 and 11.

5.2.9. Replication of segment 2 mutants following NF-κB inhibition

To further analyse the importance of the counteraction of NF-κB for the fitness of the ΔAUG viruses, drugs which block directly of indirectly block P65 activity were used. Given the augmented levels of P65 phosphorylation in ΔAUG mutant viruses' infection, it was hypothesised that the fitness of these mutants would recover in the presence of NF-κB inhibitors. To investigate this, two different compounds were used: IMD0354 and JSH23 (Figure 5.13A). IMD0354 blocks IκB phosphorylation (Sugita *et al.* 2009; Onai *et al.* 2004), while JSH-23 is a cell-permeable diamino compound that selectively blocks nuclear translocation of the NF-κB P65-P50 hetero-dimer and its ensuing transcription factor activity without affecting IκB degradation (Shin *et al.* 2004).

To determine the appropriate concentration of the inhibitors to use, 293T cells were transfected with 50ng of the IFN::Luc reporter plasmid. After 24 hours, cells were treated with several concentrations of either IMD0354 (Figure 5.12A) or JSH-23 (Figure 5.12B) for 2 hours, after which they were either transfected with poly I:C or treated with 500 ng/ml TNFα (Sakurai *et al.* 2003). Twenty-four hours post stimulation, cells were lysed and luciferase activity was measured. Values were scaled to the luciferase sample with no added drug (Figure 5.12 B and C). In general, IMD0354 was a more powerful inhibitor than JSH-23, leading to a 40 and 80% reduction of poly I:C- and TNFα-stimulated IFN-β induction, respectively, at 0.1μM

and near complete inhibition at 0.5μM. JSH-23 achieved the same blockade of poly I:C-induced IFN-β activation at 1μM but was not particularly effective against TNFα stimulation. Based on these results and considering the cytotoxicity levels of these two compounds (Figure 8.1, section 8.3.4), concentrations of 0.1μM of IMD0354 and 1μM of JSH-23 were chosen to be used in infection experiments.

In order to assess the impact of the NF-κB inhibitors on the replication of mutant viruses, A549 cells were mock-pre-treated or pre-treated with IMD0354 or JHS-23 for 2 hours followed by infection with WT and segment 2 mutants at MOI of 0.001. Forty-eight hpi, virus-containing cell supernatants were collected, and viral titres were measured by plaque assay. Titre values were scaled to WT PR8 titre in each drug data set (Figure 5.12 D and E). Infections performed in the absence of inhibitors showed the previously observed attenuation of ΔAUG10 and/or 11 viruses, whereas mutation of AUG5 did not alter virus replication. However, despite statistically insignificant, all segment 2 mutant viruses presented higher replication rates in the presence of either inhibitor with a generalised 3- to 100-fold increase in viral propagation for all the mutant viruses.

The general improved virus replication in NF-κB inhibiting conditions correlates with the P65 phosphorylation level increase generally observed in segment 2 mutant viruses. This suggests that the AUG5, 10 and 11 expressing polypeptides (PB1-N40, -N92 and -N111) may act to counteract P65 phosphorylation and NF-κB transcription factor activity.

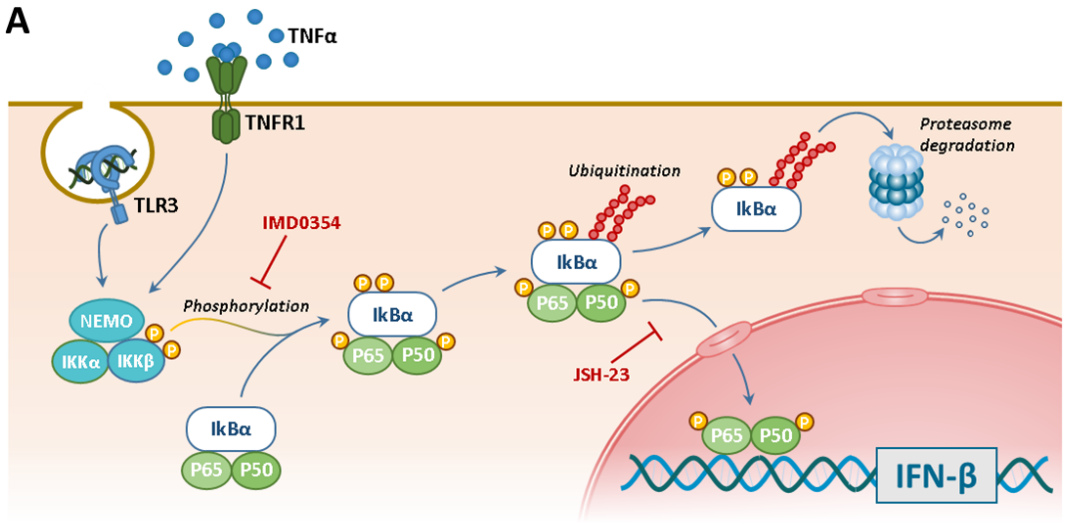
A
TNFα
TNFR1
TLR3
IMD0354
Phosphorylation
NEMO
IKKα
IKKβ
IkBα
P65
P50
Ubiquitination
Proteasome degradation
JSH-23
IFN-β

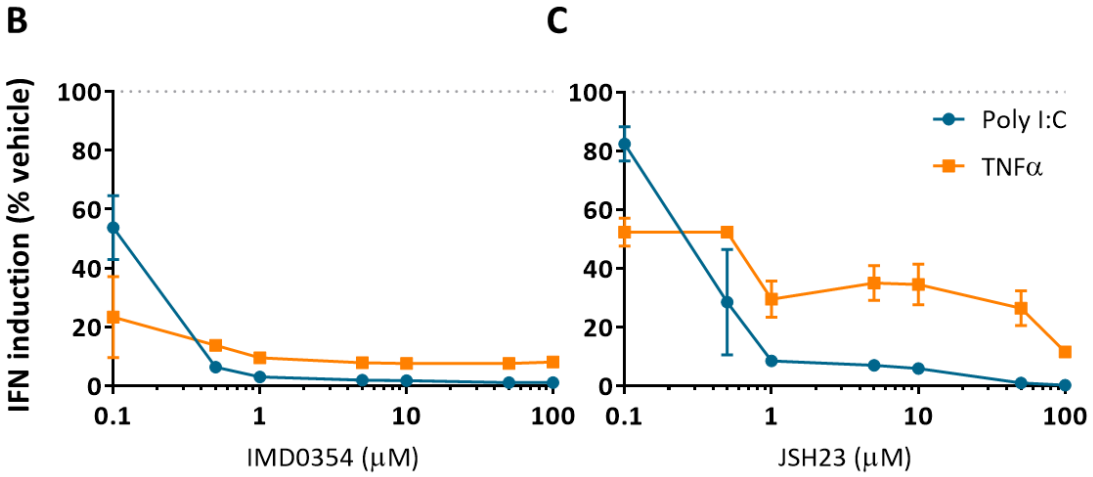
B
C
IFN induction (% vehicle)
IMD0354 (μM)
JSH23 (μM)
Poly I:C
TNFα

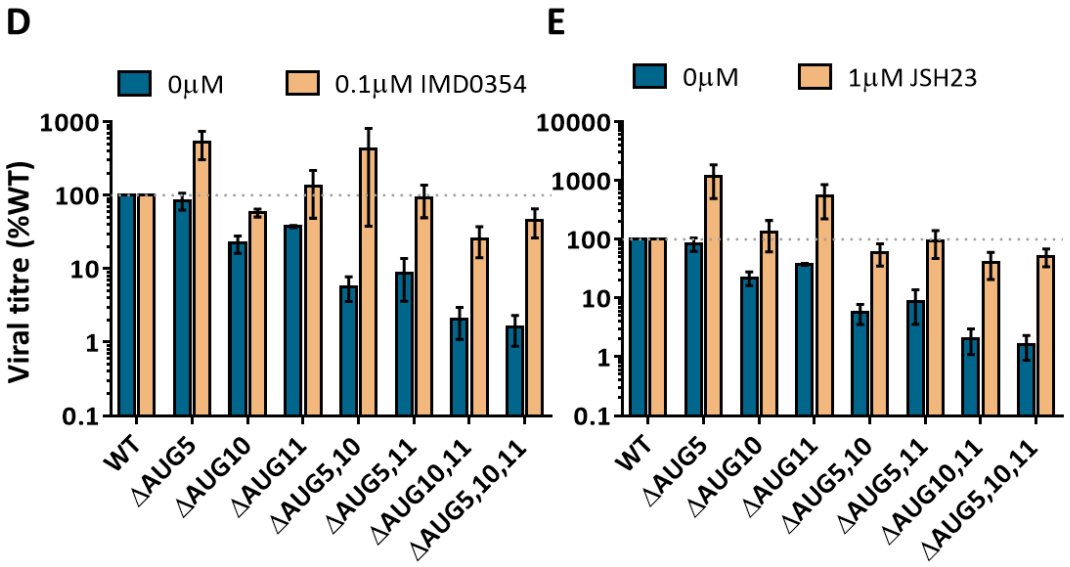
D
E
0μM
0.1μM IMD0354
1μM JSH23
Viral titre (%WT)
WT
ΔAUG5
ΔAUG10
ΔAUG11
ΔAUG5,10
ΔAUG5,11
ΔAUG10,11
ΔAUG5,10,11

Figure 5.12: ΔAUG-mutants viral propagation in the presence of NFκB inhibitors. (A) Schematic representation of the NF-κB pathway and inhibition mechanisms of IMD0354 and JSH-23. Upon stimuli such as TLR3, TNFα or RIG-I, formation and activation of the IKKα/ IKKα/NEMO complex occurs, and is responsible for phosphorylation of IkBα. This step is inhibited by IMD0354. The phosphorylated IkBα is then targeted for proteasome degradation by ubiquitylation, leaving the P65/P50 hetero-dimer free to translocate into the nucleus though nuclear pores, process which is inhibited by JSH-23. Once in the nucleus, P65/P50 functions as a transcriptional factor to induce the expression of, among other, IFN-β. (B and C) 293T cells were transfected with 25ng of IFN-β::Luc reporter plasmid. Twenty-four hours post transfection cells were stimulated with poly I:C or TNFα and incubated with different concentrations of IMD0354 (B) or JSH23 (C). After a further 24 hours, cells were lysed and luciferase activity was measured. Values were scaled to the 0μM stimulated cells sample. Data are mean ± SEM from two independent experiments performed with three technical repeats. (D and E) A549 cells were infected with PR8 WT and segment 2 mutants at a MOI of 0.001. Virus was grown for 48 hours in the presence of absence of IMD0354 (D) or JSH23 (E). Viral titres were measured by plaque assay. Data are mean ± SEM from three independent experiments performed with a single technical repeat. Statistic annotations are the result of a two-way ANOVA test. Multiple comparisons tests were performed against the untreated control and no significantly statistical differences were found.

5.2.10. Effects of TRIM25 knockout on viral fitness of segment 2 mutants

IFN induction by IAV is highly attributed to RIG-I activation (Wu *et al.* 2015; Rehwinkel *et al.* 2010; Opitz *et al.* 2007). RIG-I viral RNA recognition and pathway activation are intrinsically linked to TRIM25. This mediates RIG-I ubiquitylation, leading to its activation and efficient recruitment of RIG-I's downstream partners and triggering of interferon expression (Gack *et al.* 2007). So far, the systems employed and described in previous sections here (virus or poly I:C) induce type I IFN by signalling via TLR3 or RIG-I. To further test the importance of RIG-I activation for the attenuation of AUG mutant viruses, mock-edited and TRIM25$^{-/-}$ 293 cells (Choudhury *et al.* 2017), were infected at a MOI of 0.001 and plaque assays were used to quantify viral titres at 48 hpi (Figure 5.13). As a positive control, the NS1 R38K41A RNA-binding mutant was used, since these point mutations prevent inhibition of RNA recognition by RIG-I, causing therefore an attenuated growth phenotype (Pichlmair *et al.* 2006; Guo *et al.* 2007). WT PR8 replicated to titres of 10^7 PFU/mL in both WT and TRIM25 knockout cells and, consistent with previous data, an attenuated phenotype was seen for ΔAUG10 and/or 11 viruses in WT 293 cells. However, there was no increase in PB1 mutant virus replication on TRIM25$^{-/-}$ cells. On the other hand, the NS1 mutant virus was sensitive to TRIM25, having a 10-fold attenuation compared to WT PR8 in TRIM$^{+/+}$ cells, which recovered in the counterpart knockout cells. Thus the segment 2 mutants were insensitive to the presence of TRIM25, suggesting that PB1-N92 and –N111 do not counteract RIG-I-mediated triggering of the IFN pathway.

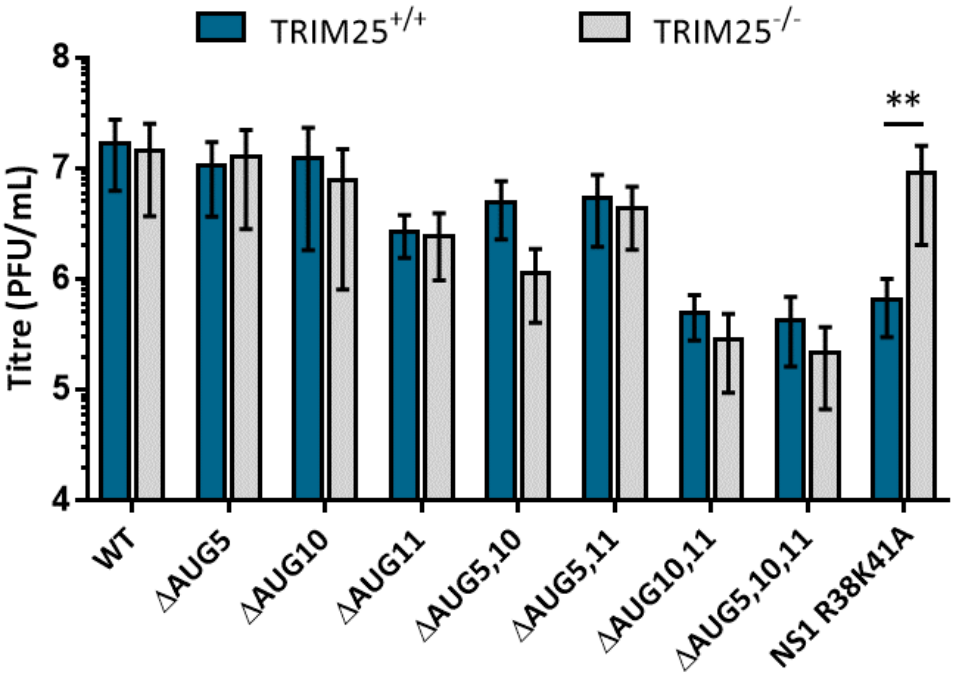

Figure 5.13: Viral replication in TRIM25$^{-/-}$ cells. Mock-edited and TRIM25$^{-/-}$ 293 cells were infected at a MOI of 0.001. Viral titres were quantified by plaque assay 48 hpi. Data represent mean ± SEM from three independent experiments performed with a single technical repeat. Statistical symbols represent the result of a two-way ANOVA test. Multiple comparison tests were performed between naïve (TRIM$^{+/+}$) and knockout (TRIM$^{-/-}$) cells. **p-value <0.01.

5.3. Discussion

Data from previous chapters showed that knocking out expression of PB1-N92 and PB1-N111 increased the levels of type I IFN induced by virus infection, leading to the hypothesis that these polypeptides could be inhibiting involved in IFN induction. To test this, both polypeptides PB1-N92 and –N111 were examined outside of the infection context, through being cloned in expression plasmids, and their effects in IFN counteraction were independently tested in transfection-based assays.

Initially, expression of PB1-related polypeptides from expression vectors showed the presence of products with corresponding predicted sizes. FLAG-tagged versions of these polypeptides were also created and used to observe their cytoplasmic localisation. The observed cytoplasmic localisation of PB1 in the absence of PA was consistent with previous studies showing a requirement for PB1-PA heterodimer formation prior to nuclear translocation. Moreover, transfection of PB1 along with a GFP-tagged PA expression plasmids resulted in the nuclear localisation of PA (Fodor and Smith 2004; Nieto *et al.* 1992). Due to their lack of PA-interacting N-terminal domain, PB1-N92 and –N111 were predicted not to localise in the nucleus regardless of the presence or absence of PA, as observed when transfecting FLAG-tagged PB1-N92 and –N111. These findings are in agreement with previous studies where PB1-N40, which also lacks this N-terminal region/function, also failed to localise in the nucleus (Wise *et al.* 2009). Nevertheless, cellular localisation was measured from FLAG-tagged CMV-driven expression plasmids, which result in more abundant protein levels than the ones detected in infected cells and therefore a potential different cellular localisation. Examples of differential protein cellular localisation dependent

on its mechanism of expression was observed in previous studies where, for instance, the single expression of PB1 from vaccinia virus resulted in its nuclear localisation (Smith *et al.* 1987), despite the fact that, in infected cells, PB1 requires the heterodimerisation with PA to undergo nuclear translocation.

Virus-driven transcriptional and translational protein shut-off mechanisms have been related to PA-X, NS1 as well as the viral polymerase (Khaperskyy and McCormick 2015; Jagger *et al.* 2012; Marazzi *et al.* 2012). IAV RdRp has been shown to interact with the C-terminal domain of the transcriptionally engaged initiating form of Pol II and also associates with the promoter region of actively transcribed Pol II genes through its interaction with the large subunit of Pol II (reviewed in Vreede and Fodor 2010). Nevertheless, this polymerase shut-off activity has been mainly attributed to the PA subunit which exhibits cap-snatching endonuclease activity (Dias *et al.* 2009) and no shut-off activity has so far been shown for PB1, fitting the obtained results.

Individual expression of PB1, PB1-N40, -N92 and –N111 did not result in a general protein shut-off effect, but were shown to inhibit poly I:C-induced IFN-β and ISRE promoter activation. As mentioned in chapter 3, IFN inhibition driven by the viral polymerase has been reported. The PB2 from human and avian viruses has been shown to accumulate in the mitochondrion and interact with MAVS (Graef *et al.* 2010; Long and Fodor 2016). Additional studies on the overall polymerase complex also reported IFN-β counteraction through MAVS inhibition in an NS1-independent manner (Iwai *et al.* 2010) and more recent studies also suggested RIG-I interaction with PB1/PA from incoming virions (Liedmann *et al.* 2014b).

Counteraction of RIG-driven IFN-β expression by PB1-expressing plasmids has been shown by Iwai *et al.* 2010. The same study has also shown that MAVS-induced IFN-β and NF-κB can also be diminished by transient PB1 expression, consistent with results obtained in section 5.2.4. However, our study showed for the first time IFN-counteraction by PB1-truncated forms by both their untagged and FLAG-tagged versions, despite the fact that the FLAG-tagged polypeptides have shown a reduced counteractive effect in comparison to their untagged counterparts. However, this may be explained by the hydrophilic nature of the FLAG tag which, although did not seem to alter the predicted cellular localisation, could possibly impair the PB1-related polypeptides folding and function.

Counteraction of the IFN-β promoter by PB1-related polypeptides was also seen following induction by RIG-I, MAVS as well as MyD88, TRIF and TBK1. However, the PB1 shorter products failed to counteract IFN-β induction by expression of IKKβ or any of the tested NF-κB subunits. Therefore, analysis of the pathway (Figure 1.6) suggested that inhibition of IFN induction by these polypeptides occurs at the stages of TBK1 or between MyD88 and the IKKα/β/NEMO complex.

The action of the shorter products of PB1 was further evaluated in infected cells. IRF3 phosphorylation was enhanced in cells infected with ΔAUG11-containing viruses and their replication recovered when TBK1 and TRIF were inhibited. A general increase in p65 phosphorylation was seen for all mutant viruses whose replication fitness was also improved in the presence of NF-κB inhibitors. However, abrogation of RIG-I recognition by the knockout of TRIM25 did not alter virus fitness for any of the segment 2 mutant viruses.

Studies on IFN counteraction by other viruses have shown that, in addition to inhibition of RNA/DNA detection, they also express proteins which act at several downstream steps on the pathway leading to IFN-β expression. Example of this on the IRF3/7 arm are:

- IE62 of varicella-zoster virus was shown to block IRF3 phosphorylation at key serine residues (Sen *et al.* 2010).
- Ebola virus protein V35 has been shown to interact with IKKε and TBK1, modifying SUMOylation of IRF-7 (Prins *et al.* 2009; Chang *et al.* 2009).
- Vpr and Vif of human immunodeficiency virus have been shown to bind to TBK1 and prevent its autophosphorylation (Harman *et al.* 2015).
- Bovine viral diarrhea virus NPro has been shown to target IRF3 for proteasomal degradation (Hilton *et al.* 2006).

Viral proteins responsible for the inhibition of the NF-κB cascade have also been described:

- Vaccinia virus A52R has been shown to bind to IRAK2 and TRAF6 and disrupts downstream interactions (Harte *et al.* 2003).
- NS5A is expressed by HCV and has been shown to prevent the interaction between IRAK and MyD88 (Abe *et al.* 2007).
- HSV ICP27 has been shown to block phosphorylation and ubiquitylation of IκB (Kim *et al.* 2008).
- West Nile virus NS1 has been shown to inhibit TLR3-induced NF-κB nuclear translocation (Wilson *et al.* 2008).

Reduction of IFN expression by IAV has been attributed to various functions of NS1, tNS1, PB1-F2, PB2-S1 and the viral polymerase (reviewed in Chapter 1). However, these are associated with counteraction of IFN at the very early stages of the pathway. Although the truncated version of NS1 (tNS1) was shown to inhibit IRF3 phosphorylation, the study did not specify whether this was a shared function with full length NS1 at the RIG-I stage or if the inhibition was actually taking place at the IRF3 step (Kuo *et al.* 2016). Given that both RIG-I and TLR3 may be required for full IFN induction following IAV infection (Wu *et al.* 2015), despite the shut-off activity of NS1 and PA-X at the level of blocking general Pol II-mediated gene expression, it would not be implausible that IAV could also encode an IFN inhibitor which acts downstream of RIG-I/MAVS to strengthen inhibition of TLR3-driven IFN induction.

Due to the nested set nature of PB1, PB1-N40, -N92 and –N111, the expression of a larger peptide results in the co-production of a shorter peptide. Hence, it was not possible to solely express PB1-N92. One could argue the possibility of deleting AUG11 from the PB1-N92 expressing plasmid. However, potential changes in the phenotype given by such mutant plasmid would not provide a clear answer to whether it was due to the lack of PB1-N111, a single point mutation in PB1-N92 or both, making the determination of the individual functions of PB1-N92 challenging using expression plasmids. Nevertheless, analysis of IRF3 and NF-κB phosphorylation in infected cells and viral fitness in the presence of inhibitors suggested that whilst PB1-N111 might counteract IRF3 phosphorylation, both PB1-N92 and –N111 could be involved in NF-κB inhibition.

Overall, this chapter added two additional polypeptides to the group of inhibitors of IFN induction coded by IAV: PB1-N92 and –N11. Moreover, it showed

that counteraction of IFN expression in IAV infection is also performed in stages downstream of the initial RIG-I/MAVS recognition which also prevents TRL3/7-driven IFN upregulation.

Chapter 6

Studies on the strain-dependency of AUG codons 10 and 11

6.1. Background and aims

Previous chapters have described the expression of two additional products expressed from segment 2 AUG codons 10 and 11. These polypeptides were shown to block TBK1- and MyD88-induced IFN-β expression; their deletion from the virus led to increased phosphorylation of IRF3 and NF-κB P65 and reduced virus propagation *in vitro* and *in vivo*. However, the work so far only examined the PR8 strain of IAV. It was therefore important to determine if segment 2 AUG codons 10 and 11 are also important in the context of other IAV strains. Studies on the overall conservation of AUG codons in IAV segments 2 and 3 have been carried out (Gong *et al.* 2014; Gog *et al.* 2007). Although these studies found high conservation of PB1 AUG codons 10 and 11, they failed to provide insights into any differential AUG conservation within specific hosts and subtypes of IAV. Therefore, a more in-depth analysis was performed

using a larger set of sequences that also considered the strength of Kozak signalling for AUG codons 5, 10 and 11, as well as their prevalence. Furthermore, in order to further test the importance of PB1 AUG codons 10 and 11 in IAV, six additional strains of virus were selected from avian, human and swine hosts. Segment 2 AUGs 10 and 11 mutations were inserted into the background of these viruses and key elements of the biological characterisations performed for the PR8 set were repeated for these strains.

6.2. Results

6.2.1. Conservation of frame 1 AUG codons in field isolates.

In order to evaluate the conservation of segment 2 AUG codons within IAV subtypes from all known hosts, the available segment 2 sequences were downloaded from GenBank's Influenza Virus Resource (http://www.ncbi.nlm.nih.gov/genomes/FLU/FLU.html) on the 6th of May 2016. The 31389 sequences found represented isolates from the main types of IAV host. Most sequences were from human isolates (45% of the total number of sequences). The next most abundant were sequences from avian hosts (42.5%), which were considered as one block, followed by swine (11.8%) and then equine (0.45%) and canine (0.25%) viruses (Figure 6.1). Sequences from other IAV hosts such as felines, aquatic mammals and bats were also retrieved but not considered due to the low number of samples (Figure 6.1). Once separated into hosts, sequences were further separated into groups of 500 using an R script. All R scripts used in this chapter were written by Dr Samantha Lycett (The Roslin Institute, The University of Edinburgh, UK). Each

A

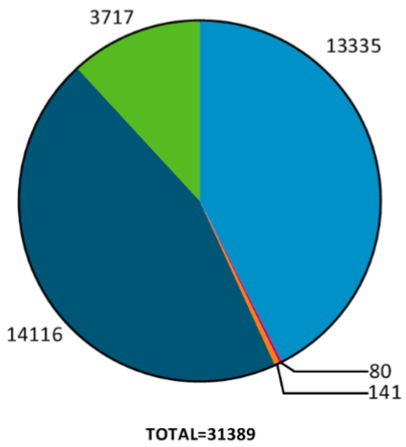

B

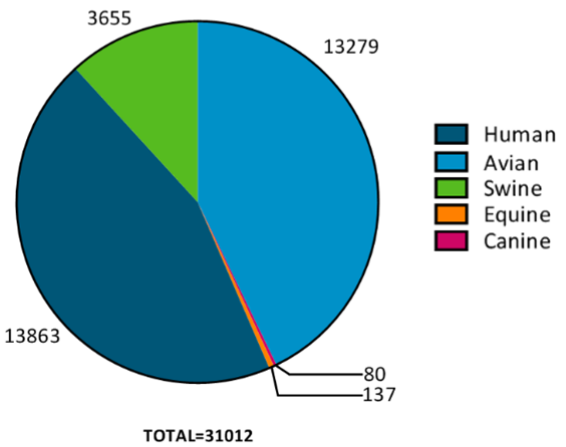

C

Hosts	Downloaded sequences		Post clean-up sequences	
	Number of sequences	%	Number of sequences	%
Human	14116	44.97	13863	44.70
Avian	13335	42.48	13279	42.82
Swine	3717	11.84	3655	11.79
Equine	141	0.45	137	0.44
Canine	80	0.25	80	0.26

Figure 6.1: Representation of the number of segment 2 sequences analysed. (A) A total of 31389 IAV segment 2 sequences were downloaded from NCBI. (B) After discarding poor quality sequences, 31012 sequences were retained, having maintained the overall representation of avian, canine, equine, human or swine sequences. (C) Numbers and percentages of total and analysed sequences.

individual group was aligned using the MUSCLE application within the MEGA6.0 software followed by the selection of incomplete and erroneous sequences which were visually detected and discarded from the analysis. Reporting of UTR information was inconsistent between sequences, so in order to ensure a clear start for the alignments, any 5' UTRs were removed. After sequence clean-up, the analysis was performed using 13278 avian, 80 canine, 134 equine, 14365 human and 3655 swine sequences, maintaining the original representation of each host category in the overall analysis (Figure 6.1 B and C). The "cleaned" alignments (containing up to 500 sequences each) were re-joined and the presence of AUGs at PB1 codons 1, 40, 92 and 111 (starting at nucleotides 1, 118, 274 and 331, respectively) was assessed using an R script (Figure 6.2A). Sequences were further classified according to their H and N subtypes; considering the wide variety of these within each host grouping, subtypes which represented less than 1.5% of the total number of sequences per host were congregated into "Others". The prevalence data were then plotted in contingency charts where the total prevalence of a specific AUG codon represents the sum of the percentage conservation for each subtype. Conservation of AUGs 5, 10 and 11 could therefore be compared to AUG1, which was always 100% conserved in every group of sequences. Overall, AUG codons 5, 10 and 11 were conserved at 99.4, 99.9 and 98.3% respectively. These high prevalence values were consistent with previous studies, which showed that AUGs 10 and 11 were present in at least 99 and 97% of the analysed sequences, respectively (Gong *et al.* 2014; Gog *et al.* 2007). Avian sequences presented a consistent AUG conservation independently of the subtype. Canine sequences presented 100% conservation of AUG codons 1, 5 and 10. AUG11 prevalence was slightly decreased in this host (98.7%) due to the absence of this codon

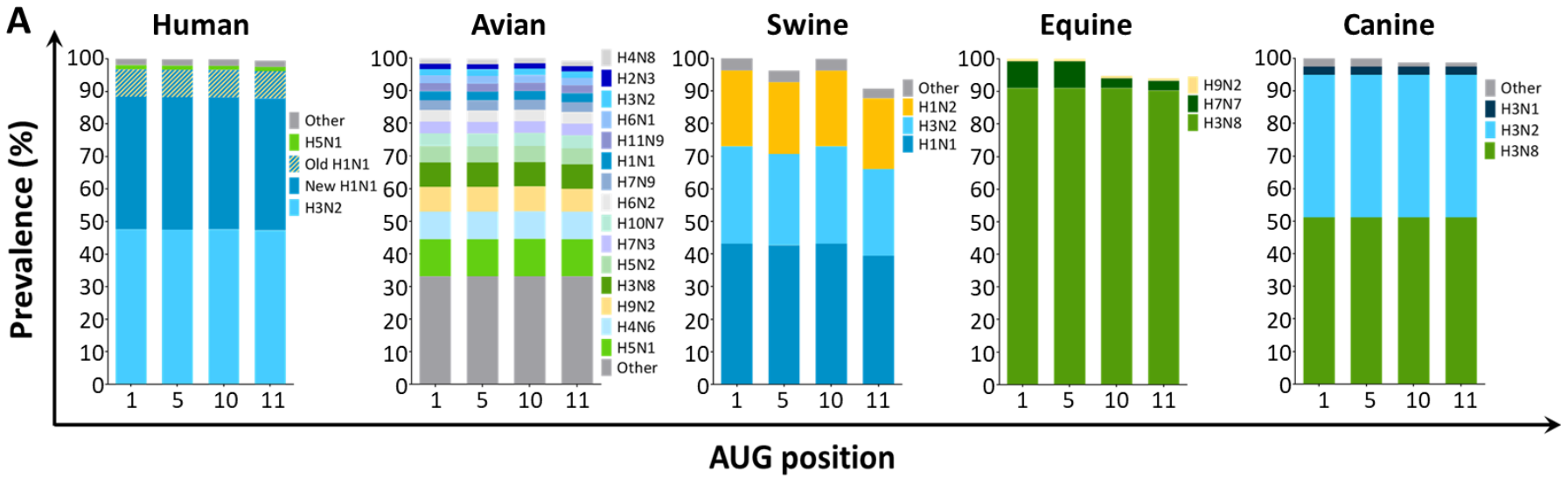

B

	AUG5				AUG10				AUG11			
	None	Weak	Medium	Strong	None	Weak	Medium	Strong	None	Weak	Medium	Strong
Human	19	-	1	14345	24	-	5	14336	77	-	1	14287
Avian	35	-	2	13241	5	-	2	13271	116	-	5	13157
Swine	136	-	3	3516	2	-	4	3649	338	-	1	3316
Equine	-	-	-	134	-	-	-	134	1	-	-	133
Canine	-	-	-	80	-	-	-	80	1	-	-	79

Figure 6.2: Conservation of segment 2 AUG codons 5, 10 and 11 and their Kozak consensus sequence. All available PB1 nucleotide sequences were downloaded from NCBI. (A) Sequences were separated into hosts and subtypes and the presence of AUGs 1, 5, 10 and 11 in individual sequences was calculated. (B) The strength of Kozak signalling around the indicated AUG codons in the dataset was categorised as strong (-3A/G and +4G), medium (-3A/G or +4G) or weak (neither -3A/G nor +4G). "None" refers to sequences where no AUG codon was found in the stated positions.

in the single H9N2 (included in "Others") sequence. Equine sequences also showed an overall 100% conservation of AUG codons 10 and 11, with the exception of H7N7 isolates where these AUGs were only present in 4 of the 11 analysed sequences (36.3%). Similarly to avian isolates, human sequences had a high prevalence of all tested AUG codons (conservation varying between 99.4 and 99.9%). Conservation of frame 1 AUG codons was more variable in swine isolates, with AUG11 having the lowest levels in this host. AUG codons 5, 10 and 11 showed prevalence values of 96.3, 99.9 and 90.8%, respectively. However, in contrast to other hosts, in swine sequences, the decrease of AUG conservation was not associated with a particular subtype.

In addition to the ORF length and conservation of initiator codon, the nature of the Kozak motif is also an important factor in potentially dual-coding transcripts (Xu *et al.* 2010). Therefore, the same alignments were used to quantify the strength of each AUG Kozak signalling (Figure 6.2B). These sequences were categorised into strong (-3A/G and +4G), medium (-3A/G or +4G) and weak (neither -3A/G nor +4G) (Kozak 1986). Analysis revealed that in the case of present AUGs at in positions 40 (AUG5), 92 (AUG10) or 111 (AUG11), Kozak sequence was strong in more than 99% of the occurrences. Cases of medium Kozak signalling represented 0.02, 0.03, 0.02% of the overall AUG-containing sequences for AUG codons 5, 10 and 11, respectively. Weak sequences were not detected. Analysis of Kozak signalling of AUG1 was not assessed, given the deletion of the 5' UTR region post alignment. Total numbers of sequences where there were no AUG detected in the mentioned positions are shown under "None". Overall, the majority of IAV strains (despite host or subtype) maintain AUG codons 10 and 11 in sequence context conducive to translation initiation.

6.2.2. Selected IAV strains

In order to study the importance of segment 2 AUG codons 10 and 11 in other IAV strains, 6 additional viruses from avian, human and swine hosts were selected based on the availability of a reverse genetics system in the laboratory (Table 6.1). Alignments between the PB1 amino acid sequences of these viruses was performed, confirming the presence of AUG codons 10 and 11 (see later in Figure 6.11). Selected viruses included:

- A pair of low- and high-virulence isolates from the 1983 United States poultry H5N2 outbreak (Kawaoka and Webster 1985) - Penn83 HP and Penn83 LP,
- A laboratory-passaged H1N1 isolate derived from the mixed population present in an original isolate from a mallard duck (Bourret *et al.* 2012) – Mallard,
- A lab-adapted human seasonal H3N2 strain (Chen *et al.* 2007) – Udorn,
- A mouse-adapted derivative of the prototype human 2009 H1N1 pandemic virus (Ye *et al.* 2010) - Cal04,
- An H3N2 swine isolate from 1987 (Wibberley *et al.* 1988) subsequently passaged 8 times in eggs (Brown 2016) - Swine87.

6.2.3. Translation initiation from segment 2 AUG codons 10 and 11 of the selected viruses

As previously described for PR8 in section 2.2.1, protein expression from AUGs 10 and 11 of the selected panel of viruses was examined in the context of

Table 6.1: Selected virus strains used for reverse genetics analysis of PB1 AUGs 10 and 11. Viral host, strain name and serotype are given. To simplify nomenclature of these viruses, abbreviations were also defined.

Host	Virus	Abbreviation	Serotype
Avian	A/chicken/Pennsylvania/1/1983	Penn83 HP	H5N2
	A/chicken/Pennsylvania/1370/1983	Penn83 LP	H5N2
	A/mallard/Netherlands/10-Cam/1999	Mallard	H1N1
Human	A/Puerto Rico/8/34	PR8	H1N1
	A/Udorn/307/1972	Udorn	H3N2
	A/California/04/2009	Cal04	H1N1
Swine	A/swine/England/87842/1990	Swine87	H3N2

plasmid transfection. In order to do this, the first 380bp of Udorn, Cal04, Swine87 and Mallard segment 2 cDNAs were also cloned into a green fluorescent protein (GFP) expression plasmid, with the reporter gene positioned into frame with AUG codons 1, 5, 10 and 11. Once confirmed by DNA sequencing, the panel of WT and mutated PR8 constructs and the four new constructs were individually transfected into 293T cells. Forty-eight hours post-transfection, the expression of GFP-fused products was assessed by SDS-PAGE and western blot, using an antibody against GFP, as well as α-tubulin as a loading control. All samples contained similar amounts of tubulin (Figure 6.3), which confirmed comparable loading.

As a negative control, a sample from mock transfected cells was included, which did not contain detectable GFP peptides, apart from the background bands (Figure 6.3, lane 1). The detection system was validated by the transfection of a GFP-only plasmid positive control, where a polypeptide product was seen at 27kDa, the expected molecular mass for GFP (lane 2). As previously described in section 2.2.1, transfected cells with WT PR8 PB1-GFP plasmid, cells expressed fusion peptides corresponding to PB1, PB1-N40, PB1-N92 and PB1-N111 (lane 3) which were absent or reduced after the mutation of AUGs 1, 5, 10 and 11, respectively (lanes 4-8). Lanes 9-12 represent GFP-tagged versions of Udorn, Cal04, Swine87 and Mallard 1-380bp of segment 2 mRNA, which also resulted in the expression of the four PB1-related polypeptides.

Hence, translation initiation from AUG codons 10 and 11 is also observed from segment 2 cDNA of Udorn, Cal04, Swine87 and Mallard in transfected cells.

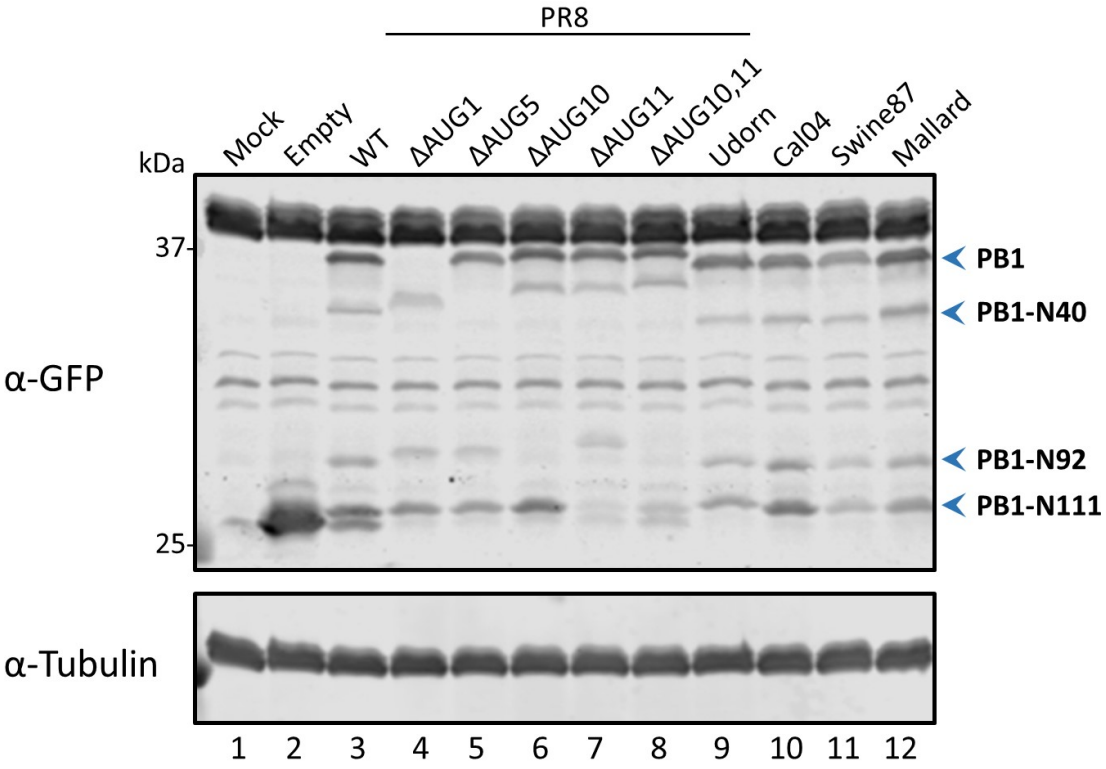

Figure 6.3. Expression of PB1 related species from Udorn, Cal04, Swine87 and Mallard segment 2 cDNA in transfected cells. 293T cells were transfected with the panel of PR8 GFP-fusion plasmids as well as the Udorn, Cal04, Swine87 and Mallard GFP-tagged segment 2 plasmids for 48 hours. Lysates from cells transfected (or mock transfected) with the indicated panel of plasmids were analysed by western blot with anti-GFP serum; α-tubulin was used as loading control. The position of molecular mass markers (in kDa) is indicated on the left. Datum is a representative of two independent experiments performed with one single technical repeat.

6.2.4. Evaluation of the transcription activity of mutant PB1 proteins of the selected viruses

Single and double mutations of AUGs 10 and 11 were introduced into the segment 2 reverse genetics plasmids of the selected viruses by site-directed mutagenesis. As described in chapter 2, alteration of AUGs 10 and 11 led to the inevitable introduction of amino acid point mutations which could alter PB1 polymerase activity. Therefore, as previously described in section 2.2.6, reverse genetics plasmids coding for the components of the viral ribonucleoprotein were used to measure transcription activity of mutant PB1 proteins of the different isolates in minireplicon assays.

Mammalian IAVs and Mallard viral polymerase activity was assessed in 293T cells which were transfected with 50ng of each RNP plasmid and 20ng of a firefly luciferase vRNA-like reporter plasmid. Forty-eight hours later, cells were lysed and luciferase activity was measured (Figure 6.4 A-D). For all the viruses, a negative control substituting the PB1 segment for an empty pDUAL plasmid (2PNP), and mock-transfected cells were included. Assay validation was seen by statistically significant over 100-fold increase in luciferase activity between the 2PNP and the WT 3PNP samples. Mutation of AUG codons 10 and/or 11 in the context of Udorn, Cal04, Swine87 or Mallard RNPs did not affect viral gene expression. Equivalent analyses were performed for the chicken viruses Penn83 HP and LP (Figure 6.4 E and F). However, these avian isolates possess a glutamic acid (E) at position 627 of PB2 which often does not support activity in mammalian cells (Luk *et al.* 2015; Subbarao *et al.* 1993; Naffakh *et al.* 2000). Therefore, transcription activity of the mutant PB1

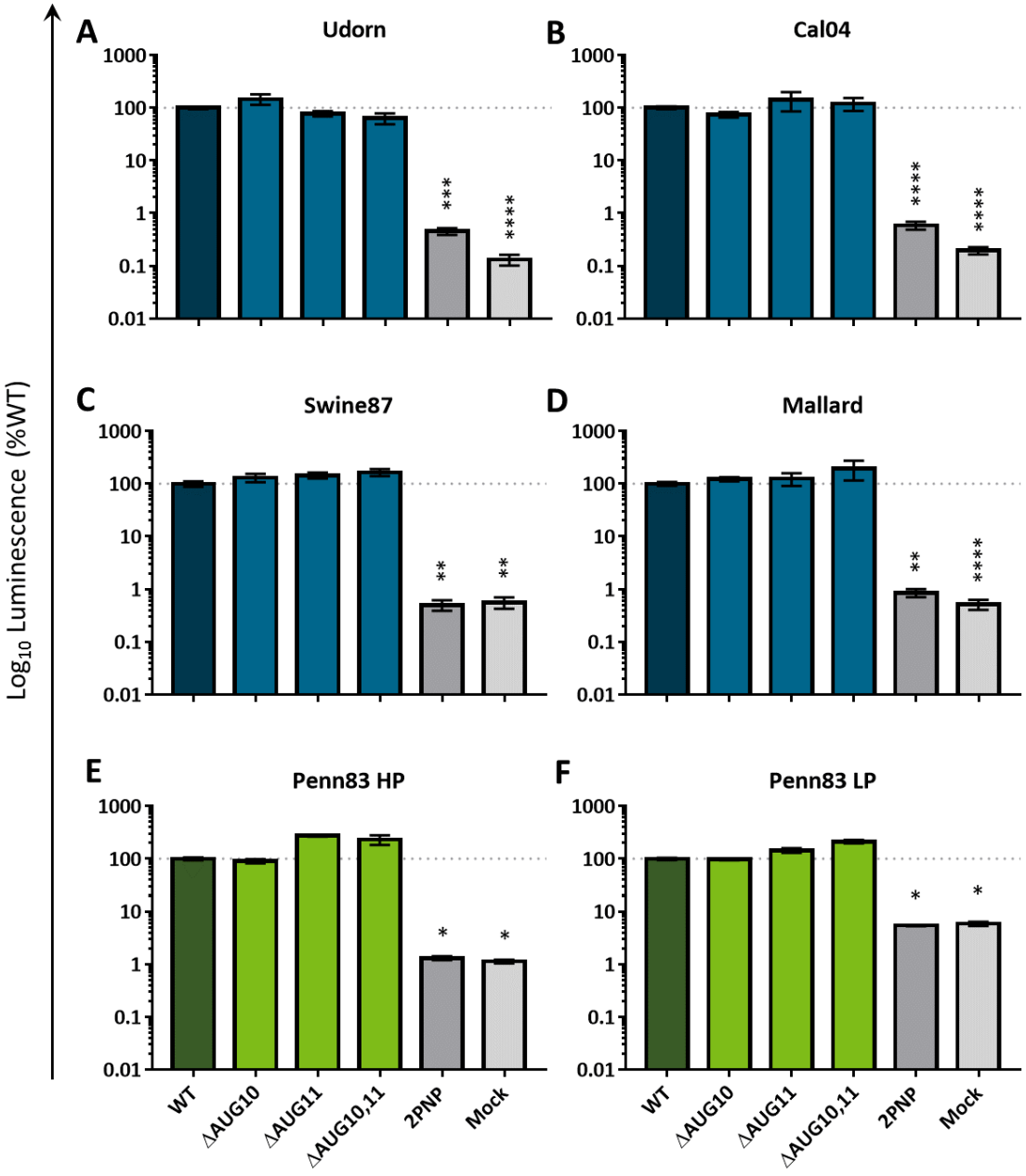

Figure 6.4: Transcription activity of segment 2 mutant RNPs. (A-D) 293T or (E, F) QT-35 cells were transfected with 3PNP expressing plasmids and a vRNA-like luciferase reporter plasmid under a human or avian RNA PolI promoter respectively. Forty-eight hours post transfection, cells were lysed, and luciferase levels measured. Data represent mean ± SEM from three independent experiments performed with three technical repeats. Statistic annotations are the result of an ordinary one-way ANOVA test. *p-value, <0.05, **p-value <0.01, ***p-value <0.001, ****p-value <0.0001.

specimens in the context of Penn83 HP and LP polymerases was performed in avian cells. QT-35 quail fibroblasts were transfected with plasmids encoding the RNP proteins of Penn83 HP or LP along with a reporter plasmid expressing vRNA-Luc from an avian PolI promoter (Figure 6.4 E and F). Transcription activity of Penn38 HP was stronger than Penn83 LP with Penn83 HP having a near 100-fold induction of 3PNP over 2PNP condition, compared with Penn83 LP where the fold induction was only 20-fold. Nonetheless, as observed for all the other tested viruses, RNPs harbouring ΔAUG10/11 PB1 subunits did not show any attenuation in transcription activity. Thus, as previously shown for PR8 ΔAUG mutants (section 2.2.6), mutated PB1 polypeptides of the the additional IAV strains tested shared a WT-like transcription phenotype.

6.2.5. Propagation of the wider panel of segment 2 mutant viruses in MDCK cells

Having tested the transcriptional activity of PB1 mutants, the reverse genetics plasmids were used to rescue the actual viruses, in WT and mutant forms. Attempts at rescuing Penn83 HP and LP viruses as either 6:2 (using HA and NA of PR8 for biosafety reasons) or 4:4 (using the chicken virus 3PNP genes with the remaining segments from PR8) reassortant combinations were made in several mammalian and avian systems. However, despite several attempts, neither WT nor mutant viruses were successfully generated in any of the reassortment arrangements (data not shown). In contrast, the other viruses were generated readily and used to create P1 stocks (as in section 2.2.2). At least two independent stocks were created for each of the mutant

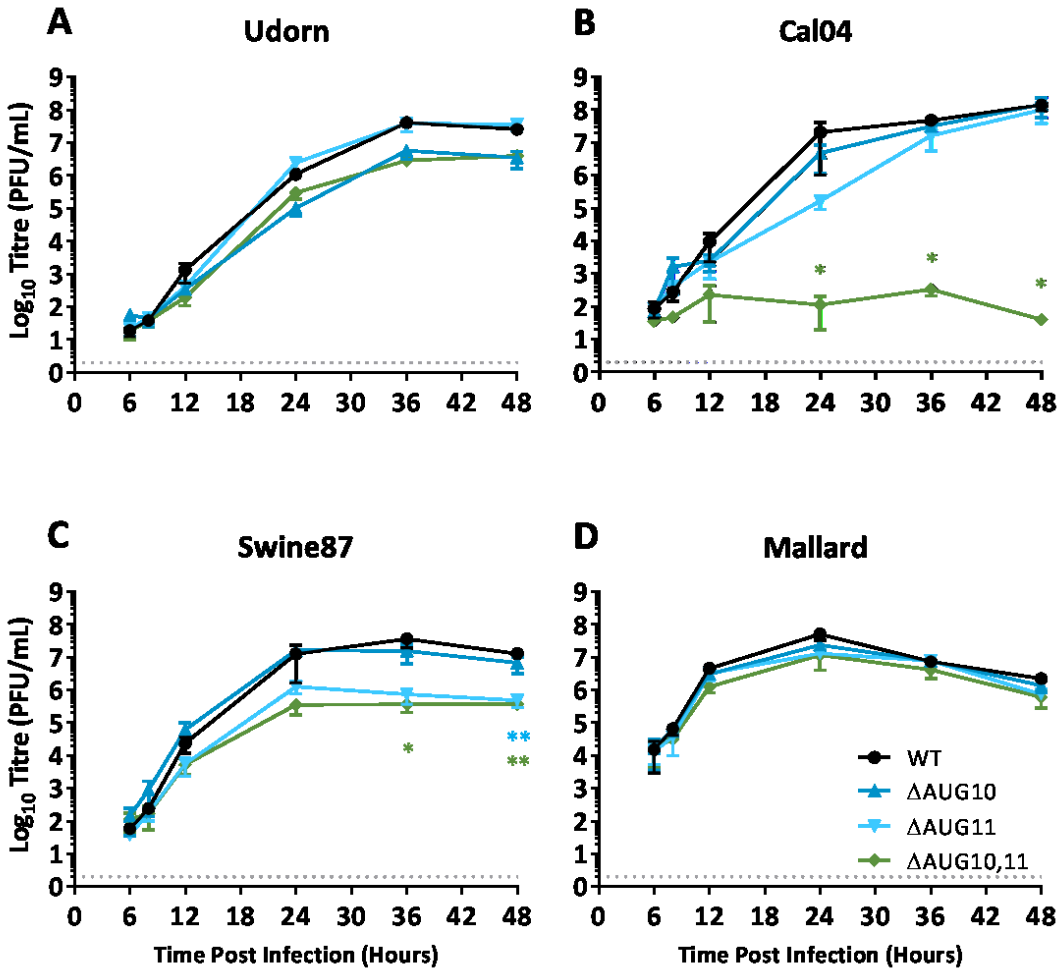

Figure 6.5: Growth kinetic analyses of WT and mutant viruses in MDCK cells. MDCK cells were infected at a MOI of 0.001 and samples were collected at the indicated times post infection. Data are mean ± SEM from three independent experiments performed with a single technical repeat. Statistic annotations are the result of an ordinary one-way ANOVA test (performed individually for each time-point). *p-value <0.05, **p-value <0.01. Dashed lines indicate the limit of detection for the plaque assays (2 PFU/ml).

viruses. Sequencing of segment 2 confirmed the presence of the desired sequences (data not shown).

Rescued P1 stocks for the Udorn, Cal04, Swine87 and Mallard sets were used to perform growth kinetic analyses. Confluent monolayers of MDCK cells were infected at a MOI of 0.001, supernatants were collected at 6, 8, 12, 24, 36, and 48 hpi and viral titres were measured by plaque assay (Figure 6.5). WT Udorn steadily increased in titre with time, reaching a maximum of 4×10^7 PFU/mL at 36 hpi (Figure 6.5A). A comparable outcome was observed for Udorn ΔAUG11, which showed no attenuation in this growth system. However, although not statistically significant, mutation of AUG10 resulted in 10-fold lower titres from 24 hours onwards. This phenotype was shared by the double mutant virus Udorn ΔAUG10,11 whose growth pattern overlapped the single mutant ΔAUG10. Cal04 WT reached titres of 10^8 PFU/mL and a WT-like phenotype was observed for Cal04 ΔAUG10 during the entire course of infection (Figure 6.5B). However, loss of AUG11 resulted in delayed virus replication kinetics which nevertheless recovered to WT-like titres at 36 and 48 hpi. An even more accentuated attenuation of replication was seen for the double mutant Cal04 ΔAUG10,11, which had a 10^6-fold decrease in viral titre compared with its WT counterpart at 24 hpi and did not show any recovery throughout the remaining course of infection. WT Swine87 virus also propagated to high titres in this system, reaching a maximum titre of 4×10^7 PFU/mL at 36 hpi (Figure 6.5C). Similar to PR8 and Cal04 mutants, deletion of AUG10 did not induce changes in virus replication. On the other hand, deletion of AUG11 led to statistically significant 100-fold decreases in virus titres, seen for both single and double mutants ΔAUG11 and ΔAUG10,11. Replication of Mallard WT resulted in titres of 5×10^7 PFU/mL which peaked at 24 hpi (Figure

6.5D). However, introduction of mutations in AUG codons 10 and/or 11 in this viral context did not affect virus titres. In general terms, this section showed that either AUG codons 10 and/or 11 are important for WT-like virus replication of mammalian isolates in MDCK cells, but dispensable in the context of the duck virus used here.

6.2.6. IFN induction by the wider panel of segment 2 mutant viruses

Next, we asked if, as found for PR8, the larger panel of segment 2 AUG mutants would induce a stronger IFN expression in the context of viruses, which might explain the attenuated phenotype of some of them. To investigate this, A549 cells were infected at a MOI of 3 (for Udorn and Cal04 sets) or 0.03 (for Swine and Mallard sets). The diminished MOI used for the last two sets was due to the lower titres acquired for some of the P1 stocks (data not shown) which did not allow high MOI infections. Infections with the mutant viruses Cal04 ΔAUG10,11 and Swine87 ΔAUG10,11 were not performed as the P1 stocks were too low titre to allow even this reduced MOI (data not shown). Twenty-four hpi, IFN levels were measured using the HEK Blue cell bioassay (as previously described in section 3.2.1). As a control for all the infections, PR8 WT and NS1 R38K41A were used as negative and positive controls, respectively. A strong IFN induction was seen for the mutant NS1 virus while background levels were observed for PR8 WT (data not shown). Moreover, a standard curve using universal type I IFN was also added and a dose-dependent increase in A_{600} was observed, confirming assay function (data not shown). WT Udorn virus infection induced only background levels of IFN, whereas the virus with a mutation in AUG10 resulted in statistically significantly increased IFN induction. Equivalent results were

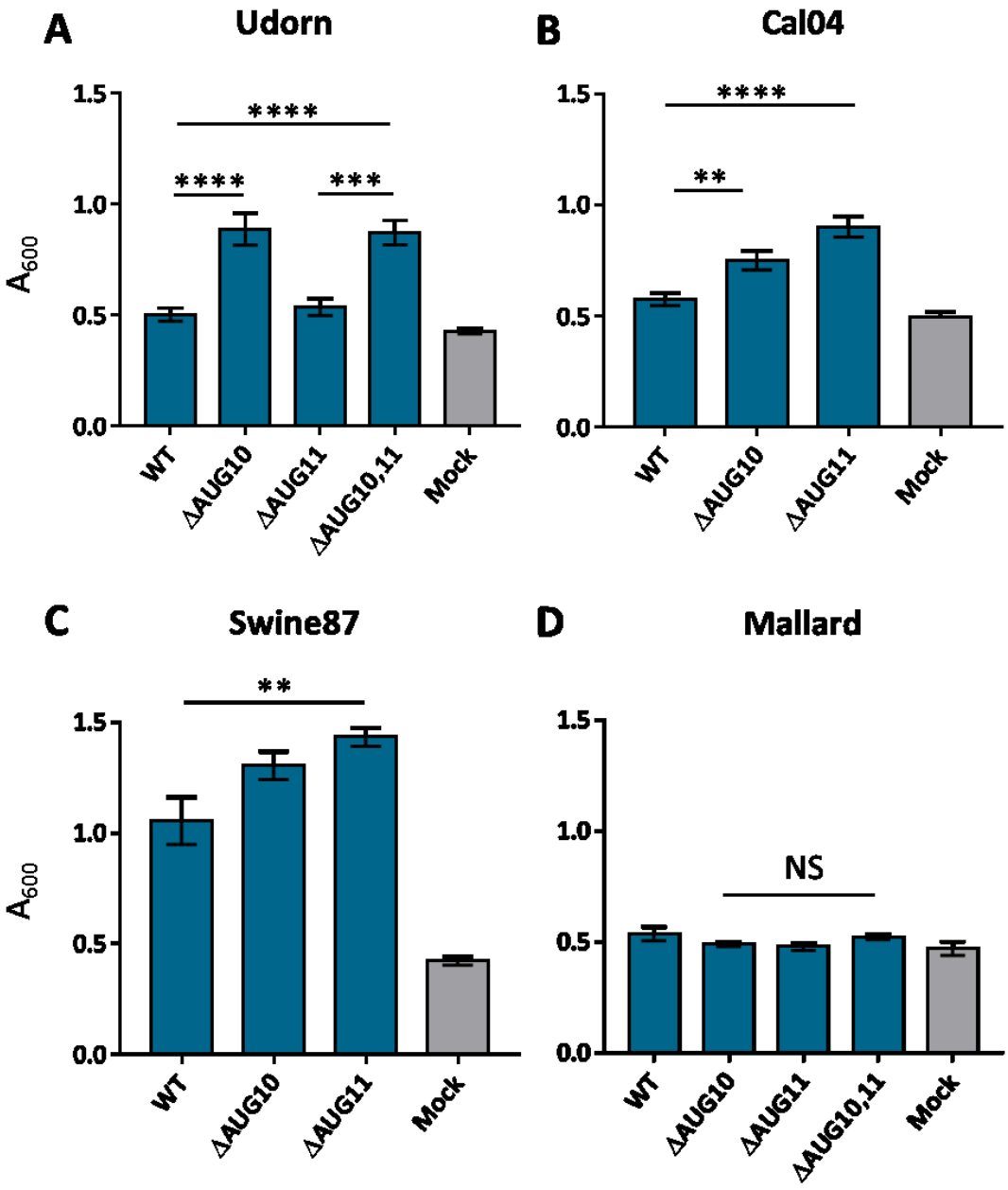

Figure 6.6: Type I IFN induction during infection with selected ΔAUG10 and/or 11 viruses isolated from different hosts. A549 cells were infected with MOI of 3 for (A) Udorn and (B) Cal04 and 0.03 for (C) Swine87 and (D) Mallard mutant viruses. Twenty-four hpi, cell supernatants were harvested, UV-inactivated and type I IFN levels measured using HEK Blue cell bioassay. Absorbance values at 600nm are shown, which are proportional to the amount of type I IFN present in the cell supernatants. Data are mean ± SEM from four independent experiments performed in duplicates. Statistical symbols represent the results of ordinary one-way ANOVA tests. **p-value <0.01, ***p-value <0.001, ****p-value <0.0001.

seen for infection with the ΔAUG10,11 virus. On the other hand, loss of AUG11 did not result in different IFN secretion from WT virus (Figure 6.6A). WT Cal04 infection also resulted in background levels of IFN induction. However, this was significantly increased in ΔAUG10, and more prominently in ΔAUG11 mutant viruses (Figure 6.6B). As with PR8, high MOI infections with the double mutant ΔAUG10,11 were not possible because of the low titres of the recovered P1 stocks (data not shown). In contrast to all the other tested WT viruses, A549 infections with WT Swine87 induced IFN levels well above background/mock levels. Nonetheless, similarly to the Cal04 and PR8 sets of viruses, mutation of AUG codons 10 and 11 resulted in augmented IFN induction, which was statistically significant when the ΔAUG11 Swine87 virus was compared to WT (Figure 6.6C). Mallard WT infections induced background levels of type I IFN. However, unlike all the ΔAUG10/11 mutant viruses so far tested, alteration of AUG codons 10 and/or 11 did not cause increased IFN expression in A549 cells (Figure 6.6D).

Overall, this section corroborated the data observed in the kinetic analysis by showing a good correlation between the inability to replicate normally *in vitro* and an increased induction of type I IFN.

6.2.7. Phosphorylation of IRF3 in cells infected with the panel of segment 2 mutants

Following the sequence of experiments performed to characterise the PR8 AUG mutant viruses, we next analysed the levels of IRF3 phosphorylation in cells infected with the mutants. As in section 6.2.5, A549 cells were infected with the

different sets of segment 2 mutant viruses at MOIs of 3 (Udorn and Cal04) or 0.03 (Swine87 and Mallard). Twenty-four hpi, phosphorylation of IRF3 was detected by western immunoblot, along with total IRF3 levels. Detection of viral NP was used to confirm infection and α-tubulin monitored as loading control (Figure 6.7). Mock-infected samples had undetectable or very low levels of IRF3 phosphorylation (Figure 6.7 A-D lanes 1). For each individual experiment of each set of viruses, PR8 NS1 R38K41A and transfection with poly I:C were used as positive controls, which showed increased levels of pIRF3 compared to the cells-only control (data not shown). Readily detectable amounts of pIRF3 were detected in Udorn WT-infected cells, which were not substantially increased by the introduction of the ΔAUG10/11 mutations (Figure 6.7A). Quantification of replicate experiments by densitometry corroborated that, despite a slight increase in pIRF3 amounts in the Udorn ΔAUG11 mutant, there were no significant differences between the mutants and WT Udorn (Figure 6.7E). Cal04 WT infections also resulted in low levels of pIRF3 detection. However, in contrast to the Udorn mutants, single deletion of AUG codons 10 or 11 resulted in substantially increased levels of IRF3 phosphorylation. This increment was more pronounced with Cal04 ΔAUG11 (Figure 6.7B). This was confirmed by quantification of IRF3 phosphorylation which showed statistically significant 3- and 5-fold increases of pIRF3 levels with ΔAUG10 and ΔAUG 11 Cal04 viruses, respectively (Figure 6.7F). Phosphorylation of IRF3 was also readily detectable in the context of Swine87 WT virus infection. However, increased levels of pIRF3 were seen following infection with AUG10 and, especially, ΔAUG11 Swine87 viruses (Figure 6.7C). Quantification by densitometry from three independent experiments showed statistically significant differences only for Swine87 ΔAUG11 in comparison to the WT virus (Figure 6.7G).

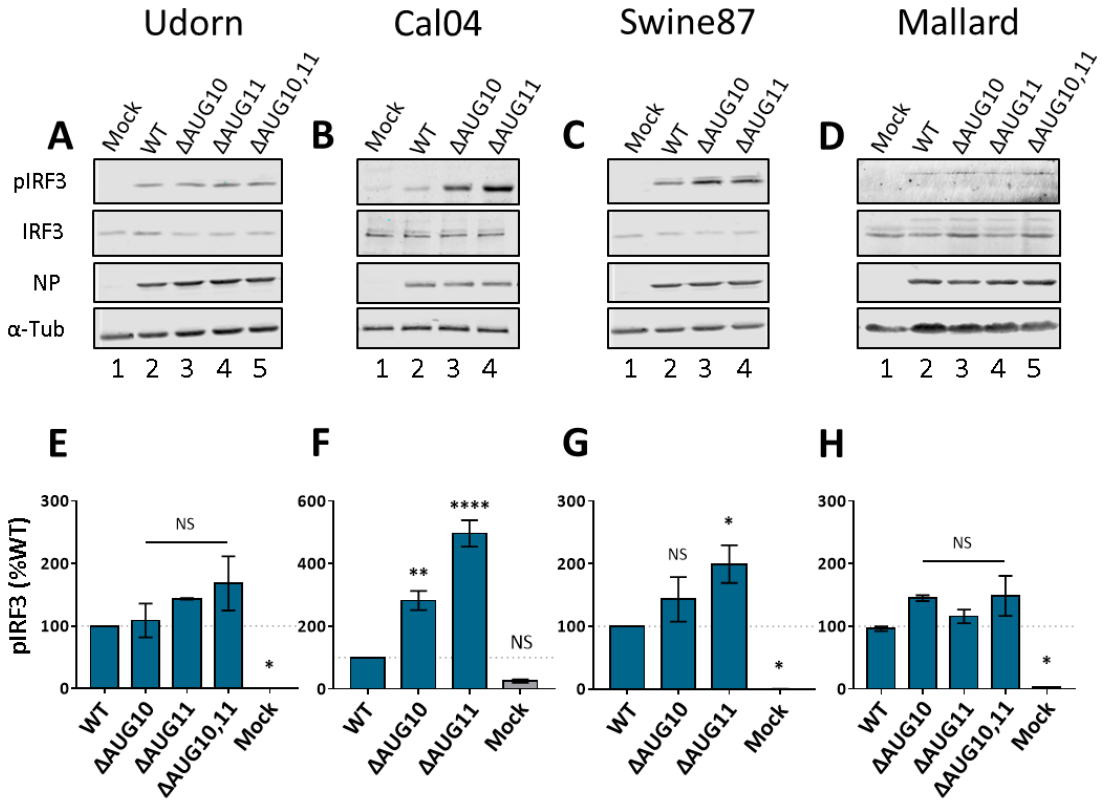

Figure 6.7: IRF3 phosphorylation in infection of selected viruses' segment 2 mutants. (A-D) A549 cells were infected at a MOI of 5 for 24 hours, after which cell lysates were collected. Lysates were subjected to SDS-PAGE followed by the detection of naïve and phosphorylated forms of IRF3 by western blot. NP and α-tubulin were detected to confirm infection and as a loading control, respectively. (E-H) Relative quantification of the phosphorylated IRF3 form was performed in ImageJ and scaled to the respective values from WT virus infections. Data represent mean ± SEM from three independent experiments performed with a single technical repeat. Statistic annotations are the result of an ordinary one-way ANOVA test. *p-value, <0.05, **p-value <0.01, ****p-value <0.0001.

In concordance with the previous sections and in contrast to the other viruses, mutation of AUG codons 10 and/or 11 in the context of a Mallard virus infection did not lead to stronger phosphorylation of IRF3 in comparison to WT virus (Figure 6.7D). Quantifications of the western blots reflected this result (Figure 6.7H). Thus, IRF3 phosphorylation levels were upregulated in ΔAUG10/11 mutant viruses in general agreement with increased IFN induction and lowered replication values.

6.2.8. Effect of BX-795 on the propagation of the panel of segment 2 mutant viruses

Next, the effects of chemically inhibiting IRF3 phosphorylation on segment 2 AUG mutant virus propagation were measured for Udorn, Cal04, Swine87 and Mallard virus sets; again following the hypothesis that if the growth defect arose from the lack of a viral IRF3 antagonist, exogenous suppression of TBK1/IKKε complex activity should complement the defect. As previously described in section 5.2.6, A549 cells were pre-treated with varying concentrations of BX-795 for 2 hours, following which cells were infected at MOI of 0.001 and overlaid with the same concentrations of drug. Virus-containing cell supernatants were collected at 48 hpi and viral titres were measured by plaque assay (Figure 6.8). For the Udorn set, in the absence of drug, deletion of AUG10 was more deleterious for virus replication than the loss of AUG11 in A549 cells (as previously seen in section 6.2.5 for MDCK cells). Infection with the ΔAUG10 mutant resulted in a 20-fold reduction in viral titre in comparison with WT Udorn, while ΔAUG11 replication was only reduced in 8-fold (Figure 6.8A). The double mutant presented an 80-fold reduction in viral titre, compared its WT

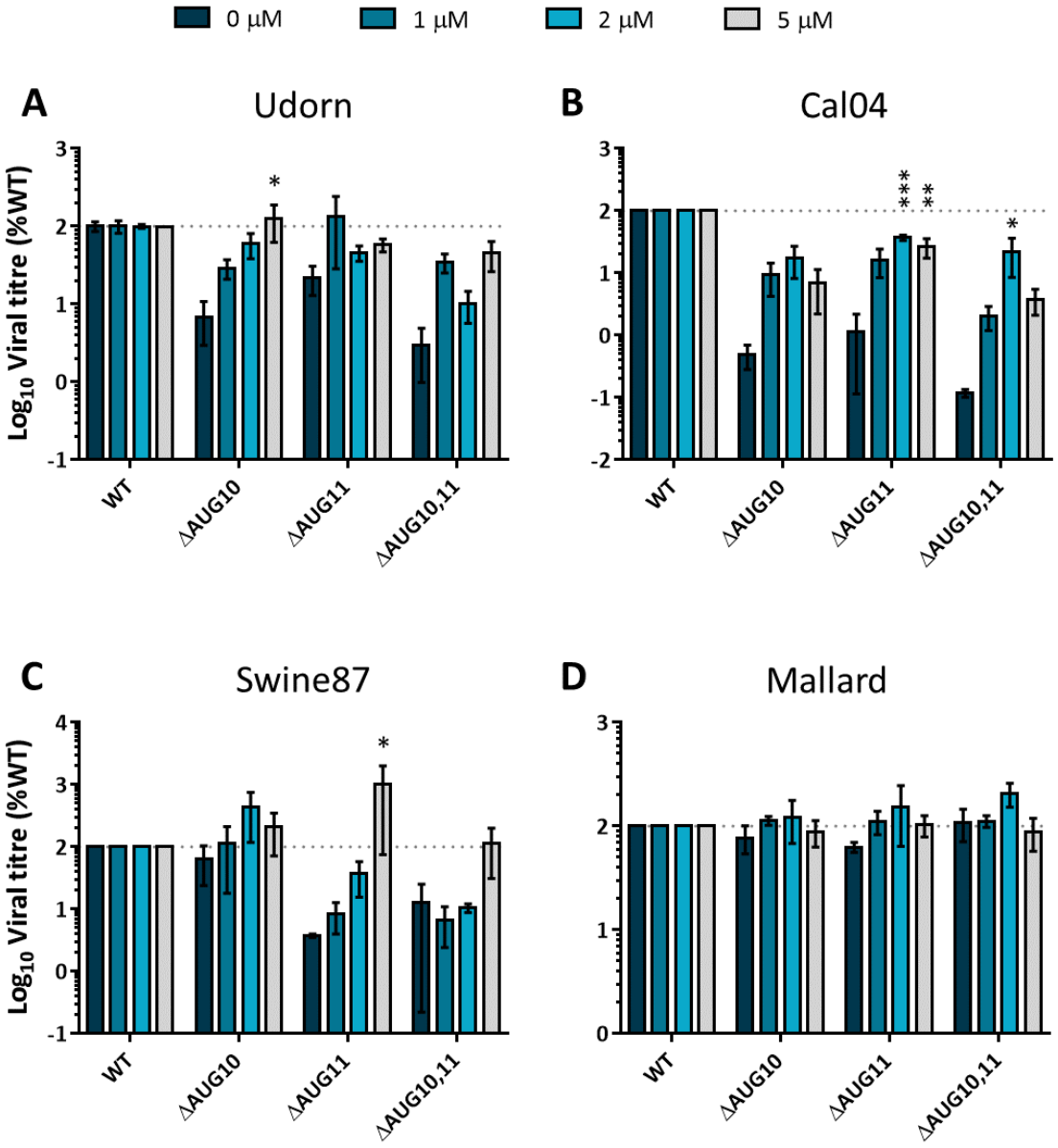

Figure 6.8: Replication of ΔAUG mutant viruses in the presence of BX-795. A549 cells were pre-treated with 1, 2, 5µM of BX-795 and infected with (A) Udorn, (B) Cal04, (C) Swine or (D) Mallard segment 2 mutant viruses at a MOI of 0.001. BX-795 concentrations were kept during the entire time course of infection. Forty-eight hpi, viral titres were measured by plaque assay. Values were scaled to the WT viral titres of each drug concentration. Data represent mean ± SEM from three independent experiments performed with a single technical repeat. Statistical symbols represent the result of a two-way ANOVA test. Multiple comparison tests were performed within each mutant, having the 0µM concentration as control. *p-value <0.05, **p-value <0.01, ***p-value <0.001.

counterpart. However, despite the modestly augmented pIRF3 levels in ΔAUG10 and/or 11 mutant viruses, replication of mutant ΔAUG10-containing Udorn viruses recovered in the presence of BX-795. This recovery was most obvious, and statistically significant, with the highest dose of inhibitor, 5μM for the ΔAUG10 virus. Cal04 ΔAUG10 and/or 11 mutants were attenuated in A549 cells in the absence of BX-795 with reductions of 100- to 1000-fold in end point viral titres in comparison to WT Cal04 (Figure 6.8B). However, the addition of BX-795 resulted in the increased virus propagation of the AUG mutants, correlating with the enriched phosphorylation levels of IRF3 in the both single ΔAUG10 and ΔAUG11 Cal04 mutant viruses. As previously seen in MDCK cells, the ΔAUG10 Swine87 mutant replicated with a WT-like phenotype in A549 cells (Figure 6.8C), while a >100-fold attenuation of AUG11 mutant viruses (ΔAUG11 and ΔAUG10,11) was observed in the absence of BX-795. However, addition of the IRF3 inhibitor resulted in the recovery of viral propagation of the attenuated mutants, this phenotype being most pronounced using 5μM of the drug. As seen for the Cal04 mutants, these data corroborated the IRF3 phosphorylation data, where the strongest levels of pIRF3 were seen with the ΔAUG11 mutant. Consistent with all the data acquired for the Mallard mutants so far in this chapter, modification of AUG codons 10 and 11 did not alter viral fitness in the absence or presence of BX-795 in A549 cells (Figure 6.8D). These findings also correlate with the lack of changes in pIRF3 in ΔAUG10/11 Mallard-infected cells.

Overall, these data supported the hypothesis that mutation of segment 2 AUGs 10 and/or 11 result in reduced control of IRF3 phosphorylation in most, but not all of a wider panel of IAVs.

6.2.9. Fitness of Mallard segment 2 mutants in avian cells

The avian virus, Mallard, was the only one of the tested IAV strains which was not sensitive to the mutation of either AUG codon 10 and/or 11. However, the fitness of, and cell responses against, WT and mutant Mallard viruses were assayed in mammalian cell lines. Type I IFN pathways in mammalian and avian cells differ in several ways, such as the absence of RIG-I in chickens and other members of the order Galliformes (Santhakumar *et al.* 2017; Karpala *et al.* 2011). Therefore, we postulated that Mallard had evolved to better counteract the IFN system in avian systems and that the products arising from AUGs 10 and 11 might more efficiently counteract components of avian IFN pathways. To test this, the fitness of Mallard WT and AUG mutant viruses was assessed in avian cells: QT-35 quail fibroblasts and DF1 chicken fibroblasts. Cells were infected at a MOI of 0.001 and a multicycle infection was allowed to proceed until 48 hpi, after which cell supernatants were collected and viral titres measured by plaque assay. In both cell lines, Mallard WT replicated to over 10^4 PFU/mL (Figure 6.9). Single mutations of AUGs 10 or 11 led to non-statistically significant 5-fold decreases in viral titre in QT-35 cells (Figure 6.9A). However, despite the lack of attenuation in mammalian systems, a 9-fold statistically significant attenuation in virus propagation was seen for the double mutant Mallard ΔAUG10,11. In DF1 cells, multicycle infection with ΔAUG10 Mallard resulted in non-significant differences compared to its WT counterpart (Figure 6.9B). However, in the same cell type, mutation of AUG11 or both AUGs 10 and 11 lead to a 40-fold statistically significant decrease in viral titre, compared to WT virus. Thus, although Mallard virus was indifferent to the loss of segment 2 AUG codons 10 and/or 11 in mammalian cells,

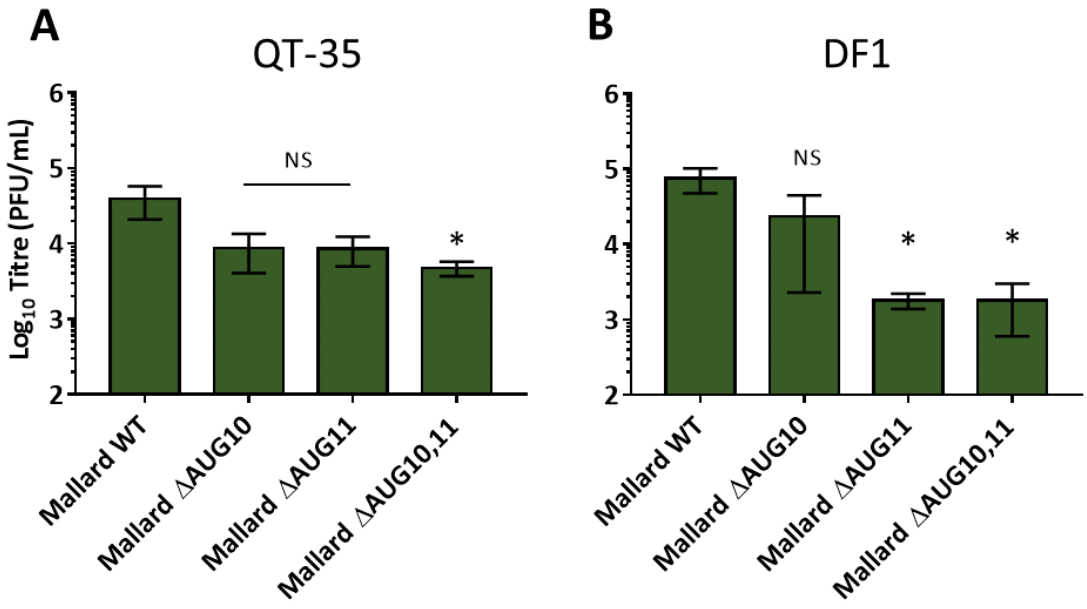

Figure 6.9: Replication of Mallard mutant viruses in avian cells. (A) QT-35 and (B) DF1 cells were infected at MOI 0.001 and supernatants were collected 48 hpi. Viral titres were quantified by plaque assay. Data are mean ± SEM from three independent experiments performed with a single technical repeat. Statistical symbols represent the result of an ordinary one-way ANOVA test. Multiple comparison tests (within data from each cell type) were performed against WT Mallard. *p-value <0.05.

the same was not the case in avian cells, where the single and/or double mutation of these codons resulted in the attenuation of the Mallard mutant viruses.

6.3. Discussion

In this chapter, in order to corroborate the characterisation performed for PR8, the importance of segment 2 AUG codons 10 and 11 was evaluated in the context of other viruses. A bioinformatics analysis of all available segment 2 sequences showed that AUGs 10 and 11 are more than 90% conserved in IAV isolates, in a host-independent manner. Moreover, Kozak signalling analysis confirmed the strong translation start potential in the majority of the sequences examined. These data complemented previous bioinformatics studies on the search for alternative open reading frames which also showed the high prevalence of AUG codons 10 and 11 of 99 and 97%, respectively (Gong *et al.* 2014; Gog *et al.* 2007). Moreover, based on criteria such as strong Kozak consensus sequence, AUG location (within the first third of the transcript), and high prevalence, the study by Gong and colleagues considered there to be a high likelihood of protein expression from these AUG codons (Gong *et al.* 2014).

However, despite the overlapping PB1-F2 ORF encoded between nucleotides 119 and 382 of PR8 segment 2, other AUG codons within that region (such as AUGs 6, 7, 8 or 9, Figure 2.1) are not highly conserved (data not shown) (Gong *et al.* 2014).

The high AUG conservation of AUGs 10 and 11 contrasts with other AUG codons present in the 5' end of IAV segment 2 (schematic representation in Figure

2.1). Parallel bioinformatics analysis also performed in this study suggested that apart from AUG4 which drives the expression of PB1-F2 (Chen *et al.* 2001) and shows high AUG prevalence and conserved strong Kozak signalling, the remaining AUG codons 4, 6, 7, 8 and 9 can be present in between 10 and 100% in field isolates and Kozak signalling is very often of medium power (Figure 6.10), despite the overlapping PB1 and PB1-F2 ORFs encoded in that same region (between nucleotides 119 and 382).

Here it is hypothesised that AUG codons 10 and 11 are conserved to drive expression of an IRF3 antagonist which were shown important for IAV life cycle, which is correlated with the observed high conservation of AUG5 driving expression of PB1-N40 (Wise *et al.* 2009). Nevertheless, given the coding restrains of IAV, it must be admitted that the observed conservation of AUG codons and respective strong Kozak consensus could reflect other reasons:

- The main product PB1 requires methionines at positions 92 and 111. However, for none of the tested viruses the deletion of AUG codons 10 and/or 11 resulted in a deficit in polymerase activity as measured by RNP reconstitution assays.
- The conserved strong Kozak signalling can be due to the need to preserve the amino acids immediately adjacent to positions M40, M92 and M111 (which was not tested by RNP reconstitution assays). A strong Kozak signalling of a given AUG was defined as having A/G in -3 and G in +4 positions (Kozak 1986). According to Gog and colleagues, PB1 position 39 fluctuates between adenine and threonine whilst 41 is invariably an asparagine (Table 6.2A). Analysis of all the possible codons of either A39 or T39 results in the first nucleotide being always G or A. Likewise, the immediately downstream

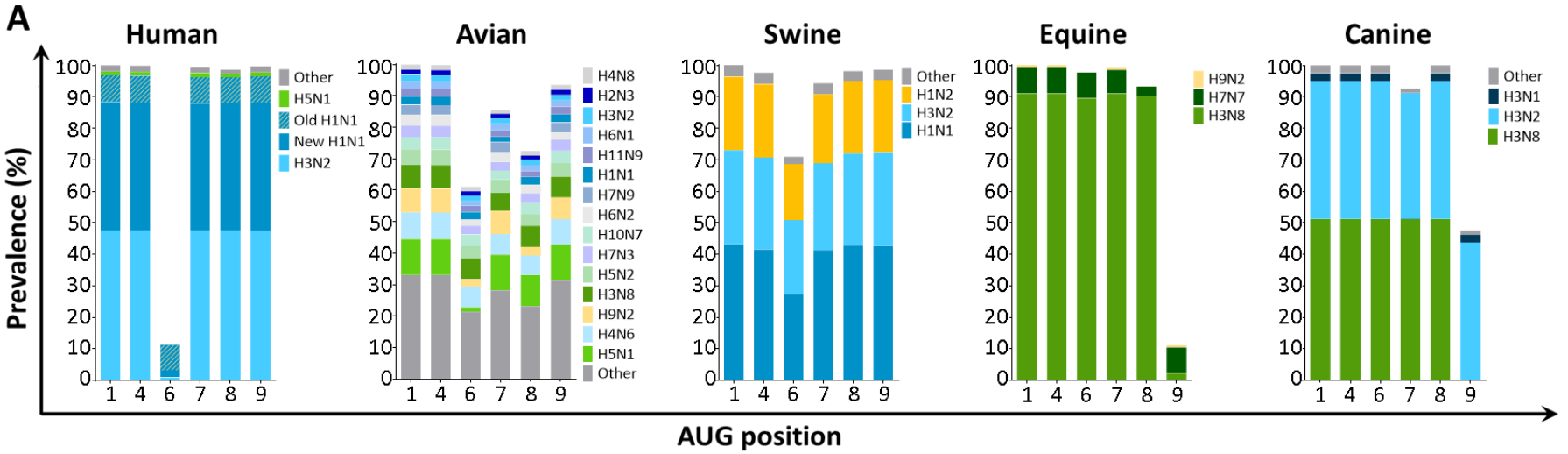

B

	AUG4				AUG6				AUG7				AUG8				AUG9			
	None	Weak	Medium	Strong	None	Weak	Medium	Strong	None	Weak	Medium	Strong	None	Weak	Medium	Strong	None	Weak	Medium	Strong
Human	17	-	1	14347	12610	0	0	1755	98	-	14266	1	194	-	14170	1	51	-	14313	1
Avian	38	-	-	13240	5167	-	5	8106	1911	-	11367	-	3652	1	9619	6	872	-	12404	2
Swine	86	-	-	3569	1062	-	8	2585	208	-	3447	-	68	-	3586	1	49	-	3606	-
Equine	-	-	-	134	3	-	-	131	-	-	134	-	3	-	131	-	126	-	8	-
Canine	-	-	-	80	6	-	-	74	-	-	80	-	1	-	79	-	42		38	-

Figure 6.10: Conservation of segment 2 AUG codons 4, 6, 7, 8 and 9 and their Kozak consensus sequence. All available PB1 nucleotide sequences were downloaded from NCBI. (A) Sequences were separated into hosts and subtypes and the presence of AUGs 4, 6, 7, 8 and 9 in individual sequences was calculated. (B) The strength of Kozak signalling around the indicated AUG codons in the dataset was categorised as strong (-3A/G and +4G), medium (-3A/G or +4G) or weak (neither -3A/G nor +4G). "None" refers to sequences where no AUG codon was found in the stated positions.

Table 6.2. Kozak context of AUG codons 5, 10 and 11. Observed neighbouring amino acids of AUG codons 5-M40 (A), 10-M92 (B) and 11-M111 and respective possible codons. Most prevalently observed amino acids are marked with an asterisk (*). Nucleotides responsible for the strength of the Kozak consensus (-3 and +4) (Kozak 1986) are highlighted in light blue. Adapted from Gog, *et al.*, 2007.

A

PB1 residue	39		40	41
Observed amino acids	Ala (A)	Thr (T)*	**Met (M)**	Asp (D)*
Potential codons	GCU GCC GCG GCA -3	ACU ACC ACA ACG -3	AUG	GAT GAC +4

B

PB1 residue	91		92	93	
Observed amino acids	Ala (A)*	Val (V)	**Met (M)**	Ala (A)*	Thr (T)
Potential codons	GCU GCC GCG GCA -3	GTT GTC GTA GTG -3	AUG	GCU GCC GCG GCA +4	ACU ACC ACA ACG +4

C

PB1 residue	110		111	112	
Observed amino acids	Ala (A)	Thr (T)*	**Met (M)**	Glu (E)*	Gly (G)
Potential codons	GCU GCC GCG GCA -3	ACU ACC ACA ACG -3	AUG	GAA GAG +4	GGT GGC GGA GGG +4

D41 is either coded by GAT or GAC, both resulting in a G in +4 and providing the strong Kozak consensus of AUG5. Parallel analysis performed for AUGs 10 and 11 revealed that AUG10 (M92) is neighboured by A91 or V91 (both giving a G in -3) and A93 (G in +4) or T93 (A in +4) (Table 6.2B). Despite not providing a strong Kozak context, T93 occurs in less than 1% of all the analysed sequences (Gog *et al.* 2007). Similar to AUG5, all the possible amino acids surrounding AUG11 (M111) always provide an A/G at -3 and G at +4 (Table 6.2C). Given the high amino acid conservation of PB1 (Gog *et al.* 2007) and the lack of diversity of the potential codons of the amino acids adjacent to M92 and M111, it is difficult to differentiate between PB1 protein conservation and PB1-N92/-111 expression conservation. This could though be tested my mutagenesis followed by RNA reconstitution assays and further explored by serial passage a ΔAUG10,11 attenuated virus in type I IFN/IRF3 knockout cells and compare their evolution/reversion.

To further test whether the findings obtained for PR8 suggesting an IRF3 antagonist are a generalised feature of IAV, 6 additional viruses were selected (but only 4 could be rescued) and ΔAUG10 and/or 11 mutant reverse genetics plasmids were constructed.

Swine87 and Cal04 viruses behaved similarly to PR8 where the deletion of AUG11 was shown to be more deleterious to virus replication and resulted in higher levels of IRF3 phosphorylation and increased IFN induction in human cells than AUG10. However, multicycle infections using H3N2 Udorn mutant viruses showed that the AUG10 was more important than AUG11, with replication defects seen only for the single mutant ΔAUG10 and the double mutant ΔAUG10,11 viruses. Udorn was

the only virus to which AUG10 seems to be more important. However, the phenotype of ΔAUG10 in the context of Udorn is not as severely attenuated as ΔAUG11 in PR8, Swine and/or Cal04. Differences between the importance of different AUG codons in different isolates can be due to:

- Differential expression of PB1-N92 and PB1-N111 in Udorn, in comparison to the other tested strains. Both GFP-tagged segment 2 constructs and infections with PR8 mutant viruses showed a stronger expression of –N111 in comparison to –N92. However, levels of expression of PB1-N92 and –N111 were not assessed from Udorn-infected cells nor Udorn segment 2-GFP plasmids. Speculating that if in Udorn expression of PB1-N92 is higher that –N111, it is reasonable to consider that its deletion would cause a more severe impact in virus replication, despite PR8 and Udorn PB1-N92 could potentially share the same function. However, given the conservation of the adjacent amino acids 91, 93, 110 and 112, as previously explained in this subchapter, the Kozak surroundings of AUG codons 10 and 11 are the same for all the tested viruses (Figure 6.11).
- Differential protein activity of PB1-N92 and PB1-N111 between Udorn and the other tested mammalian IAV strains. Comparative analysis between PB1 amino acid sequences from Udorn and the other viruses tested revealed minor differences. However, Udorn PB1 presents unique lysine residues in positions 121 and 393 whereas the other selected viruses have arginines (Figure 6.4). Given that the structures of the PB1-N92 and –N111 polypeptides have not been resolved, although both amino acids are positively charged, the loss of the

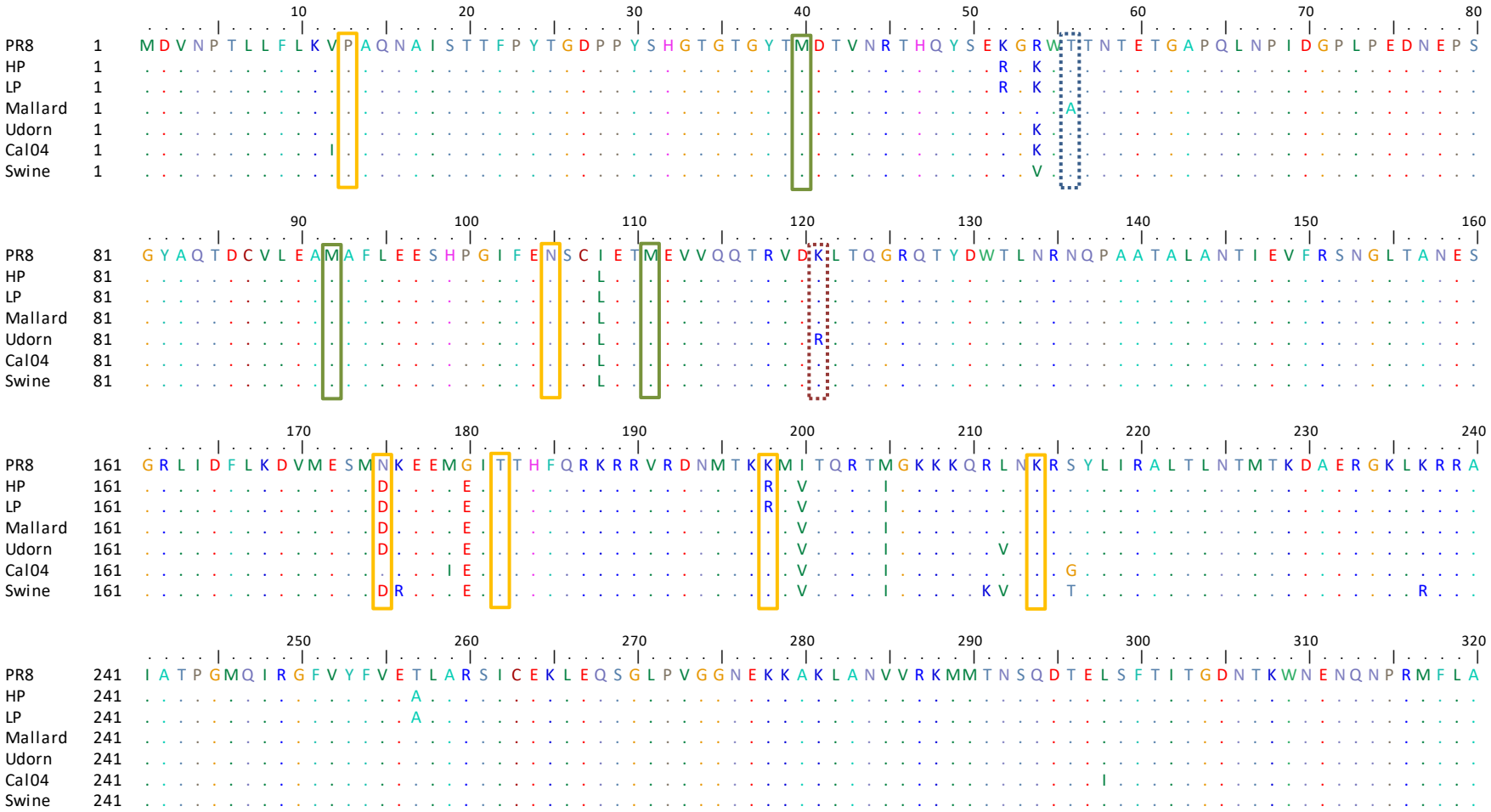
10 20 30 40 50 60 70 80
PR8 1 MDVNPTLLFLKVPAQNAISTTFPYTGDPPYSHGTGTGYTMDTVNRTHQYSEKGRWTTNTETGAPQLNPIDGPLPEDNEPS
HP 1 R K
LP 1 R K
Mallard 1 A
Udorn 1 K
Cal04 1 I K
Swine 1 V
90 100 110 120 130 140 150 160
PR8 81 GYAQTDCVLEAMAFLEESHPGIFENSCIETMEVVQQTRVDKLTQGRQTYDWTLNRNQPAATALANTIEVFRSNGLTANES
HP 81 L
LP 81 L
Mallard 81 L
Udorn 81 L R
Cal04 81 L
Swine 81 L
170 180 190 200 210 220 230 240
PR8 161 GRLIDFLKDVMESMNKEEMGITTHFQRKRRVRDNMTKKMITQRTMGKKKQRLNKRSYLIRALTLNTMTKDAERGKLKRRA
HP 161 D E R V I
LP 161 D E R V I
Mallard 161 D E V I
Udorn 161 D E V I V
Cal04 161 I E V I G
Swine 161 D R E V I K V T R
250 260 270 280 290 300 310 320
PR8 241 IATPGMQIRGFVYFVETLARSICEKLEQSGLPVGGNEKKAKLANVVRKMMTNSQDTELSFTITGDNTKWNENQNPRMFLA
HP 241 A
LP 241 A
Mallard 241
Udorn 241
Cal04 241 I
Swine 241

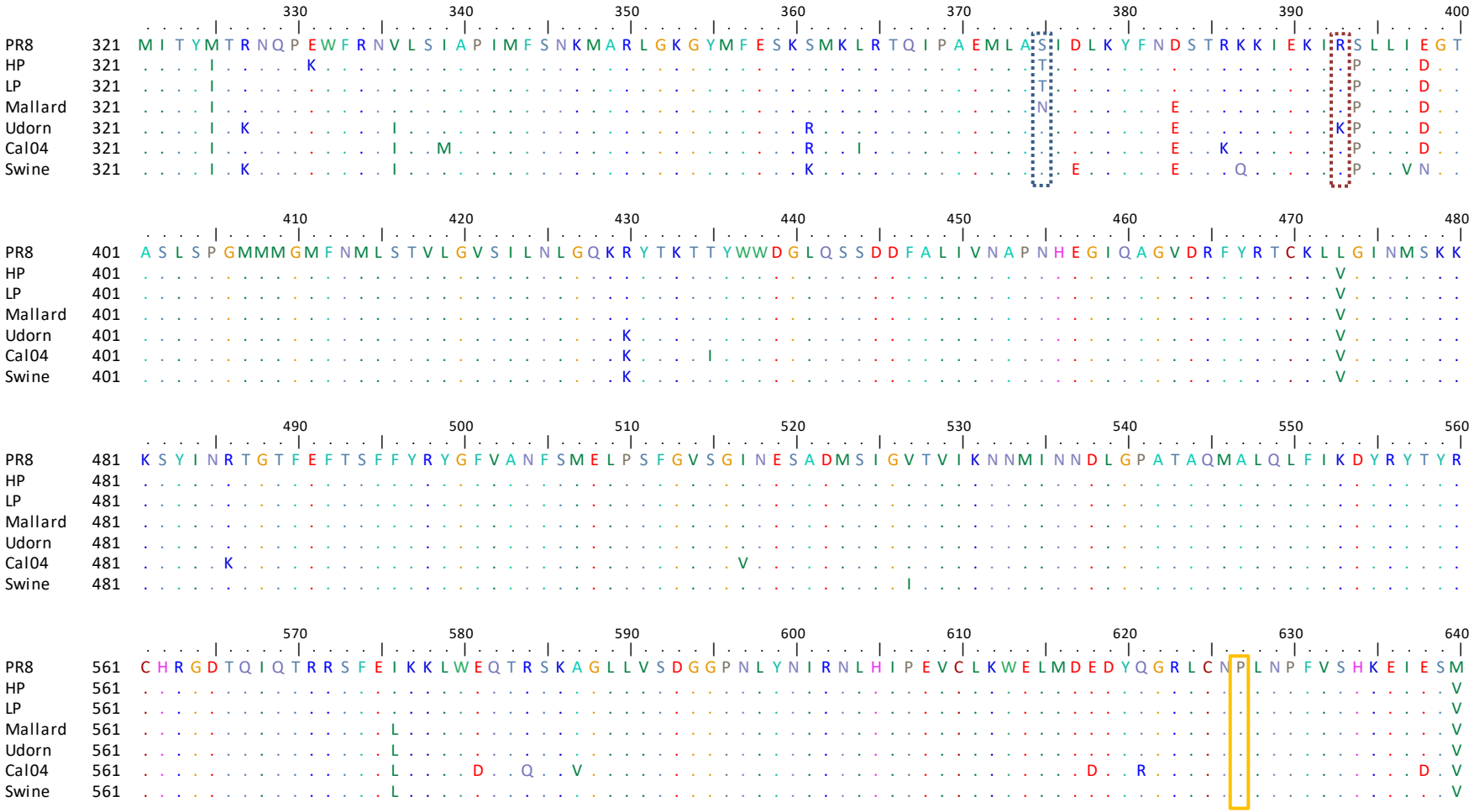
330 340 350 360 370 380 390 400
PR8 321 MITYMTRNQPEWFRNVLSIAPIMFSNKMARLGKGYMFESKSMKLRTQIPAEMLASIDLKYFNDSTRKKIEKIRSLLIEGT
HP 321 ....I....K.....T.....P...D..
LP 321 ....I.....T.....P...D..
Mallard 321 ....I.....N.....E.....P...D..
Udorn 321 ....I.K.....I.....R.....E.....KP...D..
Cal04 321 ....I.....I..M.....R..I.....E..K.....P...D..
Swine 321 ....I.K.....I.....K.....E.....E...Q.....P..VN..
410 420 430 440 450 460 470 480
PR8 401 ASLSPGMMMGMFNMLSTVLGVSILNLGQKRYTKTTYWWDGLQSSDDFALIVNAPNHEGIQAGVDRFYRTCKLLGINMSKK
HP 401 .....V.....
LP 401 .....V.....
Mallard 401 .....V.....
Udorn 401 .....K.....V.....
Cal04 401 .....K....I.....V.....
Swine 401 .....K.....V.....
490 500 510 520 530 540 550 560
PR8 481 KSYINRTGTFEFTSFFYRYGFVANFSMELPSFGVSGINESADMSIGVTVIKNNMINNDLGPATAQMALQLFIKDYRYTYR
HP 481 .....
LP 481 .....
Mallard 481 .....
Udorn 481 .....
Cal04 481 ....K.....V.....
Swine 481 .....I.....
570 580 590 600 610 620 630 640
PR8 561 CHRGDTQIQTRRSFEIKKLWEQTRSKAGLLVSDGGPNLYNIRNLHIPEVCLKWELMDEDYQGRLCNPLNPFVSHKEIESM
HP 561 V
LP 561 V
Mallard 561 .....L.....V
Udorn 561 .....L.....V
Cal04 561 .....L....D..Q..V.....D..R.....D.V
Swine 561 .....L.....V

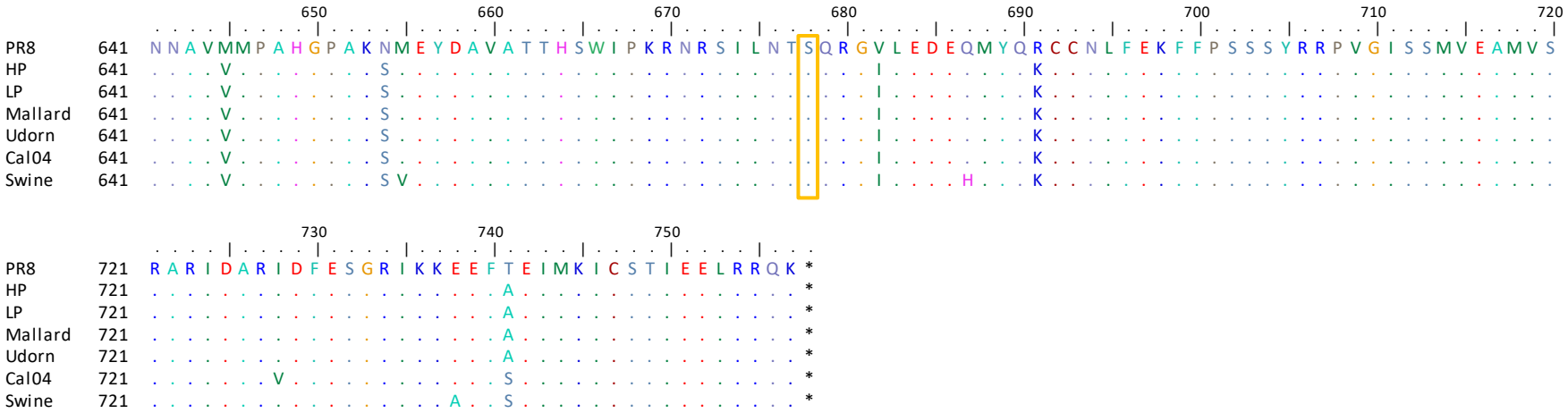

Figure 6.11: Sequence alignment of PB1 proteins of selected viruses. Nucleotide sequences of selected viruses were downloaded from NCBI. *In silico* translation and protein alignment was performed using the MEGA6 software. PR8 PB1 was used as reference sequence. Avian viruses are represented on the top, followed by two additional human strains and the swine strain. Conservation of M40, M92 and M111 is highlighted in green. Specific changes in Udorn are marked by dashed red boxes. Specific changes in Mallard are marked by dashed blue boxes. Avian-to-mammalian adaptation mutations found in the literature are marked by yellow boxes. Alignment was created and kindly provided by Dr Carina Conceição.

amino group in the lysine residues could lead to conformational and functional changes within the structure of both polypeptides and may explain the phenotypic differences between Udorn and the other tested mammalian viruses.

Assessment of the importance of AUG codons 10 and 11 in avian IAVs was only performed using the Mallard H1N1 duck isolate. In contrast to the mammalian mutants, mutations introduced in either AUG 10 or 11 did not result in attenuation of virus fitness in either of the two mammalian cell types tested; MDCK or A549 cells. Moreover, IFN induction and IRF3 phosphorylation levels were also unchanged following infection by the AUG mutant viruses in comparison to WT Mallard. Comparison of Mallard PB1 amino acid sequence to the other mammalian viruses revealed two Mallard specific residues: an alanine in position 56 and an asparagine in position 375 (Figure 6.10). Of these two, only amino acid 375 is shared by PB1-N92 and –N111, given that position 52 is upstream of their starting codons. Amino acid 375 has been shown to be a host-range signature amino acid (Kawaoka *et al.* 1989; Cauldwell *et al.* 2014). Most avian strains have an asparagine or threonine at this position, whereas the majority of human isolates have a serine. Moreover, all PB1 sequences from the 1918, 1957 and 1968 human pandemics viruses strictly possess a serine at position 375 (Naffakh *et al.* 2008; Kawaoka *et al.* 1989; Taubenberger *et al.* 2005). However, given that Mallard still harbours an avian-like 375 residue and segment 2 AUG mutants are still able to establish a successful infection in mammalian cells, the host restriction related to the residue 375 may not be related to PB1–N92 or –N111 function.

Additional PB1 residues have also been associated with avian to mammalian adaptations (Gabriel *et al.* 2007). An avian H7N7 strain showed a leucine and a serine

at positions 13 and 678 while its mouse-adapted variant showed serine and asparagine at the same residues. An independent study also identified the avian-to-mammalian N105S mutation in H5N1 *in vitro* adaptation (Taft *et al.* 2015). Moreover, additional PB1 mutations D175N, T182L, K198R, K214R, P627L have also been identified in infected patients with an H5N1 duck virus (Arai *et al.* 2016). Nevertheless, the majority of these amino acids did not differ in the selected viruses, without a specific incidence of either avian- or mammalian-associated polymorphisms. For example, all the selected isolates share P13 (mammalian), N105 (avian) and S678 (avian), and the avian-like R198 was only present in two of the three avian selected isolates (Penns HP and LP). Nevertheless, in order to possibly assess the importance of these residues, site-directed mutagenesis can be performed followed by the generation of mutant viruses and assessment of viral propagation in mammalian and avian cell lines.

As previously mentioned, despite not showing attenuation in mammalian cells, when grown in avian cells (chicken and quail fibroblasts), the Mallard AUG mutant viruses showed reduced virus fitness. Avian and mammalian type I IFN systems present several divergences (Santhakumar *et al.* 2017). Therefore, the simplest hypothesis would predict that Mallard would strongly induce IRF3 phosphorylation and present reduced growth kinetics. However, that was not the case and led the hypothesis that, perhaps the difference lays within the differences of the mechanisms which induce IRF3 phosphorylation within the mammalian and avian IFN systems. Despite the differences between these two pathways some of their constituents, such as TBK1, have been shown to be present in both pathways and is considered to be evolutionarily conserved (Wang *et al.* 2017). Therefore, even considering the high prevalence of PB1, it can be hypothesised that avian IAVs have evolved to counteract

avian IFN systems and mammalian viruses have developed to better inhibit the mammalian IFN pathway.

As introduced in chapter 1, viral-encoded mechanisms to counteract an IFN response can either be directly acting on the IFN-induction pathway or be more broad spectrum, by induction of host protein shutdown and are shared between several viral proteins, such as PB1-F2, PA-X and NS1. Studies on the NS1 CPSF30 binding have suggested that NS1 proteins encoded by H3N2 (such as Udorn), H2N2 and seasonal H1N1 viruses strongly bind to CPSF30, thereby inhibiting the 3' end processing of host pre-mRNAs and the production of mature mRNA, among which IFN-β (Nemeroff *et al.* 1998; Noah *et al.* 2003). However, NS1 proteins from PR8 and 2009 pandemic H1N1 viruses (such as Cal04) present inefficient binding to CPSF30 (Twu *et al.* 2007; Hale *et al.* 2010; Steidle *et al.* 2010). Therefore, these viruses depend on other counteractive measurements, such as the inhibition of IRF3 phosphorylation to restrain IFN induction/expression. Moreover, studies on IRF3 phosphorylation in different IAV strains have suggested a correlation between the levels of phosphorylated IRF3 and the ability of these viruses to control host proteins synthesis, therefore being able to block the consequences of IRF3 phosphorylation (Kuo *et al.* 2010).

The effects of the deletion of AUG codons as well as the predicted shut-off activity by NS1 and PA-X as well as MAVS-driven IFN counteraction by NS1 and PB1-F2 are summarised in table 6.3. Whilst PR8 NS1 exhibits weak CPSF30-binding activity, harbouring amino acids 103S and 106I, Udorn possessed a phenylalanine and a methionine in the respective positions, which are associated with a strong CPSF30-binding (Rodriguez *et al.* 2018; Das *et al.* 2008). Therefore, the counteraction of IRF3 phosphorylation is essential in PR8, but obsolete in Udorn and the deletion of an IRF3

Table 6.3. Summary of phenotypes of all tested IAV strains and respective predicted host protein shut-off activity and IFN counteraction. Observed viral fitness defects, type-I IFN induction, and IRF3 phosphorylation for all the tested viruses are resumed. The symbols "+++", "++", "+" and "-" represent the degree of the defect by the deletion of a given AUG in the measured criteria. Light grey squares represent non-performed experiments. Bold amino acid mutations represent differences between the specific virus and PR8.

Virus	Fitness defects			IFN induction			Increased IRF3 phosphorylation			Predicted host cell protein shut-off				Predicted IFN counteraction							
	Δ10	Δ11	Δ10,11	Δ10	Δ11	Δ10,11	Δ10	Δ11	Δ10,11	CPSF30 binding		mRNA nuclease activity		TRIM25 binding		dsRNA binding		MAVS inhibition	
										NS1		PA-X		NS1		NS1		PB1-F2	
PR8	+	+	+++	+	++	++	-	++		103S, 106I	-	197E, 246C	-	Y89, L95, E96, E97, S99	+	R38A, K41A	+	66N	+
Udorn	+	-	+	++	-	++	-	-	-	103**F**, 106**M**	+	197**A**, 246**F**	+	Y89, **I**95, E96, E97, S99	+	R38A, K41A	+	66N	+
Swine87	-	++	++	+	++		+	+		103**F**, 106**M**	+	197**A**, 246**F**	+	Y89, **T**95, E96, E97, S99	+	R38A, K41A	+	66N	+
Cal04	+	++	+++	+	++		+	+++		103**F**, 106**M**	+	197**A**, **Δ232**	+ / -	Y89, L95, E96, E97, S99	+	R38A, K41A	+	**Δ11**	-
Mallard	-	-	-	-	-	-	-	-	-	103**F**, 106**M**	+	197**A**, 246**F**	+	Y89, L95, E96, E97, S99	+	R38A, K41A	+	66N	+


A
PR8 NS1
Udorn NS1
Swine87 NS1
Cal04 NS1
Mallard NS1
B
PR8 PB1-F2
Udorn PB1-F2
Swine87 PB1-F2
Cal04 PB1-F2
Mallard PB1-F2

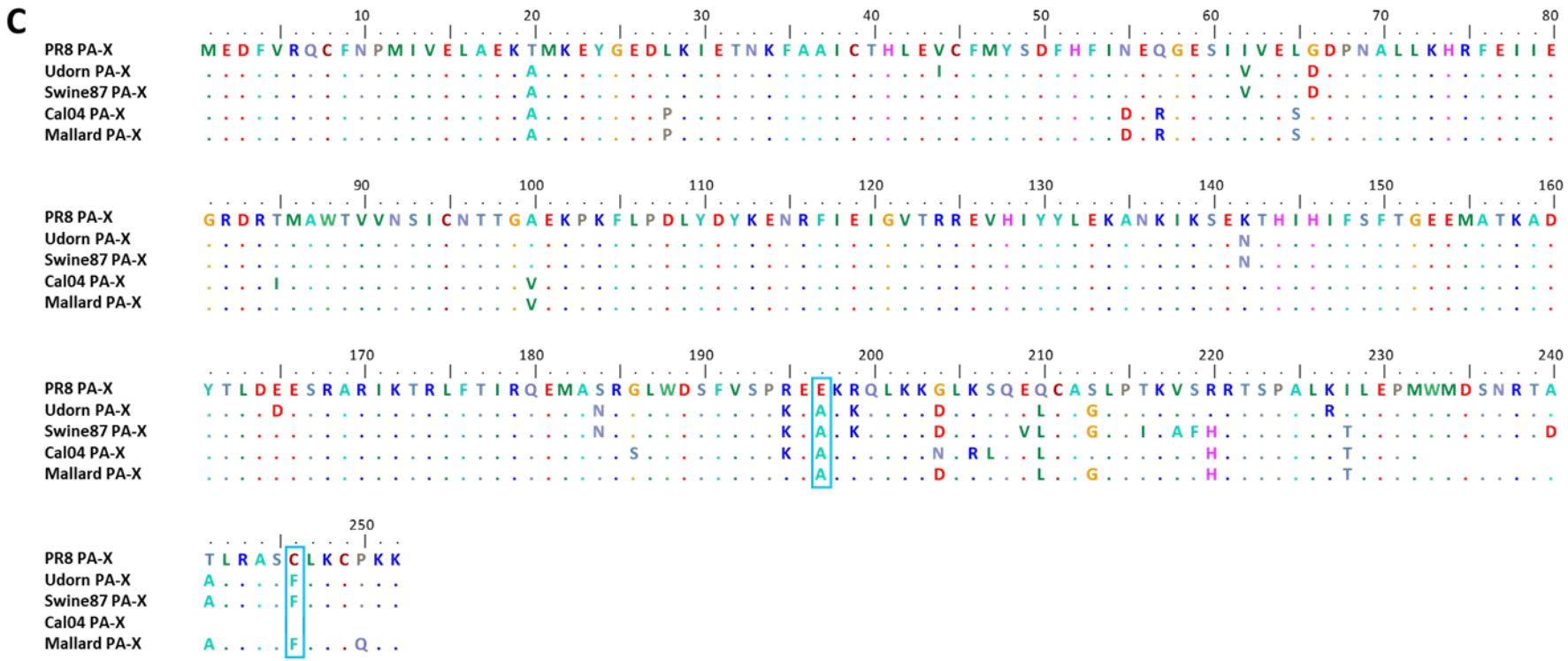

Figure 6.12: Sequence alignment of NS1, PB1-F2 and PA-X proteins of selected viruses. CDSs of NS1 (A), PB1-F2 (B) and PA-X (C) polypeptides of selected viruses were downloaded from NCBI using the accession numbers in table 8.3. *In silico* translation and protein alignment was performed using the MEGA6 software. PR8 proteins were used as reference sequence. Conservation of NS1 dsRNA binding domain key residues is highlighted in amber. NS1 CPSF30 binding domains are marked in red. The PB1-F2 determinant of virulence N66S single nucleotide polymorphism (Conenello *et al.* 2011; Conenello *et al.* 2007) is highlighted in green. Key residues in PA-X which determine shutoff activity are highlighted in blue (Chung, *et al.*, unpublished). Alignment was created and kindly provided by Dr Carina Conceição.

phosphorylation inhibitor such as PB1-N111 would not affect viral fitness (as observed throughout this chapter).

Despite presenting a predicted Udorn-like CPSF30-binding by its NS1, Cal04 was one of the viruses which was shown very sensitive to the deletion of AUG codons 10 and/or 11. However, this sensitivity can be explained by a truncated PA-X which was previously shown to impair shut-off activity in H1N1 2009 pandemic strains (Gao *et al.* 2015a; Lee *et al.* 2017). The impairment of the shut-off activity due to the truncated PA-X can justify the need to express an IRF3 inhibitor. Moreover, Cal04 also possesses a truncated PB1-F2. However, despite the expression of a short 11-amino acid PB1-F2, studies when PB1-F2 ORF was restored to its full length have shown minimal differences when compared to the original truncated version (Pena *et al.* 2012; Hai *et al.* 2010).

Although not to the same extent as Cal04, Swine87 was also shown to be sensitive to the deletion of AUG codons 10, but mainly 11. However, predicted NS1 CPSF30-binding, PA-X activity as well as PB1-F2 IFN counteraction seem to be Udorn-like. Nevertheless, levels of protein expression of NS1 and/or PA-X and/or PB1-F2 and/or PB1-N111 can perhaps be different than in Udorn and the balance between these four polypeptides may be required to ensure full IFN-counteraction and subsequent viral propagation of Swine 87.

Overall, this chapter showed that AUG codons 10 and 11 are highly conserved among IAV sequences and that PB1-N92 and -N111 potentially encoded by them could play important roles in the virus life cycle for more than one virus, thus not being an artefact of the PR8 strain.

Chapter 7

Concluding remarks

7.1. General conclusion

This project aimed to investigate initiation of translation from segment 2 AUG codons in order to identify and characterise suspected novel accessory proteins in IAV. The data presented describe the expression of two additional accessory polypeptides from AUG codons 10 and 11. The proteins, named PB1-N92 and PB1-N111, are both detected from transfected GFP-fusion plasmids and PB1-N111 was also detected in the context of virus infection. The mutation of AUGs 10 and 11 abrogated the expression of the two peptides and led to an attenuated replication phenotype in the lab adapted IAV strain PR8. However, despite the alterations of PB1 ORF (M92V and M111V), polymerase transcription and replication activity were seemingly kept unchanged in comparison to the original WT enzyme.

Infection of human cells with ΔAUG10/11 mutant viruses resulted in increased secretion of type I IFNs, while replication of the attenuated mutant viruses recovered

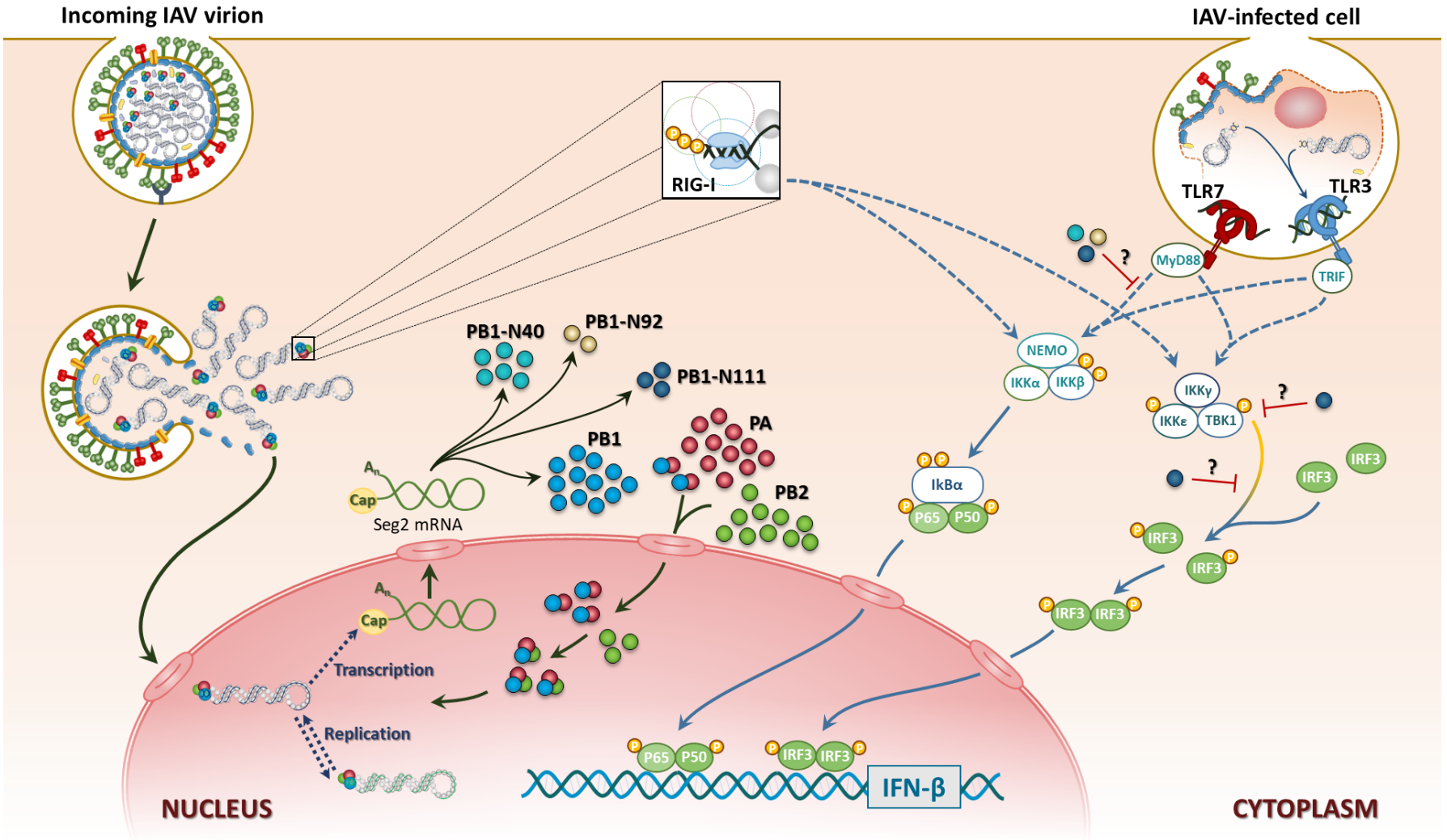
Incoming IAV virion
IAV-infected cell
RIG-I
TLR7
TLR3
MyD88
TRIF
?
NEMO
IKKα
IKKβ
IKKγ
IKKε
TBK1
IkBα
P65
P50
IRF3
PB1-N40
PB1-N92
PB1-N111
PB1
PA
PB2
Cap
Seg2 mRNA
Transcription
Replication
IFN-β
NUCLEUS
CYTOPLASM

Figure 7.1: Proposed model of expression and function of PB1-N92 and PB1-N111. Alongside PB1 and PB1-N40, PB1-N92 and PB1-N111 are expressed from segment 2 mRNA. PB1 complexes with PA which are further imported to the nucleus and interact with PB2 to support viral transcription and replication. PB1-N92 and PB1-N111 are not as strongly expressed as the main product PB1, or PB1-N40, but PB1-N111 may accumulate to higher levels than PB1-N92. Once expressed, PB1-N111 is believed to prevent the phosphorylation of IRF3, while the inhibition of the MyD88-driven NF-κB pathway is potentially carried out by all PB1-N40, PB1-N92 and N111. Nevertheless, the stages and the mechanisms by which this happens are still not fully understood.

in *in vitro*, *in ovo* and *in vivo* IFN-defective systems. Expression of the newly identified viral polypeptides from transfected plasmids made it possible to determine their ability to inhibit the induction of IFN-β at the MyD88 and TBK1 pathway stages and to prevent the phosphorylation of NF-κB subunit P65 and IRF3. However, the exact stage(s) at which this inhibition took place were not fully clarified (Figure 7.1).

An overview of the expression and potential mechanisms of action of PB1-N92 and PB1-N111 can be seen in Figure 7.1. In addition to PB1 which dimerises with PA and undergoes nuclear import to fulfil its main function of transcription and replication of the virus genome, the PB1 shorter polypeptides remain in the cytoplasm where they act to prevent induction of IFN-β.

Bioinformatic analysis showed the high conservation of AUG codons 10 and 11 in field isolates as well as a sequence context conducive to translation initiation of these codons. Therefore, in addition to the firstly tested lab adapted strain PR8, the introduction of ΔAUG10 and/or 11 mutations was carried out for further human, swine and avian viruses. Similar to PR8, minigenome reporter assays revealed a WT-like polymerase transcription and replication activity. However, the deletion of AUGs 10 and 11 did not result in the same phenotype in all the viruses. While, like PR8, Swine87 and Cal04 presented a more attenuated phenotype with the deletion of AUG11, Udorn was more affected with the deletion of AUG10 and growth of Mallard in mammalian cells was not affected by the deletion of either codon. However, these mutations conferred an attenuated phenotype in Mallard propagation in avian cells. Moreover, the importance of AUG codon 11 was associated with a lack of host shut-off activity and IFN counteraction by NS1, PA-X and PB1-F2, respectively.

7.2. Future work and directions

7.2.1. Identification of the potential function of AUG 10 and 11 in virus packaging

Work presented in chapter 2 showed that the simultaneous mutation of AUG codons 10 and 11 resulted in a worse genome copy to infectious particle ratio, which could suggest a packaging defect. Virus purification of the mutant PR8 viruses was performed aiming to determine if PB1-N92 and/or -N111 are present in virions, but only full-length PB1 was detected (data not shown). However, it is not clear whether a) these AUG codons (CAU residues in the vRNA sequence) are involved in RNA/RNA interactions between vRNP molecules at the budding site, b) PB1-N92 and -N111 are involved in trafficking of RNPs or responsible for packaging, c) the induction of type I IFN, which results in the upregulation of ISGs (e.g. BST2/tetherin) which have been shown to have an effect on budding of H1N1 influenza viruses (Gnirss *et al.* 2015), can contribute to the observed genome:PFU increased ratio.

7.2.2. Identification of binding partners of PB1-N92 and -N111

Data presented in chapter 4 went some way to identifying the stage(s) in the interferon pathway at which PB1-N92 and -N111 interfere. However, despite the low levels of TBK1- and MyD88-driven IFN-β induction in the presence of PB1-N92 and PB1-N111, the data are insufficient to conclude that there is a direct interaction between the PB1-related polypeptides and any component of the IFN induction pathway. For instance, the increased levels of phosphorylated IRF3 and, to a lesser

extent, P65 could also be due to an interaction of PB1-N92 and –N111 with phosphatases responsible for reversing activation of the transcription factors. Therefore, to fully understand the mechanisms behind the perceived inhibition of IFN-β synthesis by the truncated PB1 products, plasmids expressing the FLAG-tagged versions of PB1-N92 and –N111 could be transfected in cells and FLAG pull-down immunoprecipitations then performed followed by mass-spectrometry analysis to identify interaction partners. Moreover, given the tagged nature of some of the IFN induction plasmids (with GST or GFP, described in chapter 5 and 8), immunoprecipitations could also be performed using those tags.

7.2.3. Elucidation of the mechanism of expression of PB1-N92 and -N111

Expression of PB1-N92 and –N111 from AUG codons 10 and 11 was shown in chapter 2. However, the mechanism by which this translation initiation occurs was not fully elucidated. Previous studies on translation regulation of segment 2 coding polypeptides suggested that the expression of PB1-F2 and PB1-N40 from AUG codons 4 and 5 occurs through ribosomal leaky scanning and termination reinitiation, respectively (Wise *et al.* 2011). Nevertheless, it is still not clear how the ribosome reaches even further ahead in the mRNA to initiate protein expression from AUG codons 10 and 11. Additional data not shown in this dissertation showed the expression of individual polypeptides from segment 2 AUG codons 7, 8 and 9. However, the deletion of these AUG codons did not alter the expression of PB1-N92 and –N111 (data not shown), potentially discarding leaky scanning as the main translation control

mechanism of AUGs 10 and 11. As has been demonstrated for the expression of the IAV proteins NS2/NEP and M2, we also considered that alternative splicing might account for expression of PB1-N92 and -N111. However, the expression of PB1-related polypeptides was not decreased in the presence of splicing inhibitors (data not shown). Although never described for IAV, internal ribosomal entry sites (IRES) and ribosome shunts have been shown to be used by several RNA viruses as a mechanism to control translation initiation (reviewed in Firth and Brierley 2012). Moreover, when the same RNA region that was introduced into the eGFP-N1 plasmid (segment 2 nucleotides 1-380) was submitted into IRES prediction website (IRESPred; Kolekar *et al.* 2016), this resulted in a prediction of a "potential IRES" (data not shown). In addition to explaining the expression of AUG codons 10 and 11, the existence of an IRES/RNA loop could explain the apparently stronger expression of AUG11 in comparison to AUG10.

Overall, the work in this thesis has defined at least one further IAV gene product - PB1-N111 - and suggested a role for it in the virus life cycle as an antagonist of IRF3 activation. Future work will hopefully confirm and extend this hypothesis.

Chapter 8

Materials and Methods

8.1. Materials

8.1.1. General reagents

General purpose reagents were supplied by Sigma-Aldrich, Scientific Laboratory Supplies and Fisher Scientific. The Roslin Institute Central Services Unit (CSU) prepared and provided sterile water and phosphate-buffered saline (PBS). Additional specific reagents and kits and their respective suppliers are listed below.

- 30% acrylamide:bisacrylamide (37.5:1) — BioRad
- Agarose (UltraPure™) — Invitrogen
- Avicel — FMC Biopolymer
- BCA Protein Assay Kit — ThermoFisher Scientific
- Beetle Luciferin — Promega
- Beta-Galactosidase Enzyme Assay System — Promega
- Cell-Titre Glo — Promega
- Dimethyl sulphoxide (DMSO) — ThermoFisher Scientific
- DNA molecular weight markers — Promega
- dNTPs — Invitrogen™

• Isofluorane	Merial Animal Health
• Lipofectamine 2000	ThermoFisher Scientific
• Neutral Buffered Formalin (NBF)	Leica
• Odyssey® TBST Blocking Buffer	LI-COR
• Nitrocellulose membrane (0.2 and 0.45µm)	BioRad
• NP-40 (10%)	VWR International Ltd
• Precision plus dual colour molecular weight marker	BioRad
• Polyinosinic:polycytidylic acid (poly I:C)	InvivoGen
• Protein A-Sepharose Beads	Roche
• QIAamp Viral RNA Kit	Qiagen
• QIAGEN Plasmid Midi Kit	Qiagen
• QIAprep Spin Miniprep Kit	Qiagen
• QIAquick Gel Extraction Kit	Qiagen
• QIAquick PCR Purification kit	Qiagen
• QUANTI Blue reagent	InvivoGen
• QuikChange Lightning site-directed mutagenesis kit	Agilent Technologies
• Renilla Luciferase Assay kit	Promega
• Resolving buffer for acrylamide gels	Protogel
• RIPA lysis buffer	Source BioScience
• SensiFAST SYBR Lo-ROX One-Step Kit	Bioline
• Stacking buffer for acrylamide gels	Protogel
• Stainless Steel Beads (5 mm)	Qiagen
• SYBR DNA gel stain	Invitrogen
• Tetramethylethylenediamine (TEMED)	Protogel
• Tris-Buffered Saline with 1% Tween20 (TBST)	Santa Cruz
• Trizol reagent	Invitrogen
• TrueBlue Peroxidase Substrate	Kirkegaard & Perry Labs
• Tween20	Sigma-Aldrich
• X-ray films	ThermoFisher Scientific

8.1.2. Radiochemicals

- EasyTag™ Protein Labeling Mix (L-[^{35}S] Met and L-[^{35}S] Cys) Perkin Elmer

8.1.3. Enzymes

DNA restriction endonucleases and their respective reaction buffers were supplied by Promega and New England Biolabs and used according to manufacturer's instructions, unless otherwise stated. The following enzymes were acquired from the specified companies:

- Taq DNA polymerase Invitrogen
- (TPCK)-treated bovine pancreas trypsin Sigma-Aldrich
- T4 DNA ligase New England Biolabs

8.1.4. Bacterial cells

- XL10-Gold ultra-competent cells Agilent Technologies
- XL1-Blue competent cells Agilent Technologies

8.1.5. Eukaryotic cells

Table 8.1: Avian cell lines

Cell line	Source	Reference
Chicken Embryonic Fibroblasts (DF1)	Dr Lonneke Vervelde (The Roslin Institute, The University of Edinburgh, UK)	(Himly *et al.* 1998)
Japanese Quail Fibrosarcoma Cells (QT35)	Dr Laurence Tiley (The University of Cambridge, UK)	(Moscovici *et al.* 1977)

Table 8.2: Mammalian cell lines

Cell line	Source	Reference
HEK 293-Blue IFN-α/β Cells (HEK Blue)	InvivoGen	(Turnbull *et al.* 2016)
HEK 293 Naïve	Dr Gracjan Michlewski (The University of Edinburgh, UK)	-
HEK 293 TRIM25$^{-/-}$	Dr Gracjan Michlewski (The University of Edinburgh, UK)	-
Human Embryonic Kidney 293T Cells (293T)	American Type Culture Collection (ATCC)	(DuBridge *et al.* 1987)
Human Adenocarcinomic Alveolar Basal Epithelial Cells (A549)	ATCC	(Giard *et al.* 1973)
Madin-Darby Canine Kidney Cells (MDCK)	Prof Bernadette Dutia (The Roslin Institute, The University of Edinburgh, UK)	(Gaush *et al.* 1966)
MDCK-Sialyltransferase 1 Cells (MDCK-SIAT)	Prof John McCauley (The Francis Crick Institute, Mill Hill, UK)	(Matrosovich *et al.* 2003)

8.1.6. Solutions and media

8.1.6.1. Eukaryotic cell culture media and cell passage solutions

- 0.25% Trypsin-EDTA — Life Technologies
- Blasticidin — InvivoGen
- Bovine serum albumin (BSA) — Fisher Scientific
- Dialysed foetal bovine serum — Gibco
- Dulbecco's Modified Eagle Medium (D-MEM) — Sigma-Aldrich
- Foetal Bovine Serum (FBS) — Life Technologies
- Geneticin (G418) — Life Technologies
- L-Glutamine — Life Technologies
- Methionine- and Cysteine-free D-MEM — Gibco
- Opti-MEM — Life Technologies
- Penicillin/Streptomycin — Life Technologies
- Roswell Park Memorial Institute (RPMI) medium — Sigma-Aldrich
- Zeocin — InvivoGen

The previously listed supplies were used to prepare the following media:

- Complete medium: D-MEM or RPMI supplemented with 10% (v/v) FBS, 2mM glutamine, 100 U/ml penicillin, and 100µg/ml streptomycin.
- Serum free medium: Complete D-MEM or RPMI without FBS.
- Virus growth medium: D-MEM or RPMI supplemented with 2mM glutamine, 100 U/ml penicillin, 100µg/ml streptomycin, 0.14% (w/v) BSA, and 1µg/ml N-tosyl-L-phenylalanine chloromethyl ketone (TPCK)-treated trypsin.
- Transfection media: Complete D-MEM without penicillin and streptomycin.

8.1.6.2. Bacterial media

- Ampicillin sodium salt (used at 100µg/mL) Sigma-Aldrich
- Kanamycin sulphate salt (used at 50µg/mL) Gibco

Luria-Bertani (LB) broth and LB-agar were prepared and provided by the Roslin Institute CSU according to the following formulae:

- Luria-Bertani (LB) Broth: 10g/L tryptone, 5g/L yeast extract, 5g/L sodium chloride (pH 7.0).
- Super Optimal Broth (SOB): 20g/L tryptone, 5g/L yeast extract, 10mM NaCl, 2.5mM KCl, 10mM $MgCl_2$, and 10mM $MgSO_4$.
- LB agar 15g/L agar, 20g/L tryptone, 5g/L yeast extract, 10g/L sodium chloride (pH 7.0).

8.1.6.3. Competent bacteria preparation solutions

- CCMB buffer: 10mM potassium acetate, 10% (v/v) glycerol, 80mM $CaCl_2$, 20mM $MnCl_2$, 10mM $MgCl_2$, pH 6.4.

8.1.6.4. Nucleic acid gel electrophoresis buffers

TAE buffer was prepared and supplied by the Roslin Institute CSU according to the following formulae:

- TAE buffer: 40mM Tris, 20mM acetic acid, 1mM EDTA.
- 6x DNA loading buffer: 10mM Tris-HCl (pH 7.6) 0.15% (w/v) Orange G dye, 0.03% (w/v) xylene cyanol FF, 60% (v/v) glycerol, 60mM EDTA.

8.1.6.5. Protein buffers and solutions

8.1.6.5.1. Lysis Buffers

- Laemmli's sample buffer: 20% (v/v) glycerol, 2% (w/v) SDS, 100mM DTT, 24mM Tris, 0.016 % (v/v) bromophenol blue, 0.016% (v/v) xylene cyanol solution.

8.1.6.5.2. Acrylamide gel electrophoresis

- SDS-PAGE running buffer. 25mM Tris, 192 mM glycine, 0.1% (w/v) SDS.
- 4 x resolving buffer (Protogel) 1.5M Tris-HCl, 0.4% (w/v) SDS, pH 8.8.

- 4 x stacking buffer (Protogel) 0.5M Tris-HCl, 0.4% (w/v) SDS, pH 6.8.
- Resolving polyacrylamide gel: 7-15% acrylamide:bisacrylamide (37.5:1), 1× resolving buffer, 0.1% (w/v) APS, 0.1% (v/v) TEMED. This formula was adapted to make gels containing 7-15% polyacrylamide by altering the added amounts 30% acrylamide solution and water.
- Stacking polyacrylamide gel: 4% acrylamide:bisacrylamide (37.5:1), 1× stacking buffer, 0.5% (w/v) APS, 0.1% (v/v) TEMED.
- Polyacrylamide gel fix solution: 50% (v/v) methanol, 10% (v/v) acetic acid.

8.1.6.5.3. Western blotting

- Protein transfer buffer: 25mM Tris, 192mM glycine, 0.1% (w/v) SDS, 20% (v/v) methanol.
- Blocking solution: PBS/0.1% (v/v) Tween20, 5% (w/v) skimmed milk.
- Washing solution (PBST): PBS/0.1% (v/v) Tween20

8.1.6.5.4. Autoradiography

- Gel fixing solution: 50% methanol (v/v), 10% acetic acid (v/v)

8.1.6.6. Fluorescence-activated cell sorting buffers

- Intracellular (IC) Fixation Buffer eBioscience™

8.1.7. Drugs, inhibitors and compounds

- BX-795 (DMSO; used at 1, 2 and 5 µM) — Merck Chemicals
- IMD0325 (DMSO; used at 0.1µM) — Cayman Chemical company
- JHS-23 (DMSO; used at 1µM) — Calbiochem
- TNFα (H_2O, used at 500 ng/ml) — LifeTechnologies
- Universal type I interferon — PBL Assay Science
- Pepinh-TRIF (H_2O, used at 20µM) — InvivoGen

8.1.8. Viruses and reverse genetics systems

Table 8.3: Sequence accession numbers for the viral cDNA inserts in reverse genetics plasmids. Colour coding: Blue - segments cloned into pDUAL; Green - segments cloned into pHH21; Yellow - segments cloned into both pHH21 and pcDNA3.1.

Segment	PR8[a]	Udorn[b]	Swine87[c]	Cal04[d]	Mallard[e]	Penn83 LP[f]	Penn83 HP[g]
1	EF467818	M91712	CY116312	FJ966079	KC209512	CY015114	CY015080
2	EF467819	CY009642	CY116313	FJ966080	KC209513	GU052777	CY015079
3	EF467820	CY009641	CY116314	FJ966081	KC209514	GU052776	CY015078
4	EF467821	M54895	CY115996	FJ966082	KC209515	-	-
5	EF467822	D00051	CY115997	FJ966083	KC209516	CY015076	
6	EF467823	J02168	CY116317	FJ966084	KC209517	-	-
7	EF467824	J02167	CY116318	FJ966085	KC209518	-	-
8	EF467817	V01102	CY116000	FJ966086	KC209519	-	-

[a] A/Puerto Rico/8/34. Gift from Prof Ron Fouchier (Erasmus University Medical Center, Rotterdam, The Netherlands) (de Wit *et al.* 2004).
[b] A/Udorn/307/1972. Gift from Prof Robert Lamb (Department of Molecular Biosciences, Northwestern University, Illinois, USA) (Chen *et al.* 2007).
[c] A/swine/England/87842/1990. Cloned and kindly provided by Dr Russell Brown (Digard laboratory) (Brown 2016; Wibberley *et al.* 1988).
[d] A/California/04/2009. Gift from Dr Daniel Perez (Department of Populational Health, The University of Georgia, USA) (Ye *et al.* 2010).
[e] A/mallard/Netherlands/10-Cam/1999. Gift from Dr Laurence Tiley (The University of Cambridge) (Bourret *et al.* 2012).
[f] A/chicken/Pennsylvania/1370/1983. Cloned and kindly provided by Dr Lita Murphy (Digard laboratory) (Murphy et al, unpublished).
[g] A/chicken/Pennsylvania/1/1983. Cloned and kindly provided by Dr Lita Murphy (Digard laboratory) (Murphy et al, unpublished).

8.1.9. Plasmids

Table 8.4: Expression and reverse genetics plasmids

Name	Description	Selection	Source
pDUAL	Reverse genetics plasmid. Bidirectional pol I and pol II promoters either side of insert lead to mRNA and vRNA-like RNA synthesis. Used for PR8, Mallard, Cal 04, Penn83 LP and Penn83 HP.	Ampicillin	Gift from Prof Ron Fouchier (Erasmus University Medical Center, Rotterdam, The Netherlands
pHH21	Reverse genetics plasmid. Pol I promoter leads to vRNA-like RNA synthesis. Used to rescue Udorn.	Ampicillin	Gift from Prof Robert Lamb (Department of Molecular Biosciences, Northwestern University, Illinois, USA)
pcDNA3.1	CMV pol II promoter upstream of insert leads to constitutive high protein expression. Used for Udorn.	Ampicillin	

Table 8.5: Reporter plasmids

Name	Description	Selection	Source
pPol I vRNA FFLuc	Reporter for RNP reconstitution assays. Contains firefly luciferase reporter gene in the reverse (-) orientation, flanked by the UTRs of PR8 segment 8, under the control of a pol I promoter.	Ampicillin	Gift from Dr Laurence Tiley (The University of Cambridge, UK)
Avian pPol I vRNA FF Luc	Reporter for RNP reconstitution assays. Contains firefly luciferase reporter gene in the reverse (-) orientation, flanked by the UTRs of PR8 segment 8, under the control of an avian pol I promoter.	Ampicillin	
pPol I cRNA FF Luc	Reporter for RNP reconstitution assays. Contains firefly luciferase reporter gene in the (+) sense orientation, flanked by the UTRs of PR8 segment 8, under the control of a pol I promoter.	Ampicillin	This study
pRL	Constitutively expressed *Renilla* luciferase under the control of the SV40 promoter.	Ampicillin	Promega
pPolII β-gal	Constitutively expressed β-gal under control of CMV Immediate-Early (IE) promoter.	Ampicillin	Digard lab
pIFN-β::Luc	Firefly luciferase under control of human IFN-β promoter.	Ampicillin	Gift from Prof Rick Randall (The University of St Andrews, UK)
pISRE::Luc	Firefly luciferase under control of ISRE element.	Ampicillin	

Table 8.6: Other expression plasmids

Name	Description	Selection	Reference	Source
pEGFP-N1	Constitutively expresses eGFP under control of CMV IE promoter. Multiple cloning site upstream allows opportunity to clone C-terminally tagged proteins.	Kanamycin	-	Clontech
pGST-IRF7	SV40 pol II promoter upstream of insert leads to constitutive expression of IRF7 fused to GST.	Ampicillin	-	Kind gift from Dr Andrew MacDonald (The University of Leeds, UK)
pGST-TBK1	SV40 pol II promoter upstream of insert leads to constitutive expression of TBK1 fused to GST.	Ampicillin	(Mankouri *et al.* 2010)	
pGST-RIG-I	SV40 pol II promoter upstream of insert leads to constitutive expression of RIG-I fused to GST.	Ampicillin	-	
pGST-MAVS	SV40 pol II promoter upstream of insert leads to constitutive expression of MAVS fused to GST.	Ampicillin	-	
pGST-MyD88	SV40 pol II promoter upstream of insert leads to constitutive expression of MyD88 fused to GST.	Ampicillin	-	
pGST-TRIF	SV40 pol II promoter upstream of insert leads to constitutive expression of TRIF fused to GST.	Ampicillin	-	
pCMV-HA-IRF7	CMV IE pol II promoter upstream of insert leads to constitutive expression of HA-tagged IRF7.	Ampicillin	-	
pCMV-HA-IRF3	CMV IE pol II promoter upstream of insert leads to constitutive expression of HA-tagged IRF3.	Ampicillin	-	
pCMV-HA-IKKβ	CMV IE pol II promoter upstream of insert leads to constitutive expression of HA-tagged Ikkβ.	Ampicillin	(Richards *et al.* 2015)	
pIRF3 GFP	CMV IE pol II promoter upstream of insert leads to constitutive expression of GFP-tagged pIRF3.	Kanamycin	-	
pGFP-RelA	CMV IE pol II promoter upstream of insert leads to constitutive expression of GFP-tagged RelA.	Kanamycin	-	
pCFP-P50	CMV IE pol II promoter upstream of insert leads to constitutive expression of CFP-tagged P50	Kanamycin	-	

8.1.10. Oligonucleotides

8.1.10.1. Oligonucleotides used for sequencing of constructs and viruses

Table 8.7: Sequencing oligonucleotides

Primer name	Sequence (5'-3')	Description/Application
pDUAL Fw	ATGTCGTAACAACTCCGCCC	Forward primer to sequence the 3' end of vRNA of segments inserted in pDUAL plasmid
pDUAL Rv	TTTTTGGGGACAGGTGTCCG	Reverse primer to sequence the 5' end of vRNA of segments inserted in pDUAL plasmid
Uni 12	AGCAAAAGCAGG	Complementary to the 3' end of all IAV vRNA segments
eGFP-N1 Fw	GGCGGTAGGCGTGTA	To sequence peGFP-N1 inserts from the 5' end (closer to the MCS)
PR8 seg2 611-592 Rv	GTCATATTGTCTCTCACCCG	Reverse primer sequence for the 5' end of PR8 segment 2 cDNA
Udorn seg 2 611-592 Rv	ACCATTTTCTTGGTCATGTT	Reverse primer to sequence the 5' end of Udorn segment 2 cDNA
Cal04 seg 2 611-592 Rv	GTTCTTTGCGTGACCATCTT	Reverse primer to sequence the 5' end of Cal04 segment 2 cDNA
Swine87 seg 2 611-592 Rv	GTTCTTTGCGTGACCATTTT	Reverse primer to sequence the 5' end of Swine87 segment 2 cDNA
Mallard seg 2 611-592 Rv	GTCATGTTGTCCCTTACTCT	Reverse primer to sequence the 5' end of Mallard segment 2 cDNA

8.1.10.2. Oligonucleotides used to subclone viral sequences into the indicated vectors

Table 8.8: Cloning oligonucleotides

Name	Sequence (5'-3')	Description/Application	Enzyme
FLAG PB1 Fw	GCAAGCTTATGACTACAAGG ACGACGACGACAAGGTGGAT GTCAATCCGACCTTAC	Used to clone full length PB1 into pcDNA3.1 vector and add an N-terminal FLAG-tag	HindIII
FLAG PB1-N40 Fw	GCAAGCTTATGGACTACAAG GACGACGACGAcAAGTTGGA TACTGTCAACAGGACAC	Used to clone PB1-N40 into pcDNA3.1 vector and add n N-terminal FLAG-tag	HindIII
FLAG PB1-N92 Fw	GCAAGCTTATGGACTACAAG GACGACGACGAcAAGGTGGC TTTCCTTGAGGAATCCC	Used to clone PB1-N92 into pcDNA3.1 vector and add an N-terminal FLAG-tag	HindIII

Table 8.8: Cloning oligonucleotides (continuation)

Name	Sequence (5'-3')	Description/Application	Enzyme
FLAG PB1-N111 Fw	GCAAGCTTATGGACTACAAGGACGACGACGAcAAGGTGGAGGTTGTTCAGCAAACAC	Used to clone PB1-N111 into pcDNA3.1 vector and add a N-terminal FLAG-tag	HindIII
PB1 Fw	CCGCAAGCTTATGGATGTCAATCCGACCTTAC	Used to clone full length PB1 into pcDNA3.1 vector	HindIII
PB1-N40 Fw	CCGCAAGCTTATGGATACTGTCAACAGGACAC	Used to clone PB1-N40 into pcDNA3.1 vector	HindIII
PB1-N92 Fw	CCGCAAGCTTATGGCTTTCCTTGAGGAATCCC	Used to clone PB1-N92 into pcDNA3.1 vector	HindIII
PB1-N111 Fw	CCGCAAGCTTATGGAGGTTGTTCAGCAAACAC	Used to clone PB1-N111 into pcDNA3.1 vector	HindIII
PB1 2298-2280 Rv	GCGTCTAGACTATTTTTGCCGTCTGAGC	Used to clone tagged and untagged full-length PB1 and shorter products into pcDNA3.1 vector	XbaI

8.1.10.3. Oligonucleotides used for site-directed mutagenesis

Table 8.9: Oligonucleotides used to introduce mutations into PR8 segment 2

Primer name	Mutation	Sequence (5'-3')
PR8 ΔAUG10 Fw	A298G (M92V)	ATTGTGTATTGGAGGCGGTGGCTTTCCTTGAGGAA
PR8 ΔAUG10 Rv	A298G (M92V)	TAACACATAACCTCCGCCACCGAAAGGAACTCCTT
PR8 ΔAUG11 Fw	A355G (M111V)	AAACTCGTGTATTGAAACGGTGGAGGTTGTTCAGCAAAC
PR8 ΔAUG11 Rv	A355G (M111V)	TTTGAGCACATAACTTTGCCACCTCCAACAAGTCGTTTG

Table 8.10: Oligonucleotides used to introduce mutations into Cal04 segment 2

Primer name	Mutation	Sequence (5'-3')
Cal04 ΔAUG10 Fw	A298G (M92V)	AAACAGACTGTGTTCTAGAGGCTGTGGCTTTCCTTG
Cal04 ΔAUG10 Rv	A298G (M92V)	CAAGGAAAGCCACAGCCTCTAGAACACAGTCTGTTT
Cal04 ΔAUG11 Fw	A355G (M111V)	AGGAATATTTGAGAATTCATGCCTTGAAACAGTGGAAGTTGTTCAACA
Cal04 ΔAUG11 Rv	A355G (M111V)	TGTTGAACAACTTCCACTGTTTCAAGGCATGAATTCTCAAATATTCCT

Table 8.11: Oligonucleotides used to introduce mutations into Udorn segment 2

Primer name	Mutation	Sequence (5'-3')
Udorn ΔAUG10 Fw	A298G (M92V)	CAGACTGTGTCCTGGAAGCAGTGGCTTTCCTTGA
Udorn ΔAUG10 Rv	A298G (M92V)	TCAAGGAAAGCCACTGCTTCCAGGACACAGTCTG
Udorn ΔAUG11 Fw	A355G (M111V)	ACTCGTGCCTTGAAACGGTGGAAGTCGTTCAACAA
Udorn ΔAUG11 Rv	A355G (M111V)	TTGTTGAACGACTTCCACCGTTTCAAGGCACGAGT

Table 8.12: Oligonucleotides to introduce mutations into Swine87 segment 2

Primer name	Mutation	Sequence (5'-3')
Swine87 ΔAUG10 Fw	A298G (M92V)	AAACAGACTGCGTCTTGGAAGCAGTGGCTTTCCTTG
Swine87 ΔAUG10 Rv	A298G (M92V)	CAAGGAAAGCCACTGCTTCCAAGACGCAGTCTGTTT
Swine87 ΔAUG11 Fw	A355G (M111V)	CTCGTGCCTTGAAACGGTGGAAGTCGTTCAGCA
Swine87 ΔAUG11 Rv	A355G (M111V)	TGCTGAACGACTTCCACCGTTTCAAGGCACGAG

Table 8.13: Oligonucleotides to introduce mutations into Mallard segment 2

Primer name	Mutation	Sequence (5'-3')
Mallard ΔAUG10 Fw	A298G (M92V)	AAACAGATTGCGTGTTGGAAGCAGTGGCTTTCCTTG
Mallard ΔAUG10 Rv	A298G (M92V)	CAAGGAAAGCCACTGCTTCCAACACGCAATCTGTTT
Mallard ΔAUG11 Fw	A355G (M111V)	GGATCTTTGAAAACTCTTGTCTTGAAACAGTGGAAGTCGTTCAGC
Mallard ΔAUG11 Rv	A355G (M111V)	GCTGAACGACTTCCACTGTTTCAAGACAAGAGTTTTCAAAGATCC

Table 8.14: Oligonucleotides to introduce mutations into Penn HP/LP segment 2s

Primer name	Mutation	Sequence (5'-3')
Penns 83 ΔAUG10 Fw	A298G (M92V)	AAACAGACTGCGTTTTGGAAGCAGTGGCTTTCCTTG
Penns 83 ΔAUG10 Rv	A298G (M92V)	CAAGGAAAGCCACTGCTTCCAAAACGCAGTCTGTTT
Penns 83 ΔAUG11 Fw	A355G (M111V)	GAAAACTCGTGTCTTGAAACGGTGGAAGTTGTTCAACAAACAA
Penns 83 ΔAUG11 Rv	A355G (M111V)	TTGTTTGTTGAACAACTTCCACCGTTTCAAGACACGAGTTTTC

8.1.10.4. Oligonucleotides used for RT-qPCR

Table 8.15: Primers used for RT-qPCR analysis. Kindly designed and provided by Dr Elly Gaunt, Dr Matthew Turnbull and Dr Christine Tait-Burkark.

Primer name	Sequence (5'-3')
Segment 2 Fw	GGAACAGGATACACCATGGA
Segment 2 Rv	AGTGGYCCATCAATCGGGTT
Segment 5 Fw	ATCATGGCGTCTCAAGGCAC
Segment 5 Rv	CCGACGGATGCTCTGATTTC
Segment 7 Fw	TGCAGGGAAGAACACCGATC
Segment 7 Rv	GGGCATTTTGGACAAAGCGT
PRRSV-1 (LT3 ORF5) Fw	GGATACTATCACGGGCGGTA
PRRSV-1 (LT3 ORF5) Rv	GGCACGCCATACAATTCTTA

8.1.11. Immunological reagents and dyes

Table 8.16: Primary antibodies raised against IAV proteins

Antibody	Supplier/Reference	Applied dilution
Rabbit polyclonal anti-PA (V34/V35)	(Blok *et al.* 1996)	WB (1:500)
Rabbit polyclonal anti-PB1 (V19)	(Digard *et al.* 1989)	WB (1:500), IF (1:50)
Rabbit polyclonal anti-MBP-NP (2915)	(Digard *et al.* 1999)	WB (1:500)
Mouse monoclonal anti-PR8 NP (AA5H)	Abcam (abAA5H)	IF (1:1000)
Mouse monoclonal anti-M2	Abcam (ab5416)	WB (1:1000)
Rabbit polyclonal anti-PR8 NS1 (V29)	(Turnbull *et al.* 2016)-	WB (1:500)
Rabbit polyclonal anti-PR8 NEP (V13)	(Turnbull *et al.* 2016)	WB (1:500)

Table 8.17: Primary antibodies raised against cellular proteins

Antibody	Supplier	Applied dilution
Rat monoclonal anti-α-tubulin	BioRad	WB (1:1000)
Rabbit monoclonal anti-IRF3	Cell Signalling	WB (1:1000)
Rabbit monoclonal anti-phospho IFR3	Cell Signalling	WB (1:1000)
Rabbit monoclonal anti-P65 (NFκB)	Cell Signalling	WB (1:1000)
Rabbit monoclonal anti-phospho P65 (NFκB)	Cell Signalling	WB (1:1000)

Table 8.18: Primary antibodies raised against tags

Antibody	Supplier	Applied dilution
Rabbit monoclonal anti-DYKDDDDK Tag (D6W5B)	Cell Signalling	WB (1:1000)
Mouse monoclonal anti-DYKDDDDK Tag (9A3)	Cell Signalling	IF (1:750)
Mouse monoclonal anti-GFP	Clontech (JL8)	WB (1:5000)
Purified Rat Anti-Mouse CD16/CD32 (Mouse BD Fc Block™)	BD Bioscience	FACS (1:200)

Table 8.19: Secondary antibodies

Antibody	Supplier	Applied dilution
IRDye® 680LT Goat anti-Rat IgG (H + L)	LI-COR 926-68076	WB (1:10000)
IRDye® 800CW Donkey anti-Mouse IgG (H + L)	LI-COR 925-32212	WB (1:10000)
IRDye® 800CW Donkey anti-Rabbit IgG (H + L)	LI-COR 926-32213	WB (1:10000)
IRDye® 680LT Donkey anti-Mouse IgG (H + L)	LI-COR 925-68022	WB (1:10000)
IRDye® 680LT Donkey-anti-Rabbit IgG (H + L)	LI-COR 926-68023	WB (1:10000)
IRDye® 800CW Goat anti-Rat IgG (H + L)	LI-COR 926-32219	WB (1:10000)
IRDye® 800CW Streptavidin	LI-COR 925-32230	Cytokine array (1:2000)
Goat Anti-Rabbit IgG (H+L)-HRP Conjugate	Bio-Rad 1721019	Immunostaining (1:1000)
Donkey anti-Mouse IgG (H+L) Alexa Fluor® 488 conjugate	Thermo Fisher (A-21202)	IF (1:1000)
Donkey anti-Rabbit IgG (H+L) Alexa Fluor® 488 conjugate	Thermo Fisher (A-21206)	IF (1:1000)
Donkey anti-Rabbit IgG (H+L) Alexa Fluor® 594 conjugate	Thermo Fisher (R37119)	IF (1:1000)
Donkey anti-Mouse IgG (H+L) Alexa Fluor® 594 conjugate	Thermo Fisher (R37115)	IF (1:1000)

Table 8.20: Fluorescent dyes

Dye	Supplier	Applied dilution
ProLong Gold Antifade Mountant with 4',6-Diamidino-2-phenylindole (DAPI)	Invitrogen	IF (neat)
Hoechst 33342	Thermo Fisher	IF (1:2000)
eBioscience™ Fixable Viability Dye eFluor™ 780	Thermo Fisher	FACS (1:1000)

8.2. Molecular techniques and nucleic acid handling

8.2.1. Polymerase chain reaction (PCR)

PCR was used for cloning applications. Different size fragments were amplified using forward and reverse primers from section 8.1.10.2 (Oligonucleotides used to subclone viral sequences into indicated vectors). Each PCR mix contained

200nM of each primer, 400µM of each dNTP, 30nM of $MgCl_2$ and 2.5 units of Taq DNA polymerase. The PCR was carried out in a Veriti 96 well ThermalCycler (Applied Biosystems). PCR conditions included a denaturation step performed at 94ºC for 2 minutes, followed by 30 cycles of 30 seconds at 94°C, 30 seconds at 55-60°C and 1-6 minutes at 72°C (1 minute per 1Kb), finishing with 10 minute incubation at 72°C. Annealing temperature and extension time varied depending on melting temperature of primers and amplicon length, respectively. PCR product length was confirmed by 1% (w/v) agarose gel electrophoresis.

8.2.2. DNA gel electrophoresis

DNA electrophoresis was performed in agarose gels. 0.8-2 % agarose gels were prepared by dissolving agarose in a microwave oven in TAE buffer containing 1× SYBR DNA gel stain. Melted agarose was poured into a gel tray with a comb containing the desired number of wells. Once set, the gel was immersed in 1× TAE buffer. 8µL of 1kb DNA ladder was loaded alongside the samples containing 1× DNA loading buffer. Gels were electrophoresed at 80V for approximately 1 hour and imaged using an Ultraviolet transilluminator (FluorChem® HD2, Alpha Innotech).

8.2.3. Purification of DNA fragments

PCR amplified or restriction digested fragments were purified using the QIAquick PCR purification kit (Qiagen) according to manufacturer's instructions. Briefly, a DNA-containing sample was diluted in binding buffer which allows binding

to a silica-gel membrane. Throughout a series of centrifugation steps, contaminants were removed by an ethanol-based buffer wash and silica matrix-retained DNA was eluted with nuclease free water. Purified DNA was analysed by spectrophotometry and electrophoresis.

8.2.4. Restriction enzyme digestion

PCR product or 1µg of plasmid DNA was digested using 1-5 units of enzyme. Enzymatic reaction mixes were prepared using the manufacturer's recommended buffer and temperature and digested for at least 3 hours. When digesting with multiple enzymes with a compatible reaction buffer, enzymes were combined. Otherwise, sequential digestions were performed with an intermediate PCR purification step.

8.2.5. Extraction of DNA fragments from agarose gels

When subcloning, restriction digested vector DNA fragments were separated by electrophoresis, visualised in a UV transilluminator and excised with a scalpel. The agarose slice was extracted using the QIAquick Gel Extraction Kit in a bind-wash-elute procedure. Concisely, gel slices were dissolved at 50°C in a high salt, neutral pH buffer and the nucleic acid-containing mixture was applied to a silica membrane. Impurities were sequentially washed away using an ethanol-based solution and pure DNA was eluted in 30µL of water. DNA was assessed by spectrophotometry for its content and purity and further used in subsequent applications such as restriction digestions or ligations.

8.2.6. Ligation of DNA fragments

DNA fragments were ligated using T4 DNA ligase according to manufacturer's recommendations. A typical ligation reaction included 100ng of linearised vector DNA, insert DNA fragment at a molecular ratio of 5:1 (insert:vector), 1x reaction buffer and 2 units of T4 DNA ligase in a total volume of 20µL. The reaction was place on ice and left overnight, during which it warmed up to room temperature. Five µL aliquots of the ligation reactions were transformed into home-made competent *E. coli* according to section 8.2.8, or commercially sourced - XL10-Gold ultra-competent or XL1-Blue competent - bacterial cells according to manufacturer's instructions.

8.2.7. Preparation of antibiotic-selection agar plates

Previously prepared LB agar was microwave-heated until liquefied. After cooling, the appropriate selection antibiotic was added and mixed. Molten LB agar was poured into sterile 10cm dishes, allowed to set at room temperature and stored at 4°C until further use.

8.2.8. Preparation of competent bacterial cells

Each new batch of competent bacterial cells was prepared from a previously competent bacterial cell liquid culture. After overnight culture, in antibiotic free broth, *E. coli* DH5α were diluted 1:100 in SOB and incubated for a further 3 hours (to an

OD_{550} of 0.3). After a 10-minute incubation on ice, cells were harvested by centrifugation (3000rpm, 10 minutes at 4°C). Supernatant was decanted and cells were resuspended in CCMB buffer in 1/4 of the initial volume. Following a 4-hour incubation on-ice, bacteria were pelleted as before and resuspended in CCMB, this time in 1/12 of the starting volume. This cell suspension was aliquoted into 100µL individual dosages, snap frozen on dry ice and store at -80°C until required for plasmid transformation.

8.2.9. Transformation of competent bacterial cells

Plasmid DNA was transformed into chemically competent *E. coli* using the heat shock method. Briefly, 100ng of plasmid DNA was added to 25µL of cells. Following a 30-minute incubation on ice, cells were heated at 42°C for 45 seconds, allowing the opening of bacterial membrane pores and the entry of plasmid DNA. Following a further 2 minutes incubation on ice, 900µL of LB broth was added and cells were allowed to recover by incubating for 1 hour in a 37 °C shaker (180rpm) before being plated on previously prepared selective LB agar medium (section 8.2.7.).

8.2.10. Bacterial culture

E. coli strains were grown (from single colonies or previously amplified mini cultures) in LB broth supplemented with 100µg/mL of ampicillin or 50µg/mL of kanamycin and incubated overnight in a 180rpm shaker at 37ºC.

8.2.11. Plasmid DNA extraction and quantification

Plasmid DNA was prepared in small or large scales. Small-scale preparations (mini-prep) was performed from 2-5 mL of overnight *E. coli* cultures, whilst large-scale plasmid DNA preparations (midi-preps) used 50mL of overnight culture. Mini- and midi-preps were performed using Qiagen's Plasmid DNA Mini Prep and Plasmid *Plus* Midi kits, respectively. DNA concentration was determined by measuring the absorbance at 260nm using a Nanodrop spectrophotometer. Purity of the same preparations was assessed through the analysis of absorbance ratios A_{260}/A_{280} and A_{260}/A_{230} which indicate protein and ethanol/phenol/EDTA contaminations, respectively.

8.2.12. Site-direct mutagenesis

Introduction of single nucleotide mutations in the pDUAL-PB1 plasmid was performed using the QuikChange Lightning Site-Directed Mutagenesis kit (Agilent) according to manufacturer's instructions with minor changes. Briefly, a PCR was performed using synthetic oligonucleotides containing the desired mutation in a total volume of 25µL followed by the addition of 1µL of DpnI restriction enzyme and incubation at 37ºC for 1 hour. Five µL of the reaction mix was used to transform XL10-Gold ultra-competent cells which were plated on antibiotic-containing agar plates. Following an overnight 37°C incubation, individual colonies were selected, regrown in broth for a following overnight period and used to extract plasmid DNA.

8.3. Eukaryotic cell culture, isolation and manipulation

8.3.1. Cell passage

Madin-Darby canine kidney (MDCK), human embryonal kidney (293T) and adenocarcinomic human alveolar basal epithelial (A549) cell lines were cultured in Dulbecco's modified Eagle's medium (D-MEM) supplemented with 10% (v/v) heat inactivated foetal bovine serum (FBS), 2mM L-glutamine, 100U/mL penicillin and 100µg/mL streptomycin. HEK-Blue™ IFN-α/β cells were grown in complete medium further supplemented with 100µg/mL Zeocin and 30µg/mL Blasticidin. MDCK-SIAT cells were grown in compete medium further supplemented with 50µg/mL geneticin.

Regular cell passage was performed twice a week. Complete medium was removed, cells were washed once with PBS and incubated with 0.25% trypsin-EDTA at 37°C until cells detached from the flask (12mL of PBS and 2mL of trypsin for 75cm^2 flasks; 25mL of PBS and 4mL of trypsin for 150cm^2 flasks). Cells were resuspended in fresh complete medium and 10-50% of the cells were transferred to a clean flask containing complete medium (total volumes: 12mL for 75cm^2 and 30mL for 150cm^2 flasks).

8.3.2. Cell counting

All cell types were counted using a haemocytometer (Neubauer counting chamber). Usually, 10µL of cell suspension was supplied into one side of the chamber under a glass cover slip. Under a light microscope, the number of cells was counted in

a designated squared area equivalent to 0.1mm^3 (1×10^{-4}mL). Cell concentration was then estimated to be: number of counted cells × 1×10^4 cells/mL.

8.3.3. Isolation of bone marrow-derived macrophages

129Sv/Ev wild-type and IFN-α/β receptor knockout (IFNAR$^{-/-}$) mice on the same background were bred in the Biomedical Research Facility (BRF) at The Roslin Institute. Femurs from female mice aged 7 to 13 weeks old were extracted and the bone marrow was flushed out with 10mL of complete RPMI, using a 25G needle and syringe. Bone marrow cells were plated in 10cm bacteriological squared dishes in complete RPMI further supplemented with 1µg/mL porcine Colony Stimulating Factor 1 (CSF1). Four days post isolation, adherent cells were incubated with D-PBS and detached from the plastic by vigorous washing with an 18G needle and syringe and pelleted by centrifugation at 1500rpm. The content of each single dish was reseeded in two to three new plates in CSF1-supplemented complete RPMI. At day 7 post isolation, differentiated macrophages were harvested and seeded for infection.

8.3.4. Cytotoxicity assays

Drug cytotoxicity was measured using the CellTiter-Glo viability assay kit, which judges cell viability on cellular ATP content. Cells were seeded at 1.5 ×10^4 cells/well in a flat clear bottom, opaque-walled 96-well plate. On the following day, cells were incubated with increasing concentrations of drug and/or DMSO (vehicle) in a total volume of 100µL of complete D-MEM at 37 °C in 5 % CO_2 for 12, 24 and/or

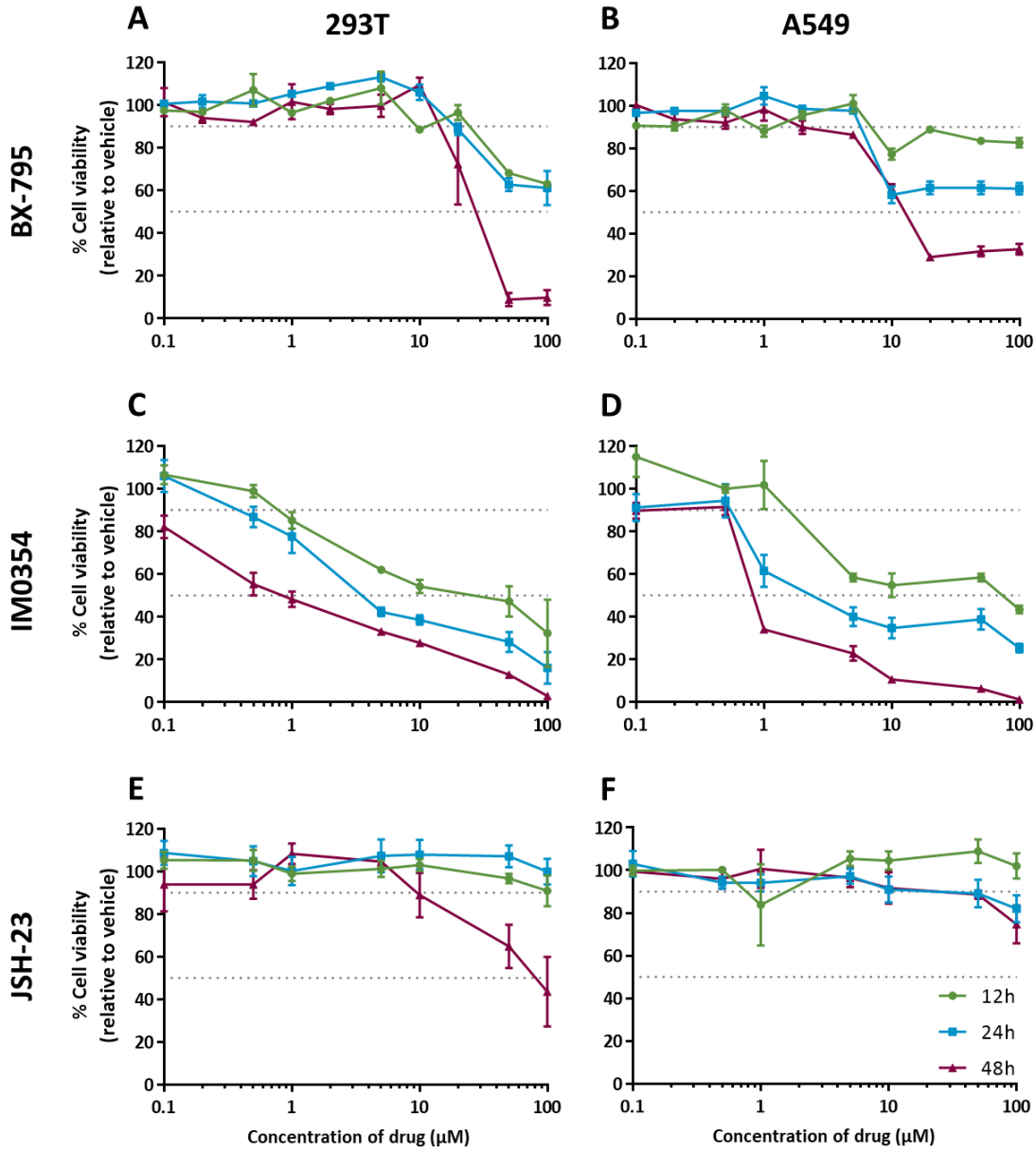

Figure 8.1: Cytotoxicity effects of IRF3- and NF-κB-inhibiting drugs. 293T and A549 cells were incubated with increasing concentrations of BX-795 (A and B), IMD0354 (C and D) or JSH-23 (E and F) for 12 (green), 24 (blue) and 48 (magenta) hours after which cell viability was measured using the CellTitre-Glo according to manufacturer's instructions. Dashed lines represent 90 and 50% of cell viability.

48 hours. At the end of each time point, 100µL of CellTiter-Glo reagent was added to each well and mixed on a horizontal orbital shaker for 2 minutes. Following a further 10-minute steady incubation at room temperature, the luminescent signal was measured in a GLOMAX® multidetection system using an integration time of 0.24 seconds per well.

This assay was used to determine cytotoxicity levels of mammalian cell lines (293T and A549 cells) in the presence of IRF3 and NF-κB inhibition drugs (BX-795, IMD0354 and JSH-23). Analysis of relative cell viability was performed at three time points (12, 24 and 48 hours), ranging the drug concentration from 100 to 0.1µM (Figure 8.1).

8.3.5. Plasmid transfection of mammalian and avian cells

Mammalian and avian cells were routinely transfected with Lipofectamine 2000 reagent following manufacturer's instructions. Briefly, cells were seeded the day before in order to get 70-80% confluency on the day of transfection. Plasmid DNA or poly I:C and lipofectamine were separately diluted in Opti-MEM (detailed amounts of plasmid and lipofectamine are later described in each section). Following a 5-minute incubation period, the two mixtures were combined and incubated for further 20 minutes. Cells culture medium was changed to Opti-MEM and the mixture was dripped over cells.

8.3.6. RNP reconstitution reporter assays

8.3.6.1. Transcription (firefly luciferase) reporter plasmid

Sub-confluent monolayers of 293T or QT-35 cells (2×10^5 cells 24-well plates seeded on the previous day) were co-transfected in triplicate with 50ng of each pDUAL plasmid encoding PB2, PA, NP along with a PolI plasmid containing a reverse oriented firefly luciferase reporter flanked by the 5 and 3' UTRs of segment 8, and various PB1 plasmids. As a negative control, transfections lacking the PB1 plasmid (empty vector was used to balance plasmid intake) were also performed (2PNP). Two days post transfection, medium was removed and cells were lysed with 120µL of reporter lysis buffer. Cell debris was scraped off, lysates were collected into clean tubes and clarified by centrifugation (10,000rpm, 5 minutes, 4°C) in a benchtop centrifuge. Luminescence was measured using 60µL of lysate in opaque 96-well plates and injecting 15pmol of luciferin using a GLOMAX® multidetection system (injection speed: 200µL/second; gap: 0.5 seconds; integration time: 5 seconds).

A dose-dependent variety of this protocol was also performed. For this, 50ng of PB2, PA and NP pDUAL plasmids were transfected into 293T cells along with varying amounts of PB1 pDUAL plasmid (from 100 to 0.001ng). 2PNP, lipofectamine only and mock controls were also included. Incubation time, lysis and luciferase activity measurements were performed as previously described. A wide-range dose-dependent experiment was performed with PB1 WT only (Figure 8.2A). Parallel western blot analysis of PB1 confirmed that PB1 accumulation and luciferase expression declined with decreasing plasmid amount without similar decreases in NP

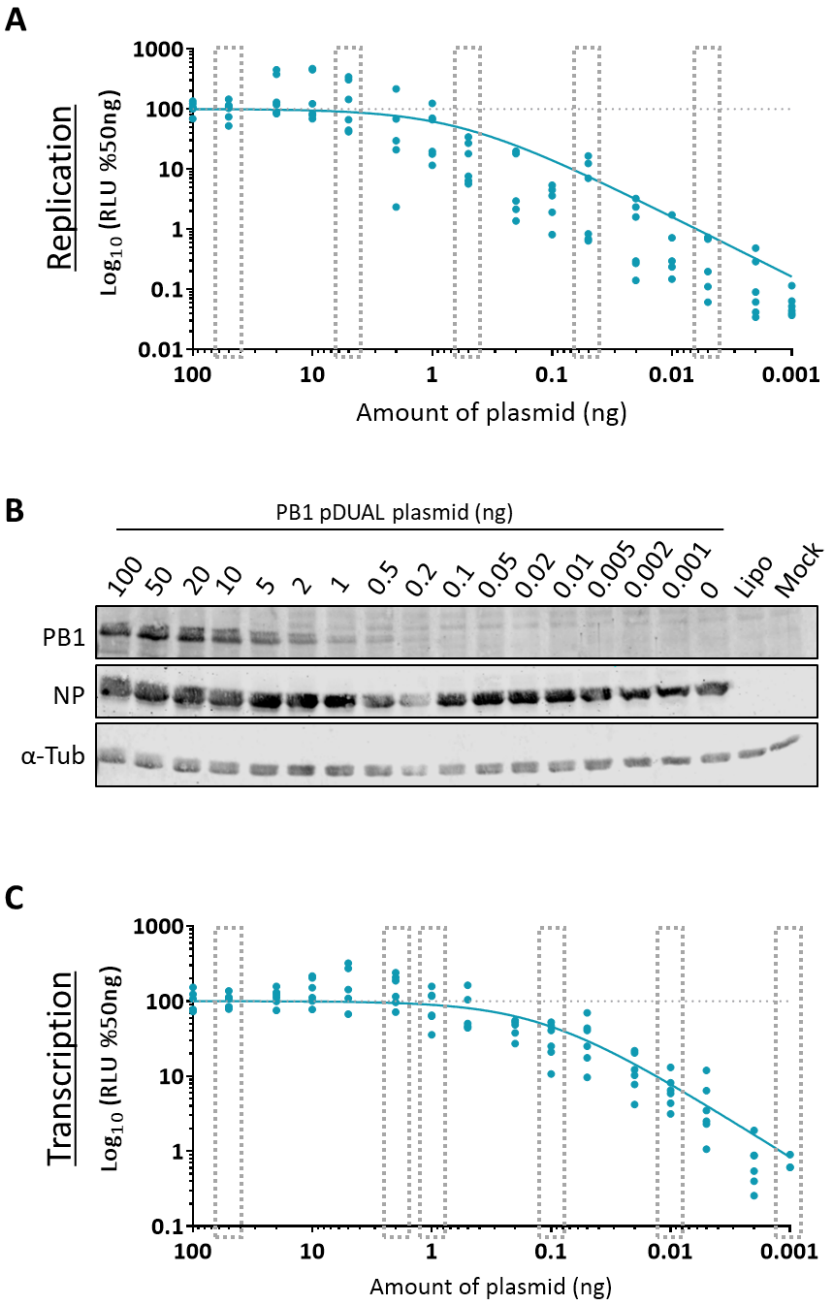

Figure 8.2. Wide-range dose-dependent replication and transcription minireplicon assays. (A) 293T cells were transfected as described in section 8.3.6.1. Luciferase levels were scaled to 50ng of PB1 pDUAL plasmid (B) Expression levels of PB1 and NP were confirmed by western blot (α-tubulin was used as loading control). Inconsistencies in the levels of NP and α-tubulin could be associated with experimental artefacts at the gel-to-membrane transfer step. (C) 293T cells were transfected as described in section 8.3.6.3. Luciferase levels were scaled to 50ng of PB1 pDUAL plasmid. In both (A) and (C), point represent independent replicated within at least 3 independent experiments. Dotted boxes represent the selected amounts of PB1 plasmid used to apply to the remaining segment 2 mutants.

abundance (Figure 8.2B). From this analysis, 6 amounts of PB1 pDUAL plasmid (50, 2, 1, 0.1, 0.01, 0.001ng) were selected and the method applied to segment 2 mutants.

8.3.6.2. Transcription (GFP) reporter plasmid

RNP reconstitution assays with a transcription GFP reporter plasmid were performed as in section 8.3.6.1. with minor changes. Transfection was performed with 100ng of each pDUAL plasmid and 1000ng of reporter plasmid. GFP readings were taken by measuring fluorescence levels (excitation: 485/20, emission: 528/20, sensitivity: 35) using a plate reader (Synergy HT, BioTek®).

8.3.6.3. Replication (firefly luciferase) reporter plasmid

293Ts (2×10^5 cells 24-well plates seeded on the previous day) were co-transfected with 50ng of each 3PNP-expressing reporter plasmids and 25ng of cRNA-like firefly luciferase reporter plasmid using 1µL of Lipofectamine2000. Twenty-four hours post transfection, cells were lysed with 120µL of 1×RLB and luciferase levels were read as in section 8.3.6.1. An equivalent wide-range as in Figure 8.2A was applied using the replication reporter plasmid (Figure 8.2C).

8.3.7. Cellular gene expression shut-off assays

Sub-confluent monolayers of 293T cells were co-transfected in triplicate with 400ng of pcDNA effector plasmids (expressing PB1-related peptides) and 100ng of

pRL or 20ng of β-gal expressing plasmids using 1μL of Lipofectamine2000 as described in 8.3.5. A pcDNA3.1 plasmid expressing A/chicken/Rostock/34 (fowl plague or FPV) PA segment was added as positive control effector plasmid (Hussain *et al.* 2018). Negative controls included a temperature-sensitive FPV PA mutant (Bell 2006) and empty control pcDNA plasmids. A mock transfection condition was also included. Successful transfection efficiencies were confirmed by western blot analysis against PB1 and PA (data not shown). Renilla luciferase or β-gal expression levels were assessed 48 hours post transfection.

8.3.7.1. *Renilla* luciferase measurement

Quantification of renilla luciferase expression was performed using a Renilla Luciferase Assay kit. Briefly, cells were lysed with 100μL of 1× lysis buffer and frozen overnight at -20°C. Cells were scraped off the plate, cell debris was removed by centrifugation (8000rpm, 5 minutes, 4°C) and 20μL of each sample was transferred to a white-bottomed 96-well plate and luminescence was measured in a Promega GloMax Multi Detection Unit injecting 100μL of 1× Renilla luciferase substrate (speed: 200μL/second, delay: 2 seconds, integration time: 10 seconds).

8.3.7.2. β-galactosidase measurement

Expression levels of β-gal were measured using a β-Galactosidase Enzyme Assay System. Cells were lysed with 100μL of 1× reporter lysis buffer. Lysates were transferred to clean 1.5mL tubes, vortexed and cleared by centrifugation. Fifty μL of

cleared lysate was transferred to a clear bottomed 96-well plate and 50µL of ortho-nitrophenyl-D-galactopyranoside (ONPG)-containing 2× assay buffer was added to each well. β-galactosidase catalyses the hydrolysis of β-galactosidase such as ONPG. Hydrolysis of ONPG results in the production of ONP anion which has a bright yellow colour. After a 30 minute incubation at 37°C, the reaction was stopped by the addition of 150µL of 1M sodium carbonate and absorbance at 420nm was measured using a plate reader (FLUOStartOmega, BGM Labtech).

8.3.8. Plasmid-based β-IFN and ISRE promoter reporter studies

Under confluent (80%) monolayers of 293T cells (2×10^5 cells per 24 well seeded on the previous day) were co-transfected with 50ng of reporter plasmid (IFN-β::Luc or ISRE::Luc) and 400ng of pcDNA3.1 expressing PB1-related peptides using 1µL of Lipofectamine 2000 as described in *section 8.3.5 Plasmid transfection of mammalian and avian cells*. For positive control, a plasmid expressing the A/green-winged teal/Ohio/175/1986 NS1 ORF was used (Turnbull *et al.* 2016). Negative controls included a plasmid expressing the PR8 NP ORF and the pcDNA3.1 empty plasmid. 24 hours post transfection, cells were stimulated with 5µg of poly I:C by transfection using 2µL of Lipofectamine/well. Mock-stimulated cells were also included where poly I:C was replaced by milliQ H_2O. Each assay was performed in triplicates. Twenty-four hours post stimulation, cells were lysed with 120µL of reporter lysis buffer and luciferase activity was measured as described in section *8.3.6.1 Transcription (firefly luciferase) reporter plasmid*.

8.4. Virological assays

8.4.1. Generation of P0 viral stocks

PR8 wild-type and mutant viruses were rescued using a previously described reverse genetics system (section *2.2.2. Virus rescue of PR8 segment 2 mutants*). Briefly, 80%-confluent monolayers of 293T cells in 6-well plates were transfected with PR8 segment cDNAs cloned into the pDUAL plasmid (250ng of each) along with 4µL of Lipofectamine2000 in a total volume of 800µL of Opti-MEM. After overnight incubation at 37ºC, the transfection medium was replaced with fresh virus growth medium (DMEM, 2mM L-glutamine, 100U/mL penicillin, 100µg/mL streptomycin, 0.14% BSA, 1µg/ml TPCK trypsin). Cells were incubated for 48 hours, after which supernatants were harvested, cleared by centrifugation and stored at -80°C until future use.

8.4.2. Generations of cell-grown P1 viral stocks

A first passage stock was grown in confluent monolayers of MDCKs (4×10^6 cells/T25 flask or 1.2×10^7 cells/T75 flask seeded the previous day) where cells were infected with an estimated MOI of 0.01 using the P0 stock. Following a minimum of 48 hour incubation, or when infected cells showed cytopathic effect (CPE), cell supernatants were harvested, cleared by centrifugation (1500rpm, 5 minutes), aliquoted and stored at -80ºC until titrated by plaque assay.

8.4.3. Quantification of viral stocks and samples by plaque assay

MDCK cells were seeded in 6-well plates (2×10^6 cells/well) in 2 mL D-MEM/10% FBS and incubated overnight at 37°C/5% CO_2. Medium was removed from the wells and the cells were washed once with 2mL of PBS and then infected with 500µL of 10-fold serial dilutions of virus and incubated for 60 minutes to allow virus adsorption to the cells. Following adsorption, medium was removed and cells were overlaid with 2mL of DMEM/0.14% BSA/1µg/mL TPCK/1.2% Avicel. Incubation continued undisturbed for 2 days at 37°C/5% CO_2 after which cells were fixed with 10% NBF. After overnight fixation, the Avicel-NBF overlay was removed and cells were stained with 0.1% Toluidine Blue. After a 1-hour incubation at room temperature, staining solution was rinsed under tap water, plates were air dried and plaques were counted.

8.4.3.1. Plaque assay staining of pandemic human IAVs (Cal04)

Plaque assays for Cal04 backbone viruses were performed essentially as described in the previous section (*8.4.3. Quantification of viral stocks and samples by plaque assay*), but using MDCK-SIAT cells and a 3 day incubation period at 35°C. Cells were then fixed as previously described, fixing solution was removed and cells were washed with PBS and permeabilised using 1 mL PBS/0.2% (v/v) Triton X-100 per well for 10 minutes. After two PBS washes, cells were incubated with 400µL/well of A2915 rabbit polyclonal anti-MBP-NP (diluted 1:1000 in PBS/2% BSA) for 1 hour on a rocking platform at room temperature. Following two PBS washes, cells were incubated with 400µL of goat anti-rabbit IgG-HRP conjugated secondary antibody

(diluted to 1:1000 in PBS/2%BSA) for 1 hour in the same conditions. Cells were washed three times with PBS, 0.5mL of TrueBlue peroxidase substrate was added per well and cells were incubated at room-temperature covered from direct light. When blue-stained plaques were visible, cells were washed with water, allowed to dry, and plaques were counted under a stereo microscope.

8.4.4. Quantification of viral stocks and samples by haemagglutination assay

Virus stocks grown in eggs were 2-fold serial diluted in PBS in a final volume of 50µL after which 50µL of 1% chicken blood cells were added to each well. After a 30 minute incubation at room-temperature, haemagglutination-positive wells were recorded. Each plate contained a negative (PBS only) and a positive sample for haemagglutination comparison.

8.4.5. Quantification of plaque sizes

After plaque assay incubation, fixation and staining (performed as described in section *8.4.3 Quantification of viral stocks and samples by plaque assay*), 6-well plates were scanned in an Epson Perfection V750 Pro Scanner at a resolution of 1200dpi. Images were converted to grey scale and a Photoshop software used to apply a level 4 posterisation. The area of each plaque was then determined in ImageJ. At least 50 plaques were analysed per condition.

Individual plaque area values of WT PR8 were averaged and used as a reference to scale the individual plaque sizes of each one of the analysed mutant PR8 segment 2 mutants.

8.4.6. Viral RNA isolation and sequencing

First passage viral stocks had RNA extracted using the QIAamp Viral RNA Kit via the spin protocol according to manufacturer's guidelines. Briefly, 140µL of P1 stock or virus sample was mixed with a lysis buffer to release RNA from the virions which was then bound to a silica-based membrane. After a series of alcohol-based washes, RNA was eluted from the column using 40µL of milliQ water.

cDNA production was performed with the Verso cDNA kit (Thermo Scientific), using 5µL of RNA and 10nM of Uni12 primer (Table 8.7) in a final volume of 10µL. For RNA denaturation, the mixture was heated to 65°C for 10 minutes in a Veriti® Thermocycler (Applied Biosystems®, LifeTechnologies) after which, final concentrations of 50nM of each dNTP, 1× RT Buffer and 1µL of Verso™ Enzyme Mix were added in a total 20µL reaction. The final mixture was incubated at 42°C for 60 minutes followed by 95ºC for 2 minutes.

A 611bp fragment of segment 2 was amplified using Uni12 and one of the Seg2 611-592 reverse oliognucleotides (for each different virus) (Table 8.7) as forward and reverse primers, respectively. Each PCR contained 200nM of each primer, 200µM of each dNTP, 1.5mM $MgCL_2$ and 2.5 units of Taq DNA Polymerase (Invitrogen, Life Technologies). PCR were carried out in a Veriti® Thermocycler, using conditions of

1 cycle of 2 minutes at 95°C, followed by 30 cycles of 30 seconds at 95°C, 1 minute at 55°C and 2.5 minutes at 72°C, finishing with a 10-minute incubation at 72°C. PCR product length was confirmed by 1% agarose gel electrophoresis. PCR products were purified according to section *8.2.3. Purification of DNA fragments*. Five µL of DNA was sent for sequencing using a final concentration of 5µM of Uni12 primer in a total volume of 10µL. Sequencing analysis was performed by GATC Biotech.

8.4.7. Quantification of viral genome by quantitative RT-PCR

Viral genome quantification was performed by single step real-time PCR in a Rotor-Gene Q cycler (Qiagen) and data were analysed using the Rotor-Gene Software. RT qPCR mixes were prepared with 400nM of primers against PR8 segments 2, 5 and 7. Other mix components included 1× SensiFAST SYBR® Lo-ROX One-Step Mix (Bioline), 2µL of template RNA, reverse transcriptase and RiboSafe RNA inhibitor in a 20µL reaction. Samples for all targets were analysed in duplicates or triplicates using the following cycling thermal profile: 45°C for 10 minutes, 95°C for 2 minutes and 40 amplification cycles at 95°C for 10 seconds and 60°C for 30 seconds. Melting curves were acquired by consecutive 1° C temperature increments from 50 to 99°C.

Alongside the RNA samples, standard curves constructed with serial diluted pDUAL plasmids of segments 2, 5 and 7 were ran (Figure 8.3). All these showed a decrease of CT values with the increase of number of copies and satisfactory efficiencies.

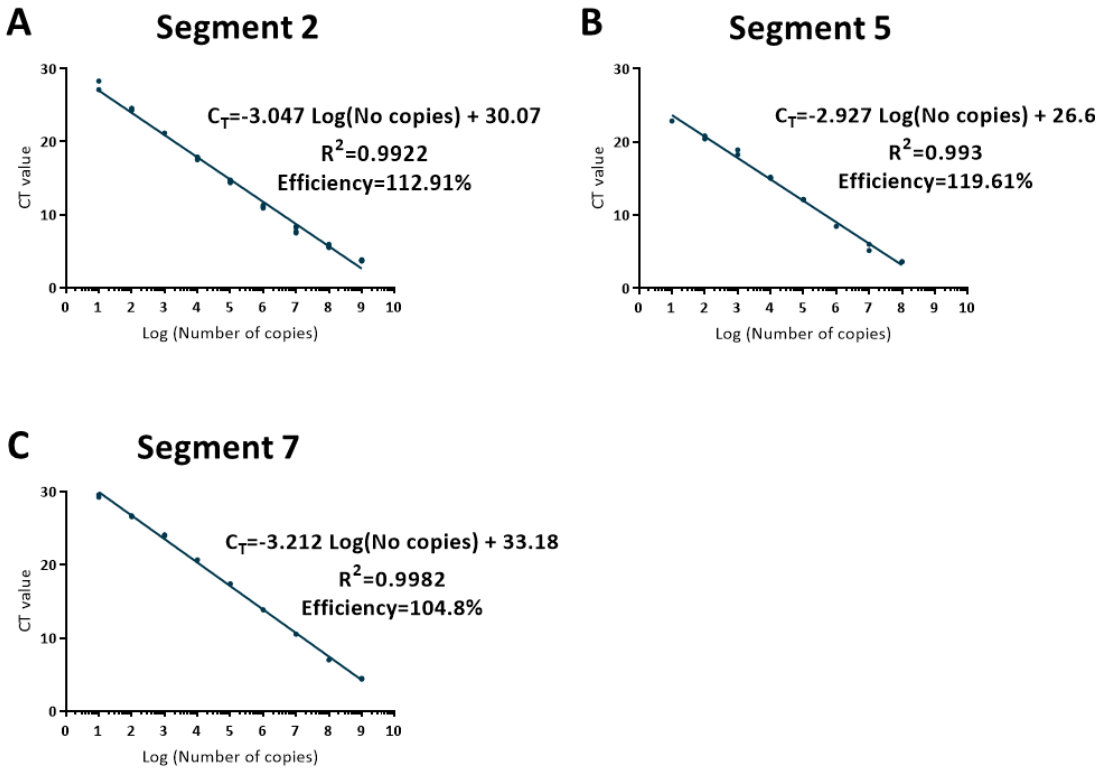

Figure 8.3: qPCR standard curves. Known concentrations of PR8 segment 2 (A), 5 (B) and 7 (C) pDUAL plasmids were run alongside viral samples. C_T equations and respective R^2 values were calculated using GraphPad Prism. Efficiencies were calculated based on: $Efficiency\ (\%) = 100 \times \frac{-1}{10^{slope}-1}$.

8.4.8. Virus infection of eukaryotic cells

To all adherent cells, a wash with the appropriate serum free medium was performed to ensure the removal of residual FBS. Infections were carried out using serum free medium in small volumes: viruses were diluted in 150µL for 24-well plates, 300µL for 12-well and 500µL for 6-well plates). Following a 1 hour incubation which allowed virus adsorption, plates were incubated at the propagation temperature for 1 hour (shaking every 15 minutes). Infectious medium was then removed and the desired medium was added to cells (generally 1mL for 24 and 12-well plates and 2mL for 6-well plates).

8.4.9. Viral multicycle growth kinetic analysis

Confluent monolayers of MDCK, QT-35 or bone-marrow derived macrophage cells were infected with PR8 viruses at a MOI of 0.001 in 300µL of serum free DMEM in 12-well plates. After a 1-hour incubation at 37°C (which allowed virus attachment to the cells) inoculum was replaced by 1mL of fresh virus growth medium (DMEM/0.14% BSA/1µg/ml TPCK trypsin). At different times post infection, supernatants were snap frozen in dry ice and samples were stored at -80°C until titrated by plaque assay.

8.4.10. HEK Blue assay

90% confluent monolayers of A549 cells were infected with the mentioned viruses at a range of different MOIs (0.003, 0.03, 0.3 and 3) in serum free medium in

triplicate. After a 1-hour virus adsorption at 37ºC, inoculum was replaced with 1mL of DMEM/0.14% BSA. Twenty-four hpi, UV inactivation was performed. 300µL of supernatant was moved to a clean 24-well plate and exposed to 120MJ/cm^2 for 10 minutes in a CL-1000 Ultraviolet Crosslinker on ice. Type I interferon levels were measured using 20µL of either original or UV inactivated supernatants along with 5×10^4 HEK Blue cells in a total volume of 200µL of heat inactivated complete medium in 96 well plates. After a 24-hour incubation (37ºC, 5% CO_2), 20µL of each sample was mixed with 180µL of QUANTI-Blue reagent in 96-well plates. Following a 1.5-2 hour incubation, absorbance values at 600nm were acquired using a GLOMAX® multidetection system.

8.5. Protein purification and detection

8.5.1. SDS Polyacrylamide gel electrophoresis

Polypeptides were separated using sodium dodecyl sulphate polyacrylamide gel electrophoresis (SDS-PAGE). Polyacrylamide gels were cast using approximately 5mL per gel of the resolving gel recipe described in 8.1.6.5.2 using 0.75 or 1mm spacer plates with appropriate short plates. Acrylamide:bisacrylamide content was dependent on the size of the proteins of interest, with smaller proteins requiring a higher polyacrylamide percentage gel to allow efficient resolution and vice-versa. Stacking gels were always cast with 4% acrylamide:bisacrylamide.

Lysates were typically generated by adding 200µL of 2× Laemmli's buffer to 24-well plates (generally 5×10^5 cells). Lysates were transferred into clean 1.5mL

tubes, boiled at 95°C for 7 minutes and centrifuged at 13000rpm for 1 minute. Each lane was loaded with 5-20µL of lysate. 3µL of protein molecular weight marker was added to the last lane and gels were run at 80V. Once the sample had past the stacking gel barrier and entered the running gel, voltage was increased up to 150V for the desired length of time.

8.5.2. Western blot

After separation by SDS-PAGE according to the previous section (section *8.5.1. SDS Polyacrylamide gel electrophoresis*), proteins were transferred to a 0.2 or 0.45µm nitrocellulose membrane in a Trans-Blot®Turbo™ apparatus using a commercial transfer buffer. Membranes were blocked with milk-based blocking buffer (or Odyssey TBS blocking buffer, when detecting phosphorylated peptides) for 1 hour and stained with primary antibodies diluted in blocking buffer overnight at 4ºC. After three 5-minute PBST washes (TBST for phosphorylated targets), a secondary antibody was incubated for one hour at room temperature protected from direct light. Following three more washes, membranes were imaged using the LI-COR Odyssey Imaging platform and the ImageStudio Lite software.

8.5.3. Densitometry

Densitometric analysis of polypeptide abundance was performed using Image J software (https://imagej.nih.gov/ij/) (Hartig 2013). Concisely, ImageStudio acquired images were compiled and saved as TIFF files. Those images were opened on ImageJ and the image type was transformed into a 32-bit format. Sample lanes were defined

using the gel analysing tool. Once selected, each lanes' pixel intensity was plotted and the area under each peak curve was calculated.

8.6. Radioactive isotope experiments

8.6.1. ^{35}S-methionine/cysteine metabolic labelling of infected cells

Confluent A549 cell monolayers were infected at a MOI of 10 in 6-well plates. Following a 7-hour infection, cells were washed twice with Methionine/Cysteine free D-MEM and incubated with 500µL of Met/Cys free D-MEM supplemented with 10% dialysed FBS and 2MBq/mL ^{35}S-Met/Cys (1MBq/well) for 1 hour (37°C, 5% CO_2). Cells were further washed with PBS and lysed with 500µL of RIPA buffer containing phosphatase inhibitors and stored overnight at -80°C.

8.6.2. Autoradiography of dried polyacrylamide gels

SDS-PAGE was performed as described in section *8.5.1. SDS Polyacrylamide gel electrophoresis* and gels were fixed in gel fixing solution for 15 minutes with the gel fixing solution being replaced every 5 minutes. Fixed gels were transferred to 3mm filter paper, covered with film and dried in a gel dryer (Model 5432, BioRad) under 80°C heating and vacuum pressure for 2 hours. Once dried, gels were placed in a flat, light-tight cassette and overlaid with an X-ray film. Overnight or longer exposures were developed using a Konica SRX-101A (FAPJ) X-ograph film processer.

8.7. Fluorescent imaging and detection

8.7.1. Immunofluorescence staining

The desired cell lines were seeded on 13mm round glass coverslips in 24 well dishes. After infection/transfection, cells were fixed with 4% neutral buffered formaldehyde (NBF) in PBS for 20 minutes followed by three 1mL PBS washes. Cells were permeabilised with 1% Triton X-100 in PBS for 10 minutes at room temperature. Following three washes with PBS, cells were blocked with 1mL of PBS/1% BSA) for 30 minutes. A single wash with PBS was then followed by incubation for 1 hour with 200µL of primary antibodies at the appropriate dilutions. Three 1mL PBS washes were then executed to remove unbound antisera followed by incubation of secondary antibodies in the same volume. 4',6-Diamidino-2-phenylindole (DAPI) (100ng/mL) was diluted in blocking buffer and incubated for 10 minutes. After labelling steps were completed, coverslips were washed three more times and mounted upside down on glass slides with ProLong reagent.

8.7.2. Confocal microscopy

Confocal fluorescent imaging was carried out using a Zeiss laser confocal microscope LSM710. Machine settings were generally kept unchanged during image acquisition for each fluorophore during an individual experiment. Post-capture tarring up of images was performed using Adobe Photoshop, using only linear transformation methods.

8.7.3. Fluorescence-activated cell sorting (FACS)

In order to verify the degree of differentiation, CSF1-differentiated bone-marrow-derived macrophages were subjected to FACS analysis. This protocol was performed in polypropylene FACS tubes. Washes were performed by a 5-minute centrifugation at 1500rpm. 5×10^5 cells were washed, resuspended in 50µL of PBS/2% FBS (FACS buffer) and blocked with FACS buffer/Fc block for 30 minutes. Staining was performed using CD11b-APC and F4/80-488 primary conjugated antibodies in a total volume of 100µL for 15 minutes. From this stage, all incubation and washing steps were performed protected from direct light. After two 500µL PBS washes, live/dead cell staining was performed in 100µL of eFluor™ 780 diluted in PBS for 30 minutes. Cells were washed once with 500µL of FACS buffer and fixed on ice with 100µL of IC Fixation buffer. After a final 500µL FACS buffer wash, cells were maintained at 4°C and read on the following day using a FACSCalibur cell analyser (BD biosciences).

Negative (secondary antibodies only), single and double staining conditions were performed for both WT (Figure 8.4A) and IFNAR$^{-/-}$ BMDM (Figure 8.4B). In average, 3000 cells per condition were scanned and gated. The secondary antibodies-only staining was used to set the regions of each quadrant. Single staining with the α-F4/80 antibody resulted in the staining of 94.3 and 94.0% of cells (for WT and KO BMDM, respectively), which shifted to Q3. A similar percentage of positive stained BMDM was observed when cells were single stained for CD11b. In this case, 97.4 and 94.6% of WT and IFNAR$^{-/-}$ cells were seen in Q1. The simultaneous use of both primary antibodies resulted in the double staining of over 92% of CSF1-differentiated

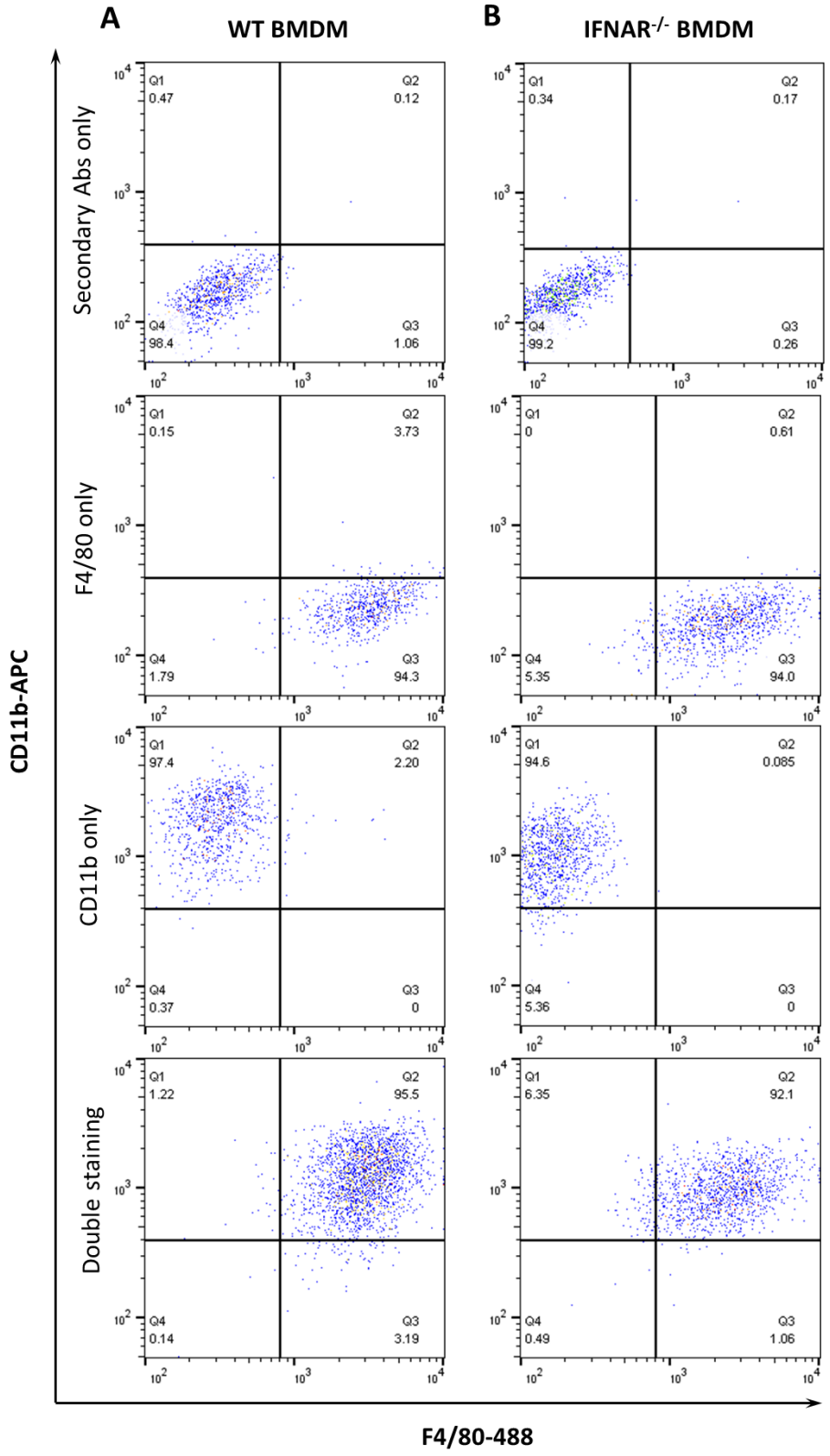

Figure 8.4: Use of FACS to verify the differentiation of BMDMs CSF1 treatment. WT (A) and IFNAR$^{-/-}$ BMDMs (B) were stained against macrophage markers CD11b and F4/80. No primary antibody, individual single staining and double staining were performed. Data acquisition was performed by Dr Marlynne Quigg-Nicol.

BMDM. These percentages are consistent with previously published studies and allowed us to be certain of the successful differentiation of the used BMDM differentiation protocol.

8.8. Mouse experiments

8.8.1. Ethics statement

The following statement was provided by Prof. Bernadette Dutia (The Roslin Institute, The University of Edinburgh, UK), under whose license and authority the experiments were performed: "All animal experiments were carried out under the authority of a UK Home Office Project Licence (60/4479) within the terms and conditions of the strict regulations of the UK Home Office 'Animals (scientific procedures) Act 1986' and the Code of Practice for the housing and care of animals bred, supplied or used for scientific purposes." Individual studies were performed after a study request protocol had been submitted to and approved by the Roslin Institute Animal Welfare and Ethics Review Board.

8.8.2. Viral infections and sampling

129Sv/Ev WT and IFNAR$^{-/-}$ mice were bred and housed in the Roslin Institute Biomedical Research Facility (BRF). All work was carried out under a UK Home Office licence according to the Animals (Scientific Procedures) Act 1986. Mouse infections were conducted by Prof. Bernadette Dutia and Dr. Marlynne Quigg-Nicol

(The Roslin Institute, The University of Edinburgh, UK). Five to seven week old female mice were anaesthetised using isoflurane in an incubation chamber and intranasally infected with 200 PFU of virus in 40µL of PBS through both nostrils simultaneously. Mice were weighed and assessed visually for clinical signs (inactivity, ruffled fur and laboured breathing) on a daily basis. At the fifth day post infection, mice were humanely euthanised by CO_2 asphyxiation. Upon confirmation of death, mice were dissected, and tissue collection was performed. The tip of the left lung was collected into 500µL of RNA later solution and the remainder of the left lung was snap frozen in 2mL tubes on dry ice and stored at -80°C until downstream processing. The left main bronchus airway was constricted, the right lung was inflated with 1mL of 10% (v/v) NBF and stored in the same solution.

8.8.3. Tissue homogenisation and viral quantification

Left lungs were added to 1.5mL of serum-free D-MEM and a 5mm diameter stainless steel bead in 2mL tubes and homogenised using a Tissue Lyser II (Qiagen) system at 28kHz for 2 sets of 2 minutes. Homogenised tissue was clarified by centrifugation (3000rpm, 5 minutes, 4°C). Mouse lung homogenates were titrated for infectious virus (as described in section *8.4.3. Quantification of viral stocks and samples by plaque assay*) and cytokine profiling (*section 8.8.6. Mouse cytokine arrays*).

8.8.4. Histopathological analysis

Inflated and formalin-fixed mouse right lungs were dehydrated and embedded in paraffin and 5µm sections were cut, applied to slides and stained with haematoxylin and eosin (performed by the University of Edinburgh Easter Bush Histopathology Laboratory). Lesion scoring was performed blindly by Dr Philippa Beard (The Pirbright Institute, Surrey, UK). The scoring system was designed by Dr Beard and provided as follows:

- 0, no lesions
- 1, mild, focal inflammation and rare degeneration and necrosis
- 2, moderate, multifocal inflammation with frequent necrotic cells
- 3, marked, multifocal inflammation with common necrosis and occasional fibrin accumulation.

8.8.5. Enzyme-linked immunosorbent assay (ELISA)

IFN-β was detected in mouse lung homogenates by ELISA using a DuoSet® ELISA Development Systems kit (R&DSystems). The capture antibody was diluted 1:3000 and used to coat 96-well plates (50µL/well). Plates were incubated overnight at room-temperature. Following 3 washes with the provided wash buffer, wells were blocked for 1 hour and individual lung homogenates and standard solutions of known IFN-β concentration were added. After 2 hours incubation at room temperature, wells were washed three times. Detection antibody was added for 2 hours at room-temperature, cells were washed three times and a streptavidin-HRP solution was

applied. A 20-minute incubation was performed in the dark, followed by the addition of a 2N sulphuric acid solution and the measurement of absorbance at 560nm.

8.8.6. Mouse cytokine arrays

Cytokines and chemokines were quantified from mouse lungs using the Mouse Cytokine Antibody Array Panel A (R&D Systems). First, protein quantification of lung homogenates was performed with a BCA Protein Assay Kit according to manufacturer's instructions.

Homogenates of up to 5 mice per cohort were pooled and applied to the array membrane according to the manufacturer's instructions. Briefly, a homogenate was incubated with a cocktail of biotinylated antibodies against 40 cytokines. This mixture was then applied overnight to a nitrocellulose membrane containing anti-cytokine antibodies spots (printed in duplicate), which capture the detection antibody/cytokine complex. After a wash to remove unbound cocktail antibodies, the nitrocellulose membrane was incubated with a streptavidin-tagged secondary antibody mixture and imaged using the LI-COR Odyssey Imaging platform and the ImageStudio Lite software. Protein quantification was measured through signal intensity, assuming a proportional correlation between the signal intensity of each membrane spot and the quantity of the specific cytokine. Subsequent analyses and heat map construction were performed in Microsoft Excel and GraphPad Prism respectively.

8.9. Bioinformatic analyses

Bioinformatic analyses were performed in collaboration with Dr Samantha Lycett (The Roslin Institute, University of Edinburgh). PB1 nucleotide sequences were acquired from the NCBI Influenza Virus Database (https://www.ncbi.nlm.nih.gov/genomes/FLU/Database/nph-select.cgi?go=database) on the 4th of May 2016. Sequences were downloaded by host (avian, canine, equine, human and swine) in combined FASTA files. Avian, human and swine sequences were separated into groups of 500 sequences using a script written in R software and each group was uploaded and aligned in MEGA6, after which poor quality/incomplete sequences were discarded. Complete sequences were then re-joined and AUG codon preservation (and respective Kozak strength) was quantified using R scripts and further analysed in Microsoft Excel. All R scripts were written and kindly provided by Dr Samantha Lycett.

8.10. Statistical analysis

All statistic tests were performed in GraphPad Prism 7 Software. Specific statistical tests were chosen for different analyses and are stated in each figure legend.

- ns: non-significant
- *: $p<0.05$
- **: $p<0.01$
- ***: $p<0.001$.

8.11. Structure modelling

The previously published model of IAV polymerase was obtained from RCSB Protein Data Bank (reference 4WSB). Protein structure predictions were performed through the i-TASSER online server, using the pre-set parameters (https://zhanglab.ccmb.med.umich.edu/I-TASSER/) (Roy *et al.* 2011; Yang *et al.* 2015). All proteins models were analysed and visualized using PyMOL Molecular graphics system using the default settings (https://pymol.org/2/).

References

Abe, K., T. Ishigami, A. B. Shyu, S. Ohno, S. Umemura, and A. Yamashita. 2012. 'Analysis of interferon-beta mRNA stability control after poly(I:C) stimulation using RNA metabolic labeling by ethynyluridine', *Biochem Biophys Res Commun*, 428: 44-9.

Abe, T., Y. Kaname, I. Hamamoto, Y. Tsuda, X. Wen, S. Taguwa, K. Moriishi, O. Takeuchi, T. Kawai, T. Kanto, N. Hayashi, S. Akira, and Y. Matsuura. 2007. 'Hepatitis C virus nonstructural protein 5A modulates the toll-like receptor-MyD88-dependent signaling pathway in macrophage cell lines', *J Virol*, 81: 8953-66.

Akarsu, H., W. P. Burmeister, C. Petosa, I. Petit, C. W. Muller, R. W. Ruigrok, and F. Baudin. 2003. 'Crystal structure of the M1 protein-binding domain of the influenza A virus nuclear export protein (NEP/NS2)', *EMBO J*, 22: 4646-55.

Ali, A., R. T. Avalos, E. Ponimaskin, and D. P. Nayak. 2000. 'Influenza virus assembly: effect of influenza virus glycoproteins on the membrane association of M1 protein', *J Virol*, 74: 8709-19.

Almond, J. W., D. McGeoch, and R. D. Barry. 1979. 'Temperature-sensitive mutants of fowl plague virus: isolation and genetic characterization', *Virology*, 92: 416-27.

Amorim, M. J., E. A. Bruce, E. K. Read, A. Foeglein, R. Mahen, A. D. Stuart, and P. Digard. 2011. 'A Rab11- and microtubule-dependent mechanism for cytoplasmic transport of influenza A virus viral RNA', *J Virol*, 85: 4143-56.

Ank, N., H. West, C. Bartholdy, K. Eriksson, A. R. Thomsen, and S. R. Paludan. 2006. 'Lambda interferon (IFN-lambda), a type III IFN, is induced by viruses and IFNs and displays potent antiviral activity against select virus infections in vivo', *J Virol*, 80: 4501-9.

Arai, Y., N. Kawashita, T. Daidoji, M. S. Ibrahim, E. M. El-Gendy, T. Takagi, K. Takahashi, Y. Suzuki, K. Ikuta, T. Nakaya, T. Shioda, and Y. Watanabe. 2016. 'Novel Polymerase Gene Mutations for Human Adaptation in Clinical Isolates of Avian H5N1 Influenza Viruses', *PLoS Pathog*, 12: e1005583.

Archetti, I. 1955. 'Appearances associated with filamentous forms of influenza viruses', *Arch Gesamte Virusforsch*, 6: 29-35.

Arranz, R., R. Coloma, F. J. Chichon, J. J. Conesa, J. L. Carrascosa, J. M. Valpuesta, J. Ortin, and J. Martin-Benito. 2012. 'The structure of native influenza virion ribonucleoproteins', *Science*, 338: 1634-7.

Babcock, H. P., C. Chen, and X. Zhuang. 2004. 'Using single-particle tracking to study nuclear trafficking of viral genes', *Biophys J*, 87: 2749-58.

Baccam, P., C. Beauchemin, C. A. Macken, F. G. Hayden, and A. S. Perelson. 2006. 'Kinetics of influenza A virus infection in humans', *J Virol*, 80: 7590-9.

Bai, L. Y., C. F. Chiu, N. P. Kapuriya, T. M. Shieh, Y. C. Tsai, C. Y. Wu, A. M. Sargeant, and J. R. Weng. 2015. 'BX795, a TBK1 inhibitor, exhibits antitumor activity in human oral squamous cell carcinoma through apoptosis induction and mitotic phase arrest', *Eur J Pharmacol*, 769: 287-96.

Baigent, S. J., and J. W. McCauley. 2003. 'Influenza type A in humans, mammals and birds: determinants of virus virulence, host-range and interspecies transmission', *Bioessays*, 25: 657-71.

Barchet, W., A. Krug, M. Cella, C. Newby, J. A. Fischer, A. Dzionek, A. Pekosz, and M. Colonna. 2005. 'Dendritic cells respond to influenza virus through TLR7- and PKR-independent pathways', *Eur J Immunol*, 35: 236-42.

Baron, S., and A. Isaacs. 1961. 'Mechanism of recovery from viral infection in the chick embryo', *Nature*, 191: 97-8.

Basler, C. F., and P. V. Aguilar. 2008. 'Progress in identifying virulence determinants of the 1918 H1N1 and the Southeast Asian H5N1 influenza A viruses', *Antiviral Res*, 79: 166-78.

Baum, A., R. Sachidanandam, and A. Garcia-Sastre. 2010. 'Preference of RIG-I for short viral RNA molecules in infected cells revealed by next-generation sequencing', *Proc Natl Acad Sci U S A*, 107: 16303-8.

Bavagnoli, L., S. Cucuzza, G. Campanini, F. Rovida, S. Paolucci, F. Baldanti, and G. Maga. 2015. 'The novel influenza A virus protein PA-X and its naturally deleted variant show different enzymatic properties in comparison to the viral endonuclease PA', *Nucleic Acids Res*, 43: 9405-17.

Beaton, A. R., and R. M. Krug. 1986. 'Transcription antitermination during influenza viral template RNA synthesis requires the nucleocapsid protein and the absence of a 5' capped end', *Proc Natl Acad Sci U S A*, 83: 6282-6.

Bell, Gwynneth Louise. 2006. 'The function of the PA polymerase subunit of influenza A virus', PhD dissertation, University of Cambridge.

Belzacq, A. S., H. L. Vieira, G. Kroemer, and C. Brenner. 2002. 'The adenine nucleotide translocator in apoptosis', *Biochimie*, 84: 167-76.

Benitez, A. A., M. Panis, J. Xue, A. Varble, J. V. Shim, A. L. Frick, C. B. Lopez, D. Sachs, and B. R. tenOever. 2015. 'In Vivo RNAi Screening Identifies MDA5 as a Significant Contributor to the Cellular Defense against Influenza A Virus', *Cell Rep*, 11: 1714-26.

Bergmann, M., A. Garcia-Sastre, E. Carnero, H. Pehamberger, K. Wolff, P. Palese, and T. Muster. 2000. 'Influenza virus NS1 protein counteracts PKR-mediated inhibition of replication', *J Virol*, 74: 6203-6.

Biswas, S. K., and D. P. Nayak. 1994. 'Mutational analysis of the conserved motifs of influenza A virus polymerase basic protein 1', *J Virol*, 68: 1819-26.

Blaas, D., E. Patzelt, and E. Kuechler. 1982. 'Identification of the cap binding protein of influenza virus', *Nucleic Acids Res*, 10: 4803-12.

Blok, V., C. Cianci, K. W. Tibbles, S. C. Inglis, M. Krystal, and P. Digard. 1996. 'Inhibition of the influenza virus RNA-dependent RNA polymerase by antisera directed against the carboxy-terminal region of the PB2 subunit', *J Gen Virol*, 77 (Pt 5): 1025-33.

Bluyssen, H. A., R. J. Vlietstra, A. van der Made, and J. Trapman. 1994. 'The interferon-stimulated gene 54 K promoter contains two adjacent functional interferon-stimulated response elements of different strength, which act synergistically for maximal interferon-alpha inducibility', *Eur J Biochem*, 220: 395-402.

Boni, M. F. 2008. 'Vaccination and antigenic drift in influenza', *Vaccine*, 26 Suppl 3: C8-14.

Bortz, E., L. Westera, J. Maamary, J. Steel, R. A. Albrecht, B. Manicassamy, G. Chase, L. Martinez-Sobrido, M. Schwemmle, and A. Garcia-Sastre. 2011. 'Host- and strain-specific regulation of influenza virus polymerase activity by interacting cellular proteins', *MBio*, 2.

Bourret, V., J. Lyall, M. F. Ducatez, J. L. Guerin, and L. Tiley. 2012. 'Development of an improved polykaryon-based influenza virus rescue system', *BMC Biotechnol*, 12: 69.

Braam, J., I. Ulmanen, and R. M. Krug. 1983. 'Molecular model of a eucaryotic transcription complex: functions and movements of influenza P proteins during capped RNA-primed transcription', *Cell*, 34: 609-18.

Brass, A. L., I. C. Huang, Y. Benita, S. P. John, M. N. Krishnan, E. M. Feeley, B. J. Ryan, J. L. Weyer, L. van der Weyden, E. Fikrig, D. J. Adams, R. J. Xavier, M. Farzan, and S. J. Elledge. 2009. 'The IFITM proteins mediate cellular resistance to influenza A H1N1 virus, West Nile virus, and dengue virus', *Cell*, 139: 1243-54.

Brisse, M., and H. Ly. 2017. 'Viral inhibitions of PACT-induced RIG-I activation', *Oncotarget*, 8: 60725-26.

Broughton, S. E., U. Dhagat, T. R. Hercus, T. L. Nero, M. A. Grimbaldeston, C. S. Bonder, A. F. Lopez, and M. W. Parker. 2012. 'The GM-CSF/IL-3/IL-5 cytokine receptor family: from ligand recognition to initiation of signaling', *Immunol Rev*, 250: 277-302.

Brown, R. H. M. 2016. 'Derivation and characterisation of temperature-sensitive mutants of swine influenza A virus', PhD dissertation, University of Cambridge.

Bruce, E. A., P. Digard, and A. D. Stuart. 2010. 'The Rab11 pathway is required for influenza A virus budding and filament formation', *J Virol*, 84: 5848-59.

Buehler, J., D. Navi, A. Lorusso, A. Vincent, K. Lager, and C. L. Miller. 2013. 'Influenza A virus PB1-F2 protein expression is regulated in a strain-specific manner by sequences located downstream of the PB1-F2 initiation codon', *J Virol*, 87: 10687-99.

Bui, M., G. Whittaker, and A. Helenius. 1996. 'Effect of M1 protein and low pH on nuclear transport of influenza virus ribonucleoproteins', *J Virol*, 70: 8391-401.

Bullido, R., P. Gomez-Puertas, M. J. Saiz, and A. Portela. 2001. 'Influenza A virus NEP (NS2 protein) downregulates RNA synthesis of model template RNAs', *J Virol*, 75: 4912-7.

Cadena, C., S. Ahmad, A. Xavier, J. Willemsen, S. Park, J. W. Park, S. W. Oh, T. Fujita, F. Hou, M. Binder, and S. Hur. 2019. 'Ubiquitin-Dependent and -Independent Roles of E3 Ligase RIPLET in Innate Immunity', *Cell*, 177: 1187-200 e16.

Cady, S. D., K. Schmidt-Rohr, J. Wang, C. S. Soto, W. F. Degrado, and M. Hong. 2010. 'Structure of the amantadine binding site of influenza M2 proton channels in lipid bilayers', *Nature*, 463: 689-92.

Calder, L. J., S. Wasilewski, J. A. Berriman, and P. B. Rosenthal. 2010. 'Structural organization of a filamentous influenza A virus', *Proc Natl Acad Sci U S A*, 107: 10685-90.

Campbell, P. J., S. Danzy, C. S. Kyriakis, M. J. Deymier, A. C. Lowen, and J. Steel. 2014. 'The M segment of the 2009 pandemic influenza virus confers increased neuraminidase activity, filamentous morphology, and efficient contact transmissibility to A/Puerto Rico/8/1934-based reassortant viruses', *J Virol*, 88: 3802-14.

Carr, C. M., and P. S. Kim. 1993. 'A spring-loaded mechanism for the conformational change of influenza hemagglutinin', *Cell*, 73: 823-32.

Carr, S. M., E. Carnero, A. Garcia-Sastre, G. G. Brownlee, and E. Fodor. 2006. 'Characterization of a mitochondrial-targeting signal in the PB2 protein of influenza viruses', *Virology*, 344: 492-508.

Cauldwell, A. V., J. S. Long, O. Moncorge, and W. S. Barclay. 2014. 'Viral determinants of influenza A virus host range', *J Gen Virol*, 95: 1193-210.

Chaimayo, C., T. Hayashi, A. Underwood, E. Hodges, and T. Takimoto. 2017. 'Selective incorporation of vRNP into influenza A virions determined by its specific interaction with M1 protein', *Virology*, 505: 23-32.

Chakrabarti, A., B. K. Jha, and R. H. Silverman. 2011. 'New insights into the role of RNase L in innate immunity', *J Interferon Cytokine Res*, 31: 49-57.

Chang, T. H., T. Kubota, M. Matsuoka, S. Jones, S. B. Bradfute, M. Bray, and K. Ozato. 2009. 'Ebola Zaire virus blocks type I interferon production by exploiting the host SUMO modification machinery', *PLoS Pathog*, 5: e1000493.

Chen, B. J., G. P. Leser, E. Morita, and R. A. Lamb. 2007. 'Influenza virus hemagglutinin and neuraminidase, but not the matrix protein, are required for assembly and budding of plasmid-derived virus-like particles', *J Virol*, 81: 7111-23.

Chen, W., P. A. Calvo, D. Malide, J. Gibbs, U. Schubert, I. Bacik, S. Basta, R. O'Neill, J. Schickli, P. Palese, P. Henklein, J. R. Bennink, and J. W. Yewdell. 2001. 'A novel influenza A virus mitochondrial protein that induces cell death', *Nat Med*, 7: 1306-12.

Chen, Z. J. 2005. 'Ubiquitin signalling in the NF-kappaB pathway', *Nat Cell Biol*, 7: 758-65.

Cheong, H. K., C. Cheong, and B. S. Choi. 1996. 'Secondary structure of the panhandle RNA of influenza virus A studied by NMR spectroscopy', *Nucleic Acids Res*, 24: 4197-201.

Chiang, C., G. W. Chen, and S. R. Shih. 2008. 'Mutations at alternative 5' splice sites of M1 mRNA negatively affect influenza A virus viability and growth rate', *J Virol*, 82: 10873-86.

Cho, M. L., J. W. Kang, Y. M. Moon, H. J. Nam, J. Y. Jhun, S. B. Heo, H. T. Jin, S. Y. Min, J. H. Ju, K. S. Park, Y. G. Cho, C. H. Yoon, S. H. Park, Y. C. Sung, and H. Y. Kim. 2006. 'STAT3 and NF-kappaB signal pathway is required for IL-23-mediated IL-17 production in spontaneous arthritis animal model IL-1 receptor antagonist-deficient mice', *J Immunol*, 176: 5652-61.

Choudhury, N. R., G. Heikel, M. Trubitsyna, P. Kubik, J. S. Nowak, S. Webb, S. Granneman, C. Spanos, J. Rappsilber, A. Castello, and G. Michlewski. 2017. 'RNA-binding activity of TRIM25 is mediated by its PRY/SPRY domain and is required for ubiquitination', *BMC Biol*, 15: 105.

Chu, C., S. Fan, C. Li, C. Macken, J. H. Kim, M. Hatta, G. Neumann, and Y. Kawaoka. 2012. 'Functional analysis of conserved motifs in influenza virus PB1 protein', *PLoS One*, 7: e36113.

Chua, M. A., S. Schmid, J. T. Perez, R. A. Langlois, and B. R. Tenoever. 2013. 'Influenza A virus utilizes suboptimal splicing to coordinate the timing of infection', *Cell Rep*, 3: 23-9.

Clark, K., L. Plater, M. Peggie, and P. Cohen. 2009. 'Use of the pharmacological inhibitor BX795 to study the regulation and physiological roles of TBK1 and IkappaB kinase epsilon: a distinct upstream kinase mediates Ser-172 phosphorylation and activation', *J Biol Chem*, 284: 14136-46.

Cobbin, J. C., C. Ong, E. Verity, B. P. Gilbertson, S. P. Rockman, and L. E. Brown. 2014. 'Influenza virus PB1 and neuraminidase gene segments can cosegregate during vaccine reassortment driven by interactions in the PB1 coding region', *J Virol*, 88: 8971-80.

Colman, P. M. 1994. 'Influenza virus neuraminidase: structure, antibodies, and inhibitors', *Protein Sci*, 3: 1687-96.

Coloma, R., J. M. Valpuesta, R. Arranz, J. L. Carrascosa, J. Ortin, and J. Martin-Benito. 2009. 'The structure of a biologically active influenza virus ribonucleoprotein complex', *PLoS Pathog*, 5: e1000491.

Compans, R. W., J. Content, and P. H. Duesberg. 1972. 'Structure of the ribonucleoprotein of influenza virus', *J Virol*, 10: 795-800.

Conenello, G. M., J. R. Tisoncik, E. Rosenzweig, Z. T. Varga, P. Palese, and M. G. Katze. 2011. 'A single N66S mutation in the PB1-F2 protein of influenza A virus increases virulence by inhibiting the early interferon response in vivo', *J Virol*, 85: 652-62.

Conenello, G. M., D. Zamarin, L. A. Perrone, T. Tumpey, and P. Palese. 2007. 'A single mutation in the PB1-F2 of H5N1 (HK/97) and 1918 influenza A viruses contributes to increased virulence', *PLoS Pathog*, 3: 1414-21.

Connor, R. J., Y. Kawaoka, R. G. Webster, and J. C. Paulson. 1994. 'Receptor specificity in human, avian, and equine H2 and H3 influenza virus isolates', *Virology*, 205: 17-23.

Cox, J. C., A. W. Hampson, and R. C. Hamilton. 1980. 'An immunofluorescence study of influenza virus filament formation', *Arch Virol*, 63: 275-84.

Cros, J. F., A. Garcia-Sastre, and P. Palese. 2005. 'An unconventional NLS is critical for the nuclear import of the influenza A virus nucleoprotein and ribonucleoprotein', *Traffic*, 6: 205-13.

Dadonaite, B., B. Gilbertson, M. L. Knight, S. Trifkovic, S. Rockman, A. Laederach, L. E. Brown, E. Fodor, and D. L. V. Bauer. 2019. 'The structure of the influenza A virus genome', *Nat Microbiol*.

Dadonaite, B., S. Vijayakrishnan, E. Fodor, D. Bhella, and E. C. Hutchinson. 2016. 'Filamentous influenza viruses', *J Gen Virol*, 97: 1755-64.

Das, K., L. C. Ma, R. Xiao, B. Radvansky, J. Aramini, L. Zhao, J. Marklund, R. L. Kuo, K. Y. Twu, E. Arnold, R. M. Krug, and G. T. Montelione. 2008. 'Structural basis for suppression of a host antiviral response by influenza A virus', *Proc Natl Acad Sci U S A*, 105: 13093-8.

Dauber, B., G. Heins, and T. Wolff. 2004. 'The influenza B virus nonstructural NS1 protein is essential for efficient viral growth and antagonizes beta interferon induction', *J Virol*, 78: 1865-72.

Dauletbaev, N., M. Cammisano, K. Herscovitch, and L. C. Lands. 2015. 'Stimulation of the RIG-I/MAVS Pathway by Polyinosinic:Polycytidylic Acid Upregulates IFN-beta in Airway Epithelial Cells with Minimal Costimulation of IL-8', *J Immunol*, 195: 2829-41.

Davis, A. R., A. L. Hiti, and D. P. Nayak. 1980. 'Influenza defective interfering viral RNA is formed by internal deletion of genomic RNA', *Proc Natl Acad Sci U S A*, 77: 215-9.

Davis, A. R., and D. P. Nayak. 1979. 'Sequence relationships among defective interfering influenza viral RNAs', *Proc Natl Acad Sci U S A*, 76: 3092-6.

de Castro Martin, I. F., G. Fournier, M. Sachse, J. Pizarro-Cerda, C. Risco, and N. Naffakh. 2017. 'Influenza virus genome reaches the plasma membrane via a modified endoplasmic reticulum and Rab11-dependent vesicles', *Nat Commun*, 8: 1396.

de Haro, C., R. Mendez, and J. Santoyo. 1996. 'The eIF-2alpha kinases and the control of protein synthesis', *FASEB J*, 10: 1378-87.

de Jong, M. D., C. P. Simmons, T. T. Thanh, V. M. Hien, G. J. Smith, T. N. Chau, D. M. Hoang, N. V. Chau, T. H. Khanh, V. C. Dong, P. T. Qui, B. V. Cam, Q. Ha do, Y. Guan, J. S. Peiris, N. T. Chinh, T. T. Hien, and J. Farrar. 2006. 'Fatal outcome of human influenza A (H5N1) is associated with high viral load and hypercytokinemia', *Nat Med*, 12: 1203-7.

de Wit, E., M. I. Spronken, T. M. Bestebroer, G. F. Rimmelzwaan, A. D. Osterhaus, and R. A. Fouchier. 2004. 'Efficient generation and growth of influenza virus A/PR/8/34 from eight cDNA fragments', *Virus Res*, 103: 155-61.

Deng, T., F. T. Vreede, and G. G. Brownlee. 2006. 'Different de novo initiation strategies are used by influenza virus RNA polymerase on its cRNA and viral RNA promoters during viral RNA replication', *J Virol*, 80: 2337-48.

Derossi, D., S. Calvet, A. Trembleau, A. Brunissen, G. Chassaing, and A. Prochiantz. 1996. 'Cell internalization of the third helix of the Antennapedia homeodomain is receptor-independent', *J Biol Chem*, 271: 18188-93.

Derossi, D., G. Chassaing, and A. Prochiantz. 1998. 'Trojan peptides: the penetratin system for intracellular delivery', *Trends Cell Biol*, 8: 84-7.

Deshmane, S. L., S. Kremlev, S. Amini, and B. E. Sawaya. 2009. 'Monocyte chemoattractant protein-1 (MCP-1): an overview', *J Interferon Cytokine Res*, 29: 313-26.

Desmet, E. A., K. A. Bussey, R. Stone, and T. Takimoto. 2013. 'Identification of the N-terminal domain of the influenza virus PA responsible for the suppression of host protein synthesis', *J Virol*, 87: 3108-18.

Desselberger, U., V. R. Racaniello, J. J. Zazra, and P. Palese. 1980. 'The 3' and 5'-terminal sequences of influenza A, B and C virus RNA segments are highly conserved and show partial inverted complementarity', *Gene*, 8: 315-28.

Detjen, B. M., C. St Angelo, M. G. Katze, and R. M. Krug. 1987. 'The three influenza virus polymerase (P) proteins not associated with viral nucleocapsids in the infected cell are in the form of a complex', *J Virol*, 61: 16-22.

Dias, A., D. Bouvier, T. Crepin, A. A. McCarthy, D. J. Hart, F. Baudin, S. Cusack, and R. W. Ruigrok. 2009. 'The cap-snatching endonuclease of influenza virus polymerase resides in the PA subunit', *Nature*, 458: 914-8.

Didcock, L., D. F. Young, S. Goodbourn, and R. E. Randall. 1999. 'Sendai virus and simian virus 5 block activation of interferon-responsive genes: importance for virus pathogenesis', *J Virol*, 73: 3125-33.

Diebold, S. S., T. Kaisho, H. Hemmi, S. Akira, and C. Reis e Sousa. 2004. 'Innate antiviral responses by means of TLR7-mediated recognition of single-stranded RNA', *Science*, 303: 1529-31.

Digard, P., V. C. Blok, and S. C. Inglis. 1989. 'Complex formation between influenza virus polymerase proteins expressed in Xenopus oocytes', *Virology*, 171: 162-9.

Digard, P., D. Elton, K. Bishop, E. Medcalf, A. Weeds, and B. Pope. 1999. 'Modulation of nuclear localization of the influenza virus nucleoprotein through interaction with actin filaments', *J Virol*, 73: 2222-31.

Dittmann, M., H. H. Hoffmann, M. A. Scull, R. H. Gilmore, K. L. Bell, M. Ciancanelli, S. J. Wilson, S. Crotta, Y. Yu, B. Flatley, J. W. Xiao, J. L. Casanova, A. Wack, P. D. Bieniasz, and C. M. Rice. 2015. 'A serpin shapes the extracellular environment to prevent influenza A virus maturation', *Cell*, 160: 631-43.

Doms, R. W., R. A. Lamb, J. K. Rose, and A. Helenius. 1993. 'Folding and assembly of viral membrane proteins', *Virology*, 193: 545-62.

Donald, H. B., and A. Isaacs. 1954. 'Counts of influenza virus particles', *J Gen Microbiol*, 10: 457-64.

Donelan, N. R., C. F. Basler, and A. Garcia-Sastre. 2003. 'A recombinant influenza A virus expressing an RNA-binding-defective NS1 protein induces high levels of beta interferon and is attenuated in mice', *J Virol*, 77: 13257-66.

Dou, D., R. Revol, H. Ostbye, H. Wang, and R. Daniels. 2018. 'Influenza A Virus Cell Entry, Replication, Virion Assembly and Movement', *Front Immunol*, 9: 1581.

Drake, J. W. 1993. 'Rates of spontaneous mutation among RNA viruses', *Proc Natl Acad Sci U S A*, 90: 4171-5.

Du, Y., L. Xin, Y. Shi, T. H. Zhang, N. C. Wu, L. Dai, D. Gong, G. Brar, S. Shu, J. Luo, W. Reiley, Y. W. Tseng, H. Bai, T. T. Wu, J. Wang, Y. Shu, and R. Sun. 2018. 'Genome-wide identification of interferon-sensitive mutations enables influenza vaccine design', *Science*, 359: 290-96.

Dubois, J., O. Terrier, and M. Rosa-Calatrava. 2014. 'Influenza viruses and mRNA splicing: doing more with less', *MBio*, 5: e00070-14.

DuBridge, R. B., P. Tang, H. C. Hsia, P. M. Leong, J. H. Miller, and M. P. Calos. 1987. 'Analysis of mutation in human cells by using an Epstein-Barr virus shuttle system', *Mol Cell Biol*, 7: 379-87.

Duesberg, P. H. 1968. 'The RNA of influenza virus', *Proc Natl Acad Sci U S A*, 59: 930-7.

Duhaut, S. D., and N. J. Dimmock. 2002. 'Defective segment 1 RNAs that interfere with production of infectious influenza A virus require at least 150 nucleotides of 5' sequence: evidence from a plasmid-driven system', *J Gen Virol*, 83: 403-11.

Duhaut, S. D., and J. W. McCauley. 1996. 'Defective RNAs inhibit the assembly of influenza virus genome segments in a segment-specific manner', *Virology*, 216: 326-37.

Duhaut, S., and N. J. Dimmock. 2000. 'Approximately 150 nucleotides from the 5' end of an influenza A segment 1 defective virion RNA are needed for genome stability during passage of defective virus in infected cells', *Virology*, 275: 278-85.

Eierhoff, T., E. R. Hrincius, U. Rescher, S. Ludwig, and C. Ehrhardt. 2010. 'The epidermal growth factor receptor (EGFR) promotes uptake of influenza A viruses (IAV) into host cells', *PLoS Pathog*, 6: e1001099.

Eisfeld, A. J., E. Kawakami, T. Watanabe, G. Neumann, and Y. Kawaoka. 2011. 'RAB11A is essential for transport of the influenza virus genome to the plasma membrane', *J Virol*, 85: 6117-26.

Engel, D. A. 2013. 'The influenza virus NS1 protein as a therapeutic target', *Antiviral Res*, 99: 409-16.

Engelhardt, O. G., M. Smith, and E. Fodor. 2005. 'Association of the influenza A virus RNA-dependent RNA polymerase with cellular RNA polymerase II', *J Virol*, 79: 5812-8.

Erkmann, J. A., and U. Kutay. 2004. 'Nuclear export of mRNA: from the site of transcription to the cytoplasm', *Exp Cell Res*, 296: 12-20.

Everitt, A. R., S. Clare, T. Pertel, S. P. John, R. S. Wash, S. E. Smith, C. R. Chin, E. M. Feeley, J. S. Sims, D. J. Adams, H. M. Wise, L. Kane, D. Goulding, P. Digard, V. Anttila, J. K. Baillie, T. S. Walsh, D. A. Hume, A. Palotie, Y. Xue, V. Colonna, C. Tyler-Smith, J. Dunning, S. B. Gordon, Isis Investigators Gen, Mosaic Investigators, R. L. Smyth, P. J. Openshaw, G. Dougan, A. L. Brass, and P. Kellam. 2012. 'IFITM3 restricts the morbidity and mortality associated with influenza', *Nature*, 484: 519-23.

Feeley, E. M., J. S. Sims, S. P. John, C. R. Chin, T. Pertel, L. M. Chen, G. D. Gaiha, B. J. Ryan, R. O. Donis, S. J. Elledge, and A. L. Brass. 2011. 'IFITM3 inhibits influenza A virus infection by preventing cytosolic entry', *PLoS Pathog*, 7: e1002337.

Ferhadian, D., M. Contrant, A. Printz-Schweigert, R. P. Smyth, J. C. Paillart, and R. Marquet. 2018. 'Structural and Functional Motifs in Influenza Virus RNAs', *Front Microbiol*, 9: 559.

Field, A. K., A. A. Tytell, G. P. Lampson, and M. R. Hilleman. 1967. 'Inducers of interferon and host resistance. II. Multistranded synthetic polynucleotide complexes', *Proc Natl Acad Sci U S A*, 58: 1004-10.

Firth, A. E., and I. Brierley. 2012. 'Non-canonical translation in RNA viruses', *J Gen Virol*, 93: 1385-409.

Firth, A. E., B. W. Jagger, H. M. Wise, C. C. Nelson, K. Parsawar, N. M. Wills, S. Napthine, J. K. Taubenberger, P. Digard, and J. F. Atkins. 2012. 'Ribosomal frameshifting used in influenza A virus expression occurs within the sequence UCC_UUU_CGU and is in the +1 direction', *Open Biol*, 2: 120109.

Fitzgerald, K. A., S. M. McWhirter, K. L. Faia, D. C. Rowe, E. Latz, D. T. Golenbock, A. J. Coyle, S. M. Liao, and T. Maniatis. 2003. 'IKKepsilon and TBK1 are essential components of the IRF3 signaling pathway', *Nat Immunol*, 4: 491-6.

Flick, R., and G. Hobom. 1999. 'Interaction of influenza virus polymerase with viral RNA in the 'corkscrew' conformation', *J Gen Virol*, 80 (Pt 10): 2565-72.

Fodor, E. 2013. 'The RNA polymerase of influenza a virus: mechanisms of viral transcription and replication', *Acta Virol*, 57: 113-22.

Fodor, E., D. C. Pritlove, and G. G. Brownlee. 1994. 'The influenza virus panhandle is involved in the initiation of transcription', *J Virol*, 68: 4092-6.

Fodor, E., and M. Smith. 2004. 'The PA subunit is required for efficient nuclear accumulation of the PB1 subunit of the influenza A virus RNA polymerase complex', *J Virol*, 78: 9144-53.

Fortes, P., A. I. Lamond, and J. Ortin. 1995. 'Influenza virus NS1 protein alters the subnuclear localization of cellular splicing components', *J Gen Virol*, 76 (Pt 4): 1001-7.

Fournier, G., C. Chiang, S. Munier, A. Tomoiu, C. Demeret, P. O. Vidalain, Y. Jacob, and N. Naffakh. 2014. 'Recruitment of RED-SMU1 complex by Influenza A Virus RNA polymerase to control Viral mRNA splicing', *PLoS Pathog*, 10: e1004164.

Fujii, Y., H. Goto, T. Watanabe, T. Yoshida, and Y. Kawaoka. 2003. 'Selective incorporation of influenza virus RNA segments into virions', *Proc Natl Acad Sci U S A*, 100: 2002-7.

Furuse, Y., A. Suzuki, and H. Oshitani. 2009. 'Large-scale sequence analysis of M gene of influenza A viruses from different species: mechanisms for emergence and spread of amantadine resistance', *Antimicrob Agents Chemother*, 53: 4457-63.

Gabriel, G., M. Abram, B. Keiner, R. Wagner, H. D. Klenk, and J. Stech. 2007. 'Differential polymerase activity in avian and mammalian cells determines host range of influenza virus', *J Virol*, 81: 9601-4.

Gack, M. U., R. A. Albrecht, T. Urano, K. S. Inn, I. C. Huang, E. Carnero, M. Farzan, S. Inoue, J. U. Jung, and A. Garcia-Sastre. 2009. 'Influenza A virus NS1 targets the ubiquitin ligase TRIM25 to evade recognition by the host viral RNA sensor RIG-I', *Cell Host Microbe*, 5: 439-49.

Gack, M. U., Y. C. Shin, C. H. Joo, T. Urano, C. Liang, L. Sun, O. Takeuchi, S. Akira, Z. Chen, S. Inoue, and J. U. Jung. 2007. 'TRIM25 RING-finger E3 ubiquitin ligase is essential for RIG-I-mediated antiviral activity', *Nature*, 446: 916-20.

Gale, M., Jr., and M. G. Katze. 1998. 'Molecular mechanisms of interferon resistance mediated by viral-directed inhibition of PKR, the interferon-induced protein kinase', *Pharmacol Ther*, 78: 29-46.

Gao, H., H. Sun, J. Hu, L. Qi, J. Wang, X. Xiong, Y. Wang, Q. He, Y. Lin, W. Kong, L. G. Seng, J. Pu, K. C. Chang, X. Liu, J. Liu, and Y. Sun. 2015a. 'Twenty amino acids at the C-terminus of PA-X are associated with increased influenza A virus replication and pathogenicity', *J Gen Virol*, 96: 2036-49.

Gao, H., Y. Sun, J. Hu, L. Qi, J. Wang, X. Xiong, Y. Wang, Q. He, Y. Lin, W. Kong, L. G. Seng, H. Sun, J. Pu, K. C. Chang, X. Liu, and J. Liu. 2015b. 'The contribution of PA-X to the virulence of pandemic 2009 H1N1 and highly pathogenic H5N1 avian influenza viruses', *Sci Rep*, 5: 8262.

Gao, H., G. Xu, Y. Sun, L. Qi, J. Wang, W. Kong, H. Sun, J. Pu, K. C. Chang, and J. Liu. 2015c. 'PA-X is a virulence factor in avian H9N2 influenza virus', *J Gen Virol*, 96: 2587-94.

Garaigorta, U., and J. Ortin. 2007. 'Mutation analysis of a recombinant NS replicon shows that influenza virus NS1 protein blocks the splicing and nucleo-cytoplasmic transport of its own viral mRNA', *Nucleic Acids Res*, 35: 4573-82.

Garcia-Sastre, A. 2011. 'Induction and evasion of type I interferon responses by influenza viruses', *Virus Res*, 162: 12-8.

Gard, S., and P. von Magnus. 1947. 'Studies on Interference in Experimental Influenza .2. Purification and Centrifugation Experiments', *Arkiv for Kemi Mineralogi Och Geologi*, 24: 1-4.

Gaush, C. R., W. L. Hard, and T. F. Smith. 1966. 'Characterization of an established line of canine kidney cells (MDCK)', *Proc Soc Exp Biol Med*, 122: 931-5.

Gaush, C. R., and T. F. Smith. 1968. 'Replication and plaque assay of influenza virus in an established line of canine kidney cells', *Appl Microbiol*, 16: 588-94.

Gavazzi, C., M. Yver, C. Isel, R. P. Smyth, M. Rosa-Calatrava, B. Lina, V. Moules, and R. Marquet. 2013. 'A functional sequence-specific interaction between influenza A virus genomic RNA segments', *Proc Natl Acad Sci U S A*, 110: 16604-9.

Gerber, M., C. Isel, V. Moules, and R. Marquet. 2014. 'Selective packaging of the influenza A genome and consequences for genetic reassortment', *Trends Microbiol*, 22: 446-55.

Giard, D. J., S. A. Aaronson, G. J. Todaro, P. Arnstein, J. H. Kersey, H. Dosik, and W. P. Parks. 1973. 'In vitro cultivation of human tumors: establishment of cell lines derived from a series of solid tumors', *J Natl Cancer Inst*, 51: 1417-23.

Gibbs, J. S., D. Malide, F. Hornung, J. R. Bennink, and J. W. Yewdell. 2003. 'The influenza A virus PB1-F2 protein targets the inner mitochondrial membrane via a predicted basic amphipathic helix that disrupts mitochondrial function', *J Virol*, 77: 7214-24.

Gnirss, K., P. Zmora, P. Blazejewska, M. Winkler, A. Lins, I. Nehlmeier, S. Gartner, A. S. Moldenhauer, H. Hofmann-Winkler, T. Wolff, M. Schindler, and S. Pohlmann. 2015. 'Tetherin Sensitivity of Influenza A Viruses Is Strain Specific: Role of Hemagglutinin and Neuraminidase', *J Virol*, 89: 9178-88.

Gog, J. R., S. Afonso Edos, R. M. Dalton, I. Leclercq, L. Tiley, D. Elton, J. C. von Kirchbach, N. Naffakh, N. Escriou, and P. Digard. 2007. 'Codon conservation in the influenza A virus genome defines RNA packaging signals', *Nucleic Acids Res*, 35: 1897-907.

Gomez-Puertas, P., C. Albo, E. Perez-Pastrana, A. Vivo, and A. Portela. 2000. 'Influenza virus matrix protein is the major driving force in virus budding', *J Virol*, 74: 11538-47.

Gong, Y. N., G. W. Chen, C. J. Chen, R. L. Kuo, and S. R. Shih. 2014. 'Computational analysis and mapping of novel open reading frames in influenza A viruses', *PLoS One*, 9: e115016.

Gonzalez, S., and J. Ortin. 1999. 'Characterization of influenza virus PB1 protein binding to viral RNA: two separate regions of the protein contribute to the interaction domain', *J Virol*, 73: 631-7.

Gonzalez, S., T. Zurcher, and J. Ortin. 1996. 'Identification of two separate domains in the influenza virus PB1 protein involved in the interaction with the PB2 and PA subunits: a model for the viral RNA polymerase structure', *Nucleic Acids Res*, 24: 4456-63.

Gottschalk, A. 1959. 'On the mechanism underlying initiation of influenza virus infection', *Ergeb Mikrobiol Immunitatsforsch Exp Ther*, 32: 1-22.

Goujon, C., O. Moncorge, H. Bauby, T. Doyle, C. C. Ward, T. Schaller, S. Hue, W. S. Barclay, R. Schulz, and M. H. Malim. 2013. 'Human MX2 is an interferon-induced post-entry inhibitor of HIV-1 infection', *Nature*, 502: 559-62.

Graef, K. M., F. T. Vreede, Y. F. Lau, A. W. McCall, S. M. Carr, K. Subbarao, and E. Fodor. 2010. 'The PB2 subunit of the influenza virus RNA polymerase affects virulence by interacting with the mitochondrial antiviral signaling protein and inhibiting expression of beta interferon', *J Virol*, 84: 8433-45.

Grandvaux, N., M. J. Servant, B. tenOever, G. C. Sen, S. Balachandran, G. N. Barber, R. Lin, and J. Hiscott. 2002. 'Transcriptional profiling of interferon regulatory factor 3 target genes: direct involvement in the regulation of interferon-stimulated genes', *J Virol*, 76: 5532-9.

Grimm, D., P. Staeheli, M. Hufbauer, I. Koerner, L. Martinez-Sobrido, A. Solorzano, A. Garcia-Sastre, O. Haller, and G. Kochs. 2007. 'Replication fitness determines high virulence of influenza A virus in mice carrying functional Mx1 resistance gene', *Proc Natl Acad Sci U S A*, 104: 6806-11.

Guo, Z., L. M. Chen, H. Zeng, J. A. Gomez, J. Plowden, T. Fujita, J. M. Katz, R. O. Donis, and S. Sambhara. 2007. 'NS1 protein of influenza A virus inhibits the function of intracytoplasmic pathogen sensor, RIG-I', *Am J Respir Cell Mol Biol*, 36: 263-9.

Hacker, H., V. Redecke, B. Blagoev, I. Kratchmarova, L. C. Hsu, G. G. Wang, M. P. Kamps, E. Raz, H. Wagner, G. Hacker, M. Mann, and M. Karin. 2006. 'Specificity in Toll-like receptor signalling through distinct effector functions of TRAF3 and TRAF6', *Nature*, 439: 204-7.

Hagmaier, K., N. Stock, S. Goodbourn, L. F. Wang, and R. Randall. 2006. 'A single amino acid substitution in the V protein of Nipah virus alters its ability to block interferon signalling in cells from different species', *J Gen Virol*, 87: 3649-53.

Hai, R., M. Schmolke, Z. T. Varga, B. Manicassamy, T. T. Wang, J. A. Belser, M. B. Pearce, A. Garcia-Sastre, T. M. Tumpey, and P. Palese. 2010. 'PB1-F2 expression by the 2009 pandemic H1N1 influenza virus has minimal impact on virulence in animal models', *J Virol*, 84: 4442-50.

Hale, B. G., R. E. Randall, J. Ortin, and D. Jackson. 2008. 'The multifunctional NS1 protein of influenza A viruses', *J Gen Virol*, 89: 2359-76.

Hale, B. G., J. Steel, R. A. Medina, B. Manicassamy, J. Ye, D. Hickman, R. Hai, M. Schmolke, A. C. Lowen, D. R. Perez, and A. Garcia-Sastre. 2010. 'Inefficient control of host gene expression by the 2009 pandemic H1N1 influenza A virus NS1 protein', *J Virol*, 84: 6909-22.

Haller, O., H. Arnheiter, J. Lindenmann, and I. Gresser. 1980. 'Host gene influences sensitivity to interferon action selectively for influenza virus', *Nature*, 283: 660-2.

Haller, O., P. Staeheli, and G. Kochs. 2009. 'Protective role of interferon-induced Mx GTPases against influenza viruses', *Rev Sci Tech*, 28: 219-31.

Hao, L., A. Sakurai, T. Watanabe, E. Sorensen, C. A. Nidom, M. A. Newton, P. Ahlquist, and Y. Kawaoka. 2008. 'Drosophila RNAi screen identifies host genes important for influenza virus replication', *Nature*, 454: 890-3.

Harman, A. N., N. Nasr, A. Feetham, A. Galoyan, A. A. Alshehri, D. Rambukwelle, R. A. Botting, B. M. Hiener, E. Diefenbach, R. J. Diefenbach, M. Kim, A. Mansell, and A. L. Cunningham. 2015. 'HIV Blocks Interferon Induction in Human Dendritic Cells and Macrophages by Dysregulation of TBK1', *J Virol*, 89: 6575-84.

Harte, M. T., I. R. Haga, G. Maloney, P. Gray, P. C. Reading, N. W. Bartlett, G. L. Smith, A. Bowie, and L. A. O'Neill. 2003. 'The poxvirus protein A52R targets Toll-like receptor signaling complexes to suppress host defense', *J Exp Med*, 197: 343-51.

Hartig, S. M. 2013. 'Basic image analysis and manipulation in ImageJ', *Curr Protoc Mol Biol*, Chapter 14: Unit14 15.

Hatada, E., and R. Fukuda. 1992. 'Binding of influenza A virus NS1 protein to dsRNA in vitro', *J Gen Virol*, 73 (Pt 12): 3325-9.

Hay, A. J., B. Lomniczi, A. R. Bellamy, and J. J. Skehel. 1977. 'Transcription of the influenza virus genome', *Virology*, 83: 337-55.

Hay, A. J., J. J. Skehel, and J. McCauley. 1980. 'Structure and synthesis of influenza virus complementary RNAs', *Philos Trans R Soc Lond B Biol Sci*, 288: 341-8.

Hayden, F. G., N. Sugaya, N. Hirotsu, N. Lee, M. D. de Jong, A. C. Hurt, T. Ishida, H. Sekino, K. Yamada, S. Portsmouth, K. Kawaguchi, T. Shishido, M. Arai, K. Tsuchiya, T. Uehara, A. Watanabe, and Group Baloxavir Marboxil Investigators. 2018. 'Baloxavir Marboxil for Uncomplicated Influenza in Adults and Adolescents', *N Engl J Med*, 379: 913-23.

He, X., J. Zhou, M. Bartlam, R. Zhang, J. Ma, Z. Lou, X. Li, J. Li, A. Joachimiak, Z. Zeng, R. Ge, Z. Rao, and Y. Liu. 2008. 'Crystal structure of the polymerase PA(C)-PB1(N) complex from an avian influenza H5N1 virus', *Nature*, 454: 1123-6.

Herold, A., M. Suyama, J. P. Rodrigues, I. C. Braun, U. Kutay, M. Carmo-Fonseca, P. Bork, and E. Izaurralde. 2000. 'TAP (NXF1) belongs to a multigene family of putative RNA export factors with a conserved modular architecture', *Mol Cell Biol*, 20: 8996-9008.

Herz, C., E. Stavnezer, R. Krug, and T. Gurney, Jr. 1981. 'Influenza virus, an RNA virus, synthesizes its messenger RNA in the nucleus of infected cells', *Cell*, 26: 391-400.

Hilton, L., K. Moganeradj, G. Zhang, Y. H. Chen, R. E. Randall, J. W. McCauley, and S. Goodbourn. 2006. 'The NPro product of bovine viral diarrhea virus inhibits DNA binding by interferon regulatory factor 3 and targets it for proteasomal degradation', *J Virol*, 80: 11723-32.

Himly, M., D. N. Foster, I. Bottoli, J. S. Iacovoni, and P. K. Vogt. 1998. 'The DF-1 chicken fibroblast cell line: transformation induced by diverse oncogenes and cell death resulting from infection by avian leukosis viruses', *Virology*, 248: 295-304.

Hiscott, J., R. Lin, P. Nakhaei, and S. Paz. 2006. 'MasterCARD: a priceless link to innate immunity', *Trends Mol Med*, 12: 53-6.

Hoffmann, E., G. Neumann, Y. Kawaoka, G. Hobom, and R. G. Webster. 2000. 'A DNA transfection system for generation of influenza A virus from eight plasmids', *Proc Natl Acad Sci U S A*, 97: 6108-13.

Holm, C. K., S. H. Rahbek, H. H. Gad, R. O. Bak, M. R. Jakobsen, Z. Jiang, A. L. Hansen, S. K. Jensen, C. Sun, M. K. Thomsen, A. Laustsen, C. G. Nielsen, K. Severinsen, Y. Xiong, D. L. Burdette, V. Hornung, R. J. Lebbink, M. Duch, K. A. Fitzgerald, S. Bahrami, J. G. Mikkelsen, R. Hartmann, and S. R. Paludan. 2016. 'Influenza A virus targets a cGAS-independent STING pathway that controls enveloped RNA viruses', *Nat Commun*, 7: 10680.

Honda, K., H. Yanai, T. Mizutani, H. Negishi, N. Shimada, N. Suzuki, Y. Ohba, A. Takaoka, W. C. Yeh, and T. Taniguchi. 2004. 'Role of a transductional-transcriptional processor complex involving MyD88 and IRF-7 in Toll-like receptor signaling', *Proc Natl Acad Sci U S A*, 101: 15416-21.

Honda, K., H. Yanai, H. Negishi, M. Asagiri, M. Sato, T. Mizutani, N. Shimada, Y. Ohba, A. Takaoka, N. Yoshida, and T. Taniguchi. 2005. 'IRF-7 is the master regulator of type-I interferon-dependent immune responses', *Nature*, 434: 772-7.

Horai, R., S. Saijo, H. Tanioka, S. Nakae, K. Sudo, A. Okahara, T. Ikuse, M. Asano, and Y. Iwakura. 2000. 'Development of chronic inflammatory arthropathy resembling rheumatoid arthritis in interleukin 1 receptor antagonist-deficient mice', *J Exp Med*, 191: 313-20.

Hsu, M. T., J. D. Parvin, S. Gupta, M. Krystal, and P. Palese. 1987. 'Genomic RNAs of influenza viruses are held in a circular conformation in virions and in infected cells by a terminal panhandle', *Proc Natl Acad Sci U S A*, 84: 8140-4.

Hu, J., Y. Mo, X. Wang, M. Gu, Z. Hu, L. Zhong, Q. Wu, X. Hao, S. Hu, W. Liu, H. Liu, X. Liu, and X. Liu. 2015. 'PA-X decreases the pathogenicity of highly pathogenic H5N1 influenza A virus in avian species by inhibiting virus replication and host response', *J Virol*, 89: 4126-42.

Huang, A. S., and D. Baltimore. 1970. 'Defective viral particles and viral disease processes', *Nature*, 226: 325-7.

Huang, I. C., C. C. Bailey, J. L. Weyer, S. R. Radoshitzky, M. M. Becker, J. J. Chiang, A. L. Brass, A. A. Ahmed, X. Chi, L. Dong, L. E. Longobardi, D. Boltz, J. H. Kuhn, S. J. Elledge, S. Bavari, M. R. Denison, H. Choe, and M. Farzan. 2011. 'Distinct patterns of IFITM-mediated restriction of filoviruses, SARS coronavirus, and influenza A virus', *PLoS Pathog*, 7: e1001258.

Huang, T. S., P. Palese, and M. Krystal. 1990. 'Determination of influenza virus proteins required for genome replication', *J Virol*, 64: 5669-73.

Hughey, P. G., R. W. Compans, S. L. Zebedee, and R. A. Lamb. 1992. 'Expression of the influenza A virus M2 protein is restricted to apical surfaces of polarized epithelial cells', *J Virol*, 66: 5542-52.

Hussain, S., M. L. Turnbull, H. M. Wise, B. W. Jagger, P. M. Beard, K. Kovacikova, J. K. Taubenberger, L. Vervelde, O. G. Engelhardt, and P. Digard. 2018. 'Mutation of influenza A virus PA-X decreases pathogenicity in chicken embryos and can increase the yield of reassortant candidate vaccine viruses', *J Virol*.

Hutchinson, E. C., P. D. Charles, S. S. Hester, B. Thomas, D. Trudgian, M. Martinez-Alonso, and E. Fodor. 2014. 'Conserved and host-specific features of influenza virion architecture', *Nat Commun*, 5: 4816.

Hutchinson, E. C., M. D. Curran, E. K. Read, J. R. Gog, and P. Digard. 2008. 'Mutational analysis of cis-acting RNA signals in segment 7 of influenza A virus', *J Virol*, 82: 11869-79.

Hutchinson, E. C., and E. Fodor. 2013. 'Transport of the influenza virus genome from nucleus to nucleus', *Viruses*, 5: 2424-46.

Hutchinson, E. C., J. C. von Kirchbach, J. R. Gog, and P. Digard. 2010. 'Genome packaging in influenza A virus', *J Gen Virol*, 91: 313-28.

Ikutani, M., T. Yanagibashi, M. Ogasawara, K. Tsuneyama, S. Yamamoto, Y. Hattori, T. Kouro, A. Itakura, Y. Nagai, S. Takaki, and K. Takatsu. 2012. 'Identification of innate IL-5-producing cells and their role in lung eosinophil regulation and antitumor immunity', *J Immunol*, 188: 703-13.

Isaacs, A., and S. Baron. 1960. 'Antiviral action of interferon in embryonic cells', *Lancet*, 2: 946-7.

Isaacs, A., and J. Lindenmann. 1957. 'Virus interference. I. The interferon', *Proc R Soc Lond B Biol Sci*, 147: 258-67.

Iwai, A., T. Shiozaki, T. Kawai, S. Akira, Y. Kawaoka, A. Takada, H. Kida, and T. Miyazaki. 2010. 'Influenza A virus polymerase inhibits type I interferon induction by binding to interferon beta promoter stimulator 1', *J Biol Chem*, 285: 32064-74.

Iwamura, T., M. Yoneyama, K. Yamaguchi, W. Suhara, W. Mori, K. Shiota, Y. Okabe, H. Namiki, and T. Fujita. 2001. 'Induction of IRF-3/-7 kinase and NF-kappaB in response to double-stranded RNA and virus infection: common and unique pathways', *Genes Cells*, 6: 375-88.

Iwasaki, A., and P. S. Pillai. 2014. 'Innate immunity to influenza virus infection', *Nat Rev Immunol*, 14: 315-28.

Jackson, D. A., A. J. Caton, S. J. McCready, and P. R. Cook. 1982. 'Influenza virus RNA is synthesized at fixed sites in the nucleus', *Nature*, 296: 366-8.

Jackson, D., and R. A. Lamb. 2008. 'The influenza A virus spliced messenger RNA M mRNA3 is not required for viral replication in tissue culture', *J Gen Virol*, 89: 3097-101.

Jagger, B. W., H. M. Wise, J. C. Kash, K. A. Walters, N. M. Wills, Y. L. Xiao, R. L. Dunfee, L. M. Schwartzman, A. Ozinsky, G. L. Bell, R. M. Dalton, A. Lo, S. Efstathiou, J. F. Atkins, A. E. Firth, J. K. Taubenberger, and P. Digard. 2012. 'An overlapping protein-coding region in influenza A virus segment 3 modulates the host response', *Science*, 337: 199-204.

James, J., W. Howard, M. Iqbal, V. K. Nair, W. S. Barclay, and H. Shelton. 2016. 'Influenza A virus PB1-F2 protein prolongs viral shedding in chickens lengthening the transmission window', *J Gen Virol*, 97: 2516-27.

Jeisy-Scott, V., J. H. Kim, W. G. Davis, W. Cao, J. M. Katz, and S. Sambhara. 2012. 'TLR7 recognition is dispensable for influenza virus A infection but important for the induction of hemagglutinin-specific antibodies in response to the 2009 pandemic split vaccine in mice', *J Virol*, 86: 10988-98.

Jennings, P. A., J. T. Finch, G. Winter, and J. S. Robertson. 1983. 'Does the higher order structure of the influenza virus ribonucleoprotein guide sequence rearrangements in influenza viral RNA?', *Cell*, 34: 619-27.

Jiao, P., G. Tian, Y. Li, G. Deng, Y. Jiang, C. Liu, W. Liu, Z. Bu, Y. Kawaoka, and H. Chen. 2008. 'A single-amino-acid substitution in the NS1 protein changes the pathogenicity of H5N1 avian influenza viruses in mice', *J Virol*, 82: 1146-54.

Johnson, C. A., D. J. Pekas, and R. J. Winzler. 1964. 'Neuraminidases and Influenza Virus Infection in Embryonated Eggs', *Science*, 143: 1051-2.

Jorba, N., R. Coloma, and J. Ortin. 2009. 'Genetic trans-complementation establishes a new model for influenza virus RNA transcription and replication', *PLoS Pathog*, 5: e1000462.

Jose, P. J., D. A. Griffiths-Johnson, P. D. Collins, D. T. Walsh, R. Moqbel, N. F. Totty, O. Truong, J. J. Hsuan, and T. J. Williams. 1994. 'Eotaxin: a potent eosinophil chemoattractant cytokine detected in a guinea pig model of allergic airways inflammation', *J Exp Med*, 179: 881-7.

Joseph, U., Y. C. Su, D. Vijaykrishna, and G. J. Smith. 2017. 'The ecology and adaptive evolution of influenza A interspecies transmission', *Influenza Other Respir Viruses*, 11: 74-84.

Josset, L., E. Frobert, and M. Rosa-Calatrava. 2008. 'Influenza A replication and host nuclear compartments: many changes and many questions', *J Clin Virol*, 43: 381-90.

Kamal, R. P., I. V. Alymova, and I. A. York. 2017. 'Evolution and Virulence of Influenza A Virus Protein PB1-F2', *Int J Mol Sci*, 19.

Kamal, R. P., A. Kumar, C. T. Davis, W. P. Tzeng, T. Nguyen, R. O. Donis, J. M. Katz, and I. A. York. 2015. 'Emergence of Highly Pathogenic Avian Influenza A(H5N1) Virus PB1-F2 Variants and Their Virulence in BALB/c Mice', *J Virol*, 89: 5835-46.

Kaminuma, O., A. Mori, N. Kitamura, T. Hashimoto, F. Kitamura, S. Inokuma, and S. Miyatake. 2005. 'Role of GATA-3 in IL-5 gene transcription by CD4+ T cells of asthmatic patients', *Int Arch Allergy Immunol*, 137 Suppl 1: 55-9.

Karakus, U., T. Thamamongood, K. Ciminski, W. Ran, S. C. Gunther, M. O. Pohl, D. Eletto, C. Jeney, D. Hoffmann, S. Reiche, J. Schinkothe, R. Ulrich, J. Wiener, M. G. B. Hayes, M. W. Chang, A. Hunziker, E. Yanguez, T. Aydillo, F. Krammer, J. Oderbolz, M. Meier, A. Oxenius, A. Halenius, G. Zimmer, C. Benner, B. G. Hale, A. Garcia-Sastre, M. Beer, M. Schwemmle, and S. Stertz. 2019. 'MHC class II proteins mediate cross-species entry of bat influenza viruses', *Nature*, 567: 109-12.

Karpala, A. J., C. Stewart, J. McKay, J. W. Lowenthal, and A. G. Bean. 2011. 'Characterization of chicken Mda5 activity: regulation of IFN-beta in the absence of RIG-I functionality', *J Immunol*, 186: 5397-405.

Kato, H., O. Takeuchi, S. Sato, M. Yoneyama, M. Yamamoto, K. Matsui, S. Uematsu, A. Jung, T. Kawai, K. J. Ishii, O. Yamaguchi, K. Otsu, T. Tsujimura, C. S. Koh, C. Reis e Sousa, Y. Matsuura, T. Fujita, and S. Akira. 2006. 'Differential roles of MDA5 and RIG-I helicases in the recognition of RNA viruses', *Nature*, 441: 101-5.

Kawaguchi, A., K. Matsumoto, and K. Nagata. 2012. 'YB-1 functions as a porter to lead influenza virus ribonucleoprotein complexes to microtubules', *J Virol*, 86: 11086-95.

Kawaguchi, A., and K. Nagata. 2007. 'De novo replication of the influenza virus RNA genome is regulated by DNA replicative helicase, MCM', *EMBO J*, 26: 4566-75.

Kawai, T., S. Sato, K. J. Ishii, C. Coban, H. Hemmi, M. Yamamoto, K. Terai, M. Matsuda, J. Inoue, S. Uematsu, O. Takeuchi, and S. Akira. 2004. 'Interferon-alpha induction through Toll-like receptors involves a direct interaction of IRF7 with MyD88 and TRAF6', *Nat Immunol*, 5: 1061-8.

Kawaoka, Y., S. Krauss, and R. G. Webster. 1989. 'Avian-to-human transmission of the PB1 gene of influenza A viruses in the 1957 and 1968 pandemics', *J Virol*, 63: 4603-8.

Kawaoka, Y., and R. G. Webster. 1985. 'Evolution of the A/Chicken/Pennsylvania/83 (H5N2) influenza virus', *Virology*, 146: 130-7.

Kawasaki, T., and T. Kawai. 2014. 'Toll-like receptor signaling pathways', *Front Immunol*, 5: 461.

Kawasaki, T., and T. Kawai. 2019. 'Discrimination Between Self and Non-Self-Nucleic Acids by the Innate Immune System', *Int Rev Cell Mol Biol*, 344: 1-30.

Khaperskyy, D. A., and C. McCormick. 2015. 'Timing Is Everything: Coordinated Control of Host Shutoff by Influenza A Virus NS1 and PA-X Proteins', *J Virol*, 89: 6528-31.

Khaperskyy, D. A., S. Schmaling, J. Larkins-Ford, C. McCormick, and M. M. Gaglia. 2016. 'Selective Degradation of Host RNA Polymerase II Transcripts by Influenza A Virus PA-X Host Shutoff Protein', *PLoS Pathog*, 12: e1005427.

Killip, M. J., E. Fodor, and R. E. Randall. 2015. 'Influenza virus activation of the interferon system', *Virus Res*, 209: 11-22.

Kim, J. C., S. Y. Lee, S. Y. Kim, J. K. Kim, H. J. Kim, H. M. Lee, M. S. Choi, J. S. Min, M. J. Kim, H. S. Choi, and J. K. Ahn. 2008. 'HSV-1 ICP27 suppresses NF-kappaB activity by stabilizing IkappaBalpha', *FEBS Lett*, 582: 2371-6.

Kim, T. K., and T. Maniatis. 1997. 'The mechanism of transcriptional synergy of an in vitro assembled interferon-beta enhanceosome', *Mol Cell*, 1: 119-29.

King, P., and S. Goodbourn. 1994. 'The beta-interferon promoter responds to priming through multiple independent regulatory elements', *J Biol Chem*, 269: 30609-15.

King, P., and S. Goodbourn. 1998. 'STAT1 is inactivated by a caspase', *J Biol Chem*, 273: 8699-704.

Klumpp, K., R. W. Ruigrok, and F. Baudin. 1997. 'Roles of the influenza virus polymerase and nucleoprotein in forming a functional RNP structure', *EMBO J*, 16: 1248-57.

Kobayashi, Y., B. Dadonaite, N. van Doremalen, Y. Suzuki, W. S. Barclay, and O. G. Pybus. 2016. 'Computational and molecular analysis of conserved influenza A virus RNA secondary structures involved in infectious virion production', *RNA Biol*, 13: 883-94.

Kochs, G., A. Garcia-Sastre, and L. Martinez-Sobrido. 2007. 'Multiple anti-interferon actions of the influenza A virus NS1 protein', *J Virol*, 81: 7011-21.

Kolekar, P., A. Pataskar, U. Kulkarni-Kale, J. Pal, and A. Kulkarni. 2016. 'IRESPred: Web Server for Prediction of Cellular and Viral Internal Ribosome Entry Site (IRES)', *Sci Rep*, 6: 27436.

Koliopoulos, M. G., M. Lethier, A. G. van der Veen, K. Haubrich, J. Hennig, E. Kowalinski, R. V. Stevens, S. R. Martin, C. Reis e Sousa, S. Cusack, and K. Rittinger. 2018. 'Molecular mechanism of influenza A NS1-mediated TRIM25 recognition and inhibition', *Nat Commun*, 9: 1820.

Kosik, I., J. Holly, and G. Russ. 2013. 'PB1-F2 expedition from the whole protein through the domain to aa residue function', *Acta Virol*, 57: 138-48.

Kouro, T., and K. Takatsu. 2009. 'IL-5- and eosinophil-mediated inflammation: from discovery to therapy', *Int Immunol*, 21: 1303-9.

Kozak, M. 1986. 'Point mutations define a sequence flanking the AUG initiator codon that modulates translation by eukaryotic ribosomes', *Cell*, 44: 283-92.

Krammer, F., G. J. D. Smith, R. A. M. Fouchier, M. Peiris, K. Kedzierska, P. C. Doherty, P. Palese, M. L. Shaw, J. Treanor, R. G. Webster, and A. Garcia-Sastre. 2018. 'Influenza', *Nat Rev Dis Primers*, 4: 3.

Krug, R. M. 2015. 'Functions of the influenza A virus NS1 protein in antiviral defense', *Curr Opin Virol*, 12: 1-6.

Kudryavtseva, K. 2014. 'Genome packaging in influenza A virus', PhD Thesis, University of Cambridge.

Kumar, A., J. Haque, J. Lacoste, J. Hiscott, and B. R. Williams. 1994. 'Double-stranded RNA-dependent protein kinase activates transcription factor NF-kappa B by phosphorylating I kappa B', *Proc Natl Acad Sci U S A*, 91: 6288-92.

Kundu, A., R. T. Avalos, C. M. Sanderson, and D. P. Nayak. 1996. 'Transmembrane domain of influenza virus neuraminidase, a type II protein, possesses an apical sorting signal in polarized MDCK cells', *J Virol*, 70: 6508-15.

Kuniyoshi, K., O. Takeuchi, S. Pandey, T. Satoh, H. Iwasaki, S. Akira, and T. Kawai. 2014. 'Pivotal role of RNA-binding E3 ubiquitin ligase MEX3C in RIG-I-mediated antiviral innate immunity', *Proc Natl Acad Sci U S A*, 111: 5646-51.

Kuo, R. L., L. H. Li, S. J. Lin, Z. H. Li, G. W. Chen, C. K. Chang, Y. R. Wang, E. H. Tam, Y. N. Gong, R. M. Krug, and S. R. Shih. 2016. 'Role of N Terminus-Truncated NS1 Proteins of Influenza A Virus in Inhibiting IRF3 Activation', *J Virol*, 90: 4696-705.

Kuo, R. L., C. Zhao, M. Malur, and R. M. Krug. 2010. 'Influenza A virus strains that circulate in humans differ in the ability of their NS1 proteins to block the activation of IRF3 and interferon-beta transcription', *Virology*, 408: 146-58.

Kutay, U., F. R. Bischoff, S. Kostka, R. Kraft, and D. Gorlich. 1997. 'Export of importin alpha from the nucleus is mediated by a specific nuclear transport factor', *Cell*, 90: 1061-71.

Lakadamyali, M., M. J. Rust, H. P. Babcock, and X. Zhuang. 2003. 'Visualizing infection of individual influenza viruses', *Proc Natl Acad Sci U S A*, 100: 9280-5.

Lamb, R. A., and P. W. Choppin. 1979. 'Segment 8 of the influenza virus genome is unique in coding for two polypeptides', *Proc Natl Acad Sci U S A*, 76: 4908-12.

Lamb, R. A., and P. W. Choppin. 1981. 'Identification of a second protein (M2) encoded by RNA segment 7 of influenza virus', *Virology*, 112: 729-37.

Lamb, R. A., P. W. Choppin, R. M. Chanock, and C. J. Lai. 1980. 'Mapping of the two overlapping genes for polypeptides NS1 and NS2 on RNA segment 8 of influenza virus genome', *Proc Natl Acad Sci U S A*, 77: 1857-61.

Lamb, R. A., P. R. Etkind, and P. W. Choppin. 1978. 'Evidence for a ninth influenza viral polypeptide', *Virology*, 91: 60-78.

Lamb, R. A., and C. J. Lai. 1980. 'Sequence of interrupted and uninterrupted mRNAs and cloned DNA coding for the two overlapping nonstructural proteins of influenza virus', *Cell*, 21: 475-85.

Lamb, R. A., C. J. Lai, and P. W. Choppin. 1981. 'Sequences of mRNAs derived from genome RNA segment 7 of influenza virus: colinear and interrupted mRNAs code for overlapping proteins', *Proc Natl Acad Sci U S A*, 78: 4170-4.

Landeras-Bueno, S., N. Jorba, M. Perez-Cidoncha, and J. Ortin. 2011. 'The splicing factor proline-glutamine rich (SFPQ/PSF) is involved in influenza virus transcription', *PLoS Pathog*, 7: e1002397.

Le Goffic, R., J. Pothlichet, D. Vitour, T. Fujita, E. Meurs, M. Chignard, and M. Si-Tahar. 2007. 'Cutting Edge: Influenza A virus activates TLR3-dependent inflammatory and RIG-I-dependent antiviral responses in human lung epithelial cells', *J Immunol*, 178: 3368-72.

Lee, J., H. Yu, Y. Li, J. Ma, Y. Lang, M. Duff, J. Henningson, Q. Liu, Y. Li, A. Nagy, B. Bawa, Z. Li, G. Tong, J. A. Richt, and W. Ma. 2017. 'Impacts of different expressions of PA-X protein on 2009 pandemic H1N1 virus replication, pathogenicity and host immune responses', *Virology*, 504: 25-35.

Leser, G. P., and R. A. Lamb. 2005. 'Influenza virus assembly and budding in raft-derived microdomains: a quantitative analysis of the surface distribution of HA, NA and M2 proteins', *Virology*, 342: 215-27.

Leung, Y. H., J. M. Nicholls, C. K. Ho, S. F. Sia, C. K. Mok, S. A. Valkenburg, P. Cheung, K. P. Hui, R. W. Chan, Y. Guan, S. Akira, and J. S. Peiris. 2014. 'Highly pathogenic avian influenza A H5N1 and pandemic H1N1 virus infections have different phenotypes in Toll-like receptor 3 knockout mice', *J Gen Virol*, 95: 1870-9.

Leymarie, O., C. Embury-Hyatt, C. Chevalier, L. Jouneau, M. Moroldo, B. Da Costa, Y. Berhane, B. Delmas, H. M. Weingartl, and R. Le Goffic. 2014. 'PB1-F2 attenuates virulence of highly pathogenic avian H5N1 influenza virus in chickens', *PLoS One*, 9: e100679.

Li, C., C. Z. Ni, M. L. Havert, E. Cabezas, J. He, D. Kaiser, J. C. Reed, A. C. Satterthwait, G. Cheng, and K. R. Ely. 2002. 'Downstream regulator TANK binds to the CD40 recognition site on TRAF3', *Structure*, 10: 403-11.

Li, W., H. Chen, T. Sutton, A. Obadan, and D. R. Perez. 2014. 'Interactions between the influenza A virus RNA polymerase components and retinoic acid-inducible gene I', *J Virol*, 88: 10432-47.

Liang, Y., Y. Hong, and T. G. Parslow. 2005. 'cis-Acting packaging signals in the influenza virus PB1, PB2, and PA genomic RNA segments', *J Virol*, 79: 10348-55.

Liang, Y., T. Huang, H. Ly, T. G. Parslow, and Y. Liang. 2008. 'Mutational analyses of packaging signals in influenza virus PA, PB1, and PB2 genomic RNA segments', *J Virol*, 82: 229-36.

Liedmann, S., E. R. Hrincius, D. Anhlan, J. A. McCullers, S. Ludwig, and C. Ehrhardt. 2014a. 'New virulence determinants contribute to the enhanced immune response and reduced virulence of an influenza A virus A/PR8/34 variant', *J Infect Dis*, 209: 532-41.

Liedmann, S., E. R. Hrincius, C. Guy, D. Anhlan, R. Dierkes, R. Carter, G. Wu, P. Staeheli, D. R. Green, T. Wolff, J. A. McCullers, S. Ludwig, and C. Ehrhardt. 2014b. 'Viral suppressors of the RIG-I-mediated interferon response are pre-packaged in influenza virions', *Nat Commun*, 5: 5645.

Liu, G., Y. Lu, Q. Liu, and Y. Zhou. 2019. 'Inhibition of Ongoing Influenza A Virus Replication Reveals Different Mechanisms of RIG-I Activation', *J Virol*, 93.

Liu, G., Y. Lu, S. N. Thulasi Raman, F. Xu, Q. Wu, Z. Li, R. Brownlie, Q. Liu, and Y. Zhou. 2018. 'Nuclear-resident RIG-I senses viral replication inducing antiviral immunity', *Nat Commun*, 9: 3199.

Liu, G., H. S. Park, H. M. Pyo, Q. Liu, and Y. Zhou. 2015. 'Influenza A Virus Panhandle Structure Is Directly Involved in RIG-I Activation and Interferon Induction', *J Virol*, 89: 6067-79.

Liu, T., L. Zhang, D. Joo, and S. C. Sun. 2017. 'NF-kappaB signaling in inflammation', *Signal Transduct Target Ther*, 2.

Lo, C. Y., Y. S. Tang, and P. C. Shaw. 2018. 'Structure and Function of Influenza Virus Ribonucleoprotein', *Subcell Biochem*, 88: 95-128.

Long, J. C., and E. Fodor. 2016. 'The PB2 Subunit of the Influenza A Virus RNA Polymerase Is Imported into the Mitochondrial Matrix', *J Virol*, 90: 8729-38.

Long, J. S., E. S. Giotis, O. Moncorge, R. Frise, B. Mistry, J. James, M. Morisson, M. Iqbal, A. Vignal, M. A. Skinner, and W. S. Barclay. 2016. 'Species difference in ANP32A underlies influenza A virus polymerase host restriction', *Nature*, 529: 101-4.

Lousberg, E. L., C. K. Fraser, M. G. Tovey, K. R. Diener, and J. D. Hayball. 2010. 'Type I interferons mediate the innate cytokine response to recombinant fowlpox virus but not the induction of plasmacytoid dendritic cell-dependent adaptive immunity', *J Virol*, 84: 6549-63.

Ludwig, S., X. Wang, C. Ehrhardt, H. Zheng, N. Donelan, O. Planz, S. Pleschka, A. Garcia-Sastre, G. Heins, and T. Wolff. 2002. 'The influenza A virus NS1 protein inhibits activation of Jun N-terminal kinase and AP-1 transcription factors', *J Virol*, 76: 11166-71.

Luk, G. S., C. Y. Leung, S. F. Sia, K. T. Choy, J. Zhou, C. C. Ho, P. P. Cheung, E. F. Lee, C. K. Wai, P. C. Li, S. M. Ip, L. L. Poon, W. G. Lindsley, M. Peiris, and H. L. Yen. 2015. 'Transmission

of H7N9 Influenza Viruses with a Polymorphism at PB2 Residue 627 in Chickens and Ferrets', *J Virol*, 89: 9939-51.

Lutz, A., J. Dyall, P. D. Olivo, and A. Pekosz. 2005. 'Virus-inducible reporter genes as a tool for detecting and quantifying influenza A virus replication', *J Virol Methods*, 126: 13-20.

Luzina, I. G., A. D. Keegan, N. M. Heller, G. A. Rook, T. Shea-Donohue, and S. P. Atamas. 2012. 'Regulation of inflammation by interleukin-4: a review of "alternatives"', *J Leukoc Biol*, 92: 753-64.

Maeda, T., and S. Ohnishi. 1980. 'Activation of influenza virus by acidic media causes hemolysis and fusion of erythrocytes', *FEBS Lett*, 122: 283-7.

Malathi, K., B. Dong, M. Gale, Jr., and R. H. Silverman. 2007. 'Small self-RNA generated by RNase L amplifies antiviral innate immunity', *Nature*, 448: 816-9.

Malur, M., M. Gale, Jr., and R. M. Krug. 2012. 'LGP2 downregulates interferon production during infection with seasonal human influenza A viruses that activate interferon regulatory factor 3', *J Virol*, 86: 10733-8.

Mankouri, J., R. Fragkoudis, K. H. Richards, L. F. Wetherill, M. Harris, A. Kohl, R. M. Elliott, and A. Macdonald. 2010. 'Optineurin negatively regulates the induction of IFNbeta in response to RNA virus infection', *PLoS Pathog*, 6: e1000778.

Manz, B., L. Brunotte, P. Reuther, and M. Schwemmle. 2012. 'Adaptive mutations in NEP compensate for defective H5N1 RNA replication in cultured human cells', *Nat Commun*, 3: 802.

Marazzi, I., J. S. Ho, J. Kim, B. Manicassamy, S. Dewell, R. A. Albrecht, C. W. Seibert, U. Schaefer, K. L. Jeffrey, R. K. Prinjha, K. Lee, A. Garcia-Sastre, R. G. Roeder, and A. Tarakhovsky. 2012. 'Suppression of the antiviral response by an influenza histone mimic', *Nature*, 483: 428-33.

Marcos-Villar, L., A. Pazo, and A. Nieto. 2016. 'Influenza Virus and Chromatin: Role of the CHD1 Chromatin Remodeler in the Virus Life Cycle', *J Virol*, 90: 3694-707.

Marcus, P. I., J. M. Rojek, and M. J. Sekellick. 2005. 'Interferon induction and/or production and its suppression by influenza A viruses', *J Virol*, 79: 2880-90.

Marion, R. M., T. Zurcher, S. de la Luna, and J. Ortin. 1997. 'Influenza virus NS1 protein interacts with viral transcription-replication complexes in vivo', *J Gen Virol*, 78 (Pt 10): 2447-51.

Marsh, G. A., R. Rabadan, A. J. Levine, and P. Palese. 2008. 'Highly conserved regions of influenza a virus polymerase gene segments are critical for efficient viral RNA packaging', *J Virol*, 82: 2295-304.

Martin, K., and A. Helenius. 1991a. 'Nuclear transport of influenza virus ribonucleoproteins: the viral matrix protein (M1) promotes export and inhibits import', *Cell*, 67: 117-30.

Martin, K., and A. Helenius. 1991b. 'Transport of incoming influenza virus nucleocapsids into the nucleus', *J Virol*, 65: 232-44.

Martinez-Alonso, M., N. Hengrung, and E. Fodor. 2016. 'RNA-Free and Ribonucleoprotein-Associated Influenza Virus Polymerases Directly Bind the Serine-5-Phosphorylated Carboxyl-Terminal Domain of Host RNA Polymerase II', *J Virol*, 90: 6014-21.

Matlin, K. S., H. Reggio, A. Helenius, and K. Simons. 1981. 'Infectious entry pathway of influenza virus in a canine kidney cell line', *J Cell Biol*, 91: 601-13.

Matrosovich, M., T. Matrosovich, J. Carr, N. A. Roberts, and H. D. Klenk. 2003. 'Overexpression of the alpha-2,6-sialyltransferase in MDCK cells increases influenza virus sensitivity to neuraminidase inhibitors', *J Virol*, 77: 8418-25.

Mayer, D., K. Molawi, L. Martinez-Sobrido, A. Ghanem, S. Thomas, S. Baginsky, J. Grossmann, A. Garcia-Sastre, and M. Schwemmle. 2007. 'Identification of cellular interaction partners of the influenza virus ribonucleoprotein complex and polymerase complex using proteomic-based approaches', *J Proteome Res*, 6: 672-82.

McCown, M. F., and A. Pekosz. 2006. 'Distinct domains of the influenza a virus M2 protein cytoplasmic tail mediate binding to the M1 protein and facilitate infectious virus production', *J Virol*, 80: 8178-89.

Medcalf, L., E. Poole, D. Elton, and P. Digard. 1999. 'Temperature-sensitive lesions in two influenza A viruses defective for replicative transcription disrupt RNA binding by the nucleoprotein', *J Virol*, 73: 7349-56.

Melikyan, G. B., W. D. Niles, and F. S. Cohen. 1993. 'Influenza virus hemagglutinin-induced cell-planar bilayer fusion: quantitative dissection of fusion pore kinetics into stages', *J Gen Physiol*, 102: 1151-70.

Mibayashi, M., L. Martinez-Sobrido, Y. M. Loo, W. B. Cardenas, M. Gale, Jr., and A. Garcia-Sastre. 2007. 'Inhibition of retinoic acid-inducible gene I-mediated induction of beta interferon by the NS1 protein of influenza A virus', *J Virol*, 81: 514-24.

Min, J. Y., and R. M. Krug. 2006. 'The primary function of RNA binding by the influenza A virus NS1 protein in infected cells: Inhibiting the 2'-5' oligo (A) synthetase/RNase L pathway', *Proc Natl Acad Sci U S A*, 103: 7100-5.

Min, J. Y., S. Li, G. C. Sen, and R. M. Krug. 2007. 'A site on the influenza A virus NS1 protein mediates both inhibition of PKR activation and temporal regulation of viral RNA synthesis', *Virology*, 363: 236-43.

Moeller, A., R. N. Kirchdoerfer, C. S. Potter, B. Carragher, and I. A. Wilson. 2012. 'Organization of the influenza virus replication machinery', *Science*, 338: 1631-4.

Momose, F., T. Sekimoto, T. Ohkura, S. Jo, A. Kawaguchi, K. Nagata, and Y. Morikawa. 2011. 'Apical transport of influenza A virus ribonucleoprotein requires Rab11-positive recycling endosome', *PLoS One*, 6: e21123.

Mondal, A., G. K. Potts, A. R. Dawson, J. J. Coon, and A. Mehle. 2015. 'Phosphorylation at the homotypic interface regulates nucleoprotein oligomerization and assembly of the influenza virus replication machinery', *PLoS Pathog*, 11: e1004826.

Mori, N., and D. Prager. 1996. 'Transactivation of the interleukin-1alpha promoter by human T-cell leukemia virus type I and type II Tax proteins', *Blood*, 87: 3410-7.

Moscovici, C., M. G. Moscovici, H. Jimenez, M. M. Lai, M. J. Hayman, and P. K. Vogt. 1977. 'Continuous tissue culture cell lines derived from chemically induced tumors of Japanese quail', *Cell*, 11: 95-103.

Mosley, R. T., T. E. Edwards, E. Murakami, A. M. Lam, R. L. Grice, J. Du, M. J. Sofia, P. A. Furman, and M. J. Otto. 2012. 'Structure of hepatitis C virus polymerase in complex with primer-template RNA', *J Virol*, 86: 6503-11.

Mosley, V. M., and R. W. Wyckoff. 1946. 'Electron micrography of the virus of influenza', *Nature*, 157: 263.

Mudhasani, R., J. P. Tran, C. Retterer, S. R. Radoshitzky, K. P. Kota, L. A. Altamura, J. M. Smith, B. Z. Packard, J. H. Kuhn, J. Costantino, A. R. Garrison, C. S. Schmaljohn, I. C. Huang, M. Farzan, and S. Bavari. 2013. 'IFITM-2 and IFITM-3 but not IFITM-1 restrict Rift Valley fever virus', *J Virol*, 87: 8451-64.

Muller, U., U. Steinhoff, L. F. Reis, S. Hemmi, J. Pavlovic, R. M. Zinkernagel, and M. Aguet. 1994. 'Functional role of type I and type II interferons in antiviral defense', *Science*, 264: 1918-21.

Mullin, A. E., R. M. Dalton, M. J. Amorim, D. Elton, and P. Digard. 2004. 'Increased amounts of the influenza virus nucleoprotein do not promote higher levels of viral genome replication', *J Gen Virol*, 85: 3689-98.

Muramoto, Y., T. Noda, E. Kawakami, R. Akkina, and Y. Kawaoka. 2013. 'Identification of novel influenza A virus proteins translated from PA mRNA', *J Virol*, 87: 2455-62.

Murphy, T. L., M. G. Cleveland, P. Kulesza, J. Magram, and K. M. Murphy. 1995. 'Regulation of interleukin 12 p40 expression through an NF-kappa B half-site', *Mol Cell Biol*, 15: 5258-67.

Naffakh, N., P. Massin, N. Escriou, B. Crescenzo-Chaigne, and S. van der Werf. 2000. 'Genetic analysis of the compatibility between polymerase proteins from human and avian strains of influenza A viruses', *J Gen Virol*, 81: 1283-91.

Naffakh, N., A. Tomoiu, M. A. Rameix-Welti, and S. van der Werf. 2008. 'Host restriction of avian influenza viruses at the level of the ribonucleoproteins', *Annu Rev Microbiol*, 62: 403-24.

Nakajima, K., M. Ueda, and A. Sugiura. 1979. 'Origin of small RNA in von Magnus particles of influenza virus', *J Virol*, 29: 1142-8.

Nayak, D. P. 1980. 'Defective interfering influenza viruses', *Annu Rev Microbiol*, 34: 619-44.

Nayak, D. P., N. Sivasubramanian, A. R. Davis, R. Cortini, and J. Sung. 1982. 'Complete sequence analyses show that two defective interfering influenza viral RNAs contain a single internal deletion of a polymerase gene', *Proc Natl Acad Sci U S A*, 79: 2216-20.

Nemeroff, M. E., S. M. Barabino, Y. Li, W. Keller, and R. M. Krug. 1998. 'Influenza virus NS1 protein interacts with the cellular 30 kDa subunit of CPSF and inhibits 3'end formation of cellular pre-mRNAs', *Mol Cell*, 1: 991-1000.

Netherton, C. L., J. Simpson, O. Haller, T. E. Wileman, H. H. Takamatsu, P. Monaghan, and G. Taylor. 2009. 'Inhibition of a large double-stranded DNA virus by MxA protein', *J Virol*, 83: 2310-20.

Neumann, G., M. T. Hughes, and Y. Kawaoka. 2000. 'Influenza A virus NS2 protein mediates vRNP nuclear export through NES-independent interaction with hCRM1', *EMBO J*, 19: 6751-8.

Newby, C. M., L. Sabin, and A. Pekosz. 2007. 'The RNA binding domain of influenza A virus NS1 protein affects secretion of tumor necrosis factor alpha, interleukin-6, and interferon in primary murine tracheal epithelial cells', *J Virol*, 81: 9469-80.

Nieto, A., S. de la Luna, J. Barcena, A. Portela, J. Valcarcel, J. A. Melero, and J. Ortin. 1992. 'Nuclear transport of influenza virus polymerase PA protein', *Virus Res*, 24: 65-75.

Ning, S., J. S. Pagano, and G. N. Barber. 2011. 'IRF7: activation, regulation, modification and function', *Genes Immun*, 12: 399-414.

Noah, D. L., K. Y. Twu, and R. M. Krug. 2003. 'Cellular antiviral responses against influenza A virus are countered at the posttranscriptional level by the viral NS1A protein via its binding to a cellular protein required for the 3' end processing of cellular pre-mRNAS', *Virology*, 307: 386-95.

Nobusawa, E., T. Aoyama, H. Kato, Y. Suzuki, Y. Tateno, and K. Nakajima. 1991. 'Comparison of complete amino acid sequences and receptor-binding properties among 13 serotypes of hemagglutinins of influenza A viruses', *Virology*, 182: 475-85.

Noda, T., H. Sagara, A. Yen, A. Takada, H. Kida, R. H. Cheng, and Y. Kawaoka. 2006. 'Architecture of ribonucleoprotein complexes in influenza A virus particles', *Nature*, 439: 490-2.

Nogales, A., L. Rodriguez, M. L. DeDiego, D. J. Topham, and L. Martinez-Sobrido. 2017. 'Interplay of PA-X and NS1 Proteins in Replication and Pathogenesis of a Temperature-Sensitive 2009 Pandemic H1N1 Influenza A Virus', *J Virol*, 91.

Noton, S. L., M. Simpson-Holley, E. Medcalf, H. M. Wise, E. C. Hutchinson, J. W. McCauley, and P. Digard. 2009. 'Studies of an influenza A virus temperature-sensitive mutant identify a late role for NP in the formation of infectious virions', *J Virol*, 83: 562-71.

O'Neill, R. E., R. Jaskunas, G. Blobel, P. Palese, and J. Moroianu. 1995. 'Nuclear import of influenza virus RNA can be mediated by viral nucleoprotein and transport factors required for protein import', *J Biol Chem*, 270: 22701-4.

O'Neill, R. E., J. Talon, and P. Palese. 1998. 'The influenza virus NEP (NS2 protein) mediates the nuclear export of viral ribonucleoproteins', *EMBO J*, 17: 288-96.

Odagiri, T., and M. Tashiro. 1997. 'Segment-specific noncoding sequences of the influenza virus genome RNA are involved in the specific competition between defective interfering RNA and its progenitor RNA segment at the virion assembly step', *J Virol*, 71: 2138-45.

Oganesyan, G., S. K. Saha, B. Guo, J. Q. He, A. Shahangian, B. Zarnegar, A. Perry, and G. Cheng. 2006. 'Critical role of TRAF3 in the Toll-like receptor-dependent and -independent antiviral response', *Nature*, 439: 208-11.

Ohtsu, Y., Y. Honda, Y. Sakata, H. Kato, and T. Toyoda. 2002. 'Fine mapping of the subunit binding sites of influenza virus RNA polymerase', *Microbiol Immunol*, 46: 167-75.

Olson, A. C., E. Rosenblum, and R. D. Kuchta. 2010. 'Regulation of influenza RNA polymerase activity and the switch between replication and transcription by the concentrations of the vRNA 5' end, the cap source, and the polymerase', *Biochemistry*, 49: 10208-15.

Onai, Y., J. Suzuki, T. Kakuta, Y. Maejima, G. Haraguchi, H. Fukasawa, S. Muto, A. Itai, and M. Isobe. 2004. 'Inhibition of IkappaB phosphorylation in cardiomyocytes attenuates myocardial ischemia/reperfusion injury', *Cardiovasc Res*, 63: 51-9.

Onoguchi, K., M. Yoneyama, A. Takemura, S. Akira, T. Taniguchi, H. Namiki, and T. Fujita. 2007. 'Viral infections activate types I and III interferon genes through a common mechanism', *J Biol Chem*, 282: 7576-81.

Opitz, B., A. Rejaibi, B. Dauber, J. Eckhard, M. Vinzing, B. Schmeck, S. Hippenstiel, N. Suttorp, and T. Wolff. 2007. 'IFNbeta induction by influenza A virus is mediated by RIG-I which is regulated by the viral NS1 protein', *Cell Microbiol*, 9: 930-8.

Ortega, J., J. Martin-Benito, T. Zurcher, J. M. Valpuesta, J. L. Carrascosa, and J. Ortin. 2000. 'Ultrastructural and functional analyses of recombinant influenza virus ribonucleoproteins suggest dimerization of nucleoprotein during virus amplification', *J Virol*, 74: 156-63.

Oshiumi, H., M. Matsumoto, S. Hatakeyama, and T. Seya. 2009. 'Riplet/RNF135, a RING finger protein, ubiquitinates RIG-I to promote interferon-beta induction during the early phase of viral infection', *J Biol Chem*, 284: 807-17.

Palese, P., K. Tobita, M. Ueda, and R. W. Compans. 1974. 'Characterization of temperature sensitive influenza virus mutants defective in neuraminidase', *Virology*, 61: 397-410.

Paterson, D., and E. Fodor. 2012. 'Emerging roles for the influenza A virus nuclear export protein (NEP)', *PLoS Pathog*, 8: e1003019.

Peiris, J. S., W. C. Yu, C. W. Leung, C. Y. Cheung, W. F. Ng, J. M. Nicholls, T. K. Ng, K. H. Chan, S. T. Lai, W. L. Lim, K. Y. Yuen, and Y. Guan. 2004. 'Re-emergence of fatal human influenza A subtype H5N1 disease', *Lancet*, 363: 617-9.

Pena, L., A. L. Vincent, C. L. Loving, J. N. Henningson, K. M. Lager, A. Lorusso, and D. R. Perez. 2012. 'Restored PB1-F2 in the 2009 pandemic H1N1 influenza virus has minimal effects in swine', *J Virol*, 86: 5523-32.

Perez-Cidoncha, M., M. J. Killip, J. C. Oliveros, V. J. Asensio, Y. Fernandez, J. A. Bengoechea, R. E. Randall, and J. Ortin. 2014. 'An unbiased genetic screen reveals the polygenic nature of the influenza virus anti-interferon response', *J Virol*, 88: 4632-46.

Perez, D. R., and R. O. Donis. 1995. 'A 48-amino-acid region of influenza A virus PB1 protein is sufficient for complex formation with PA', *J Virol*, 69: 6932-9.

Perreira, J. M., C. R. Chin, E. M. Feeley, and A. L. Brass. 2013. 'IFITMs restrict the replication of multiple pathogenic viruses', *J Mol Biol*, 425: 4937-55.

Pflug, A., D. Guilligay, S. Reich, and S. Cusack. 2014. 'Structure of influenza A polymerase bound to the viral RNA promoter', *Nature*, 516: 355-60.

Pichlmair, A., O. Schulz, C. P. Tan, T. I. Naslund, P. Liljestrom, F. Weber, and C. Reis e Sousa. 2006. 'RIG-I-mediated antiviral responses to single-stranded RNA bearing 5'-phosphates', *Science*, 314: 997-1001.

Pindel, A., and A. Sadler. 2011. 'The role of protein kinase R in the interferon response', *J Interferon Cytokine Res*, 31: 59-70.

Pinto, L. H., L. J. Holsinger, and R. A. Lamb. 1992. 'Influenza virus M2 protein has ion channel activity', *Cell*, 69: 517-28.

Platanias, L. C. 2005. 'Mechanisms of type-I- and type-II-interferon-mediated signalling', *Nat Rev Immunol*, 5: 375-86.

Plotch, S. J., M. Bouloy, I. Ulmanen, and R. M. Krug. 1981. 'A unique cap(m7GpppXm)-dependent influenza virion endonuclease cleaves capped RNAs to generate the primers that initiate viral RNA transcription', *Cell*, 23: 847-58.

Pomerantz, J. L., and D. Baltimore. 1999. 'NF-kappaB activation by a signaling complex containing TRAF2, TANK and TBK1, a novel IKK-related kinase', *EMBO J*, 18: 6694-704.

Ponath, P. D., S. Qin, D. J. Ringler, I. Clark-Lewis, J. Wang, N. Kassam, H. Smith, X. Shi, J. A. Gonzalo, W. Newman, J. C. Gutierrez-Ramos, and C. R. Mackay. 1996. 'Cloning of the human eosinophil chemoattractant, eotaxin. Expression, receptor binding, and functional properties suggest a mechanism for the selective recruitment of eosinophils', *J Clin Invest*, 97: 604-12.

Poole, E. L., L. Medcalf, D. Elton, and P. Digard. 2007. 'Evidence that the C-terminal PB2-binding region of the influenza A virus PB1 protein is a discrete alpha-helical domain', *FEBS Lett*, 581: 5300-6.

Poon, L. L., D. C. Pritlove, E. Fodor, and G. G. Brownlee. 1999. 'Direct evidence that the poly(A) tail of influenza A virus mRNA is synthesized by reiterative copying of a U track in the virion RNA template', *J Virol*, 73: 3473-6.

Portela, A., and P. Digard. 2002. 'The influenza virus nucleoprotein: a multifunctional RNA-binding protein pivotal to virus replication', *J Gen Virol*, 83: 723-34.

Prins, K. C., W. B. Cardenas, and C. F. Basler. 2009. 'Ebola virus protein VP35 impairs the function of interferon regulatory factor-activating kinases IKKepsilon and TBK-1', *J Virol*, 83: 3069-77.

Qiu, Y., M. Nemeroff, and R. M. Krug. 1995. 'The influenza virus NS1 protein binds to a specific region in human U6 snRNA and inhibits U6-U2 and U6-U4 snRNA interactions during splicing', *RNA*, 1: 304-16.

Rabinowitz, S. G., and J. Huprikar. 1979. 'The influence of defective-interfering particles of the PR-8 strain of influenza A virus on the pathogenesis of pulmonary infection in mice', *J Infect Dis*, 140: 305-15.

Rajsbaum, R., R. A. Albrecht, M. K. Wang, N. P. Maharaj, G. A. Versteeg, E. Nistal-Villan, A. Garcia-Sastre, and M. U. Gack. 2012. 'Species-specific inhibition of RIG-I ubiquitination and IFN induction by the influenza A virus NS1 protein', *PLoS Pathog*, 8: e1003059.

Randall, R. E., and S. Goodbourn. 2008. 'Interferons and viruses: an interplay between induction, signalling, antiviral responses and virus countermeasures', *J Gen Virol*, 89: 1-47.

Rash, A., A. Woodward, N. Bryant, J. McCauley, and D. Elton. 2014. 'An efficient genome sequencing method for equine influenza [H3N8] virus reveals a new polymorphism in the PA-X protein', *Virol J*, 11: 159.

Read, E. K., and P. Digard. 2010. 'Individual influenza A virus mRNAs show differential dependence on cellular NXF1/TAP for their nuclear export', *J Gen Virol*, 91: 1290-301.

Rehwinkel, J., C. P. Tan, D. Goubau, O. Schulz, A. Pichlmair, K. Bier, N. Robb, F. Vreede, W. Barclay, E. Fodor, and C. Reis e Sousa. 2010. 'RIG-I detects viral genomic RNA during negative-strand RNA virus infection', *Cell*, 140: 397-408.

Reich, S., D. Guilligay, A. Pflug, H. Malet, I. Berger, T. Crepin, D. Hart, T. Lunardi, M. Nanao, R. W. Ruigrok, and S. Cusack. 2014. 'Structural insight into cap-snatching and RNA synthesis by influenza polymerase', *Nature*, 516: 361-6.

Ribatti, D. 2016. 'The chick embryo chorioallantoic membrane (CAM). A multifaceted experimental model', *Mech Dev*, 141: 70-7.

Richards, K. H., C. W. Wasson, O. Watherston, R. Doble, G. E. Blair, M. Wittmann, and A. Macdonald. 2015. 'The human papillomavirus (HPV) E7 protein antagonises an Imiquimod-induced inflammatory pathway in primary human keratinocytes', *Sci Rep*, 5: 12922.

Richardson, J. C., and R. K. Akkina. 1991. 'NS2 protein of influenza virus is found in purified virus and phosphorylated in infected cells', *Arch Virol*, 116: 69-80.

Rigby, R. E., H. M. Wise, N. Smith, P. Digard, and J. Rehwinkel. 2019. 'PA-X antagonises MAVS-dependent accumulation of early type I interferon messenger RNAs during influenza A virus infection', *Sci Rep*, 9: 7216.

Robb, N. C., and E. Fodor. 2012. 'The accumulation of influenza A virus segment 7 spliced mRNAs is regulated by the NS1 protein', *J Gen Virol*, 93: 113-8.

Robb, N. C., M. Smith, F. T. Vreede, and E. Fodor. 2009. 'NS2/NEP protein regulates transcription and replication of the influenza virus RNA genome', *J Gen Virol*, 90: 1398-407.

Robertson, J. S. 1979. '5' and 3' terminal nucleotide sequences of the RNA genome segments of influenza virus', *Nucleic Acids Res*, 6: 3745-57.

Robertson, J. S., M. Schubert, and R. A. Lazzarini. 1981. 'Polyadenylation sites for influenza virus mRNA', *J Virol*, 38: 157-63.

Rodriguez-Boulan, E., K. T. Paskiet, and D. D. Sabatini. 1983. 'Assembly of enveloped viruses in Madin-Darby canine kidney cells: polarized budding from single attached cells and from clusters of cells in suspension', *J Cell Biol*, 96: 866-74.

Rodriguez-Boulan, E., and D. D. Sabatini. 1978. 'Asymmetric budding of viruses in epithelial monlayers: a model system for study of epithelial polarity', *Proc Natl Acad Sci U S A*, 75: 5071-5.

Rodriguez, A., A. Perez-Gonzalez, and A. Nieto. 2011. 'Cellular human CLE/C14orf166 protein interacts with influenza virus polymerase and is required for viral replication', *J Virol*, 85: 12062-6.

Rodriguez Boulan, E., and D. D. Sabatini. 1978. 'Asymmetric budding of viruses in epithelial monlayers: a model system for study of epithelial polarity', *Proc Natl Acad Sci U S A*, 75: 5071-5.

Rodriguez, L., A. Nogales, M. Iqbal, D. R. Perez, and L. Martinez-Sobrido. 2018. 'Identification of Amino Acid Residues Responsible for Inhibition of Host Gene Expression by Influenza A H9N2 NS1 Targeting of CPSF30', *Front Microbiol*, 9: 2546.

Rossman, J. S., X. Jing, G. P. Leser, and R. A. Lamb. 2010. 'Influenza virus M2 protein mediates ESCRT-independent membrane scission', *Cell*, 142: 902-13.

Rossman, J. S., and R. A. Lamb. 2011. 'Influenza virus assembly and budding', *Virology*, 411: 229-36.

Rossman, J. S., G. P. Leser, and R. A. Lamb. 2012. 'Filamentous influenza virus enters cells via macropinocytosis', *J Virol*, 86: 10950-60.

Roy, A., D. Xu, J. Poisson, and Y. Zhang. 2011. 'A protocol for computer-based protein structure and function prediction', *J Vis Exp*: e3259.

Sabbah, A., T. H. Chang, R. Harnack, V. Frohlich, K. Tominaga, P. H. Dube, Y. Xiang, and S. Bose. 2009. 'Activation of innate immune antiviral responses by Nod2', *Nat Immunol*, 10: 1073-80.

Saira, K., X. Lin, J. V. DePasse, R. Halpin, A. Twaddle, T. Stockwell, B. Angus, A. Cozzi-Lepri, M. Delfino, V. Dugan, D. E. Dwyer, M. Freiberg, A. Horban, M. Losso, R. Lynfield, D. N. Wentworth, E. C. Holmes, R. Davey, D. E. Wentworth, E. Ghedin, Insight Flu Study Group, and Insight Flu Study Group. 2013. 'Sequence analysis of in vivo defective interfering-like RNA of influenza A H1N1 pandemic virus', *J Virol*, 87: 8064-74.

Sakurai, H., S. Suzuki, N. Kawasaki, H. Nakano, T. Okazaki, A. Chino, T. Doi, and I. Saiki. 2003. 'Tumor necrosis factor-alpha-induced IKK phosphorylation of NF-kappa B p65 on serine 536 is mediated through the TRAF2, TRAF5, and TAK1 signaling pathway', *Journal of Biological Chemistry*, 278: 36916-23.

Salk, J., and D. Salk. 1977. 'Control of influenza and poliomyelitis with killed virus vaccines', *Science*, 195: 834-47.

Sallman Almen, M., N. Bringeland, R. Fredriksson, and H. B. Schioth. 2012. 'The dispanins: a novel gene family of ancient origin that contains 14 human members', *PLoS One*, 7: e31961.

Santhakumar, D., D. Rubbenstroth, L. Martinez-Sobrido, and M. Munir. 2017. 'Avian Interferons and Their Antiviral Effectors', *Front Immunol*, 8: 49.

Sarkar, S. N., K. L. Peters, C. P. Elco, S. Sakamoto, S. Pal, and G. C. Sen. 2004. 'Novel roles of TLR3 tyrosine phosphorylation and PI3 kinase in double-stranded RNA signaling', *Nat Struct Mol Biol*, 11: 1060-7.

Sato, S., M. Sugiyama, M. Yamamoto, Y. Watanabe, T. Kawai, K. Takeda, and S. Akira. 2003. 'Toll/IL-1 receptor domain-containing adaptor inducing IFN-beta (TRIF) associates with TNF receptor-associated factor 6 and TANK-binding kinase 1, and activates two distinct transcription factors, NF-kappa B and IFN-regulatory factor-3, in the Toll-like receptor signaling', *J Immunol*, 171: 4304-10.

Satterly, N., P. L. Tsai, J. van Deursen, D. R. Nussenzveig, Y. Wang, P. A. Faria, A. Levay, D. E. Levy, and B. M. Fontoura. 2007. 'Influenza virus targets the mRNA export machinery and the nuclear pore complex', *Proc Natl Acad Sci U S A*, 104: 1853-8.

Sauter, N. K., M. D. Bednarski, B. A. Wurzburg, J. E. Hanson, G. M. Whitesides, J. J. Skehel, and D. C. Wiley. 1989. 'Hemagglutinins from two influenza virus variants bind to sialic acid derivatives with millimolar dissociation constants: a 500-MHz proton nuclear magnetic resonance study', *Biochemistry*, 28: 8388-96.

Schattgen, S. A., T. H. Oguin, and P. G. Thomas. 2016. 'The antiviral molecule Mx1 positively regulates the induction of type I IFN in response to influenza infection', *Journal of Immunology*, 196.

Scheiffele, P., A. Rietveld, T. Wilk, and K. Simons. 1999. 'Influenza viruses select ordered lipid domains during budding from the plasma membrane', *J Biol Chem*, 274: 2038-44.

Schmolke, M., and A. Garcia-Sastre. 2010. 'Evasion of innate and adaptive immune responses by influenza A virus', *Cell Microbiol*, 12: 873-80.

Scholtissek, C., and H. Becht. 1971. 'Binding of ribonucleic acids to the RNP-antigen protein of influenza viruses', *J Gen Virol*, 10: 11-6.

Scholtissek, C., W. Rohde, V. Von Hoyningen, and R. Rott. 1978. 'On the origin of the human influenza virus subtypes H2N2 and H3N2', *Virology*, 87: 13-20.

Schutze, S., K. Wiegmann, T. Machleidt, and M. Kronke. 1995. 'TNF-induced activation of NF-kappa B', *Immunobiology*, 193: 193-203.

Selman, M., S. K. Dankar, N. E. Forbes, J. J. Jia, and E. G. Brown. 2012. 'Adaptive mutation in influenza A virus non-structural gene is linked to host switching and induces a novel protein by alternative splicing', *Emerg Microbes Infect*, 1: e42.

Sen, N., M. Sommer, X. Che, K. White, W. T. Ruyechan, and A. M. Arvin. 2010. 'Varicella-zoster virus immediate-early protein 62 blocks interferon regulatory factor 3 (IRF3) phosphorylation at key serine residues: a novel mechanism of IRF3 inhibition among herpesviruses', *J Virol*, 84: 9240-53.

Seo, S. U., H. J. Kwon, H. J. Ko, Y. H. Byun, B. L. Seong, S. Uematsu, S. Akira, and M. N. Kweon. 2011. 'Type I interferon signaling regulates Ly6C(hi) monocytes and neutrophils during acute viral pneumonia in mice', *PLoS Pathog*, 7: e1001304.

Seth, R. B., L. Sun, C. K. Ea, and Z. J. Chen. 2005. 'Identification and characterization of MAVS, a mitochondrial antiviral signaling protein that activates NF-kappaB and IRF 3', *Cell*, 122: 669-82.

Shapira, S. D., I. Gat-Viks, B. O. Shum, A. Dricot, M. M. de Grace, L. Wu, P. B. Gupta, T. Hao, S. J. Silver, D. E. Root, D. E. Hill, A. Regev, and N. Hacohen. 2009. 'A physical and regulatory map of host-influenza interactions reveals pathways in H1N1 infection', *Cell*, 139: 1255-67.

Shapiro, G. I., T. Gurney, Jr., and R. M. Krug. 1987. 'Influenza virus gene expression: control mechanisms at early and late times of infection and nuclear-cytoplasmic transport of virus-specific RNAs', *J Virol*, 61: 764-73.

Shaw, A. E., J. Hughes, Q. Gu, A. Behdenna, J. B. Singer, T. Dennis, R. J. Orton, M. Varela, R. J. Gifford, S. J. Wilson, and M. Palmarini. 2017. 'Fundamental properties of the mammalian innate immune system revealed by multispecies comparison of type I interferon responses', *PLoS Biol*, 15: e2004086.

Shaw, M. L., K. L. Stone, C. M. Colangelo, E. E. Gulcicek, and P. Palese. 2008. 'Cellular proteins in influenza virus particles', *PLoS Pathog*, 4: e1000085.

Shen, Y. F., Y. H. Chen, S. Y. Chu, M. I. Lin, H. T. Hsu, P. Y. Wu, C. J. Wu, H. W. Liu, F. Y. Lin, G. Lin, P. H. Hsu, A. S. Yang, Y. S. Cheng, Y. T. Wu, C. H. Wong, and M. D. Tsai. 2011. 'E339...R416 salt bridge of nucleoprotein as a feasible target for influenza virus inhibitors', *Proc Natl Acad Sci U S A*, 108: 16515-20.

Shi, J., G. Deng, H. Kong, C. Gu, S. Ma, X. Yin, X. Zeng, P. Cui, Y. Chen, H. Yang, X. Wan, X. Wang, L. Liu, P. Chen, Y. Jiang, J. Liu, Y. Guan, Y. Suzuki, M. Li, Z. Qu, L. Guan, J. Zang, W. Gu, S. Han, Y. Song, Y. Hu, Z. Wang, L. Gu, W. Yang, L. Liang, H. Bao, G. Tian, Y. Li, C. Qiao, L. Jiang, C. Li, Z. Bu, and H. Chen. 2017. 'H7N9 virulent mutants detected in chickens in China pose an increased threat to humans', *Cell Res*, 27: 1409-21.

Shi, J., G. Deng, S. Ma, X. Zeng, X. Yin, M. Li, B. Zhang, P. Cui, Y. Chen, H. Yang, X. Wan, L. Liu, P. Chen, Y. Jiang, Y. Guan, J. Liu, W. Gu, S. Han, Y. Song, L. Liang, Z. Qu, Y. Hou, X. Wang, H. Bao, G. Tian, Y. Li, L. Jiang, C. Li, and H. Chen. 2018. 'Rapid Evolution of H7N9 Highly Pathogenic Viruses that Emerged in China in 2017', *Cell Host Microbe*, 24: 558-68 e7.

Shi, M., B. W. Jagger, H. M. Wise, P. Digard, E. C. Holmes, and J. K. Taubenberger. 2012. 'Evolutionary conservation of the PA-X open reading frame in segment 3 of influenza A virus', *J Virol*, 86: 12411-3.

Shih, S. R., M. E. Nemeroff, and R. M. Krug. 1995. 'The choice of alternative 5' splice sites in influenza virus M1 mRNA is regulated by the viral polymerase complex', *Proc Natl Acad Sci U S A*, 92: 6324-8.

Shimizu, T., N. Takizawa, K. Watanabe, K. Nagata, and N. Kobayashi. 2011. 'Crucial role of the influenza virus NS2 (NEP) C-terminal domain in M1 binding and nuclear export of vRNP', *FEBS Lett*, 585: 41-6.

Shin, H. M., M. H. Kim, B. H. Kim, S. H. Jung, Y. S. Kim, H. J. Park, J. T. Hong, K. R. Min, and Y. Kim. 2004. 'Inhibitory action of novel aromatic diamine compound on lipopolysaccharide-induced nuclear translocation of NF-kappaB without affecting IkappaB degradation', *FEBS Lett*, 571: 50-4.

Shin, N., C. W. Pyo, K. I. Jung, and S. Y. Choi. 2015. 'Influenza A virus PB1-F2 is involved in regulation of cellular redox state in alveolar epithelial cells', *Biochem Biophys Res Commun*, 459: 699-705.

Silverman, R. H. 2007. 'Viral encounters with 2',5'-oligoadenylate synthetase and RNase L during the interferon antiviral response', *J Virol*, 81: 12720-9.

Simonsen, M. 1957. 'The impact on the developing embryo and newborn animal of adult homologous cells', *Acta Pathol Microbiol Scand*, 40: 480-500.

Sivasubramanian, N., and D. P. Nayak. 1983. 'Defective interfering influenza RNAs of polymerase 3 gene contain single as well as multiple internal deletions', *Virology*, 124: 232-7.

Skehel, J. J. 1972. 'Polypeptide synthesis in influenza virus-infected cells', *Virology*, 49: 23-36.

Skehel, J. J. 1973. 'Early polypeptide synthesis in influenza virus-infected cells', *Virology*, 56: 394-9.

Skehel, J. J., and A. J. Hay. 1978. 'Nucleotide sequences at the 5' termini of influenza virus RNAs and their transcripts', *Nucleic Acids Res*, 5: 1207-19.

Smith, G. J., D. Vijaykrishna, J. Bahl, S. J. Lycett, M. Worobey, O. G. Pybus, S. K. Ma, C. L. Cheung, J. Raghwani, S. Bhatt, J. S. Peiris, Y. Guan, and A. Rambaut. 2009. 'Origins and evolutionary genomics of the 2009 swine-origin H1N1 influenza A epidemic', *Nature*, 459: 1122-5.

Smith, G. L., and A. J. Hay. 1982. 'Replication of the influenza virus genome', *Virology*, 118: 96-108.

Smith, G. L., J. Z. Levin, P. Palese, and B. Moss. 1987. 'Synthesis and cellular location of the ten influenza polypeptides individually expressed by recombinant vaccinia viruses', *Virology*, 160: 336-45.

Smith, M. F., Jr., D. Eidlen, W. P. Arend, and A. Gutierrez-Hartmann. 1994. 'LPS-induced expression of the human IL-1 receptor antagonist gene is controlled by multiple interacting promoter elements', *J Immunol*, 153: 3584-93.

Son, Y. H., Y. T. Jeong, K. A. Lee, K. H. Choi, S. M. Kim, B. Y. Rhim, and K. Kim. 2008. 'Roles of MAPK and NF-kappaB in interleukin-6 induction by lipopolysaccharide in vascular smooth muscle cells', *J Cardiovasc Pharmacol*, 51: 71-7.

Spruce, A. E., A. Iwata, J. M. White, and W. Almers. 1989. 'Patch clamp studies of single cell-fusion events mediated by a viral fusion protein', *Nature*, 342: 555-8.

Sriwilaijaroen, N., and Y. Suzuki. 2012. 'Molecular basis of the structure and function of H1 hemagglutinin of influenza virus', *Proc Jpn Acad Ser B Phys Biol Sci*, 88: 226-49.

Staeheli, P., P. Danielson, O. Haller, and J. G. Sutcliffe. 1986a. 'Transcriptional activation of the mouse Mx gene by type I interferon', *Mol Cell Biol*, 6: 4770-4.

Staeheli, P., R. Grob, E. Meier, J. G. Sutcliffe, and O. Haller. 1988. 'Influenza virus-susceptible mice carry Mx genes with a large deletion or a nonsense mutation', *Mol Cell Biol*, 8: 4518-23.

Staeheli, P., O. Haller, W. Boll, J. Lindenmann, and C. Weissmann. 1986b. 'Mx protein: constitutive expression in 3T3 cells transformed with cloned Mx cDNA confers selective resistance to influenza virus', *Cell*, 44: 147-58.

Steel, J., and A. C. Lowen. 2014. 'Influenza A virus reassortment', *Curr Top Microbiol Immunol*, 385: 377-401.

Stegmann, T. 2000. 'Membrane fusion mechanisms: the influenza hemagglutinin paradigm and its implications for intracellular fusion', *Traffic*, 1: 598-604.

Steidle, S., L. Martinez-Sobrido, M. Mordstein, S. Lienenklaus, A. Garcia-Sastre, P. Staheli, and G. Kochs. 2010. 'Glycine 184 in nonstructural protein NS1 determines the virulence of influenza A virus strain PR8 without affecting the host interferon response', *J Virol*, 84: 12761-70.

Stewart, C. E., R. E. Randall, and C. S. Adamson. 2014. 'Inhibitors of the interferon response enhance virus replication in vitro', *PLoS One*, 9: e112014.

Stewart, M. 2007. 'Molecular mechanism of the nuclear protein import cycle', *Nat Rev Mol Cell Biol*, 8: 195-208.

Subbarao, E. K., W. London, and B. R. Murphy. 1993. 'A single amino acid in the PB2 gene of influenza A virus is a determinant of host range', *J Virol*, 67: 1761-4.

Sugita, A., H. Ogawa, M. Azuma, S. Muto, A. Honjo, H. Yanagawa, Y. Nishioka, K. Tani, A. Itai, and S. Sone. 2009. 'Antiallergic and anti-inflammatory effects of a novel I kappaB kinase beta inhibitor, IMD-0354, in a mouse model of allergic inflammation', *Int Arch Allergy Immunol*, 148: 186-98.

Sugiyama, K., A. Kawaguchi, M. Okuwaki, and K. Nagata. 2015. 'pp32 and APRIL are host cell-derived regulators of influenza virus RNA synthesis from cRNA', *Elife*, 4.

Sun, X., Y. Shi, X. Lu, J. He, F. Gao, J. Yan, J. Qi, and G. F. Gao. 2013. 'Bat-derived influenza hemagglutinin H17 does not bind canonical avian or human receptors and most likely uses a unique entry mechanism', *Cell Rep*, 3: 769-78.

Swayne, D. E., E. Spackman, and M. Pantin-Jackwood. 2014. 'Success factors for avian influenza vaccine use in poultry and potential impact at the wild bird-agricultural interface', *Ecohealth*, 11: 94-108.

Taft, A. S., M. Ozawa, A. Fitch, J. V. Depasse, P. J. Halfmann, L. Hill-Batorski, M. Hatta, T. C. Friedrich, T. J. Lopes, E. A. Maher, E. Ghedin, C. A. Macken, G. Neumann, and Y. Kawaoka. 2015. 'Identification of mammalian-adapting mutations in the polymerase complex of an avian H5N1 influenza virus', *Nat Commun*, 6: 7491.

Takeda, K., and S. Akira. 2005. 'Toll-like receptors in innate immunity', *Int Immunol*, 17: 1-14.

Talon, J., C. M. Horvath, R. Polley, C. F. Basler, T. Muster, P. Palese, and A. Garcia-Sastre. 2000. 'Activation of interferon regulatory factor 3 is inhibited by the influenza A virus NS1 protein', *J Virol*, 74: 7989-96.

Tang, X., J. S. Gao, Y. J. Guan, K. E. McLane, Z. L. Yuan, B. Ramratnam, and Y. E. Chin. 2007. 'Acetylation-dependent signal transduction for type I interferon receptor', *Cell*, 131: 93-105.

Tapia, K., W. K. Kim, Y. Sun, X. Mercado-Lopez, E. Dunay, M. Wise, M. Adu, and C. B. Lopez. 2013. 'Defective viral genomes arising in vivo provide critical danger signals for the triggering of lung antiviral immunity', *PLoS Pathog*, 9: e1003703.

Taubenberger, J. K., A. H. Reid, R. M. Lourens, R. Wang, G. Jin, and T. G. Fanning. 2005. 'Characterization of the 1918 influenza virus polymerase genes', *Nature*, 437: 889-93.

Tauber, S., Y. Ligertwood, M. Quigg-Nicol, B. M. Dutia, and R. M. Elliott. 2012. 'Behaviour of influenza A viruses differentially expressing segment 2 gene products in vitro and in vivo', *J Gen Virol*, 93: 840-9.

Tawaratsumida, K., V. Phan, E. R. Hrincius, A. A. High, R. Webby, V. Redecke, and H. Hacker. 2014. 'Quantitative proteomic analysis of the influenza A virus nonstructural proteins NS1 and NS2 during natural cell infection identifies PACT as an NS1 target protein and antiviral host factor', *J Virol*, 88: 9038-48.

Tchatalbachev, S., R. Flick, and G. Hobom. 2001. 'The packaging signal of influenza viral RNA molecules', *RNA*, 7: 979-89.

Te Velthuis, A. J., and E. Fodor. 2016. 'Influenza virus RNA polymerase: insights into the mechanisms of viral RNA synthesis', *Nat Rev Microbiol*, 14: 479-93.

Tiley, L. S., M. Hagen, J. T. Matthews, and M. Krystal. 1994. 'Sequence-specific binding of the influenza virus RNA polymerase to sequences located at the 5' ends of the viral RNAs', *J Virol*, 68: 5108-16.

Tomescu, A. I., N. C. Robb, N. Hengrung, E. Fodor, and A. N. Kapanidis. 2014. 'Single-molecule FRET reveals a corkscrew RNA structure for the polymerase-bound influenza virus promoter', *Proc Natl Acad Sci U S A*, 111: E3335-42.

Tong, S., Y. Li, P. Rivailler, C. Conrardy, D. A. Castillo, L. M. Chen, S. Recuenco, J. A. Ellison, C. T. Davis, I. A. York, A. S. Turmelle, D. Moran, S. Rogers, M. Shi, Y. Tao, M. R. Weil, K. Tang, L. A. Rowe, S. Sammons, X. Xu, M. Frace, K. A. Lindblade, N. J. Cox, L. J. Anderson, C. E. Rupprecht, and R. O. Donis. 2012. 'A distinct lineage of influenza A virus from bats', *Proc Natl Acad Sci U S A*, 109: 4269-74.

Tong, S., X. Zhu, Y. Li, M. Shi, J. Zhang, M. Bourgeois, H. Yang, X. Chen, S. Recuenco, J. Gomez, L. M. Chen, A. Johnson, Y. Tao, C. Dreyfus, W. Yu, R. McBride, P. J. Carney, A. T. Gilbert, J. Chang, Z. Guo, C. T. Davis, J. C. Paulson, J. Stevens, C. E. Rupprecht, E. C. Holmes, I. A. Wilson, and R. O. Donis. 2013. 'New world bats harbor diverse influenza A viruses', *PLoS Pathog*, 9: e1003657.

Toshchakov, V. U., S. Basu, M. J. Fenton, and S. N. Vogel. 2005. 'Differential involvement of BB loops of toll-IL-1 resistance (TIR) domain-containing adapter proteins in TLR4- versus TLR2-mediated signal transduction', *J Immunol*, 175: 494-500.

Toyoda, T., D. M. Adyshev, M. Kobayashi, A. Iwata, and A. Ishihama. 1996. 'Molecular assembly of the influenza virus RNA polymerase: determination of the subunit-subunit contact sites', *J Gen Virol*, 77 (Pt 9): 2149-57.

Trifilo, M. J., C. C. Bergmann, W. A. Kuziel, and T. E. Lane. 2003. 'CC chemokine ligand 3 (CCL3) regulates CD8(+)-T-cell effector function and migration following viral infection', *J Virol*, 77: 4004-14.

Trinchieri, G. 1994. 'Interleukin-12: a cytokine produced by antigen-presenting cells with immunoregulatory functions in the generation of T-helper cells type 1 and cytotoxic lymphocytes', *Blood*, 84: 4008-27.

Trnka, Z., and I. Riha. 1959. 'Antibody formation by isolated spleen cells transferred to recipients in absence of homotransplantation reaction', *Nature*, 183: 546-7.

Tsai, P. L., N. T. Chiou, S. Kuss, A. Garcia-Sastre, K. W. Lynch, and B. M. Fontoura. 2013. 'Cellular RNA binding proteins NS1-BP and hnRNP K regulate influenza A virus RNA splicing', *PLoS Pathog*, 9: e1003460.

Tsurudome, M., R. Gluck, R. Graf, R. Falchetto, U. Schaller, and J. Brunner. 1992. 'Lipid interactions of the hemagglutinin HA2 NH2-terminal segment during influenza virus-induced membrane fusion', *J Biol Chem*, 267: 20225-32.

Turan, K., M. Mibayashi, K. Sugiyama, S. Saito, A. Numajiri, and K. Nagata. 2004. 'Nuclear MxA proteins form a complex with influenza virus NP and inhibit the transcription of the engineered influenza virus genome', *Nucleic Acids Res*, 32: 643-52.

Turnbull, M. L. 2017. 'The Role of the NS Segment of Influenza A Virus in Setting Host Range and Pathogenicity', PhD Thesis, University of Edinburgh.

Turnbull, M. L., H. M. Wise, M. Q. Nicol, N. Smith, R. L. Dunfee, P. M. Beard, B. W. Jagger, Y. Ligertwood, G. R. Hardisty, H. Xiao, D. J. Benton, A. M. Coburn, J. A. Paulo, S. P. Gygi, J. W. McCauley, J. K. Taubenberger, S. J. Lycett, M. P. Weekes, B. M. Dutia, and P. Digard. 2016. 'Role of the B Allele of Influenza A Virus Segment 8 in Setting Mammalian Host Range and Pathogenicity', *J Virol*, 90: 9263-84.

Turrell, L., J. W. Lyall, L. S. Tiley, E. Fodor, and F. T. Vreede. 2013. 'The role and assembly mechanism of nucleoprotein in influenza A virus ribonucleoprotein complexes', *Nat Commun*, 4: 1591.

Twu, K. Y., R. L. Kuo, J. Marklund, and R. M. Krug. 2007. 'The H5N1 influenza virus NS genes selected after 1998 enhance virus replication in mammalian cells', *J Virol*, 81: 8112-21.

Ueda, M., K. Nakajima, and A. Sugiura. 1980. 'Extra RNAs of von Magnus particles of influenza virus cause reduction of particular polymerase genes', *J Virol*, 34: 1-8.

Uematsu, S., and S. Akira. 2008. 'Toll-Like receptors (TLRs) and their ligands', *Handb Exp Pharmacol*: 1-20.

Varga, Z. T., A. Grant, B. Manicassamy, and P. Palese. 2012. 'Influenza virus protein PB1-F2 inhibits the induction of type I interferon by binding to MAVS and decreasing mitochondrial membrane potential', *J Virol*, 86: 8359-66.

Varga, Z. T., and P. Palese. 2011. 'The influenza A virus protein PB1-F2: killing two birds with one stone?', *Virulence*, 2: 542-6.

Vasilijevic, J., N. Zamarreno, J. C. Oliveros, A. Rodriguez-Frandsen, G. Gomez, G. Rodriguez, M. Perez-Ruiz, S. Rey, I. Barba, F. Pozo, I. Casas, A. Nieto, and A. Falcon. 2017. 'Reduced accumulation of defective viral genomes contributes to severe outcome in influenza virus infected patients', *PLoS Pathog*, 13: e1006650.

Verhelst, J., E. Parthoens, B. Schepens, W. Fiers, and X. Saelens. 2012. 'Interferon-inducible protein Mx1 inhibits influenza virus by interfering with functional viral ribonucleoprotein complex assembly', *J Virol*, 86: 13445-55.

Vestergaard, C., M. Deleuran, B. Gesser, and C. G. Larsen. 2004. 'Thymus- and activation-regulated chemokine (TARC/CCL17) induces a Th2-dominated inflammatory reaction on intradermal injection in mice', *Exp Dermatol*, 13: 265-71.

Vijayakrishnan, S., C. Loney, D. Jackson, W. Suphamungmee, F. J. Rixon, and D. Bhella. 2013. 'Cryotomography of budding influenza A virus reveals filaments with diverse morphologies that mostly do not bear a genome at their distal end', *PLoS Pathog*, 9: e1003413.

von der Malsburg, A., I. Abutbul-Ionita, O. Haller, G. Kochs, and D. Danino. 2011. 'Stalk domain of the dynamin-like MxA GTPase protein mediates membrane binding and liposome tubulation via the unstructured L4 loop', *J Biol Chem*, 286: 37858-65.

von Magnus, P. 1951a. 'Propagation of the PR8 strain of influenza A virus in chick embryos. II. The formation of incomplete virus following inoculation of large doses of seed virus', *Acta Pathol Microbiol Scand*, 28: 278-93.

von Magnus, P. 1951b. 'Propagation of the PR8 strain of influenza A virus in chick embryos. III. Properties of the incomplete virus produced in serial passages of undiluted virus', *Acta Pathol Microbiol Scand*, 29: 157-81.

Vreede, F. T., and G. G. Brownlee. 2007. 'Influenza virion-derived viral ribonucleoproteins synthesize both mRNA and cRNA in vitro', *J Virol*, 81: 2196-204.

Vreede, F. T., and E. Fodor. 2010. 'The role of the influenza virus RNA polymerase in host shut-off', *Virulence*, 1: 436-9.

Vreede, F. T., T. E. Jung, and G. G. Brownlee. 2004. 'Model suggesting that replication of influenza virus is regulated by stabilization of replicative intermediates', *J Virol*, 78: 9568-72.

Wack, A., E. Terczynska-Dyla, and R. Hartmann. 2015. 'Guarding the frontiers: the biology of type III interferons', *Nat Immunol*, 16: 802-9.

Wang, C., L. Deng, M. Hong, G. R. Akkaraju, J. Inoue, and Z. J. Chen. 2001. 'TAK1 is a ubiquitin-dependent kinase of MKK and IKK', *Nature*, 412: 346-51.

Wang, P., P. Palese, and R. E. O'Neill. 1997. 'The NPI-1/NPI-3 (karyopherin alpha) binding site on the influenza a virus nucleoprotein NP is a nonconventional nuclear localization signal', *J Virol*, 71: 1850-6.

Wang, Q., Q. Li, T. Liu, G. Chang, Z. Sun, Z. Gao, F. Wang, H. Zhou, R. Liu, M. Zheng, H. Cui, G. Chen, H. Li, X. Yuan, J. Wen, D. Peng, and G. Zhao. 2018. 'Host Interaction Analysis of PA-N155 and PA-N182 in Chicken Cells Reveals an Essential Role of UBA52 for Replication of H5N1 Avian Influenza Virus', *Front Microbiol*, 9: 936.

Wang, Q., R. Liu, Q. Li, F. Wang, B. Zhu, M. Zheng, H. Cui, J. Wen, and G. Zhao. 2019. 'Host cell interactome of PB1 N40 protein of H5N1 influenza A virus in chicken cells', *J Proteomics*, 197: 34-41.

Wang, W., Z. Q. Cui, H. Han, Z. P. Zhang, H. P. Wei, Y. F. Zhou, Z. Chen, and X. E. Zhang. 2008. 'Imaging and characterizing influenza A virus mRNA transport in living cells', *Nucleic Acids Res*, 36: 4913-28.

Wang, W., and R. M. Krug. 1998. 'U6atac snRNA, the highly divergent counterpart of U6 snRNA, is the specific target that mediates inhibition of AT-AC splicing by the influenza virus NS1 protein', *RNA*, 4: 55-64.

Wang, W., K. Riedel, P. Lynch, C. Y. Chien, G. T. Montelione, and R. M. Krug. 1999. 'RNA binding by the novel helical domain of the influenza virus NS1 protein requires its dimer structure and a small number of specific basic amino acids', *RNA*, 5: 195-205.

Wang, X., E. R. Hinson, and P. Cresswell. 2007. 'The interferon-inducible protein viperin inhibits influenza virus release by perturbing lipid rafts', *Cell Host Microbe*, 2: 96-105.

Wang, X., M. Li, H. Zheng, T. Muster, P. Palese, A. A. Beg, and A. Garcia-Sastre. 2000. 'Influenza A virus NS1 protein prevents activation of NF-kappaB and induction of alpha/beta interferon', *J Virol*, 74: 11566-73.

Wang, Y., Y. Yin, X. Lan, F. Ye, K. Tian, X. Zhao, H. Yin, D. Li, H. Xu, Y. Liu, and Q. Zhu. 2017. 'Molecular characterization, expression of chicken TBK1 gene and its effect on IRF3 signaling pathway', *PLoS One*, 12: e0177608.

Watanabe, R., G. P. Leser, and R. A. Lamb. 2011. 'Influenza virus is not restricted by tetherin whereas influenza VLP production is restricted by tetherin', *Virology*, 417: 50-6.

Watanabe, T., S. Watanabe, and Y. Kawaoka. 2010. 'Cellular networks involved in the influenza virus life cycle', *Cell Host Microbe*, 7: 427-39.

Webster, R. G., W. J. Bean, O. T. Gorman, T. M. Chambers, and Y. Kawaoka. 1992. 'Evolution and ecology of influenza A viruses', *Microbiol Rev*, 56: 152-79.

Webster, R. G., and H. G. Pereira. 1968. 'A common surface antigen in influenza viruses from human and avian sources', *J Gen Virol*, 3: 201-8.

Webster, R. G., M. Yakhno, V. S. Hinshaw, W. J. Bean, and K. G. Murti. 1978. 'Intestinal influenza: replication and characterization of influenza viruses in ducks', *Virology*, 84: 268-78.

Wei, X., and J. Cui. 2018. 'Why were so few people infected with H7N9 influenza A viruses in China from late 2017 to 2018?', *Sci China Life Sci*, 61: 1442-44.

Weis, W., J. H. Brown, S. Cusack, J. C. Paulson, J. J. Skehel, and D. C. Wiley. 1988. 'Structure of the influenza virus haemagglutinin complexed with its receptor, sialic acid', *Nature*, 333: 426-31.

Wibberley, G., C. Swallow, and D. H. Roberts. 1988. 'Characterization of an influenza A (H3N2) virus isolated from pigs in England in 1987', *Br Vet J*, 144: 196-201.

Wickremasinghe, M. I., L. H. Thomas, C. M. O'Kane, J. Uddin, and J. S. Friedland. 2004. 'Transcriptional mechanisms regulating alveolar epithelial cell-specific CCL5 secretion in pulmonary tuberculosis', *J Biol Chem*, 279: 27199-210.

Wilson, J. R., P. F. de Sessions, M. A. Leon, and F. Scholle. 2008. 'West Nile virus nonstructural protein 1 inhibits TLR3 signal transduction', *J Virol*, 82: 8262-71.

Wise, H. M., C. Barbezange, B. W. Jagger, R. M. Dalton, J. R. Gog, M. D. Curran, J. K. Taubenberger, E. C. Anderson, and P. Digard. 2011. 'Overlapping signals for

translational regulation and packaging of influenza A virus segment 2', *Nucleic Acids Res*, 39: 7775-90.

Wise, H. M., A. Foeglein, J. Sun, R. M. Dalton, S. Patel, W. Howard, E. C. Anderson, W. S. Barclay, and P. Digard. 2009. 'A complicated message: Identification of a novel PB1-related protein translated from influenza A virus segment 2 mRNA', *J Virol*, 83: 8021-31.

Wise, H. M., E. C. Hutchinson, B. W. Jagger, A. D. Stuart, Z. H. Kang, N. Robb, L. M. Schwartzman, J. C. Kash, E. Fodor, A. E. Firth, J. R. Gog, J. K. Taubenberger, and P. Digard. 2012. 'Identification of a novel splice variant form of the influenza A virus M2 ion channel with an antigenically distinct ectodomain', *PLoS Pathog*, 8: e1002998.

Wolff, T., R. E. O'Neill, and P. Palese. 1998. 'NS1-Binding protein (NS1-BP): a novel human protein that interacts with the influenza A virus nonstructural NS1 protein is relocalized in the nuclei of infected cells', *J Virol*, 72: 7170-80.

Wong, S. S., and R. J. Webby. 2013. 'Traditional and new influenza vaccines', *Clin Microbiol Rev*, 26: 476-92.

Wu, W. W., L. L. Weaver, and N. Pante. 2009. 'Purification and visualization of influenza a viral ribonucleoprotein complexes', *J Vis Exp*.

Wu, W., W. Zhang, E. S. Duggan, J. L. Booth, M. H. Zou, and J. P. Metcalf. 2015. 'RIG-I and TLR3 are both required for maximum interferon induction by influenza virus in human lung alveolar epithelial cells', *Virology*, 482: 181-8.

Xia, C., M. Vijayan, C. J. Pritzl, S. Y. Fuchs, A. B. McDermott, and B. Hahm. 2015. 'Hemagglutinin of Influenza A Virus Antagonizes Type I Interferon (IFN) Responses by Inducing Degradation of Type I IFN Receptor 1', *J Virol*, 90: 2403-17.

Xing, F., T. Matsumiya, K. Onomoto, R. Hayakari, T. Imaizumi, H. Yoshida, M. Yoneyama, T. Fujita, and K. Satoh. 2012. 'Foreign RNA induces the degradation of mitochondrial antiviral signaling protein (MAVS): the role of intracellular antiviral factors', *PLoS One*, 7: e45136.

Xu, G., X. Zhang, Y. Sun, Q. Liu, H. Sun, X. Xiong, M. Jiang, Q. He, Y. Wang, J. Pu, X. Guo, H. Yang, and J. Liu. 2016. 'Truncation of C-terminal 20 amino acids in PA-X contributes to adaptation of swine influenza virus in pigs', *Sci Rep*, 6: 21845.

Xu, H., P. Wang, Y. Fu, Y. Zheng, Q. Tang, L. Si, J. You, Z. Zhang, Y. Zhu, L. Zhou, Z. Wei, B. Lin, L. Hu, and X. Kong. 2010. 'Length of the ORF, position of the first AUG and the Kozak motif are important factors in potential dual-coding transcripts', *Cell Res*, 20: 445-57.

Xu, L. G., Y. Y. Wang, K. J. Han, L. Y. Li, Z. Zhai, and H. B. Shu. 2005. 'VISA is an adapter protein required for virus-triggered IFN-beta signaling', *Mol Cell*, 19: 727-40.

Yamamoto, M., S. Sato, H. Hemmi, K. Hoshino, T. Kaisho, H. Sanjo, O. Takeuchi, M. Sugiyama, M. Okabe, K. Takeda, and S. Akira. 2003. 'Role of adaptor TRIF in the MyD88-independent toll-like receptor signaling pathway', *Science*, 301: 640-3.

Yamayoshi, S., M. Watanabe, H. Goto, and Y. Kawaoka. 2016. 'Identification of a Novel Viral Protein Expressed from the PB2 Segment of Influenza A Virus', *J Virol*, 90: 444-56.

Yang, J., R. Yan, A. Roy, D. Xu, J. Poisson, and Y. Zhang. 2015. 'The I-TASSER Suite: protein structure and function prediction', *Nat Methods*, 12: 7-8.

Yang, N., J. S. Gibbs, H. D. Hickman, G. V. Reynoso, A. K. Ghosh, J. R. Bennink, and J. W. Yewdell. 2016. 'Defining Viral Defective Ribosomal Products: Standard and Alternative Translation Initiation Events Generate a Common Peptide from Influenza A Virus M2 and M1 mRNAs', *J Immunol*, 196: 3608-17.

Yasuda, J., S. Nakada, A. Kato, T. Toyoda, and A. Ishihama. 1993. 'Molecular assembly of influenza virus: association of the NS2 protein with virion matrix', *Virology*, 196: 249-55.

Ye, J., E. M. Sorrell, Y. Cai, H. Shao, K. Xu, L. Pena, D. Hickman, H. Song, M. Angel, R. A. Medina, B. Manicassamy, A. Garcia-Sastre, and D. R. Perez. 2010. 'Variations in the hemagglutinin of the 2009 H1N1 pandemic virus: potential for strains with altered virulence phenotype?', *PLoS Pathog*, 6: e1001145.

Ye, Q., R. M. Krug, and Y. J. Tao. 2006. 'The mechanism by which influenza A virus nucleoprotein forms oligomers and binds RNA', *Nature*, 444: 1078-82.

Ye, Z., T. Liu, D. P. Offringa, J. McInnis, and R. A. Levandowski. 1999. 'Association of influenza virus matrix protein with ribonucleoproteins', *J Virol*, 73: 7467-73.

Yoneyama, M., and T. Fujita. 2004. '[Virus-induced expression of type I interferon genes]', *Uirusu*, 54: 161-7.

York, A., and E. Fodor. 2013. 'Biogenesis, assembly, and export of viral messenger ribonucleoproteins in the influenza A virus infected cell', *RNA Biol*, 10: 1274-82.

York, A., N. Hengrung, F. T. Vreede, J. T. Huiskonen, and E. Fodor. 2013. 'Isolation and characterization of the positive-sense replicative intermediate of a negative-strand RNA virus', *Proc Natl Acad Sci U S A*, 110: E4238-45.

Yoshimoto, T., H. Nagase, T. Ishida, J. Inoue, and H. Nariuchi. 1997. 'Induction of interleukin-12 p40 transcript by CD40 ligation via activation of nuclear factor-kappaB', *Eur J Immunol*, 27: 3461-70.

Yoshizumi, T., T. Ichinohe, O. Sasaki, H. Otera, S. Kawabata, K. Mihara, and T. Koshiba. 2014. 'Influenza A virus protein PB1-F2 translocates into mitochondria via Tom40 channels and impairs innate immunity', *Nat Commun*, 5: 4713.

Zaid, H., S. Abu-Hamad, A. Israelson, I. Nathan, and V. Shoshan-Barmatz. 2005. 'The voltage-dependent anion channel-1 modulates apoptotic cell death', *Cell Death Differ*, 12: 751-60.

Zamarin, D., M. B. Ortigoza, and P. Palese. 2006. 'Influenza A virus PB1-F2 protein contributes to viral pathogenesis in mice', *J Virol*, 80: 7976-83.

Zaraket, H., R. Saito, Y. Suzuki, Y. Suzuki, I. Caperig-Dapat, C. Dapat, Shabana, II, T. Baranovich, and H. Suzuki. 2010. 'Genomic events contributing to the high prevalence of amantadine-resistant influenza A/H3N2', *Antivir Ther*, 15: 307-19.

Zhang, J., A. Pekosz, and R. A. Lamb. 2000. 'Influenza virus assembly and lipid raft microdomains: a role for the cytoplasmic tails of the spike glycoproteins', *J Virol*, 74: 4634-44.

Zhang, Z., J. Liu, M. Li, H. Yang, and C. Zhang. 2012. 'Evolutionary dynamics of the interferon-induced transmembrane gene family in vertebrates', *PLoS One*, 7: e49265.

Zhao, T., L. Yang, Q. Sun, M. Arguello, D. W. Ballard, J. Hiscott, and R. Lin. 2007. 'The NEMO adaptor bridges the nuclear factor-kappaB and interferon regulatory factor signaling pathways', *Nat Immunol*, 8: 592-600.

Zurcher, T., J. Pavlovic, and P. Staeheli. 1992. 'Mouse Mx2 protein inhibits vesicular stomatitis virus but not influenza virus', *Virology*, 187: 796-800.

Zvonarjev, A. Y., and Y. Z. Ghendon. 1980. 'Influence of membrane (M) protein on influenza A virus virion transcriptase activity in vitro and its susceptibility to rimantadine', *J Virol*, 33: 583-6.